Novel cellulose particles by regeneration from homogeneous solution

Master's Thesis

Matti Leskinen

University of Helsinki

Faculty of Science

Department of Chemistry

Materials Chemistry Division

04/2018

Tiedekunta – Fakultet – Faculty	Koulutusohjelma – Utbildningsprogram – Degree programme
Matemaattis-luonnontieteellinen tiedekunta	Kemia, FM

Tekijä – Författare – Author
Matti Lauri Kalevi Leskinen

Työn nimi – Arbetets titel – Title
Novel cellulose particles by regeneration from homogeneous solution

Työn laji – Arbetets art – Level	Aika – Datum – Month and year	Sivumäärä – Sidoantal – Number of pages
Pro gradu -tutkielma	04.2018.	180

Tiivistelmä – Referat – Abstract

The theme of the thesis has been the preparation of cellulose particles from homogeneous ionic liquid solutions. The work approaches this topic from the materials chemistry perspective and focuses on physical properties of the obtained materials and the methodological details of their preparation.

Novel cellulose macro- and microparticles have been prepared from two cellulose solvents systems, [DBNH][OAc]/DMSO and [P$_{4441}$][OAc]/GVL. The two types of particles and their preparation methods are very different and distinct. The large beads are prepared using remarkably simple hands-on method, while the small particles are prepared by exploiting a thermally triggered gelation of cellulose. Both particles are scientifically interesting and observations made during their preparation provide insight to the field of cellulose materials chemistry. Special attention has been given to exploring their potential applications outside the laboratory in the commercial and industrial sectors.

The laboratory work examines the experimental parameters of the cellulose particle production methods in detail. The particle preparation methods are very simple in practice. Emphasis has been given to describing the observed novel phenomena and fine-tuning the processes for efficiency. The procured cellulose particles have been analysed using a variety of methods including optical microscopy, SEM, XRD, WAXS, CP-MAS, VSM and H-NMR.

Avainsanat – Nyckelord – Keywords
Cellulose, Ionic Liquids, Microparticles, Superbase-ILs, Phosphonium-ILs

Säilytyspaikka – Förvaringställe – Where deposited
Kumpula campus library, E-Thesis

Muita tietoja – Övriga uppgifter – Additional information

Table of contents

List of abbreviations

Aerosol-OT 100: Sodium 1,4-bis(2-ethylhexoxy)-1,4-dioxobutane-2-sulfonate/Sodium dioctyl sulfosuccinate/Docusate

AGU: AnhydroGlucose Unit

[amim]Cl: 1-allyl-3-methylimidazoliumchrolide

BNC: Bacterial nanocellulose

[bmim]Cl: 1-butyl-3-methylimidazoliumchrolide

Brij-52/Brij-C2: Polyethylene glycol hexadecyl ether, Polyoxyethylene (2) cetyl ether

Brij 72/Brij S2: Polyethylene glycol octadecyl ether, Polyoxyethylene (2) stearyl ether

Brij 76/Brij S10: Polyethylene glycol octadecyl ether, Polyoxyethylene (10) stearyl ether

CMC: Carboxymethyl cellulose

DBN: 1,5-diazabicyclo[4.3.0]non-5-ene

[DBNH]$^+$: 1,5-diazabicyclo[4.3.0]non-5-enium

[DBNH][OAc]: 1,5-diazabicyclo[4.3.0]non-5-enium acetate

DBU: 1,8-diazabicyclo[5.4.0]undec-7-ene

[DBUH]$^+$: 1,8-diazabicyclo[5.4.0]undec-7-enium

DIL: Distillable ionic liquid

DMA: Dimethylacetamide

DMAN: 1,8-bis-(dimethylamino)naphthalene

DMF: *N,N*-dimethylformamide

DMI: 1,3-dimethyl-2-imidazolidinone

[DMPH]$^+$: 1,2-dimethyl-1,4,5,6-tetrahydropyrimidinium

DMPU: 1,3-dimethyl-3,4,5,6-tetrahydro-2-pyrimidinone

DMSO: Dimethyl sulfoxide

DP: Degree of Polymerisations

DR: Draw ratio

DS: Degree of Substitution

[emim]Cl: 1-ethyl-3-methylimidazoliumchrolide

EPDM: Ethylene Propylene Diene Monomer

GVL: Gamma-γ-Valerolactone

IUBMB: International Union of Biochemistry and Molecular Biology

IUPAC: International Union of Pure and Applied Chemistry

LS: Light scattering

MCC: Microcrystalline cellulose

MF: Microfluidizer

MFC: Microfibrillated cellulose

MMCF: Man-made cellulosic fibre

mPEG–PTMC: Monomethoxy poly(ethylene glycol)-*block*-poly(trimethylene carbonate)

MWCO: Molecular weight cut-off

$[N_{4444}]F$: tetra-n-butylammonium fluoride

NCC: Nanocrystalline cellulose

NMMO: N-methylmorpholine N-oxide

NMP: N-methyl-2-pyrrolidone

OAc: Acetate

OAcH: Acetic acid

$[P_{4441}][OAc]$: tributylmethylphosphonium acetate

PACA: Polyalkylcyanoacrylate

PCL: Poly(ε-caprolactone)

PDI: Polydispersity index

PEG-PLA: poly(ethylene glycol)-poly(lactic acid) copolymer

PEO-mPAE: poly(ethylene oxide)-modified poly(β-amino ester)

PHDFDA: Poly(heptadecafluorodecyl acrylate)

PLA: Polylactid acid

PLGA: Poly(lactic-co-glycolic acid)

PMMA: Poly(methyl methacrylate)

PNP: Polymer nanoparticle

POP: Poly(organo phosphazene)

PTMC: Poly(lactide-co-trimethylene carbonate)

PVA: Polyvinyl alcohol

RESS: Rapid expansion of supercritical solution

RESOLV: Rapid expansion of supercritical solution into liquid solvent

RTIL: Room temperature ionic liquid

SAXS: Small-angle x-ray scattering

SDS: Sodium dodecyl sulfate/Sodium lauryl sulfate

SEM: Scanning electron microscopy

SIL: Superbase Ionic Liquid

TBA: tetra-n-butylammonium fluoride

[TBDH]$^+$: 5,7-triazabicyclo[4.4.0]dec-5-enium

TEMPO: 2,2,6,6-tetramethylpiperidine-1-oxyradical

THF: Tetrahydrofuran

[TMGH]$^+$: 1,1,3,3-tetra-methylguanidinium

TMU: 1,1,3,3-tetramethylurea

VSM: Vibrating-sample Magnetometer

1. Introduction

Three main topics tie together to form the main emphasis of this thesis: cellulose, ionic liquids, and particles. These are examined from the perspective of an organic materials chemist, focusing on the dissolution of cellulose in ionic liquids and the preparation of cellulose particles from said solutions. The literature review portion is divided into three main themes: properties of cellulose, cellulose solvents and polymeric particles. The topics considered within these themes are aimed at providing the reader with a solid grasp of the current state of scientific knowledge on the matter and affording answers to key findings and observations gathered in the experimental laboratory works carried out during the course of this thesis. The experimental laboratory portion of this thesis is divided into two independent units. The first unit explores the capacity and potential of preparing millimetre scale cellulose macroparticles by dissolution and regeneration of cellulose from organic electrolyte [DBNH][OAc]/DMSO. The second unit studies a thermoresponsive phase separation phenomenon observed with cellulose dissolved in $[P_{4441}][OAc]$/GVL and the properties of cellulose microparticles resulting from said phenomenon.

1.1. Cellulose as a material

Cellulose as the most abundant biopolymer on earth, with an annual biological production of $1,5 \cdot 10^{12}$ tonnes, forms a promising platform for the development of novel value-added products with sustainable goals.[1] The repeating unit of cellulose is β-D-glucopyranose,[2] which's multiple hydroxyl functionalities create the basis of the polymer's chemical reactivity. The degree of polymerization in cellulose is usually high, especially when it is derived from natural sources. This makes behaviour of cellulose as a material highly dependent on the physicochemical properties of large polymer aggregates. However, unlike many man made polymers, it still retains a high capacity and sensitivity for a range of chemical reactions.[1] These initial chemical reactions are oftentimes vital for the efficiency of subsequent follow-up modifications,[3] as unmodified cellulose is notoriously difficult to dissolve and hence to modify in a controlled manner.[4]

Materials incorporating cellulose in its chemically unmodified form have been utilised by humans for many thousands of years; the applications ranging from timber to straw-mattresses to hemp fibre. More derived forms of chemically unmodified cellulose were employed in the making of papyrus and later still paper, which enabled efficient transfer of information between generations and communities. This efficient transfer of written knowledge has accelerated the cultural evolution of major civilizations already since the Egyptian times. Presently the bulk of processed cellulose is refined from wood or cotton and the majority of it still goes towards the production of relatively simple materials such as paper, plywood and cotton fibres.

The next steps in the history of derivatisation of cellulose-based materials were regeneration and chemical modification. Early forms of chemically modified cellulose materials include the nitrocelluloses such as celluloid,[5] which is a thermoplastic nitrocellulose plasticised with camphor used in early photography, and guncotton,[6] which is a nitrocellulose used in smokeless gunpowder. Viscose,[7] which is regenerated cellulose xanthate, cupro silk and cuprophane,[8] which are regenerated in the cuprammonium process, and more recently Tencel,[9] know at the time of its development as Newcell, represent cellulose derivates designed for use as fibres. Especially Tencel, a regenerated cellulose fibre produced in the Lyocell process by dissolving bleached wood pulp in N-methylmorpholine N-oxide (NMMO), portrays aspects of efficient utilisation of cellulose in novel ways.

Presently, a variety of derived cellulose materials are being produced in many forms and functions such as fibres, films, coatings, membranes, wrappings, gels, absorbents, sponges, fillers, thickeners, stabilizers, matrix material in food and medicines, basis and carriers for drugs as well as abraders, opacifiers and moisturizers in cosmetics. This wide range of applications demonstrates the great versatility of cellulose and the remarkable interest the scientific community has shown towards the development of cellulose-based materials. Furthermore, the need to design new and innovative solutions to pressing issues brought forth by the growing global population, continued urbanisation and increasing awareness of environmental concerns emanating from said developments, creates substantial incentives for the invention of even more cellulose-derived materials. Especially the demand for new environmentally friendly fibrous, membranous and particulate materials, designed to replace their conventional plastic counterparts in consumer and industrial applications, has gained considerable attention in the public eye. This demand for novel approaches, alongside the

natural curiosity of the author, have been the driving forces that have ultimately led to the discovery of several new and intriguing materials relevant to the field of cellulose materials chemistry.

1.1.1. Cellulose in biomass and its extraction

By far the most prevalent source of cellulose used in the research and industrial sectors is plant matter, with for example cotton presenting an almost pure form of cellulose in its seed hairs. On the other hand, trees are the most voluminous and abundant cellulose containing biomass on the planet. Wood is composed of several polymeric and molecular compounds with cellulose, hemicellulose and lignin being the polymeric compounds constructing the bulk of the wood cell wall. Cellulose and hemicellulose are carbohydrate polymers, while lignin is an aromatic polymer.

Out of these compounds, cellulose, with its structurally homogenous and simple long linear chains, forms the most desirable platform for many chemical and material applications. The mainstream extraction method for separating cellulose from the rest of the cell wall material is called pulping. In pulping cellulose is isolated by breaking the lignin matrix, which acts as an adhesive holding the cellulose fibres together. Pulping can be achieved using a variety of methods and from a variety of cellulose sources with the most common ones being mechanical, thermomechanical and chemithermomechanical pulping from wood and chemical pulping from wood or recycled paper.[10] The most commonly used pulping process is the Kraft process, in which NaOH and hydrogen sulphide are utilised in the breakdown of the lignin network.[11] Because pure mechanical pulping damages the cellulose fibres considerably, steam (thermomechanical) and chemical additives (chemithermomechanical) can be used to supplement the pulping process to yield better-preserved fibres. However, these hybrid methods differ from pure chemical pulping in the sense that the role of the steam and chemicals is not to break up the lignin network, but to make it easier for the mechanical grinder to produce the pulp. It is quite common that the pulp is bleached after the pulping process using an oxidizing agent such as oxygen, ozone and hydrogen peroxide,[12] and this bleaching process can be catalysed with various metal complexes.[13]

Plant-based biomass is also frequently used in the biofuels industry, with one of the more notable applications being the fermentation of cellulose and other carbohydrates to ethanol and methanol.[10] The obvious downsides of using petroleum-based materials are the carbon positive effect on the atmosphere, the finite quantity of raw materials available in the future and the

possible plastic pollution afflicted on the environment. Hence, the possibility of producing fuel from non-petroleum-based sources has gathered wide-scale interest from the industrial and research communities. At present, the biofuels industry is using primarily non-wood-based biomass, such as sugar cane, as the fermentation base due to their cost efficient fermentation.[14] Despite the obvious environmental benefits of using bioethanol and biomethanol instead of fossil fuels, the source of the polysaccharide raw material plays an important role in determining the true environmental viability of using biomass for fuel purposes. The use of food grade biomass such as barley, sugar cane or maize for the production of biofuels raises ethical questions about the use of arable land for fuel purposes, rather than for food. This issue is made especially problematic when the shortage of food in third world countries is becoming an ever-increasing problem and the global population is estimated to rise considerably in the future.[15] Therefore, the role of ethically and environmentally sustainable cellulosic materials for the production of biofuels will surely grow in importance, when the availability and feasibility of fossil fuels will begin to dwindle in the upcoming decades.

1.2. Structural characteristics of cellulose

1.2.1. General structure and properties

Cellulose polymer is composed of a repetition of β-D-glucopyranose rings bridged with acetal groups, which are formed from the hydroxyl group O4 of the C4 carbon of one ring and the hydroxyl 05 of the C5 carbon of the other ring (**Figure 1. A**). This bond is designated as a β-1,4-glycosidic bond. Notice that the oxygen bridging the two β-D-glucopyranose rings is always O4 and not O1. This is a result of a condensation reaction that originally assembled the polymer, the O1 oxygen of glucose having been cleaved off as water during the acetal formation. Due to the bond angle preference of the acetal oxygen, every other AGU unit is rotated 180° along the axis of the cellulose backbone, which gives rise to an extended linear geometry differing from the helical structure observed in starch, another common glucopyranose-based biopolymer.[16] The two oppositely oriented AGU units make up a disaccharide unit known as cellobiose, which can be considered the repeating unit of cellulose (**Figure 1. B**).[1] However, there has been recent discussion that the use of the cellobiose as the repeating unit of cellulose brings confusion and unwarranted limitation to the visualisation and understanding of the shape and structure of cellulose. Hence, A. French[2] suggests that the repeating unit in cellulose should be preferably called β-D-glucopyranose, better known as glucose.
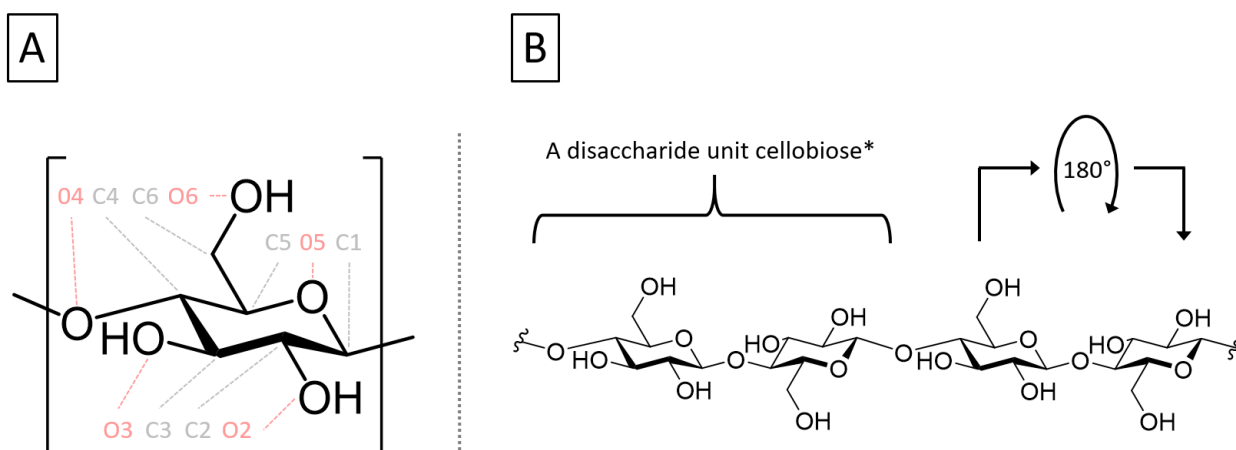
Figure 1. A: The chemical structure of cellulose and the numbering system used to designate the various carbon and oxygen atoms present in the structure. Note that the bridging oxygen is always O4 and not O1. **B:** The repeating unit of cellulose is a disaccharide composed of two β-D-glucopyranose monomers oriented in a 180° angle relative to each other along the linear axis of the polymer. *This disaccharide is referred to as cellobiose and has been traditionally considered to be the repeating unit of cellulose. However, some authors disagree with this notation and would preferentially use β-D-glucopyranose as the repeating unit.[2]

This approach would also comply with the naming conventions of IUPAC and IUBMB (International Union of Biochemistry and Molecular Biology).

In colloquial terms, cellulose is commonly used to refer to the main constituent of most plants, especially trees. More precisely, cellulose refers to the polymeric material that is responsible for the fibrous character portrayed by any plant material. These fibres in the cell wall give the plant structural support and enable some species such as the Coast Redwood *Sequoia sempervirens* to grow to remarkable heights of over 110 m.[17, 18] A plant cell can be divided into to four major structural components: cell interior, secondary cell wall, primary cell wall and middle lamella or cell exterior. The cell interior is filled with fluid (protoplasm) and contains the all of the cell organelles, whereas the secondary and primary cell walls as well as the middle lamella are composed of solid polymeric material that gives the cell structural support. The structural hierarchy of cellulose in a cell wall of a plant originates from the smallest individual component, a single cellulose chain (**Figure 2**). Individual cellulose chains come together to form elementary fibrils, which further combine to form micro fibrils. These micro fibrils are then bundled together into macrofibrils, which are the primary structural motif of the plant cell wall. An elementary fibril has a roughly square cross section and a diameter of ca. 5 nm, while microfibrils usually have diameters of ca. 20 nm, albeit this can vary depending on the plant species and the life history of the individual.[19] The cellulose fibrils are much longer than they are wide, hence their aspect ratio can be as high as several hundred (length divided width). Most reports of measured fibril lengths are in the range of hundreds of nanometres to several micrometres.[20] Hemicellulose, lignin and pectins act as an adhesive, binding together all of the cellulose fibres of the various hierarchical orders from elementary fibrils to macrofibrils. Cellulose and hemicellulose are predominantly found in the primary and secondary cell walls, whereas lignin and pectins are especially abundant in the middle lamella, where they plaster together the cell walls of adjacent cells.
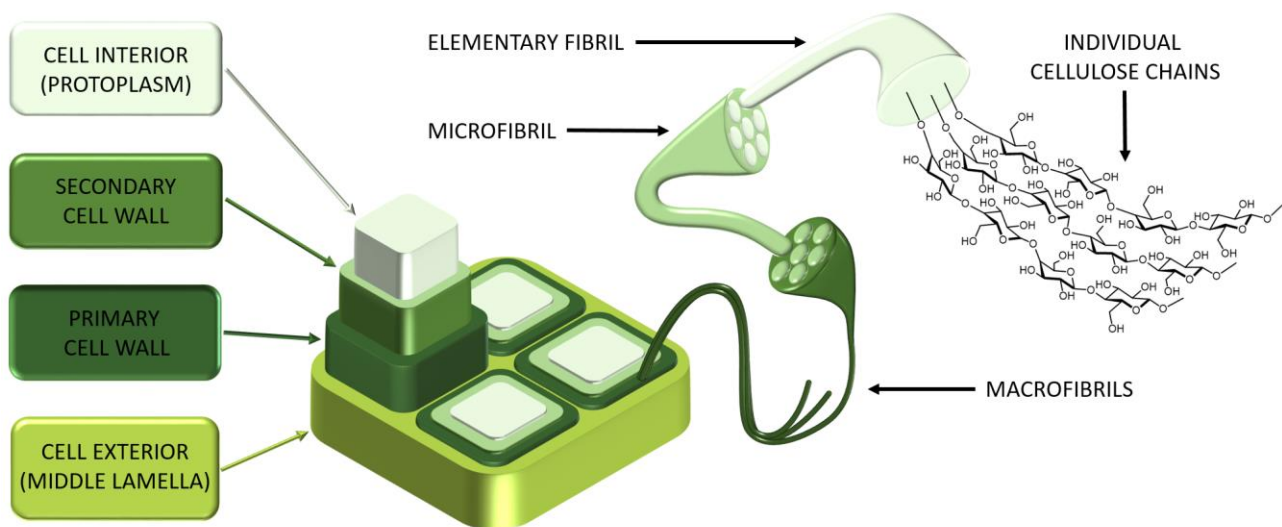
Figure 2. The primary division of structural components of a plant cell and the hierarchy of cellulose fibres in a plant cell wall. Hemicellulose, lignin and pectins act as an adhesive, binding together all of the cellulose fibres of the various hierarchical orders.

The length of a cellulose chain is an important property that defines many of the physical characteristics of a cellulose-based material. A short oligosaccharide can have vastly dissimilar physical and chemical properties compared to a long polysaccharide. The length of a cellulose chain can be expressed as the Degree of Polymerization (DP), which is equal to the number of repeating AnhydroGlucose Units (AGU) constituting the cellulose backbone. The DP of cellulose varies widely depending on the source material and the subsequent treatment of the fibres. Usually wood pulp has DP values between 300 and 1700, while plant fibres and bacterial cellulose has values between 800 and 10 000. There is a general trend, where the treatment of cellulose with a variety of chemicals and changing physical conditions reduces the DP of the resulting cellulose fibres, usually to between 250 and 500, but this is largely dependent on the DP of the starting material and employed treatment methods.[1]

A linear cellulose chain has two ends labelled as the reducing end and the non-reducing end. The reducing end terminates in the hydroxyl group of the C1 carbon, while the non-reducing end is capped off by the hydroxyl of the C4 carbon. Why the reducing end has come to be known by the name, is due to the tendency of the β-D-glucopyranose ring at the reducing end to adopt an open chain form. Unlike the closed hemiacetal forms making up the rest of the cellulose chain links, the open chain aldehyde can act as a reducing agent towards a variety of reagents. However, these two singular hydroxyls (reducing and non-reducing end) make up only a fraction of the total hydroxyl

functionalities of the cellulose chain, which's intra- and intermolecular hydrogen bond formation is dominated by the O2, O3 (secondary hydroxyls) and O6 hydroxyls (primary hydroxyl). The three hydroxyl groups are also the most chemically reactive functionalities of cellulose and can take part in a wide range of reactions characteristic to alcohols, with alkylation, acetylation and carboxymethylation being some of the most common ones.[3] These modified cellulose compounds, also known as cellulose derivatives, make up the vast majority of target molecules in the field of cellulose chemistry. Cellulose acetates are used in packaging and filtration applications and cellulose ethers such as methyl cellulose are used as thickeners in the food and materials industry. Carboxymethylcellulose (CMC) is used to adjust the rheological properties of a wide variety of products from foodstuff to wallpaper paste.[10]

1.2.2. Crystalline morphology

The most prominent intermolecular bond type expressed by cellulose is the hydrogen bond. These bonds form an extensive network, which determines the solubility, crystalline and amorphous morphology, solvent affinity and absorption of cellulose.[1] The understanding of the structure of cellulose hydrogen bond networks has been developing alongside structure-analysis methods such as X-ray diffraction, solid state NMR and electron microscopy. Cellulose is composed of crystalline and amorphous regions, a dichotomy which arises from the supramolecular structure of cellulose. Crystalline regions are composed of uniformly oriented bundles of cellulose chains and larger fibres, whereas amorphous regions are by definition non-crystalline and lack coherent orientation of the cellulose chains relative to each other. However, the structural morphology, as well as the distribution and distinction between crystalline and amorphous regions, in any one sample of cellulose is not as clear-cut as can be envisioned from this simplistic partition. Rather, the ambiguous nature of cellulose structural morphology is best expressed by what is called a Fringed Fibrillar - model (**Figure 3**).[21, 22, 23] In this model, amorphous cellulose forms numerous connections between crystallite bundles – the amorphous and crystalline regions are entwined in an intimate embrace. This makes the theoretical distinction between a crystalline and amorphous cellulose rather vague and their physical separation from each other very challenging.
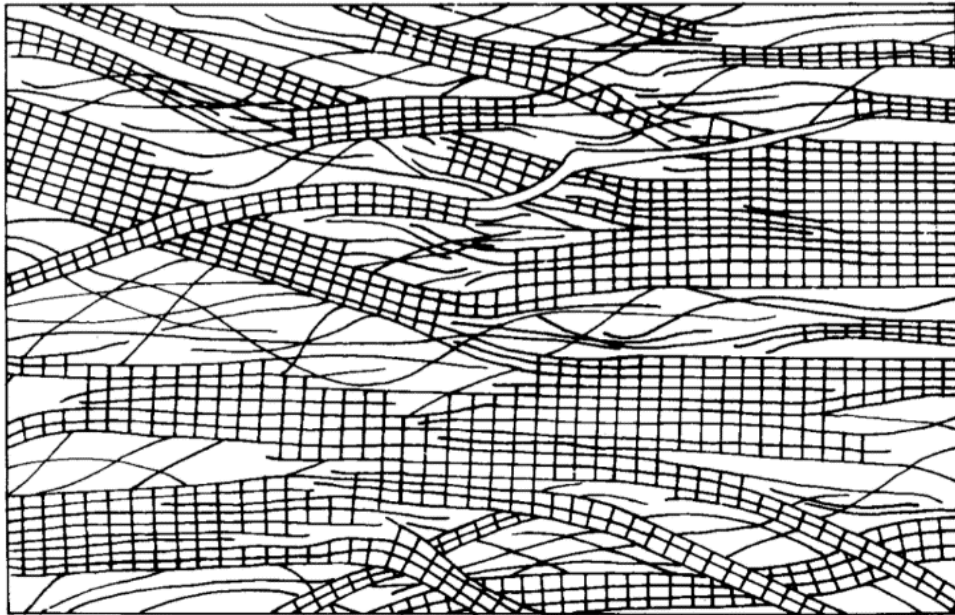
Figure 3. The Fringed Fibrillar -model of cellulose as presented by Fink et al.[26] The crystalline and amorphous regions are intimately connected. Figure reused with permission from "Fink, H. and Philipp, B., *J. Appl. Polym. Sci.* **30**(9) 1985 3779." Copyright 2003 John Wiley and Sons.

The fibres are the most crystalline as well as chemically and mechanically strongest parts of native cellulose. Highly crystalline cellulose material, in which the cellulose chains are very homogeneously oriented, is difficult to produce by conventional laboratory methods such as enzymatic treatment, polymerizing a monomer or dissolving and regenerating. If the cellulose producing system does not have the correct steering mechanism to arrange the forming cellulose polymer into an oriented crystalline structure, the resulting material will be more amorphous. These type of steering mechanisms are mostly found in biological systems such as plants and microbes but also in some man-made systems such as a fibre spinning process, where the crystallinity of formed cellulose is surprisingly high in these systems.[24] However, the presence of large amounts of completely crystalline or completely amorphous cellulose in any cellulosic material is very rare, in most cases a partly crystalline, partly amorphous configuration is observed.

The chemical reactivity of the two morphologies differ from each other as amorphous cellulose can be readily degraded in an acidic environment, leaving mostly just the crystalline regions intact. This property is utilised in the manufacture of microcrystalline cellulose (MCC, Avicel), which has DP values between 150 and 300.[25, 26] The fibrous and crystalline fractions of cellulose are concentrated when native cellulose is broken down in mechanical or chemical processing. This is a result of the less fibrous and more amorphous parts of native cellulose being the most accessible and chemically

labile towards hydrolysis, and hence end up being the sites where the cellulose matrix is most easily broken down. Nonetheless, crystalline cellulose is also degraded in the process and the degree of crystallinity of cellulose never reaches 100 %. This implies that either, not all of the amorphous cellulose is ever hydrolysed, or that new amorphous cellulose is constantly forming during the degradation process. Overall, the degradation process of cellulose in the scale of fibrils is still not well understood.

1.2.3. Cellulose I

Crystalline cellulose can be divided into several polymorphs. Cellulose I is the form of native cellulose, and in the crystal structure there are two cellulose chains running in parallel. Cellulose I can further be divided into Cellulose I_{α} and I_{β}, with both co-occurring in native cellulose.[27] Furthermore, the ratio of I_{α} to I_{β} has been shown to differ with different native cellulose sources. Cellulose derived from bacteria contain a larger portion of cellulose I_{α} compared to I_{β}, whereas cellulose from plants shows an opposite trend. Cellulose I_{β} has a space group $P2_1$ monoclinic unit cell containing two parallel chains, which form into sheets packed in a way described as "parallel up".[28] The two chains in I_{β} (named center and origin) have differing conformations for both the backbone of the chain and the glucose units. The glucose units in center chain are strained and the chains are offset axially close to a quarter of the length of a repeating unit relative to each other. On the other hand, Cellulose I_{α} has a space group P_1 triclinic unit cell containing only one cellulose chain, but also assembles into "parallel up" sheets. The chains in Cellulose I_{α} adopt a conformation resembling a twofold screw. The hydroxymethyl groups in Cellulose I_{β} and I_{α} are in a trans-gauche conformation and the chains within a sheet are held together by a network of hydrogen bonds. A representation of the hydrogen bonds present in origin and center chains of Cellulose I_{β} can be seen in **Figure 4.**[29] All of the hydroxyl groups and the acetal oxygens O4 and O5 take part in forming the intrachain cellulose backbone, while O2, O3 and O6 are also able to interact with multiple possible interchain hydrogen bonding partners. However, these hydrogen bond networks are mobile and enable a certain degree of rotational freedom in the hydroxyl groups, especially at O6 and O2. This coupled with the directionality of the free electron pairs of oxygen can lead to situations where there is no interchain hydrogen bonding present, such as is observable in the right portion of **Figure 4. A**. Unlike the chains within the sheet, stacks of "parallel up" sheets are held together only by

means of hydrophobic interactions and weak C-H⋯O bonds, there are no intersheet hydrogen bonds.
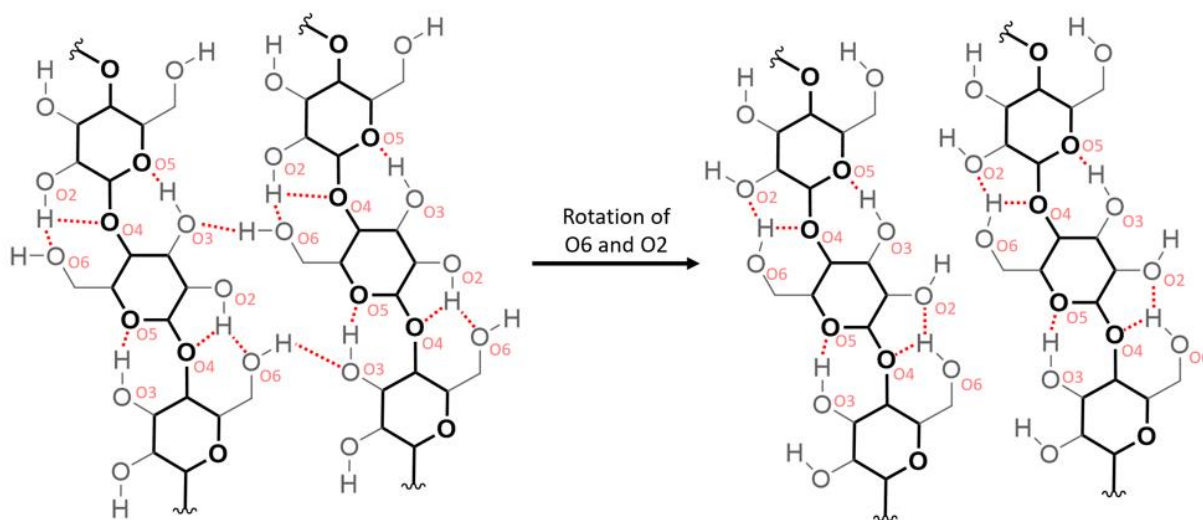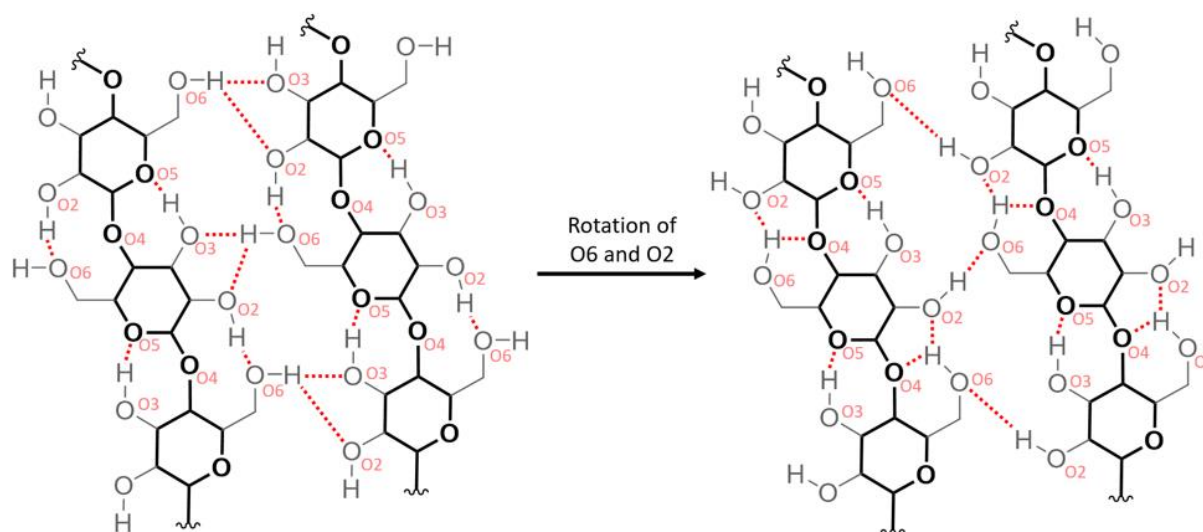
Figure 4. A representation of the intra- and intermolecular hydrogen bonds present in the "origin" and "center" chains of the crystalline structure of Cellulose I_β.[29] Red dashed lines represent hydrogen bonds. The hydrogen-bonding pattern can change as a result of the rotation of the hydroxyl groups O2 and O6. For the sake of clarity, atoms belonging to the cellulose backbone have been rendered in bold and only the oxygens partaking in hydrogen bonding have been labelled. Figure adapted with permission from "Nishiyama, Y., Langan, P. and Chanzy, H., *J. Am. Chem. Soc.* **124**(31) 2002 9074". Copyright 2002 American Chemical Society.

1.2.4. Cellulose II

Even though Cellulose I is the native form of cellulose, it is not as thermodynamically stable as Cellulose II. Cellulose II can be derived from Cellulose I by two general methods: mercerization or regeneration. In mercerization, Cellulose I is treated with an alkali solution, which ends up converting the structure into Cellulose II without properly dissolving or dispersing the cellulose chains. When Cellulose I is homogenously dissolved in a solvent, such as an ionic liquid, it will recrystallize to Cellulose II when introduced to an antisolvent.[28] This process of dissolving and precipitating cellulose is known as regeneration. Albeit, in both cases some of the cellulose will most certainly adopt an amorphous morphology as well. Similarly to Cellulose I, Cellulose II has a space group $P2_1$ monoclinic unit cell containing two chains, but in an antiparallel orientation (**Figure 5.**).[28, 30] Similarly, the two chains (origin and center) in Cellulose II have differing conformations for both the backbone of the chain and the glucose units. However, unlike in cellulose I, the hydroxymethyl groups in the center chain are disordered and occupy both trans-gauche and gauche-trans orientations. Cellulose II obtained through mercerization seems to show lower amounts of disorder in the orientation of the center chain hydroxymethyl groups (10 % *gauche-trans* to 90 % *trans-gauche*) compared to that obtained by regeneration (30 % *gauche-trans* to 70 % *trans-gauche*).[30] Both center and origin chains contain a prominent three component intrachain hydrogen bonding between O5 and O6

CELLULOSE II ANTIPARALLEL CHAINS (UP & DOWN)
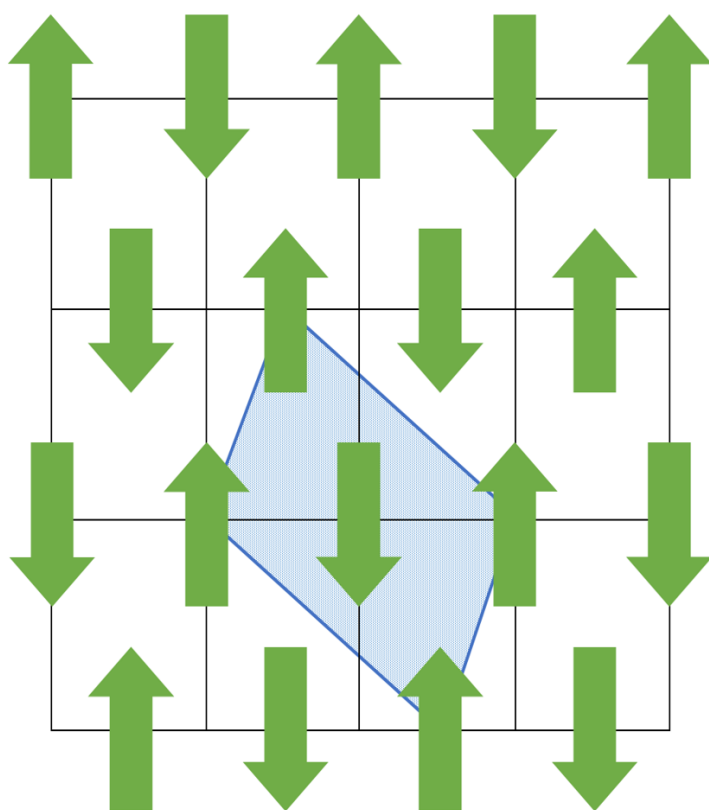
Figure 5. A schematic representation of the antiparallel orientation of the two cellulose chains (here upwards and downwards facing arrows) in the crystal structure of Cellulose II.[34] The nature of the chains (Origin or Center) is not specified. Blue rectangle represents the monoclinic unit cell in Cellulose II. Figure adapted with permission from "Wada, M., Heux, L., Nishiyama, Y. and Langan, P. *Biomacromolecules* **10**(2) 2009 302." Copyright 2008 American Chemical Society.

as acceptors and 03 as a donor, forming a bifurcated bond system with the 05-H···O3 bond acting as the main component. Due to the different orientation between the chains, the O6 of the origin chain is capable of acting as a interchain hydrogen bond donor to three possible acceptors of the center chain (O5, O6 and O3), all of which are linked by their intrachain three body bond system. For visualisation of the intrachain hydrogen bonding see **Figure 4**.

1.2.5. Cellulose III and IV

Cellulose III, like cellulose I, can also be divided into two morphologies: Cellulose III_I and III_{II}. Cellulose III can be prepared from either Cellulose I or II by treating it with liquid ammonia, the subscript depicting the original morphology of the pre-treatment cellulose.[31] Cellulose III_I has a space group $P2_1$ monoclinic unit cell containing a single chain. The chains in the crystal structure of III_I are running parallel and the hydroxymethyl groups occupy *gauche-trans* orientations.[32] X-ray crystallographic studies imply that Cellulose III_{II} has a space group $P2_1$ monoclinic unit cell, which is made up of one chain that is the average of statistically disordered antiparallel chains. However, X-ray crystallographic and ^{13}C CP/MAS NMR data together suggest that this average is composed of three different molecular conformations. Overall, the crystalline structure of Cellulose III_{II} has been the subject of very few studies.

Cellulose IV has been cited in the literature as an allomorph of cellulose derived from Cellulose III_I or III_{II} , which in turn were derived from Cellulose I (resulting in Cellulose IV_I) or Cellulose II (resulting in Cellulose IV_{II}). [33] This conversion from Cellulose III to IV can be obtained by thermal treatment. However, Cellulose IV_I has been confirmed not to be a true polymorph of cellulose, but consisting of Cellulose I_β fragmented into nanocrystals with relatively small cross-sectional dimensions.[33]

1.2.6. X-Ray measurements of cellulose morphology

X-Ray diffraction techniques (XRD), such as Wide Angle X-ray Scattering (WAXS) and Small Angle X-ray Scattering (SAXS), can be used to study the morphology and crystallinity of cellulose. Especially WAXS is useful in determining the proportion of crystalline regions relative to the amorphous regions (i.e. Crystallinity Index, CI) and the morphology (I, II, III, IV) of the cellulose crystallites.[34, 35] Each of the cellulosic morphologies present in this thesis (Cellulose I, Cellulose II and amorphous

cellulose) have their characteristic signals in the WAXS-diffractogram.[24] However, the amorphous peaks are very broad and not very pronounced. Hence, it can be practical to consider the contribution of amorphous regions to the combined signal of all cellulose morphological regions in a WAXS-diffractogram as a background of sorts for any cellulose sample. In fact, several methods of CI determination are based on the subtraction of this amorphous background from the complete diffractogram. The contribution of different cellulose crystalline morphologies (I, II, amorphous) to the total signal, and therefore also to the degree of crystallinity of the cellulosic material, can be determined by way of a computational deconvolution method (see experimental section **4.1.7. X-Ray Diffraction (XRD) measurements for determining Crystallinity Index (CI)**). In this method, the WAXS-diffractogram of a cellulose sample is compared to a fully amorphous standard, and the portion of amorphous signal contributing to the total area of the WAXS-diffractogram is calculated. In this case, the Crystallinity Index is the ratio of the area of crystalline contribution to that of the total area.

Another common method, the Ruland/Vonk method, was used to measure the degree of crystallinity of fibres derived from the IONCELL-F fibre spinning process, the products of which resemble the materials produced in this thesis to a high degree.[24] The Ruland/Vonk method is based on the subtraction of a fully amorphous standard spectrum from the sample spectrum, which is done by adjusting and scaling the amorphous spectrum so that it barely parallels the bottom of the sample spectrum.[36] Hence, the resulting spectrum should only be composed of the crystalline contribution to the original spectrum and, if the scaling and adjusting were done correctly, no portion of it should display a negative signal.

2. Cellulose solvents and dissolution of cellulose

2.1. Cellulose solvents

2.1.1. Cellulose solvents and their development

In general, cellulose solvents can be divided into two sub-classes based on their mode of dissolution: derivatizing solvents and non-derivatizing solvents, also known as direct solvents. Derivatizing solvents react with the cellulose polymer to form a derivate, which is then dissolved by the solvent systems, whereas direct solvents can dissolve cellulose without modifying it chemically. Most of the early and commercially successful processes, such as the viscose process, utilise derivatizing solvents. The solvents can be further divided, independently of their status as a direct or derivatizing cellulose solvent, based on their ionic constitution resulting in three classes: ionic solvents (ionic liquids), neutral solvents and mixed solvents (electrolytes). Electrolytes are comprised of a mixture of ionic and neutral species. Electrolytes can be further classified into aqueous and non-aqueous systems.[10] The cellulose solvent systems studied in this thesis, [DBNH][OAc]/DMSO and [P$_{4441}$][OAc]/GVL, are direct cellulose solvents composed of ionic and neutral components, i.e. electrolytes. They are also sometimes called organic electrolyte solutions.[10]

Dissolving cellulose has been a subject of great interest during the past century and a plethora of solvent systems have been studied for their cellulose dissolving capabilities. The solvents studied have been chemically very diverse, including solvent systems based on mineral acids, aqueous inorganic bases (NaOH, LiOH), transition metal amine complexes (cuam, cuen), inorganic salt hydrates (LiClO$_4$·3H$_2$O), combinations of inorganic salts and organic solvents (LiCl/DMA and DMF/N$_2$O$_4$), as well as organic salt hydrates (NMMO·H$_2$O, **Figure 6. A**). Despite their ability to dissolve and process cellulosic material, most of these aforementioned solvent systems have their limitations including harsh reaction conditions, acutely or environmentally harmful ingredients, thermal or chemical instability, high viscosity and recyclability issues. These limitations have led to the continued search for better cellulose solvating systems, such as ionic liquids, which have gathered a great deal of attention from the research community during the past two decades.
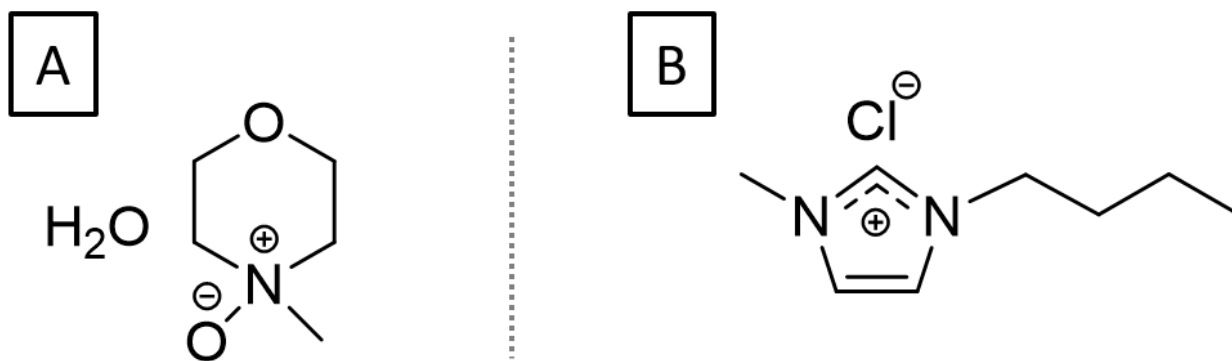
Figure 6. The chemical structure of two direct cellulose dissolving systems, **A:** NMMO·H_2O and **B:** 1-butyl-3-methylimidazolium chloride, [bmim]Cl.

The earliest observation of homogenous cellulose dissolution in what could be described as an ionic liquid dates back to 1934, when Graenacher demonstrated in his patent that alkyl pyridinium chlorides are able to dissolve cellulose.[37] However, the pyridinium salts had high melting points (>100° C) and thus were not particularly useful in the practical sense. Other cellulose solvent systems based on organic compounds were discovered later during the 20th century with the Lyocell process, utilising NMMO·H_2O as the cellulose solvent, being the most successful commercially. Regardless of their superior qualities compared to the early pyridinium salts, the new solvents still possessed high melting points and NMMO additionally had a tendency for violent run away reactions.[38] The dissolution of high molecular weight polymer compounds, such as cellulose, was brought to the spotlight of research interest again, when Swalotski *et al.*[4] published their findings on ionic liquids in 2002. The focal point of the subsequent burst of research activity was on the study of imidazolium-based ILs, which were shown to be able to dissolve cellulose in a much safer and more controllable way than prior direct cellulose solvents like NMMO.[24] The most effective of the new generation of ionic liquids was probably 1-butyl-3-methylimidazolium chloride ([bmim]Cl, **Figure 6. B**), which, in contrast to earlier solvents, had a melting point below 100° C. However, the early imidazolium ILs also had downsides, such as some solvents not being totally inert towards cellulose. For example, certain substituents of the imidazole ring caused severe cellulose degradation at elevated temperatures (90° C).[39] In addition, the corrosive nature of the commonly used halide anions on steel containers[40] and the loss of dissolving power due to extreme sensitivity to the presence of moisture[41] presented additional difficulties for the efficient utilisation of imidazolium-ILs in cellulose processing.

The next iteration of ionic liquids were the Room Temperature Ionic Liquids (RTILs). As their name suggests, RTILs have melting points below or near room temperature and additionally have relatively low viscosities. The lowered viscosity allows for lower processing temperatures and decreases the thermal degradation of cellulose. A prime example of an RTIL is [emim][OAc], which is a highly efficient and fast cellulose solvent.[42] Despite its superior dissolving capabilities and lower viscosity compared to earlier types of ILs, [emim][OAc] also has increased chemical reactivity towards cellulose at elevated temperatures, leading to solvent degradation and formation of unwanted cellulose derived contaminants.[43] These shortcomings have given rise to the need to develop even more IL-families with ever-superior cellulose dissolving properties. As recent examples, the superbase and phosphonium ionic liquid families, and more precisely two individual solvents ([DBNH][OAc] and [P_{4441}][OAc]), are the subject of investigation in this thesis.

2.1.2. Ionic liquids

Ionic liquids (ILs) are a group of ionic compounds composed of an anion and a cation, which together form an organic salt.[10] Most commonly the cation is an organic compound, while the anion can be organic or inorganic. What sets ILs apart from the majority of ionic compounds is their generally low melting points. The earliest example, of what could be considered an IL, is reported as early as 1914, when Walden described ethyl ammonium nitrate.[44] The term "molten salts" was traditionally used to describe "ionic liquids" that were composed of inorganic salts with high melting points. Presently, an ionic liquid is commonly defined as an organic salt with a melting point below 100° C.[45] Within the assemblage of ILs is embedded a subgroup called the Room Temperature Ionic Liquids (RTILs), which are liquid at RT.[46] However, studies in the field of low melting ILs have progressed much during the past two decades, and the nomenclature as well as definitions are in a state of constant refinement. For this reason, a general definition for Ionic liquids that least disagrees with the various definitions set for the group of compounds would go along the lines of "Ionic Liquid is an organic salt with a low melting point". Albeit this definition is vague, it contains the most important characteristics of ILs, their ionic nature and low melting point.

Ionic liquids can be organized into families based on the cation used to form the ion pair. A typical example of a family of ionic liquids, which has seen a great number of studies during the past two decades, is the imidazolium-based ILs. In these ILs, the imidazolium cation can be paired with a great

number of different anions such as halides, phosphonates, phosphates and carboxylates. Other examples, of how ionic liquids have been classified into families, are the phosphonium-, onium- (umbrella term for both phosphonium and ammonium) and superbase-families (**Figure 7.**).[10] This flexibility of combining different cations with anions has made it possible to tailor ionic liquids for specific applications, giving ionic liquids a designation of "designer solvents". To take the scope of design possibilities even further, ILs can also be composed of more than two ionic components as well as a non-ionic co-solvent, to fine-tune the physicochemical attributes of the solvent system.[47]
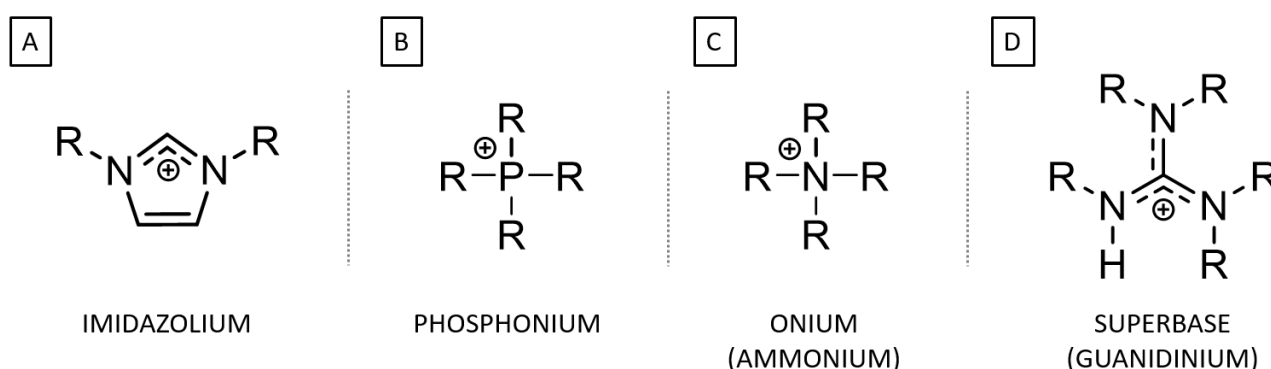
Figure 7. Examples of cations, based on which ionic liquids are classified into families such as the Imidazolium-, Phosphonium-, Onium- and Superbase-families. An ammonium cation is given as an example of the Onium IL-family, which is an umbrella term withholding both ammonium and phosphonium ILs. Guanidinium cation is given as an example of the Superbase IL-family. The R-substituent in the structures can be one of a vast number of possible substituents, but alkyl, ether and ester functionalities are most commonly used.

Ionic liquids are quite frequently described as being "green" due to their low vapour pressure. The greenness is implied to derive from the fact that ILs lose very little solvent due to evaporation at normal operating conditions compared to traditional organic solvents. This in turn is proposed to be good for recycling of the liquids. On the other hand, presently the recycling of ILs in semi-industrial to industrial scale can pretty much be considered a necessity, as it is a crucial that the markedly expensive ILs are recycled for the total process to remain economically feasible. Even when they are recycled, the loss of IL due to side reactions, hydrolysis and degradation[39] can prove to be very expensive due to the high price of the solvent. For example, DBN (1,5-Diazabicyclo[4.3.0]non-5-ene), the starting material for the superbase-IL [DBNH][OAc], costs hundreds of euros per kilogram.[48, 49] Even in a perfect system where all the IL could be recycled, getting rid of the commonly used antisolvent H_2O is possible only by distillation. This distillation process is energy intensive and has limited economical feasibility in the industrial scale – more efficient alternative

purification methods are much sought after by businesses wishing to capitalise on the novel properties of various ILs. Additionally, there is very limited experimental data on the environmental impact of ILs. In light of the body of knowledge collected during the 20th century on the bioaccumulation of synthetic compounds in the food web, the possible acutely or chronically toxic nature and the potentially lacklustre biodegradability of ILs raise significant concern about their wide-scale application in the industry.[50] Hence, the economic feasibility of IL recycling and the possible ramifications of the use of toxic ionic liquids must be properly weighed before ionic liquids can be declared truly "green".

Two ionic liquids are the main emphasis of this thesis: [DBNH][OAc] and [P$_{4441}$][OAc]. While these particular ILs were not chosen for study on this basis, both of their respective IL families have examples that exhibit characteristics making them inherently better candidates for a recyclable biomass-processing solvent than the majority of ILs. [DBNH][OAc], apart from being a Superbase-IL (SIL), can also be classified as a Distillable Ionic Liquid (DIL, see sections **2.1.5. Superbase Ionic Liquids** and **2.1.6. Distillable Ionic Liquids**).[51] Briefly, it itself can be distilled to get rid of solid or high molecular mass contaminants, such as cellulose and other biomacromolecules. Phosphonium ILs, such as [P$_{8881}$][OAc], show interesting phase-separation behaviour, where the hydrophobic IL component can be phase separated from an antisolvent (such as water). This makes these ILs representative of the group of phase-separable ionic liquids (PSIL, see section **2.1.4. Phase-Separable Ionic Liquids**).[52] [P$_{4441}$][OAc], while itself not expressing the same phase behaviour without the addition of a kosmotropic salt, is part of the same family of phosphonium ILs and hence can provide valuable insights about the interaction of the family of ILs with cellulose, which can then be applied further in future studies.

2.1.3. Phosphonium ionic liquids

The phosphonium-based ionic liquids are a family of ILs with high thermal stability and, when coupled with a co-solvent, a high dissolution capacity towards cellulose. The phosphonium cation is centered around a sp[3]-hybridized phosphorus atom with four carbon substituents, with straight or cyclic alkyl and alkyl esters being some of the most common substituents.[45, 53] Two examples of tetra-alkyl phosphonium ILs are pictured in **Figure 8.** ([P$_{4441}$][OAc] and [P$_{8881}$][OAc]). The absence of even moderately acidic protons on the cation affords them increased resilience to chemical degradation, making them more stable in basic and nucleophilic environments. Additionally, the density of phosphonium ILs is lower than that of water.[45]
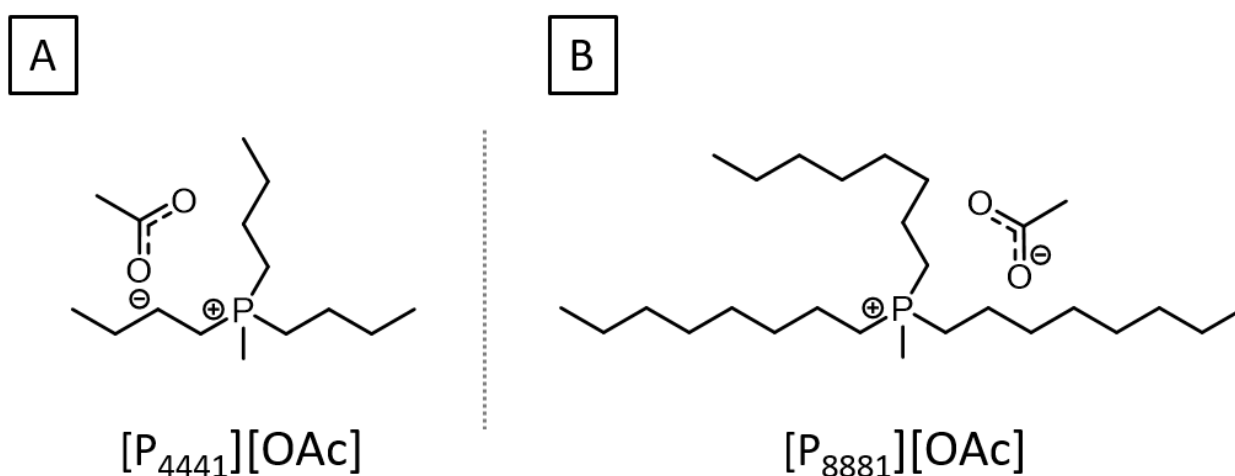
Figure 8. The chemical structure of [P$_{4441}$][OAc] (**A**) and [P$_{8881}$][OAc] (**B**), two phosphonium ILs.

McNulty *et al.*[53] documented some of the successful applications of phosphonium ILs, over their nitrogen-based counterparts, as solvents as well as catalysts. These applications included palladium-catalysed reactions such as Heck and Suzuki, rhodium-catalysed hydroformulations, Grignard reaction, zinc-based additions as well as the Diels-Alder reaction. Based on these applications and on their own observations, the authors suggested that the phosphonium cations acts as a mild Lewis acids, especially activating the carbonyl group towards nucleophilic addition in several reactions. This difference in reactivity, in comparison to nitrogen based ILs, was proposed to be due to the ability of the phosphorus atom to adopt pentacoordinate structures.

Pure tetra-alkylphosphonium ILs have only shown the ability to dissolve lignin but not cellulose.[10] However, with the addition of a polar aprotic co-solvent such as γ-valerolactone (GVL) or dimethyl sulfoxide (DMSO), the electrolyte mixture attains a high capacity for cellulose dissolution. In fact, these ionic liquids can dissolve cellulose in very high molar concentrations, with up to 1:1 ratio of

anhydroglucose units (AGU) to electrolyte pair possible. Long-chained phosphonium ionic liquids are able to dissolve cellulose at room temperature, but short-chained ILs can only do so at elevated temperatures. Holding[10] observed that the dissolution capacity of cellulose in $[P_{8881}][OAc]$/DMSO is at its maximum at IL/co-solvent weight ratio of 40 %. At this constitution of the IL and at maximum cellulose load, the AGU:IL molar ratio is above 1, meaning that there is less than 0,33 moles of ionic liquid per hydroxyl moiety in cellulose. This result is surprising when considering prior literature, where a minimum of one mole of IL per hydroxyl group was determined at maximum dissolution capacity of various ILs.[54] Cellulose solutions of certain phosphonium ILs and their electrolyte mixtures, such as $[P_{4441}][OAc]$/GVL, exhibit intriguing thermoresponsive properties, which resemble those observed in polymers having UCST-type phase behaviour (see sections **2.2.3. Thermoresponsive phase behaviour in cellulose solutions** and **2.4. $[P_{4441}][OAc]$ in cellulose processing**). This behaviour manifest as formation of microparticles when a mixture of cellulose and IL/co-solvent is heated to 120° C to dissolve cellulose, and subsequently cooled down to RT or below. However, further unpublished results seem to point to an antisolvent (impurity) driven process as the driver of the particle formation.

2.1.4. Phase-Separable Ionic Liquids

Some phosphonium ILs, such as $[P_{8881}][OAc]$, show interesting phase-behaviour, where the hydrophobic IL component can be phase-separated from antisolvent water, which makes them representative of the group of phase-separable ionic liquids (PSIL).[52] In an experiment by Holding,[10] cellulose was dissolved in $[P_{8888}][OAc]$/DMSO, regenerated in bulk with H_2O, and finally the IL was phase separated from water. The final recovery yield of IL was 97 %, but initially 30 % of it was adhered to the cellulose mass and needed separate ethanol washing procedures to recover. This disadvantage could potentially be remedied by precipitating the cellulose not as a bulk mass, but as an elongated fibre, similar to what is done in a fibre-spinning process such as IONCELL-F.[24] Even if the fibres produced would not possess great mechanical properties, the IL would much more readily diffuse out of the precipitated cellulose material. Compared to a bulk mass, the resulting cellulose fibres would be easier to wash afterwards. Holding also noted the formation of an emulsion, the presence of which is somewhat problematic for the phase separation process. However, this emulsion forming behaviour could also prove useful later on, if it were to be utilized in the preparation of cellulose micro- or nanoparticles. Holding also found that the phosphonium

based IL, in this and other studies, could uptake as much as 10 wt-% H_2O into the hydrophobic IL phase. This is problematic, as the water needs to be removed separately during the recycling process.[10]

2.1.5. Superbase Ionic Liquids

Superbase Ionic liquids (SILs), which are based on a superbase conjugate acid cation and are classified as a subgroup of protic ionic liquids (PILs), are an effective tool for dissolution and chemical modification of range of compounds.[55] As the name suggest, the cationic part of the IL, the superbase conjugate acid, is derived from a range of highly basic organic compounds known as superbases. A superbase has been defined as a compound more basic than 1,8-bis-(dimethylamino)naphthalene (DMAN), meaning that it has an absolute proton affinity higher than 245,3 kcal·mol^{-1} and gas-phase basicity of higher than 239 kcal·mol^{-1}.[56] For the purpose of cellulose dissolution, the limit of a superbase is found at a closely matching value of ca. 240 kcal·mol^{-1} (proton affinity), with values lower than that not being suitable for dissolving cellulose.[57] Some of the more common cations used in SILs include those based on derivates of the guanidinium cation, which can be acyclic ([TMGH]$^+$) or bicyclic ([TBDH]$^+$), and those based on cyclic ([DMPH]$^+$) and bicyclic derivates of the amidinium cation ([DBNH]$^+$ and [DBUH]$^+$, see list of abbreviations for full names of the cations). Two groups of superbases, guanidine and amidine derivatives, as well as their conjugate acid cations are shown in **Figure 9.**

Figure 9. The common structure of the guanidine (**A**) and amidine (**B**) superbases and some of the conjugate acid cations used in the composition of SILs.
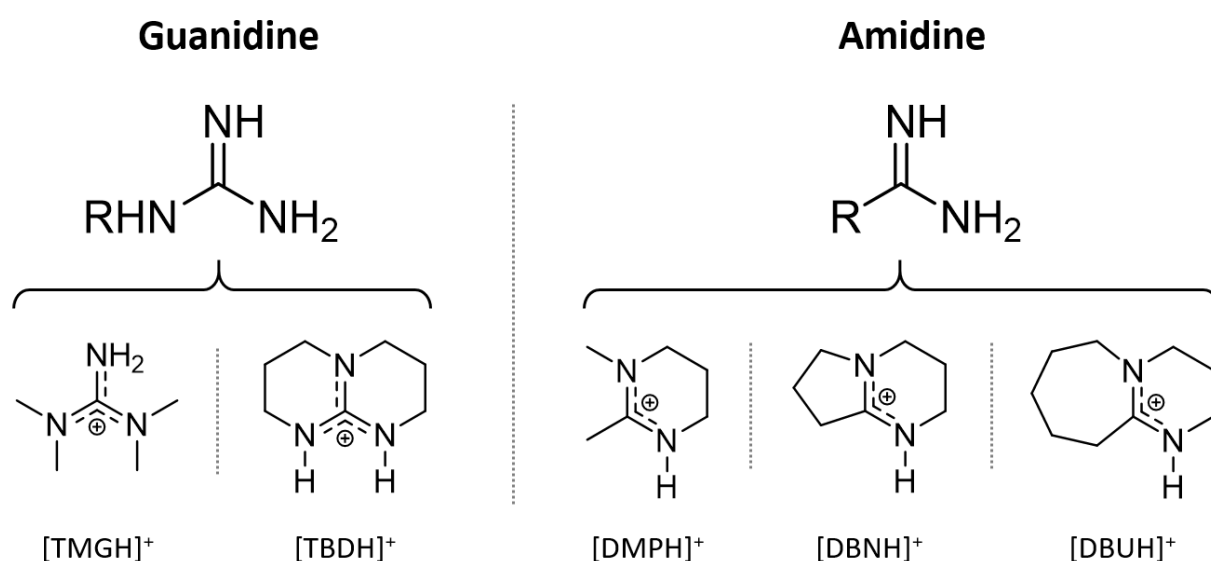
In iminoamines, the presence of two nitrogen atoms in β-position from each other, i.e. the N=C-N - motif, is the source of the high basicity of the compound prior to protonation, and is the defining feature of all the superbase cations listed in **Figure 9**.[58] The high basicity arises from the stability of the conjugated system of the protonated compound. In the case of the guanidine derivates (TMG and TBD), the additional nitrogen atom, again in β-position, makes the bases even stronger than their amidine counterparts due to the increased number of isoelectric forms.[56] In general, the more extensive the cation's conjugated π-network is, the more stable the cation is and hence, the more basic the unprotonated form is. However, the introduction of electron-deficient π-system containing substituents onto the nitrogen atoms lowers the basicity of the compound.[56] The protonation of a superbase occurs on the imine nitrogen, and hence the substitution of said nitrogen has the greatest effect on the basicity of the compound. With alkyl substituted amidines, it was noted that the addition of a larger and more electron donating alkyl group on the imine nitrogen resulted in the most basic compounds, with 1-adamantyl substituent having been estimated to contribute ca. 8,4 kcal·mol^{-1} to the basicity of the superbase.[59] An additional group of superbases, called phosphazenes, have an even greater basicity compared to the other two groups. They have also seen limited usage in ILs, but are not discussed further in the extent of this thesis.[60, 61, 62]

The anion of the SIL can be chosen from a range of common ions, with phosphates[55] and especially carboxylates seeing use in studies cellulose solvents.[57, 63] In the most simple case, such as is the synthesis of [DBNH][OAc], the superbase IL can be synthesised by allowing the superbase (DBN) to deprotonate an organic acid (AcOH), producing the SIL in the process. As with many ILs, the division of the solvent into two independent chemical moieties affords a great deal of customisation of the solvent system by changing the nature of the anion and cation independently. Especially the optimisation of viscosity, melting point as well as thermal and hydrolytic stability are decisive in designing an efficient and successful cellulose dissolving SIL. Unlike ILs based on phosphonium cations, such as [P$_{4441}$][OAc], many of the SILs do not require a co-solvent to be able to dissolve cellulose. The SIL [DBNH][OAc] solvent system was partly developed to be used in the IONCELL-F fibre spinning process and has been proven to be a notably efficient solvent in this context.[24]

2.1.6. Distillable ionic liquids

A great number of ILs have very low vapour pressures, but others like [DBNH][OAc] have vapour pressures high enough to be distillable – collectively these ILs are known as Distillable Ionic Liquids (DILs). DILs make up only a tiny fraction of the full range of ILs, but they show novel properties that could make their wide spread usage more viable than that of other types of ILs. An ionic liquid having a low vapour pressure can be purified of volatile impurities by means of evaporation and from solid impurities by filtration. However, due to their high viscosities and relatively high melting points, the filtration of ILs is not without its problems, and usually needs a low viscosity co-solvent that must be subsequently removed by evaporation. This makes the distillable ILs like [DBNH][OAc] interesting, as they can be more effectively separated from non-volatile or solid impurities by distillation of the IL itself.[64] Distillable ionic liquids composed of a protonated superbase and a deprotonated carboxylic acid were first implemented into the field of cellulose dissolution in the form of a patent in 2008 by D'Andola *et al.*[65] for BASF and laboratory study in 2011 by King *et. al.*[51] Distillable ionic liquids hold great promise from the viewpoint of recyclability – purifying the ionic liquid from high molecular weight impurities accumulated during processing of biomass, by way of solvent distillation, would solve one of the key issues currently limiting the application of high cost ionic liquids into the semi-industrial or industrial scale. For example, 1,1,3,3-tetramethylguanidium propionate ([TMGH][CO_2Et]) is thermally stable and can dissolve cellulose at 100° C, but is also distillable at higher temperatures (100-200° C) and lowered pressures (as low as 0,01 mbar).[51] In these conditions, the ion pair dissociates into the appropriate neutral species, which are then recoverable.[57] The DILs also include several superbases such as 1,5-diazabicyclo[4.3.0]non-5-ene (DBN) and 1,8-diazabicyclo[5.4.0]undec-7-ene (DBU), which are paired with a propionate counter anion.

2.2. Dissolution of cellulose

2.2.1. General aspects of dissolution

In cellulose, that has not been prior dissolved in an IL or other cellulose solvent, the packing of the anhydroglucose chains encases two different types of intermolecular forces that keep the cellulose fibrils together. Arguably, the more prominent interaction type is the hydrophilic interchain hydrogen bonding, which produce intermolecular networks that arrange individual cellulose chains into sheets. These sheets are then held together by the more elusive hydrophobic intersheet C-H···O interactions and van der Waals -forces. Why the hydrophilic and hydrophobic forces have different spatial directionality, can be mostly explained by the conformation adopted by the β-D-glucopyranose ring: the heavier hydroxyl groups occupy the equatorial positions, whereas the hydrogens are in axial positions. A generalised scheme of the directionality of the intermolecular forces in cellulose, and a hypothetical arrangement of the cations and anions of $[P_{4441}][OAc]$ around a β-D-glucopyranose unit is presented in **Figure 10.** The presence of both strong oriented hydrophilic and hydrophobic interactions, which in tandem keep the cellulose chains tightly together, has proven problematic when homogenous dissolution of cellulose has been the objective. A multitude of polar solvents can lodge themselves between the interchain hydrogen bonds, which bridge cellulose fibrils as well as individual cellulose chains on the surface of a cellulose fibril. However, without the means to stabilize and replace the intersheet hydrophobic interactions, the process will only result at the most in swelling of the fibrils, where solvent molecules temporarily push the fibrils or chains apart but are unable keep them solvated.

Certain ionic liquids, which have both a basic and small anion as well as a large and hydrophobic cation, can portray amphiphilic characteristics when it comes to interacting with the intermolecular bonds of the cellulose framework. This way they are able to break the bonds adhering cellulose chains to each other and stabilize the chains in solution, by presenting suitable interaction partners for both intermolecular hydrophilic and hydrophobic bonds present in cellulose. Many studies seem to agree that the role of the anion, with high enough basicity, is mainly to interact and force apart the interchain hydrogen bonds,[10, 66, 67] while the role of the cation is more elusive.
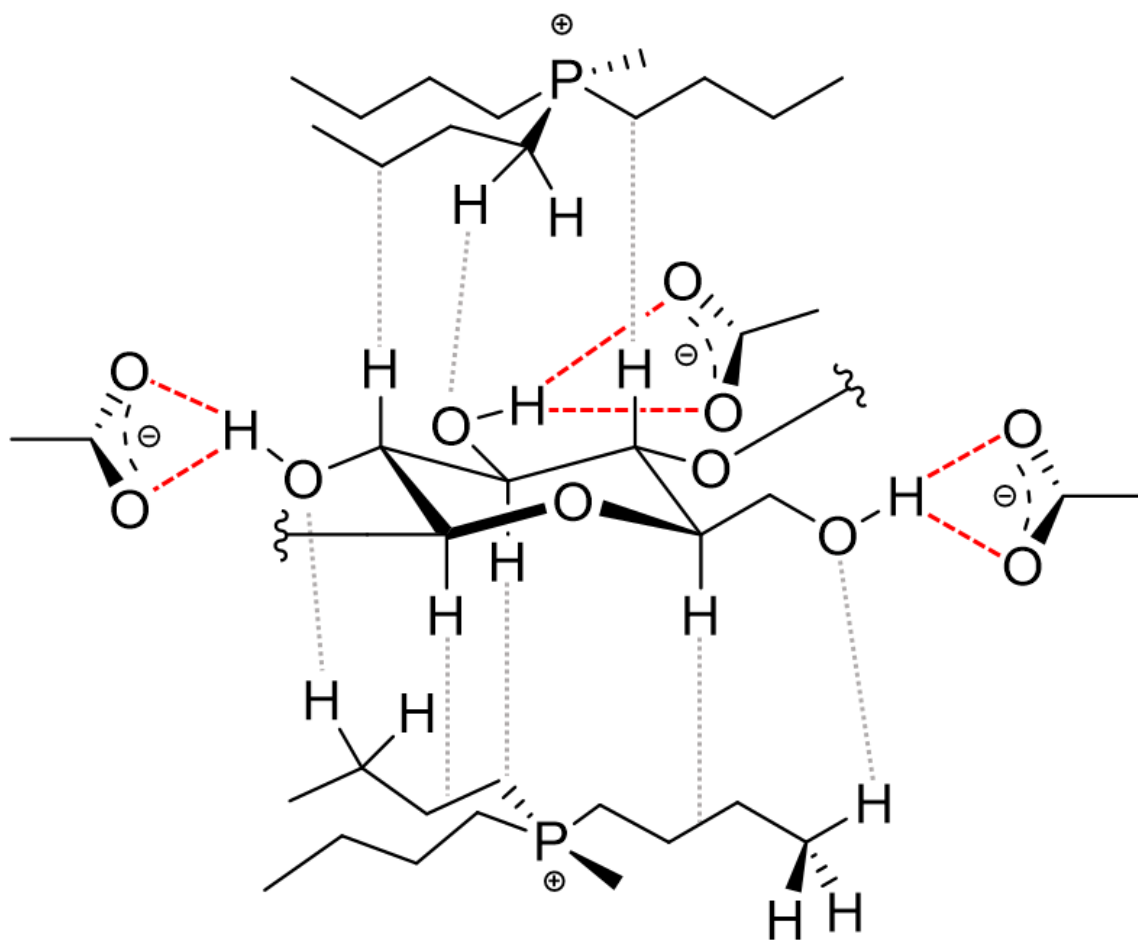
Figure 10. The general scheme for the solvation of cellulose in [P₄₄₄₁][OAc]. Notice the directionality of the hydrophilic (hydrogen bonding, red) and hydrophobic interactions (C-H···O interactions and van der Waals -forces, grey). The scheme is only used to illustrate the directionality of the intermolecular forces and the general positions of the IL anions and cations; it should not be viewed as an accurate depiction of the arrangement of ions or interactions in the solvation of cellulose.

Based on their findings, Holding *et al.*[52] postulated that dissolution of cellulose, an amphiphilic polymer, would be enhanced in a similarly amphiphilic solvent, which could favourably interact with both the polar and non-polar domains of cellulose. Hence, in comparison to some earlier polar cellulose solvents, a good cellulose solvent should possess a degree of hydrophobicity to increase beneficial interactions between solvent and solute. This hypothesis is supported by recent computational studies by Rabideau *et al.*[68, 69] The effect of the cation size on the solution power of an IL can be hypothesized based on these findings. When starting from small cations and increasing their size, initially the enlargement in cation size and resulting increase in the proportion of hydrophobic components enhances the dissolution capacity of an IL, by offering a better complement of interactions for cellulose. However, with even larger cations, the effect reverses and

they start to hamper the hydrogen bond basicity of the anion by in a way "diluting" the anion, ultimately lessening the solution power of the IL.

The Kamlet-Taft parameter β, i.e. the hydrogen bond accepting capacity also known as hydrogen bond basicity, of a cellulose solvent is important in determining whether cellulose remains in solution, and if it can be solvated in the first place. It, however, is not singly responsible in determining a successful cellulose solvent, as is shown in recent studies where it shows very little correlation with the cellulose dissolution capacity of an organic electrolyte mixture [P$_{4441}$][OAc]/GVL.[70] Hydrogen bond basicity of the solution is primarily based on the characteristics of the anion, which with a high enough specific basicity can bond with cellulose hydroxyl functionalities.[66, 71, 72] When an antisolvent with a high hydrogen bond acidity α (such as water) is added to the solution, it replaces the cellulose hydroxyl groups as the primary species interacting with the anion, drawing some of them away from the cellulose chains. The removal of anions from the vicinity of the cellulose chains also draws away some of the cations due to coulombic attraction – cations, which are interacting with the hydrophobic C-H functionalities and stabilizing cellulose in solution. This interplay, between the interionic coulombic forces and the intermolecular hydrophobic and hydrophilic forces between cellulose and IL ions, ultimately determines whether cellulose is dissolved or not. The same interactions also dictate the concentration of antisolvent needed to de-solvate cellulose, which is mostly dependent on the nature of the IL cation.[71]

Regardless of the mechanism of cellulose solvation, true solvation of cellulose necessitates that solvent molecules force their way between, and subsequently stabilize, both the interchain hydrogen bonds as well as the intersheet C-H bonds. The solvation power of an ionic liquid towards cellulose instinctively depends on the nature of the ions it is composed of and how closely the interactions displayed by the ions match those present in cellulose.[71, 73]

2.2.2. Thermodynamics of cellulose dissolution

The ability or inability of a solvent to dissolve a polymeric material is largely decided by the free energy of mixing (ΔG_{mix}, **Equation 1.**). If the value is negative, then the dissolution process is spontaneous.[10] When the molecular weight of a polymer increases, the entropy of mixing becomes less important, while the enthalpy of mixing becomes increasingly important in determining whether dissolution happens or not. However, the entropy gain for the polymer is always positive

when it dissolves in a good solvent, which is due to the increase in the number of possible states the polymer can adopt. On the other hand, the inverse is true for the solvent, which experiences a decrease in entropy due to the increase in the ordering of the solvent molecules.[10]

$$\Delta G_{mix} = \Delta H_{mix} - TS_{mix}$$ **Equation 1.**

In the context of polymer dissolution, solvents can be roughly divided into two types: "good" and "poor". Polymer-polymer interactions dominate in a "poor" solvent, whereas polymer-solvent interactions are dominant in a "good" solvent. A "good" cellulose solvent should possess a suitable mixture of interactions (H-bonding, coulombic, van der Waals, hydrophobic and hydrophilic) of the correct magnitude, so it can properly stabilise cellulose in the solution phase and overcome the low entropy gain of dissolution of cellulose. The poor entropy gain upon dissolution of cellulose in more polar solvents (including most cellulose solvents) is mostly attributed to the amphiphilic nature of cellulose. In these environments, cellulose molecules are susceptible towards self-organization due to hydrophobic effects, which prevents them from occupying the maximum number of states theoretically available.[10] The importance of amphiphilic and hydrophobic interactions in cellulose dissolution has been emphasized in recent literature.[74, 75]

Beside the thermodynamic aspects of a polymer solvent system, the kinetic characteristics of the systems are also important in determining whether dissolution happens. A thermodynamically good cellulose solvent might be incapable of dissolving cellulose due to excessively high viscosity, which can prevent the proper mixing of the components in a reasonable timeframe. Alternatively, the temperature required for dissolution of cellulose can be beyond the thermally stable range of the system components.

In his dissertation Holding pointed out several of his key observations about the dissolution of cellulose in ILs.[10] The author of this thesis found these points insightful in highlighting the novel features of cellulose among other polymeric materials. Firstly, an adequately strong hydrogen-bond accepting anion is needed to compete with the cellulose-cellulose hydrogen bonds. Secondly, an amphiphilic solvent that can stabilise both types of cellulose interactions, the polar interchain hydrogen bonds and the non-polar intersheet van der Waals forces & C-H···O interactions, is a better solvent than one that is less amphiphilic. Thirdly, a sufficient ion-pair separation leads to enhanced

dissolution capabilities due to both species (anion and cation) being more free to interact with the appropriate part of the cellulose molecule. Inclusion of a co-solvent to the IL is a good way to increase the ion-pair separation. Fourthly, the co-solvent must be of sufficiently high polarity to properly dissolve the ionic species. It must also not interfere with the hydrogen bonding between the anion and cellulose, which is best guaranteed by having the co-solvent be of only hydrogen bond donor -type.

2.2.3. Thermoresponsive phase behaviour in cellulose solutions

Two closely related thermoresponsive phase behaviours, Upper Critical Solution Temperature (UCST) and Lower Critical Solution Temperature (LCST), can be observed in various polymer-solvent mixtures. These phenomena are based on the emergence of a negative ΔG_{mix} as a result of a change in temperature. These changes can only manifest within a certain range of values for ΔH_{mix} and ΔS_{mix} for the polymer and for the solvent (**Equation 1.**). For example, if a polymer in solvent has positive or negative ΔH_{mix} and small ΔS_{mix} of the same sign, it should display UCST (positive) or LCST (negative) behaviour as a result of changing temperature. On a phase diagram with temperature and mole fraction of a component as the variables (**Figure 11.**), UCST and LCST are defined as follows: Above the UCST and below the LCST, a single phase is found for all compositions (of the polymer and solvent).[76] Which means that, if it exist, UCST is a critical temperature above which the two components are fully miscible independent of their proportions. The solvent system changes thermodynamically from poor to good with an increase in temperature. As the entropy of mixing is always positive and the enthalpy of mixing is also positive, the increase in the value of T is what causes the change from positive ΔG_{mix} value to negative value. The temperature, in which the sift in sign is observed, is called a "Theta (θ) temperature" – a temperature where the potential of mixing for the polymer is zero and the polymer-expanding excluded volume -interactions are cancelled, making the polymer behave like an ideal chain.[10] In the case of UCST, solvent-polymer interactions dominate above the θ-temperature, whereas polymer-polymer interactions dominate below it.
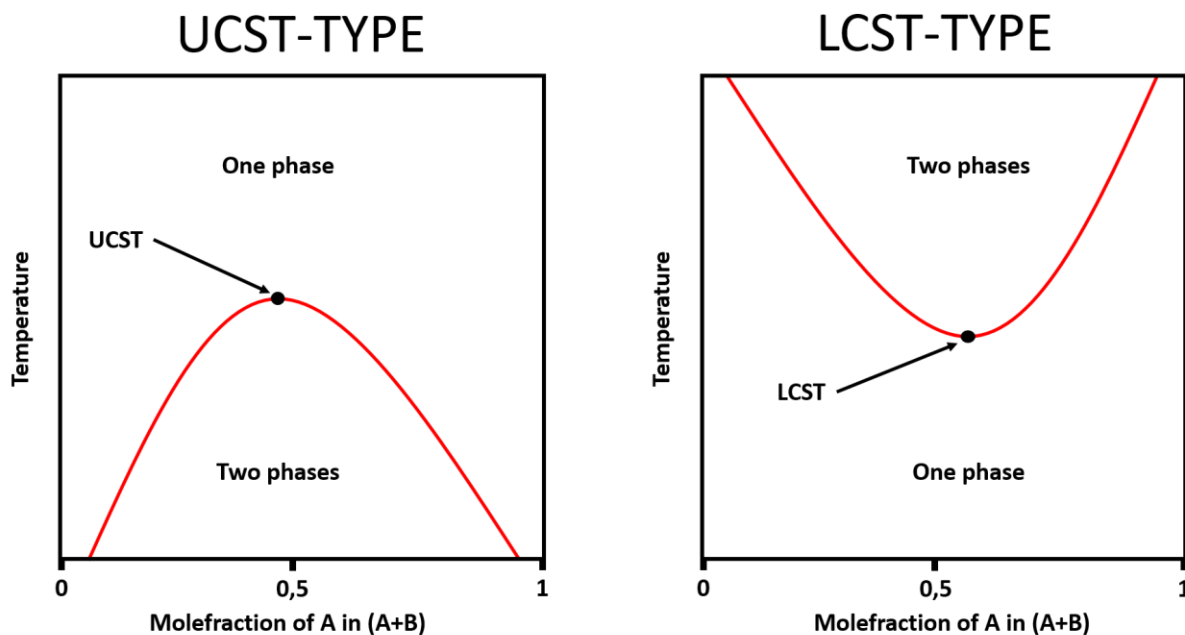
Figure 11. Phase diagrams describing the two common types of thermoresponsive phase behaviour (UCST & LCST) observed with certain polymer-solvent combinations. The two points represent the temperature above (UCST) or below (LCST) which the two components A and B are fully miscible with each other in all proportions. In such case, only one phase is observed.

In simple terms, if you adequately heated a UCST-expressing -mixture of polymer and solvent, which were not miscible at the starting temperature in the current composition, they would become miscible and the polymer would dissolve. Subsequently, when the temperature was lowered back to its starting value, the polymer would precipitate out of the solution. The same applies to LCST, albeit the temperature relationship is inverse – the components are fully miscible below a certain temperature.

The use of the terms UCST and LCST in the context of cellulose dissolution in a liquid solvent system is problematic due to certain properties of cellulose. Firstly, the presence of true UCST-type behaviour would entail that cellulose would have to be in a liquid state as the concentration nears 100 %. However, the presence of a liquid state of cellulose and the true miscibility of the components in all proportions above a certain temperature is impossible to verify, due to the decomposition of cellulose in higher concentrations at elevated temperatures. For example, the determination of the actual UCST, in a system of >15 wt-% cellulose in $[P_{4441}][OAc]$/GVL, is infeasible in practice, as the phase-transition temperature of such a system would rise above 140° C. At this temperature and above, rapid decomposition of cellulose is observed.[70] Secondly, the high viscosity of cellulose solutions puts a kinetic limitation on the mixing of the system and hence, also

on the determination of miscibility. Thirdly, the formation of a gel-state cellulosic material after the final decrease (UCST) or increase (LCST) in temperature in a cellulose/IL system is not compatible with the strict definition of UCST, as cellulose does not truly return to the solid state. Despite these inconsistencies with the definitions of UCST and LCST, the thermoresponsive phase behaviour expressed by certain cellulose/solvent systems (such as cellulose in [P$_{4441}$][OAc]/GVL, one of the solvent systems under study in this thesis) most closely resembles those of the UCST and LCST systems in a thermodynamical sense. Hence, the phase behaviour observed in [P$_{4441}$][OAc]/GVL would be best described to be "UCST-like phase behaviour".[10] However, there have been further unpublished results, which seem to point to an antisolvent (impurity) driven process as the driver of the particle formation in the cellulose/[P$_{4441}$][OAc]/GVL system. In addition to UCST-like phase behaviour, the presence of LCST-like phase behaviour has been documented for cellulose, with exemplary systems including aqueous NaOH/urea and LiOH/urea.[77]

2.2.4. Kamlet-Taft parameters of a cellulose solvent

The Kamlet-Taft parameters of a solvent can be used to assess its suitability for dissolving a certain compound, for example cellulose. The parameters are determined by observing the wavelength shift of certain UV-active dyes, which gives information (polarity, polarizability π^*, hydrogen bond basicity β, hydrogen bond acidity α) about the solvent environment in which the dye resides. However, all of the obtained parameters are relative and cannot be used as individual values outside of the study context. In the case of cellulose solvation, the Kamlet-Taft solubility parameters are useful in describing the potential for a solvent or a solvent mixture to act as either an H-bond donor or acceptor. The specific parameters related to hydrogen bonding are the hydrogen bond basicity β, which describes a solvent molecules ability to be a H-bond acceptor, and hydrogen bond acidity α, which describes the ability to be a H-bond donor.[78] It has been shown that the net basicity (β-α as a function of β) of a solvent, and especially of ionic liquids, is a good predictor of the solvent's cellulose dissolving capabilities.[57, 71] The net basicity values of superbase/acid ILs such as [DBNH][OAc] plot very close to other known good cellulose solvents such as NMMO·H$_2$O.

The hydrogen bond basicity β of a cellulose solution is important in determining whether cellulose remains in solution and if it can be solvated in the first place. In the case of ionic liquids as cellulose solvents, the hydrogen bond basicity of the solution is primarily based on the characteristics of the anion, which can bond with cellulose hydroxyl functionalities if they exhibit a high enough specific

basicity.[66, 71, 72] On the other hand, other studies by Holding observed no clear effect of the β-parameter on cellulose dissolution capability of an IL.[10] Despite ([P$_{14666}$]/Cl)/DMSO (40 wt-% DMSO) having a high β value, it was unable to dissolve cellulose, whereas [P$_{14666}$][OAc]/DMSO (40 wt-% DMSO), which also has a high β value, was able to dissolve cellulose in the same conditions. Additionally, several neat ILs also had high β values but were similarly unable to dissolve cellulose. Hence, Holding postulates that factors other than hydrogen bond basicity play a more important role in determining the solubility of cellulose in an IL.[10] The cation size was suggested as another important factor on determining cellulose solvation, the large size of a cation might hinder its intercalation between cellulose chains and hamper the cation-anion separation. Huo *et al.*[79] suggested that the presence of a certain level of acidity α in the co-solvent, is also important for the efficient dissolution of cellulose. The acidity is hypothesized to enhance the ion pair separation of the IL, and may be the reason that the more acidic [emim][OAc] can dissolve cellulose in the neat state, whereas the tetra-alkyl phosphonium acetate ILs cannot. Then again, the asymmetry of the [emim]-cation might also lead to a better charge screening on the anion, resulting in enhanced anion-cation separation.[70]

Holding studied the Kamlet-Taft parameters of [P$_{4441}$][OAc] in both DMSO and GVL in order to determine the effect of the co-solvent concentration on the parameters (**Figure 12.**).[10] The steady addition of both co-solvents slightly decreases the β of the electrolyte until about 80 wt-% of co-solvent (with DMSO showing a more pronounced shift), after which both show a drastic decrease in the value. However, GVL retains a higher and more stable β value for almost all points despite being able to dissolve less cellulose, which makes it highly improbable that β alone is the single most influential factor determining cellulose dissolution. The α value is also very slightly lowered with increasing co-solvent concentration until roughly 90 wt-% co-solvent, after which GVL shows a major decrease while approaching 100 wt-% GVL. At the same time, the mixture with DMSO does not demonstrate such drastic decrease in acidity at high DMSO-concentrations, which means that pure DMSO is much more acidic than pure GVL. This could partly explain the very effective nature of DMSO as a co-solvent in cellulose dissolution, by allowing more efficient ion pair separation.[79]
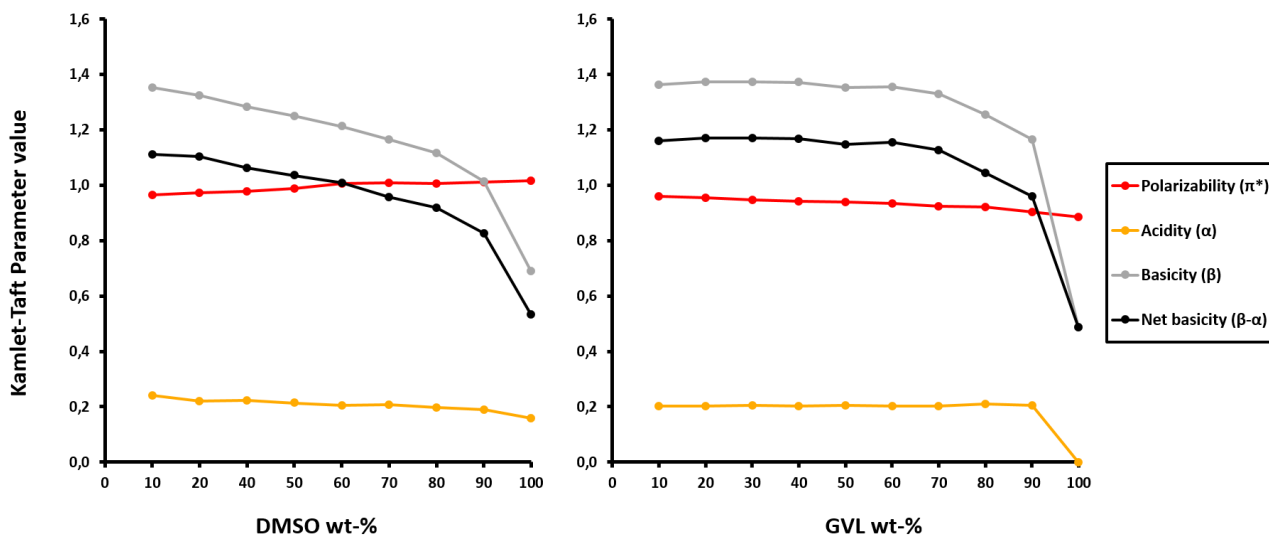
Figure 12. Kamlet-Taft parameters of [P$_{4441}$][OAc]/co-solvent mixtures as a function of co-solvent concentration (DMSO or GVL).[10] Figure modified with permission from "Holding, A.J., 2016. *Ionic Liquids and Electrolytes for Cellulose Dissolution*, University of Helsinki".

In both systems (with DMSO or GVL), the polarizability π* has a change roughly similar in magnitude but opposite in sign from one co-solvent to other. GVL shows a steady but very slight decrease, while DMSO shows a steady but slight increase.[10] A notable difference in the development of the Kamlet-Taft parameter values, between DMSO and GVL, is that the β and π* of GVL remain very stable from 0 wt-% GVL all the way to the 70-90 wt-% region, whereas those in DMSO change steadily along with the growing co-solvent concentration. This would imply that the ion pair in the GVL electrolyte favourably interacts with the dyes for essentially all of the composition range, until a higher degree of solvation occurs when approaching 100 wt-% GVL. This could mean, that the ion pair in GVL is more separated, i.e. more "naked". In general, a high polarizability is required from a co-solvent in order to solvate the also highly polarizable IL species. The co-solvent also should not form hydrogen bonds with the IL. This is supported by a test where the [P$_{4441}$][OAc]/co-solvent weight ratio was kept stable at 60:40, while the co-solvent was chosen from acetone, DMA, GVL and DMSO. The cellulose saturation point, i.e. dissolution capacity of the solvent, was shown to be highly correlative with the π* of the electrolyte mixture.

2.2.5. The role of co-solvents in the solvation of cellulose

The addition of low viscosity organic co-solvents into an IL has made certain otherwise ponderous solvent systems far more functional. Lowered viscosity, enhanced transport properties and overall tunability of thermodynamic and kinetic properties of the solvents mixtures has enabled faster, more efficient processing of cellulose along with an elevated dissolution capacity.[16, 80, 81] The use of co-solvent has been a common practice with the imidazolium-based ionic liquid family, but more recent studies have focused on also applying the same concept into other IL families, such as the phosphonium- and superbase-ILs.[10]

Co-solvents like DMSO and GVL interact strongly with an IL cation by solvating it, and hence compete with the hydrophobic IL/cellulose interactions. This should result in less effective solvation of cellulose, but somewhat counterintuitively, this solvation of the cation can in fact lead to faster and more efficient dissolution of cellulose. Even though the co-solvents might not have strong enough specific interactions with the cellulose hydroxyl and C-H groups to dissolve them on their own, they do make the solvent mixture dramatically less viscous compared to the pure IL. This increase in the mobility of the solvent molecules makes it faster and much more likely that a cellulose chain can become fully surrounded by solvent molecules and break away from the neighbouring cellulose chains, becoming truly solvated in the process. Especially when a high DP polymer like cellulose is concerned, the kinetic requirements for solvation are very important. In addition to kinetic benefits the inclusion of co-solvent has on the solvation of cellulose, the fact that the addition of a co-solvent also significantly lowers the freezing point of the solvent mixture is very useful in the practical sense. For example, this allows 5 wt-% MCC solutions in [DBNH][OAc]/DMSO (40 wt-% DMSO) to be relatively free flowing liquids at RT, while even high cellulose load dopes (>10 wt-%) remain as very high viscosity malleable liquids. This malleability makes the handling of the dope much more convenient at lower temperatures compared to pure IL dopes, which are solid at RT. Despite the apparent benefits the use of co-solvents brings to cellulose dissolution, the inclusion of a co-solvent into a solvent system is not axiomatic, as the presence of multiple solvent components can bring considerable additional costs and complications in the recycling steps of an up-scaled industrial process.

Rinaldi *et al.*[80] studied a range of co-solvents in a system of [emim][OAc]/co-solvent/cellulose. The co-solvents included in the study were N,N,-dimethylformamide (DMF), N,N-dimethylacetamide (DMA), 2-pyrrolidinone, N-methyl-2-pyrrolidone (NMP), δ-calerolactam, ε-caprolactam, 1,1,3,3-

tetramethylurea (TMU), 1,3-dimethyl-2-imidazolidinone (DMI), 1,3-dimethyl-3,4,5,6-tetrahydro-2-pyrimidinone (DMPU), dimethyl sulfoxide (DMSO), sulfolane, acetylacetone, t-butanol and t-pentanol (**Figure 13.**). The common structural motifs starting from DMF to DMPU are clearly visible, but what these amides have in common with DMSO and sulfolane is a high polarizability value. Meanwhile acetylacetone, t-butanol and t-pentanol are decisively less polarizable. The compatibility of the co-solvent-cellulose interactions varied from co-solvent to co-solvent. When the molar fraction of IL needed to dissolve cellulose was used as a measure of compatibility, DMSO showed the most promising results out of the co-solvents listed. A molar ratio of as low as 8:92 IL:DMSO was already able to dissolve 10 wt-% of cellulose. The observed ranking of the rest of the solvents, based on their performance in the experiment, is rationalized with Kamlet-Taft parametrisation (see section **2.2.4. Kamlet-Taft parameters of a cellulose solvent**). Using DMI as an example, when the IL concentration is increased, the largest change observed is the major increase in the hydrogen bond accepting Kamlet-Taft parameter (β) of the bulk solution. When a certain concentration of IL (18 mol-%) was reached, the change in the parameters levelled out – near instantaneous dissolution
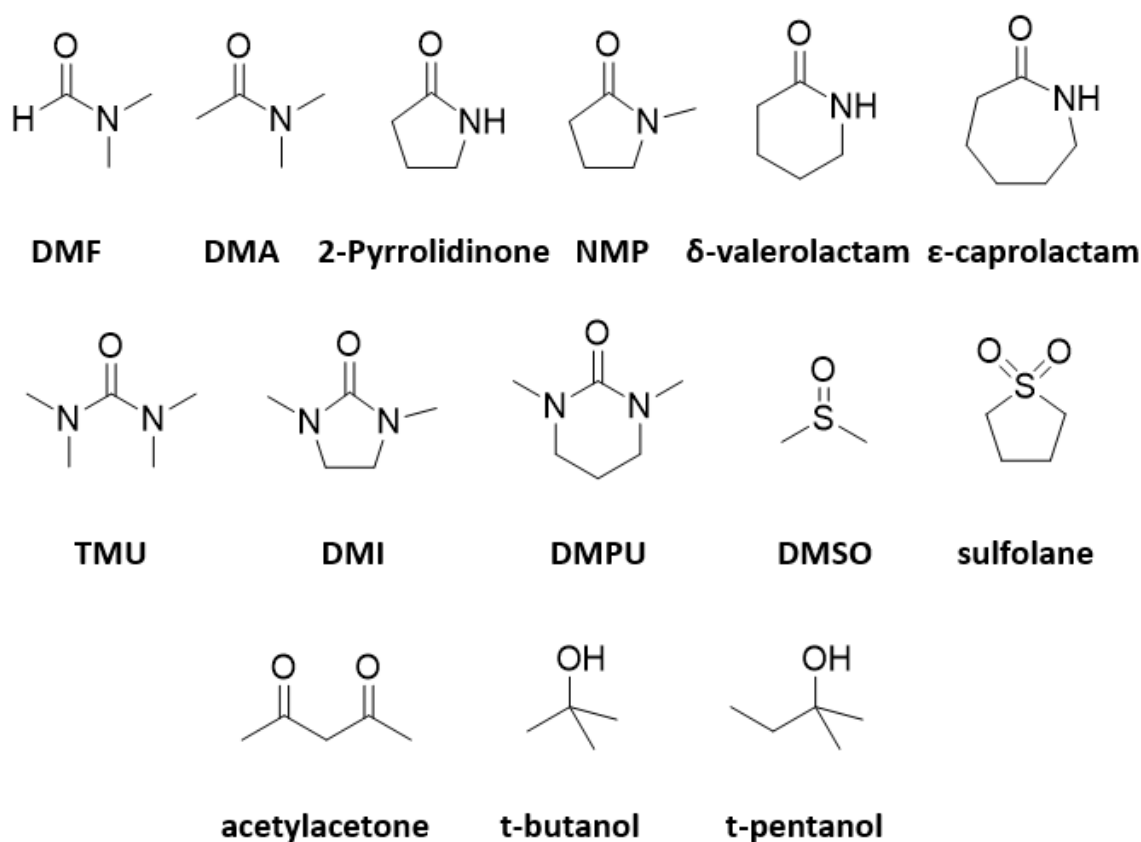
Figure 13. The various organic solvents studied by Rinaldi *et al.*[98] for their compatibility as a co-solvent of [emim][OAc] for dissolving cellulose.

was observed beyond this point. The β value of the bulk solution at these concentrations resembled that of many known cellulose solvents.[71]

The effect on dissolution capacity of three of the most promising co-solvents (DMSO, DMA, DMF), mixed with [bmim][OAc], was studied by Xu *et al.*[82] At 25° C and a co-solvent:IL ratio of 2,54:1, the ranking of the co-solvents from high to low by amount of cellulose dissolved was DMSO (15 wt-%), DMF (12,5 wt-%) and DMA (5,5 wt-%). The amount dissolved varied greatly with changing temperature, but the order of the three co-solvents did not change. The authors gathered from conductivity measurements that, apart from the obvious kinetic benefit from lowered viscosity, the major factor enhancing the dissolution of cellulose with increasing co-solvent concentrations was the better availability of free acetate ions. This increased availability was a result of the preferential solvation of the IL cation [bmim]$^+$ by the aprotic co-solvent. Dissolution of cellulose in the [bmim][OAc]/DMSO system was further studied as a function of the molar concentration of DMSO. It was found that the solubility raised rapidly from zero to 15 wt-%, when progressing from DMSO:IL molar ratio of 0 to 2,54, after which it steadily declined with further addition of DMSO. At DMSO:IL molar ratio of 22,5, the solubility of cellulose was only ca. 4 wt-%.

Holding studied several phosphonium-based ILs, which incapable of dissolving cellulose as neat solvents, and observed a general trend in the cellulose dissolution capacity with the inclusion of a co-solvent (DMSO).[10] When moving from 0 wt-% DMSO concentration to 100 wt-%, all of the solvents ([P$_{4444}$], [P$_{4441}$], [P$_{8888}$], [P$_{8881}$], and [P$_{14888}$][OAc]) expressed a similar trend of initial increasing dissolution capacity, followed by a comparably stable period and subsequent significant drop-off in capacity at high DMSO concentrations. This final drop-off is due to the solution becoming too dilute in relation to IL, which hampers the hydrogen bonding ability of the solvent system. In this case, the IL is too diluted to form enough hydrogen bonds with cellulose to properly solvate it. An ^{1}H-NMR-study using [P$_{4444}$][OAc]/D$_6$-DMSO found out that there was no significant change in the methyl signal in DMSO with changing cellulose concentration, which suggest that DMSO is not hydrogen bonded to cellulose nor to the IL anion, and that its role in cellulose solvation is passive (i.e. it solvates the cation).[10] The acetate carbonyl carbon moves downfield with increasing cellulose concentration, which is likely a result of acting as a hydrogen bond acceptor to cellulose.

Out of the traditionally used co-solvents for the dissolution of cellulose in an ionic liquid, probably the most effective ones are N,N-dimethylacetamide (DMA), N,N-dimethylformamide (DMF), 1,3-dimethyl-2imidazolidinone (DMI) and DMSO. Especially DMSO has many positive features related to its ability to favourably interact with cellulose, and hence make the dissolution easier, faster and possible at a low temperature. Additionally, its level of toxicity is very low compared to DMA, DMF and DMI.[52, 80] Due to these beneficial qualities, DMSO was chosen as one of two co-solvents used in this thesis. Despite all the positive properties, DMSO also has negative ones, which have driven people to consider other co-solvent options for their reactions.[70] One solvent in particular, γ-valerolactone (GVL), has raised a lot of interest recently as a replacement due to the relative ease with which it can be removed from a cellulose/solvent mixture (see experimental section **4.4.5. Removal of GVL under vacuum**) and its "green" background, being synthesizable from biomass. Hence, GVL was chosen as the other co-solvent used in this thesis. Despite this, DMSO is still a better co-solvent than GVL when used alongside [P$_{4441}$][OAc] and [DBNH][OAc], enabling the dissolution of more cellulose (Enocell) over the whole concentration range and the maximum amount overall in [P$_{4441}$][OAc] (DMSO 22 wt-%, GVL 15 wt-%). In addition, GVL acts almost like an antisolvent in [DBNH][OAc].[10, 70] This antisolvent-like behaviour was attributed to the high hydrogen bond acidity of GVL, which could result in GVL hydrogen bonding with the IL anion. In the case of [emim][OAc]/GVL, GVL is observed to act as a better co-solvent, while still not as good as DMSO.[10] These findings in tandem with the appearance of UCST-like thermoresponsive behaviour when [emim][OAc] and [DBNH][OAc] are coupled with GVL, a phenomenon not observed with DMSO as a co-solvent, suggest that GVL does make these electrolyte systems worse cellulose solvents in a thermodynamic sense.[70]

2.3. [DBNH][OAc] in cellulose processing

Even when the solvation of cellulose in an ionic liquid should be possible enthalpy-wise (based on the IL's net basicity and entropy), high viscosity of the solvent can place practical limitations on its ability to dissolve cellulose. This is why low viscosity ionic liquids such as [DBNH][OAc] (**Figure 14.**), which can dissolve large amounts of cellulose in a short time and at reasonably low temperatures, make for a novel, intriguing research subject and a promising base for applications such as fibre spinning.[24] The low operating temperature of 60-80° C during cellulose dissolution coupled with a good thermal stability of both polymer and solvent, makes the use of [DBNH][OAc] very convenient and benign. Compared to the high operating temperatures of other direct cellulose solvents, such as NMMO or [P_{4441}][OAc], the low temperature of [DBNH][OAc]-based processes incurs considerable energy savings and results in fast and efficient operation. These superior qualities are further emphasised when [DBNH][OAc] is combined with viscosity-lowering co-solvents such as DMSO or GVL, which leads to even faster dissolution and lower necessary operating temperature. However, the use of such beneficial co-solvents in cellulose dissolution is not self-evident, as the presence of multiple solvent components can bring unwanted costs and complications in the recycling steps of the processes.
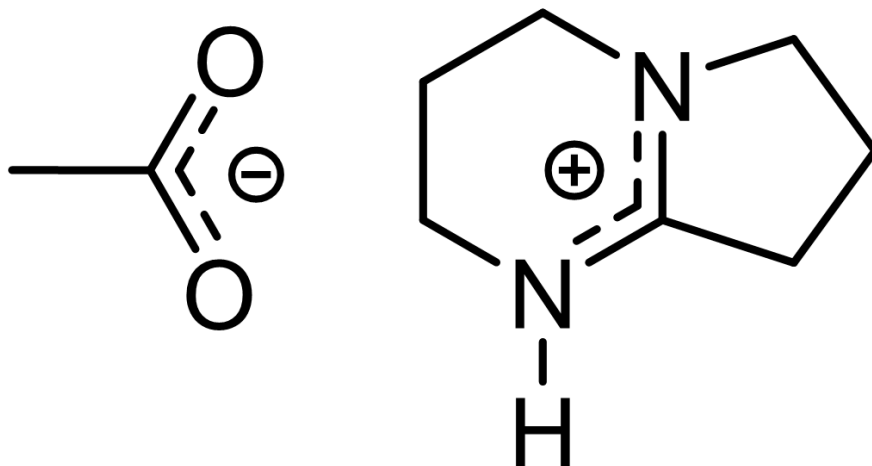
Figure 14. The chemical structure of 1,5-diazabicyclo[4.3.0]non-5-enium acetate, [DBNH][OAc].

Very high concentrations of cellulose (up to 17 wt-%) can be dissolved in [DBNH][OAc] even at relatively low temperatures of 80° C. However, due to the correspondingly high viscosity of a concentrated cellulose dope, a specialized mixing apparatus such as a kneader is needed to achieve

a homogenous solution.[71] When dissolving cellulose for the purpose of fibre spinning, the cellulose dope needs to be of constant quality, which can be achieved by press filtration after the initial dissolution step, and letting the dope solidify in the shape of the spinning cylinder. When this solid dope is loaded into the spinning cylinder and heated to 70° C, an air bubble free and homogenous dope is formed. With the addition of 40 wt-% DMSO, cellulose concentrations of ≤10 wt-% are dissolvable already at 60° C.

In their studies on fibre spinning of cellulose, Kuzmina et al.[55] demonstrated that if the nitrogen in the six-membered ring is substituted with a methyl or ethyl group, the solvent's ability to dissolve cellulose is drastically reduced. Similarly, an effect of diminishing returns was observed as a result of increasing the length of the alkyl chain in the anion series acetate-propanoate-butanoate-hexanoate. On the other hand, the replacement of 10 % of acetates in [DBNH][OAc] with hexanoates produced stronger fibres than those obtained from pure acetate IL.

2.3.1. Fibre spinning from [DBNH][OAc] dope

One process where the superbase IL [DBNH][OAc] has recently seen significant study and nascent commercial success is fibre spinning. In any process where cellulose is spun into semi-synthetic fibres, cellulose is first dissolved in a direct or derivatizing solvent. The formed dope is drawn through a spinneret into a coagulation tank, where the dissolved cellulose precipitates in the shape of a fibre. Spinning of cellulose fibres from a [DBNH][OAc] dope has been studied Hauru et al.[83] and it has been shown that the resulting fibres possess excellent spin stability and tenacity, superior to those obtained from the viscose or Lyocell processes. The fibres can be spun using higher cellulose concentration dopes as well as using a lower operating temperatures during spinning and cellulose dissolution, than what is possible in the two traditional processes.[24] Compared to NMMO, [DBNH][OAc] as a pure solvent also has very low viscosity, which helps to speed up the initial cellulose dissolution step. Because of the more benign operating conditions, there appears to be less cellulose degradation during spinning, which results in superior fibre strength characteristics as well as better yields.

A general dry-jet wet spinning apparatus is portrayed in **Figure 15**. When cellulosic material, dissolved in [DBNH][OAc] or NMMO·H_2O, is spun into fibres using dry-jet wet spinning, the dissolved cellulose is first extruded from a nozzle (a) into an air gap (b) and subsequently into a coagulation
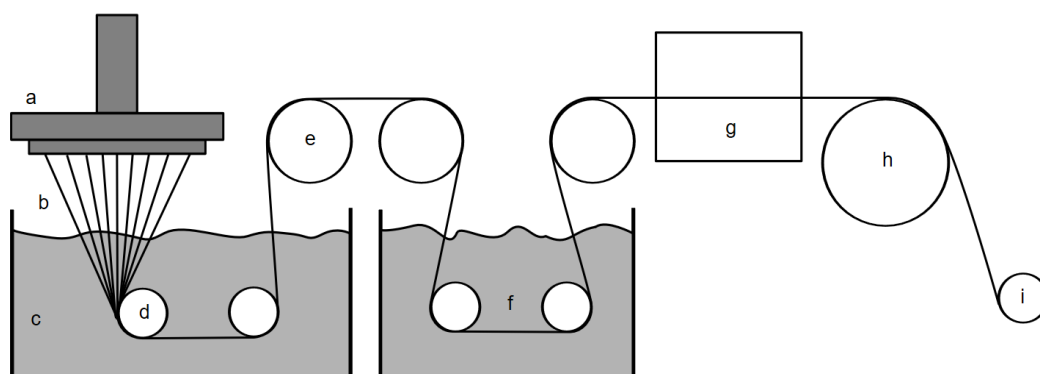
Figure 15. A sketch of the various components in a general dry-jet wet spinning apparatus. The components include: (a) spinneret, (b) air gap, (c) coagulation bath, (d & e) guides, (f) washing bath, (g) drying unit, (h) heated roller, (i) storage spool. Picture used with permission from the author Lauri Hauru.

bath (c). As the spun dope enters the coagulation bath, it starts to regenerate when the antisolvent (H_2O) starts to diffuse into the fibre and the IL starts to diffuse out of the fibre. In the case of NMMO, the coagulation bath is composed of a 4:1 mixture of water:NMMO, which helps to keep the rate of diffusion down at a low enough level.[84] The fibre also experiences a quick drop in temperature from the spinneret, held usually at 65° - 80° C in the case of [DBNH][OAc] dope, to the coagulation bath at 15° C. The use of a cooled bath has been shown to produce stronger fibres out of cellulose than a room temperature one.[83] The temperature drop helps in regenerating the fibre by decreasing the dissolution power of the IL. The regenerated fibre is directed by guides (d) in the coagulation bath and after a suitable distance in the bath, it is guided out of the bath (e) and directed onto a pure water bath (f) for washing the fibre to get rid of any residual solvent. After washing, the fibre is yet again directed out of the bath into a drying unit (g) and finally it passes over a heated roller (h) and is collected onto spools (i) for storage and further processing. The nozzle or spinneret used in the study by Hauru *et al.*,[83] on spinning a cellulose-[DBNH][OAc] dope, was a monofilament spinneret with a diameter of 100 µm unlike the multifilament spinneret shown in the figure.

The ca. 1 cm long air gap plays a major role in producing strong cellulosic fibres, by acting as a space where the fibre can be drawn prior to regeneration. Drawing on the filament from the regenerated end translates a force onto the non-regenerated part of the dope in the air gap, leading to a longitudinal orientation of the cellulose chains. This force imposed on the non-regenerated fibre has a beneficial effect on the strength of the resulting regenerated fibre. When the fibre does regenerate, some of the orientation of cellulose chains remains. A representation of the orientation of cellulose chains during the spinning process is shown in **Figure 16**. In theory, the higher the draw

ratio, the more the cellulose chains orient themselves and the stronger the resulting fibres will become. However, there is a practical limit to the maximum beneficial draw ratio and in the studies on [DBNH][OAc]-cellulose-dope,[83, 85] draw ratios of up to 7,5 were still possible. Nevertheless, using this higher draw ratio did not produce fibres of notably better quality than ones produced using a draw ratio of 4,5 in this study. The draw ratio was investigated further in later studies, where much higher draw ratios were achieved.[24, 86] After all of the fibres or, in the case of continuous operation, enough of the fibres are spun and collected to fill a spool, the fibres are treated for drying by immersing them into a cold water bath at 5° C to solidify the structure. Subsequently the fibres are washed with 50° water for five minutes and finally dried in a controlled atmosphere of 50 % relative humidity and 23° C.[73] The remaining orientation of the cellulose chains in the regenerated fibre encourages crystallization as well as longitudinal fixation of the remaining amorphous portions during the drying process. This directionality procures an axially oriented composite like structure that has vastly superior mechanical properties compared to undrawn fibres.
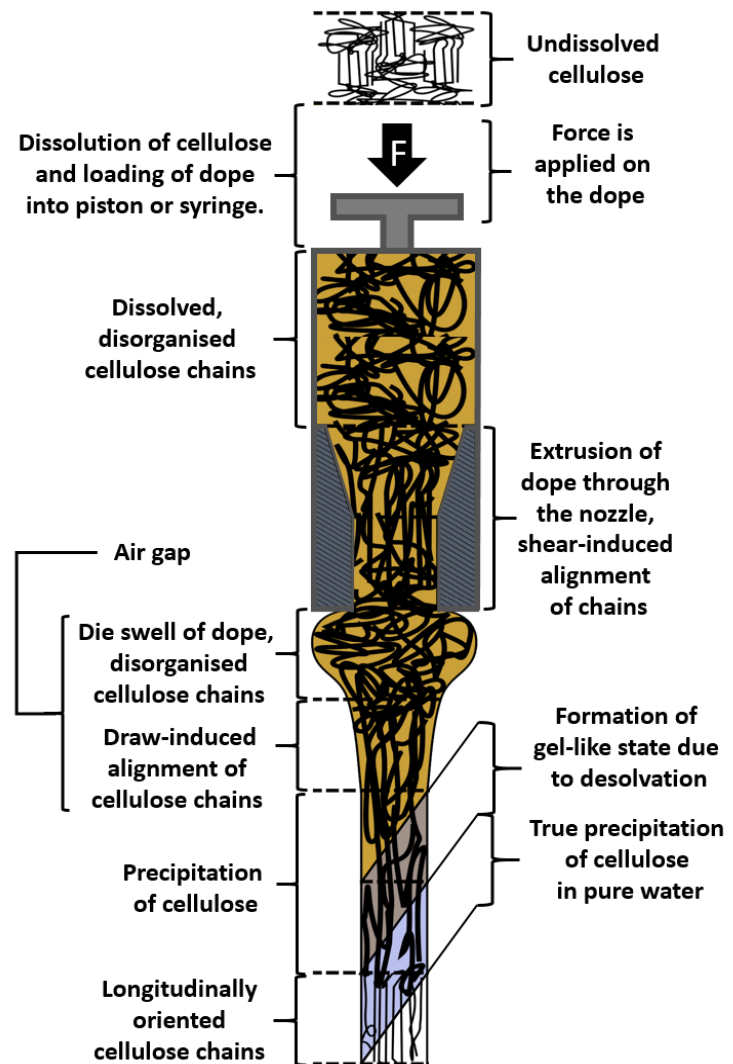
Figure 16. The orientation of cellulose chains (black lines) and the progression from undissolved cellulose to dissolved, to a gel-like state and back to undissolved during a generalised dry-jet wet spinning process. Picture modified with permission from the author Lauri Hauru.

Spinning parameters such as extrusion velocity, draw ratio and air gap as well as properties of the pulp, such as the amount of residual hemicellulose, viscosity and cellulose molecular weight distribution, play a role in determining the final mechanical characteristics of the regenerated

cellulose fibre.[86] It has also been observed that the process extracts some amount of the residual hemicellulose in the cellulosic raw material, which stays in solution during regeneration, leading to fibres with a lower hemicellulose content compared to the original pulp. This property of the solvent has been exploited in the IONCELL-P process (see section **2.3.4. IONCELL-P**), where the hemicellulose content of wood pulp can be reduced by treating the pulp with a mixture of [DBNH][OAc] and water.[86] The spinning of cellulose fibres by using [DBNH][OAc] as the direct cellulose solvent was shown to have a mild decreasing effect on the polydispersity index (PDI) of the regenerated material compared to the starting material. This was attributed to the slight degradation of the long cellulose chains, albeit the effect was shown to be much smaller compared to those observed in spinning with NMMO or imidazolium-based ILs.[85]

2.3.2. IONCELL-F

The before described process, of dry-jet wet spinning cellulose using [DBNH][OAc] as the solvent, was further refined and branded IONCELL-F (IONCELL-Fibre) by Sixta *et al*.[24] IONCELL-F is a fibre spinning method using dry-jet wet spinning to produce MMCFs (Man-Made Cellulosic Fibres), with consistent tenacities above 50 cN/tex and Young's modulus' of 24-34 GPa – mechanical properties superior to those of commercial viscose and Lyocell fibres.[85, 86] Additionally, cellulose concentrations in the dope can reach as high as 17 wt-% and still be perfectly spinnable. The fibres formed have also been fashioned into clothing, which have been found to be comfortable to wear in skin contact due to their superb moisture transport properties superior to viscose. This makes IONCELL-F a very promising process, with the potential of becoming at least a partial replacement for the environmentally or ethically unsustainable processes of today. In fact, the process has seen nascent commercial success and has received attention and praise even in the public media.[87]

Instead of a single filament spinneret used in the earlier study,[83] a 36-hole multifilament spinneret with diameters of 100 μm was used in the IONCELL-F process. The rate of extrusion was kept constant at 5,7 m/min, while the take-up velocity was varied between 5-100 m/min. This translates into draw ratios from 0,88 to values much exceeding those of the previous study,[83] with usable values of 15,9 and maximum values of 17,7 reported. The fibres were also washed after regeneration using 60° C water instead of 50° C used previously. The Ruland/Vonk X-Ray method[36] was used to measure the degree of crystallinity of fibres derived from the IONCELL-F fibre spinning

process, the products structurally resembling the cellulose beads produced in this thesis, and values between 28-36 % were obtained.[24] The crystallinity was shown to increase in tandem with the Draw Ratio (DR) used in the spinning process. The various X-Ray methods are further described in earlier section **1.2.6. X-Ray measurements of cellulose morphology.**

In an applied study, fibres were spun from a dope containing cellulose either from untreated kraft pulp, with just a viscosity adjusting treatment, or IONCELL-P extracted pulp, with various pre-treatments (see section **2.3.4. IONCELL-P**).[86] This was the first case of spinning birch (hardwood) paper pulp into fibres. It was shown that the IONCELL-P extracted pulp, which had a much lower hemicellulose content (4,23 % compared to 25,11 %), was able to be spun with a higher draw-ratio and resulted in much stronger fibres than the untreated pulp. The weakening effect of increasing hemicellulose content has been attributed to disruption of the cellulose chain orientation. Hemicellulose and cellulose regenerate together as a mixture, and as hemicelluloses are much shorter polymers than cellulose, they tend to orient themselves to a much lower degree when tension is applied to the fibre while spinning. Therefore, when the fibre is drawn during spinning, it breaks down at a lower and lower draw ratio the higher the hemicellulose content is. The resulting fibres also have inferior mechanical properties compared to ones with low hemicellulose contents. This inference is not surprising, as the importance of hemicellulose removal in man-made cellulosic fibre production is well known.[88]

2.3.3. Regeneration of cellulose from [DBNH][OAc] and other ILs – Case study in fibre spinning

In a general sense, cellulose regenerates or desolvates when the molecules of a cellulose solvent around the cellulose chains are replaced by antisolvent molecules. The regeneration behaviour of cellulose has been studied in the context of dry-jet wet spinning by Hauru *et al.*[73] In the study, cellulose was dissolved in direct cellulose solvents such as [DBNH][OAc], NMMO·H_2O, [emim][OAc] and [TMGH][OAc]. In the case of fibre spinning, the regeneration process of cellulose starts when the fibre hits the coagulation bath – the solvent molecules start to diffuse outwards into the antisolvent bath, while the antisolvent molecules start to diffuse inwards towards the core of the fibre (**Figure 17.**).

CROSS-SECTION OF A REGENERATING CELLULOSE FIBRE

Fast inwards diffusion of water.

Slower outwards diffusion of IL.

Outer section of dense regenerated cellulose that slows down the further diffusion of solvents, especially of the IL.
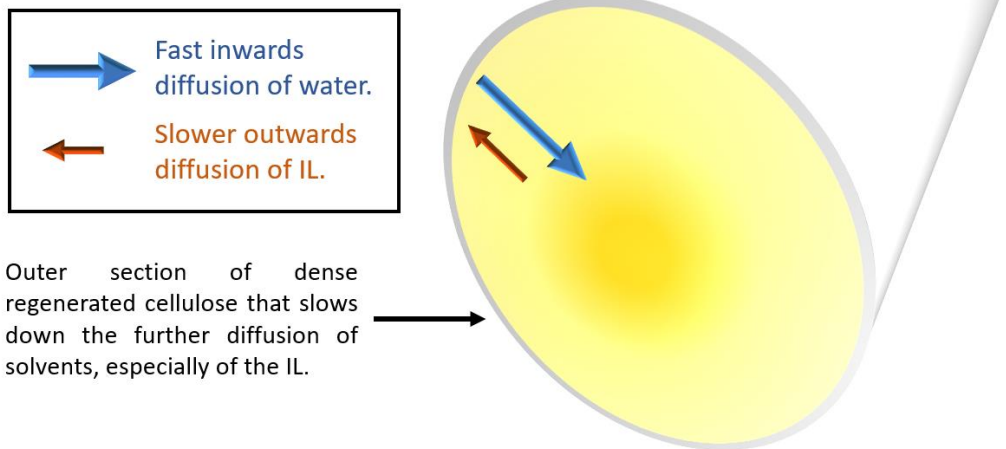
Figure 17. The direction of diffusion of the cellulose solvent (IL) and antisolvent (H_2O) over the cross-section of a cellulose fibre in the coagulation bath during a dry-jet wet spinning process. Cellulose in the outer section of the fibre regenerates almost instantly upon entering the coagulation bath. This outer regenerated network forms a barrier for the diffusion of the solvents, slowing down further regeneration inside the fibre.

In the Lyocell process, the inward diffusion of antisolvent (e.g. water) into the fibre is much faster than the outwards diffusion of the cellulose solvent, with a diffusion coefficient of one magnitude higher having been determined for H_2O compared to NMMO by Biganska *et al*.[89] According to the authors, this difference in scale is an expression of the highly hygroscopic nature of NMMO. Furthermore, the diffusion of water was found to be mainly independent of the pulp type used in the experiments, but dependent on the cellulose concentration in the dope. The diffusion constant of NMMO was shown to be inversely correlated with the cellulose concentration, as well as by the degree of regeneration of the cellulose filament. Initially, the diffusion is relatively fast, but along with increasing antisolvent concentrations, the diffusion of NMMO slows down. This slowing down of the diffusion of the cellulose solvent is only observed with good cellulose solvents like NMMO and [DBNH][OAc], and not in poorer solvents like [emim][OAc] and [TMGH][OAc], which have a fairly stable diffusion constant throughout the full diffusion process.[73] This slowing down in good solvents could be attributed to the formation of a gelatinous cellulose network – regeneration of the polymer on the outside portions of the fibre occurs after a certain amount of antisolvent is present around the cellulose chains. This newly formed cellulose network inhibits the movement of the solvent molecules, slowing down the diffusion process. Why such slowing down behaviour is

not seen with poor cellulose solvents, is most likely due to the presence of a gel-like cellulose network even prior to true regeneration of the fibres occurs in the antisolvent bath. In other words, good cellulose solvents are able to fully dissolve cellulose in the absence of antisolvent and are free to move around in the solution, while poor cellulose solvents do not truly dissolve cellulose, and hence are unable to freely move around the more gelatinous cellulose network (see section **2.2.2. Thermodynamics of cellulose dissolution** for definitions of good and poor solvents). The presence of a pre-existing gelation has implications for the orientation of the cellulose chains before regeneration. For example, the presence of a cellulose network prior to spinning inhibits the movement of the cellulose chains themselves, resulting in inferior mechanical properties.[73]

2.3.4. IONCELL-P

IONCELL-P (IONCELL-Pulp), a related process to IONCELL-F, is a fractionation process in which bleached wood pulp with a high hemicellulose content can be converted into a high quality dissolving pulp by treating it with a mixture of ionic liquid (IL) and water. The process has been shown to be highly reproducible, with average standard deviations in hemicellulose content of the resulting pulp being only 0,2 %.[86] One of the ILs usable in the IONCELL-P process is [DBNH][OAc], which is capable of fully dissolving cellulose and other assorted polymers in wood pulp, when the IL is pure. However, when it is mixed with 15 wt-% H_2O, it is capable of selectively dissolving most of the hemicellulose content (mainly xylans) of a 2-5 wt-% wood pulp load and leaving the cellulose chains largely unaffected. The IONCELL-P extraction was initially shown to be capable of producing pulps with hemicellulose content of 7,53 % from the birch kraft pulp, compared to the original hemicellulose content of circa 25 %. However, a hemicellulose content of 7,53 % is too high for the pulp to be considered of dissolving pulp quality, which is classified as having a content of less than 5 %. To prepare dissolving quality pulps with the IONCELL-P process, a number of pre-treatments such as enzymatic degradation by Pulpzyme xylanase or viscosity adjustment by H_2SO_4 are needed. How fast and effective the hemicellulose extraction is depends on the use of pre-treatments as well as the dissolved-pulp-to-IL –ratio. A higher amount of IL used leads to faster and more effective diffusion of hemicellulose to the liquid phase, leading to more efficient extractions. On the downside, this also leads to an unwanted increase in the amount of IL needed to run the process. The enzymatic degradation using Pulpzyme xylanase cocktail in conjunction with the H_2SO_4 treatment was shown to produce pulps, which after IONCELL-P extractions had hemicellulose

contents between 4,23-4,75 %. These values are low enough for them to be classified as high quality dissolving pulps. The dissolved hemicellulose can be recovered from the IL/water mixture and used in various applications ranging from films to pharmaceuticals.

Combining the pulp refining process IONCELL-P with the fibre spinning process IONCELL-F, both systems using the same solvent [DBNH][OAc], shows great promise as a means to obtain value added products in the form of regenerated cellulose fabrics from bleached birch kraft pulp. In effect the process is bringing together the paper and textile industries.[86] This study was also an attempt at cutting down on the recycling costs for the two processes, as the solvent systems of the IONCELL-P and -F could be recycled in the same plant. This consolidation of processes would lead to a more economical combined process both recycling-wise as well as logistics-wise. Improving the recycling efficiency is crucial not just to these two applications, but to most processes involving ionic liquids, as the initial costs of the solvents are currently still very high.

2.4. [P$_{4441}$][OAc] in cellulose processing

While neat [P$_{4441}$][OAc] does not dissolve cellulose, it is shown to be an effective cellulose solvent at temperatures exceeding 100° C when combined with a co-solvent. Holding *et al.*[70] explored the effect of co-solvent choice (DMSO, GVL) and concentration on the dissolution capacity of [P$_{4441}$][OAc] and found out that, out of the two co-solvents, DMSO was able to dissolve more cellulose at all co-solvent concentrations. The maximum dissolution capacity of DMSO was 20 wt-% cellulose and that of GVL was 15 %. Both of the maxima occurred at circa 30 wt-% co-solvent concentration, after which dissolution capacity linearly decreased until reaching 0 wt-% cellulose when approaching 100 wt-% co-solvent concentration. The effectiveness of GVL as a co-solvent was also tested with two other direct cellulose solvents [DBNH][OAc] and [emim][OAc]. Both of the solvents had their maximum dissolution capacity already at 0 wt-% GVL (15 wt-% [DBNH][OAc], 25 wt-% [emim][OAc]), but it was found that GVL suited [emim][OAc] much more than it did [DBNH][OAc]. The dissolution capacity of [emim][OAc]/GVL, at different co-solvent concentrations, conformed very closely to values obtained from a [emim][OAc]/DMSO system, albeit the final drop-off in dissolution capacity occurred at lower co-solvent concentration in GVL, reaching 0 wt-% already at 80 wt-% GVL concentration.[52] On the other hand, GVL worked more as an antisolvent with [DBNH][OAc], making the initial dissolution capacity of 15 wt-% drop to zero already at 50 wt-% GVL. The trajectory of the drop was also steeper than that observed with [emim][OAc]. Based on these results, and those presented in section **2.2.2. Thermodynamics of cellulose dissolution**, it can be said that while GVL is not thermodynamically as suited for the dissolution of cellulose as DMSO, it is a viable and easy-to-use co-solvent in conjunction with tetra-alkyl phosphonium ILs.

2.4.1. UCST in [P$_{4441}$][OAc]/GVL

The use of the concept UCST (Upper Critical Solution Temperature) is problematic in the context of cellulose dissolved in ILs. Hence, the thermoresponsive phase behaviour expressed by [P$_{4441}$][OAc] is here referred to as "UCST-like", and the matter is more thoroughly discussed in an earlier sections **2.2.2. Thermodynamics of cellulose dissolution** and **2.2.3. Thermoresponsive phase behaviour in cellulose solutions.** In addition, there has been further unpublished results, which point to an antisolvent driven mechanism for the peculiar phase behaviour of cellulose in these solutions.

Overall, the mechanism behind the sol-gel transition of cellulose in [P$_{4441}$][OAc]/GVL and the formation of gel-like particles is not fully understood.

The [P$_{4441}$][OAc]/GVL (as well as DMSO) solvent system shows peculiar phase change characteristics in a limited cellulose concentration range, where dissolved cellulose forms into spherical particles in the gel state, when the mixture is let to cool back to RT or below after heating. This has been described as UCST-like thermoresponsive phase behaviour by Holding.[10] Holding first observed that [P$_{4441}$][OAc]/GVL and [P$_{4444}$][OAc]/GVL only dissolved cellulose when heated to above 100° C and that the solutions turned cloudy when they were left to cool to RT.[10] This cloudiness turned out to be due to the formation of gel-like cellulose microparticles (**Figure 18.**). The DSC-analysis of a concentrated sample (20 wt-%) using DMSO as a co-solvent, revealed a clear one-step endotherm on mixing and an exotherm on demixing, while the analysis of a 12 wt-% sample with GVL indicated a more complex dissolution process. It was observed that a previously undissolved cellulose sample exhibited an exotherm on mixing when it was first dissolved (heated), but after it was let to cool down, it subsequently showed a clear endotherm during all consecutive heating cycles. While the consecutive endotherm signals were associated with a UCST-like sol-gel transition, the origin of the

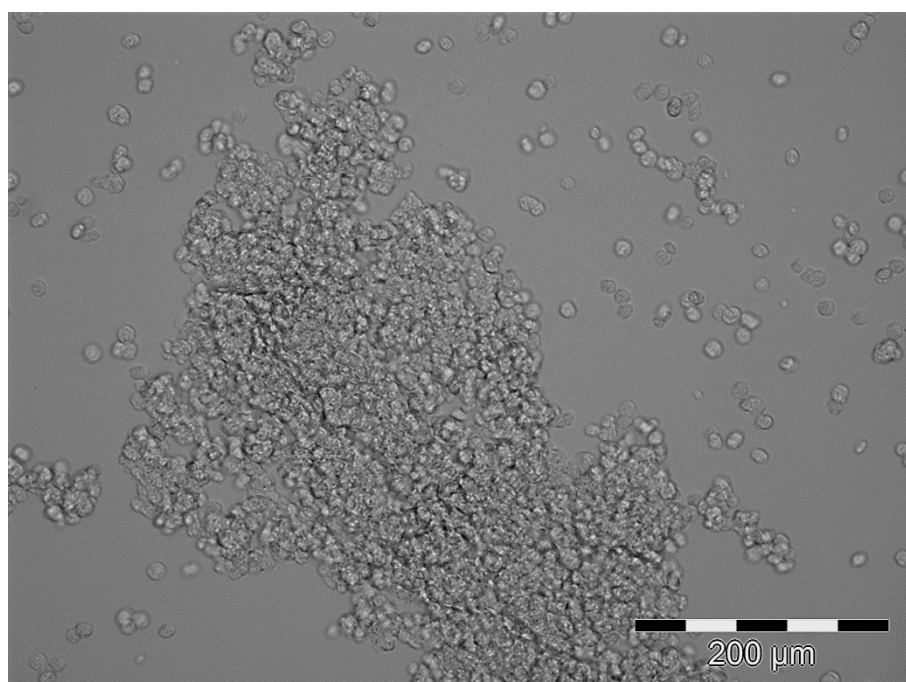**Figure 18.** Optical microscope image of the gel-like cellulose microparticles observed to have formed upon cooling of a solution of MCC in [P$_{4441}$][OAc]/GVL (30 wt-% GVL).

first exotherm, which was never found in any pre-dissolved samples, is uncertain. Despite lacking

direct proof, Holding reasoned accordingly: because the initial exotherm is not repeatable, in addition to dissolution of the polymer it might be composed of the breakage of crystalline regions as well as first time swelling and penetration of the cellulose fibres by the solvent.[10]

Holding explained that the occurrence of the UCST-like behaviour is at least partly due to neat [P$_{4441}$][OAc] being a "poor" cellulose solvent at low temperatures. This in turn is most likely due to several factors: lack of acidic hydrogen and lacking degree of hydrophobicity as well as ion-pair-separation. While the cation is bulky (and in the case of tetra-alkyl phosphoniums, hydrophobic), it is not as bulky as those of the [P$_{888R}$]-subfamily of ILs, which do not portray UCST-like behaviour. In larger phosphonium cations, the increased hydrophobicity likely leads to more favourable interactions with the intersheet cellulose dispersion forces. The presence of an acidic hydrogen has been shown to be favourable for cellulose dissolution,[90] and phosphonium cations not having such a hydrogen makes them conceptually worse cellulose solvents. The addition of a co-solvent to [P$_{4441}$][OAc] increases the anion-cation pair-separation to the point of actually leading to a negative ΔH_{mix} value at a certain constitution, which equals to both of the ionic species interacting more strongly with cellulose than individual cellulose chains do with each other.

While there have been observations of UCST-like behaviour for cellulose acetates in acetone[91] and in butanone,[92] according to Holding *et al.*,[70] this was the first occurrence of UCST-like phase behaviour of a underivatized cellulose in solution. de Oliveira *et al.*[93] recently published their findings on a system of MCC in [emim][OAc]/DMI, in which a closely UCST-resembling phenomena was observed with a change in temperature. In this case, turbidity manifests in the mixture when the concentration of the co-solvent DMI is relatively low, and the hot cellulose solution is left to cool. This turbidity closely resembles the particle formation in [P$_{4441}$][OAc] observed by Holding *et al.*[70] However, the systems are not exactly alike, as when the co-solvent concentration is higher (at least 70 wt-%), the electrolyte separates into two distinctly separate liquid phases. These phases can be divided into an upper co-solvent-rich layer and a lower IL-rich layer, where also cellulose is concentrated. In addition, there are previous observations of LCST-like behaviour of cellulose in cold aqueous NaOH.[94] In a similar system, the LCST-like behaviour observed by Medronho *et al.*[74] has been attributed to conformational changes of cellulose due to decreasing temperature. The favoured conformation of cellulose at lower temperatures is more polar, and hence it has better matching interactions with the polar solvent, water.

Holding studied the rheology and shear properties of the cellulose/[P$_{4441}$][OAc]/GVL mixture, and from the results he obtained the complex viscosity, the dynamic modulus and the sol-gel transition temperature.[10] In the case of the solvent system in study, the sol-gel state transition was expected to match the temperatures observed in the DSC-measurements. The point of transition from solution state to gel state was determined from the crossover point in the dynamic modulus. The dynamic modulus (stress to strain) obtained in the analysis is made up of the storage modulus, which describes the energy stored in elastic displacement, and the loss modulus, which describes the energy lost as heat. In the context of the dynamic modulus, the crossover point means the point in which the loss modulus equals the storage modulus in energy. Holding found that the phase transition temperature decreased from 105° to 75° C along with the increase of co-solvent concentration from 30 to 50 wt-% GVL – a point when UCST behaviour also disappears. The sol-gel transition temperature also increased from 70° to 135° C along with increasing cellulose concentrations (2-12 wt-%). The 9 wt-% cellulose concentration, which expresses phase-transition behaviour at the 75 – 110° C range (T$_{S-G}$), was deemed optimum composition for this system.

3. Particulate material from cellulose and other polymers

3.1. Polymeric microparticles

3.1.1. Synthetic microplastics

The use of synthetic, petroleum-based polymeric microparticles is widespread and commonplace in the modern industry. Their popularity is founded on the low price of the raw materials (oil), ease of manufacturing, chemical stability and their fundamental tunability. Due to their inherent stability in aquatic environments and lack of acute toxicity, they have been mostly considered environmentally benign. However, late findings of hidden negative properties of environmentally widespread plastic particles has raised plenty of concern among scientists and general public alike. It has also fuelled further study of their biological impact, the extent of usage in various industries and emission pathways into the environment, especially the aquatic ecosystems.[95] The adverse effects are elaborated on in section **3.1.2. Environmental impact and biodegradability of plastic microbeads**. The concerns raised have resulted in many governments, including USA, France, Italy, Canada, UK and Sweden, as well as multinational institutions such as the European Union banning or significantly restricting the use of plastic microbeads in cosmetic, personal care and hygiene products, abrasives, paints and coatings. However, most of the bans are only partial, for example being directed towards rinse-off personal care products only. The definition of a plastic microparticle used in the industry has been rather vague, with common definitions restricting it to particles smaller than 5 mm in diameter consisting of man-made polymeric materials. In the extent of this thesis, the terms microplastics, plastic microbeads and plastic microparticle are used synonymously. An example of 300 - 600 µm diameter plastic styrene-divinylbenzene microbeads is shown in **Figure 19**.

Figure 19. Plastic microbeads between 300 and 600 µm in diameter, consisting of styrene-divinylbenzene copolymer.

On request by the European Commission in 2017, Amec Foster Wheeler Consultancy Company conducted an exhaustive review on the previous ambiguous definitions, risk assessment, industrial applications as well as market and socio-economic analysis of intentional microplastics.[95] The report highlighted the widespread and voluminous usage of synthetic polymer particles in fields of application such as personal care products, paints and coatings, detergents, oil and gas industry, agriculture, industrial abrasives, pharmaceuticals, waste water treatment and construction. The functions of the microplastics in these applications include but are not limited to abrasives, emulsifiers, dispersers, binders, fillers, thickeners, density and rheology modifiers, flocculants, film forming and surface coating agents, insulators, aesthetics, glitters, polishers, crack inhibitors in paints, opacifying and anti-static agents, gellants, filters, absorbents and vessels for the controlled release of a substance. Overall the report estimated that a total of 10 000 to 15 000 tons of plastic microparticles are used in industry every year in the European Union region, but that the figures are careful estimates and could be significantly higher in certain fields of application. The most common polymers used in plastic microparticles include polyethylene, polypropylene, polytetrafluoroethylene, polyacrylonitrile, poly(styrene-acrylate) copolymer,

polymethylmethacrylate, polyurethane, polyamide, poly-ε-caprolactone and polylactide (**Figure 20.**). The largest fields of application by tonnage were the agricultural industry with 8 000 tons, the industrial abrasives with 1 000 - 5 000 tons and the personal care industry with 1 250 - 1 910 tons. Despite these stark figures, an atmosphere of voluntary change has been clearly visible in some parts of the industrial sector, with the personal care industry having lowered their usage of plastic microparticles by 82 % between years 2012 and 2015.

polyethylene	polypropylene	tetrafluoro-ethylene	polyacrylonitrile

poly(styrene-acrylate) copolymer	polymethyl-methacrylate	polyurethane

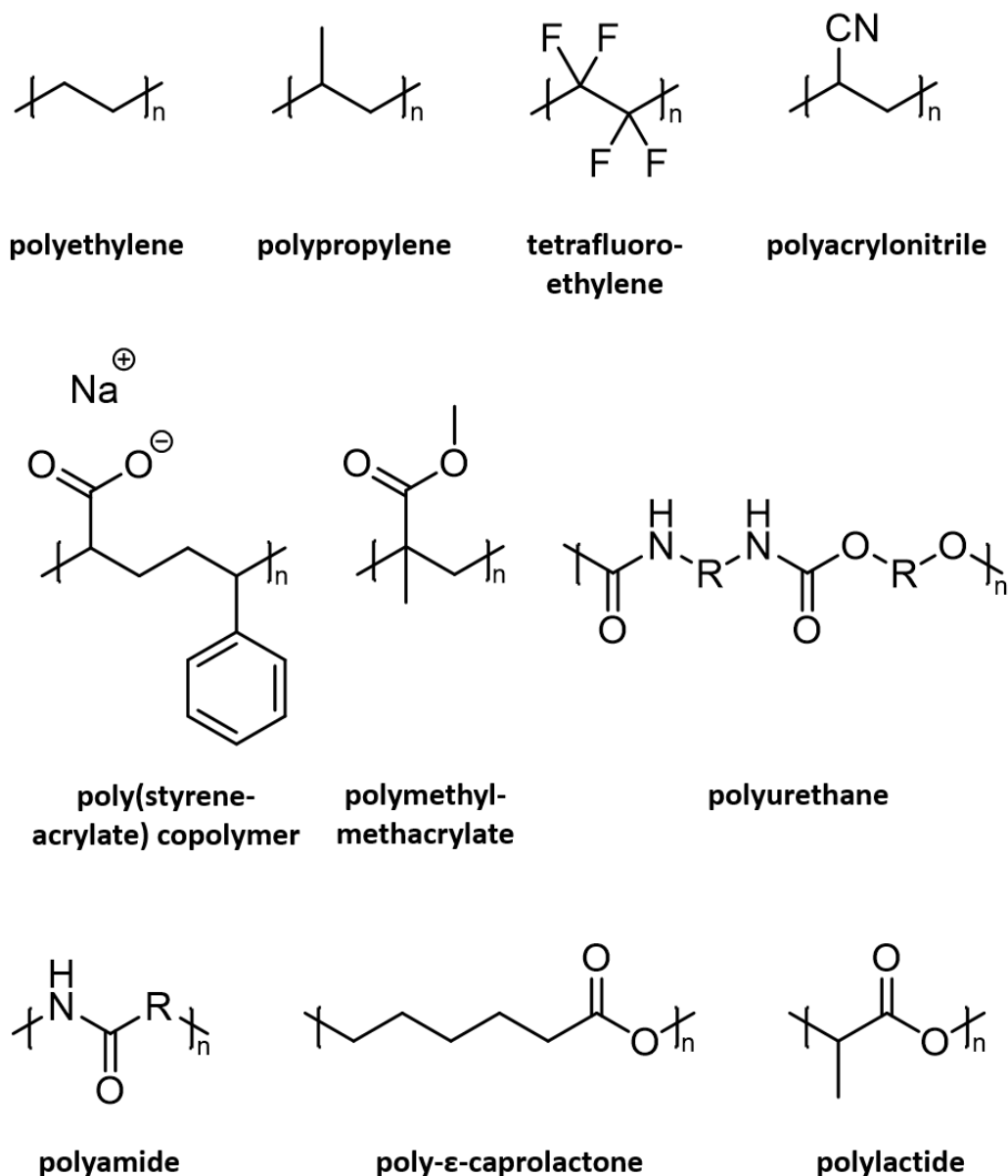| polyamide	poly-ε-caprolactone	polylactide

Figure 20. Chemical structures of common polymers used in commercial microplastics.

IUPAC defines a microparticle as "Particle with dimensions between $1 \cdot 10^{-7}$ and 10^{-4} m. (Note: The lower limit between micro- and nano-sizing is still a matter of debate.)"[96] The report by Amec Foster Wheeler[95] used the following working definition to describe microplastics: "Microplastics consist of man-made, conventional plastics. Microplastics also include biodegradable plastics, bio-based analogue plastics, and bio-based alternative plastics. Microplastics are solid and water-insoluble particles. Microplastics have particle size below 5 mm and include nanometer sized plastics as well as (nanoparticles)." However, the report highlights that the IUPAC definition of a microparticle suggests a minimum size of 100 nm for microplastics, which could prove useful in restricting future regulation to the substances intended (intentional plastic microbeads) and in establishing molecular level materials under their own legislation. For example, the particle size of microbeads used in personal care products in Denmark was found to vary between 2 μm (in toothpaste) and 1240 μm (facial cleaner) in diameter,[97] so including particles smaller than 100 nm under the same legislation would appear unnecessary from the practical point of view and could lead to undesirable complications in the future.

3.1.2. Environmental impact of plastic microbeads

Plastic microbeads have raised substantial attention in the academic circles and especially the mainstream media due to their significantly high abundance observed in the aquatic environment and the perceived negative effects they can have on the organisms in said environments. The microplastics are usually of similar size to plankton and other edible detritus available in an aquatic environment. Therefore, the particles are readily available and possible even tempting targets for ingestion by detritus-, filter- and suspension-feeding aquatic species.[98, 99] Humans can also be exposed to these microbeads either indirectly through the environment or directly via ingestion or inhalation. In addition, large-bodied, long-lived animals with comparatively slow metabolism can possibly accumulate considerable amounts of microplastics in their tissues.

In the report by Amec Foster Wheeler,[95] the number of microplastics per unit-volume or mass of water/sediment were listed from several locations within the EU. The highest in-water values were attained in the west coast of Sweden (100 000 particles/m^3, >80 μm), whereas the smallest reported values were measured in coastal water of Denmark (0,39 particles/m^3, >100 μm). Highest in-sediment values were determined in the Rhine river estuary in Netherlands (3 300 particles/kg of

dry sediment, >1 μm), while the lowest values were found in beach sediment in Belgium (14 particles/kg of dry sediment, no size reported). As can be seen from the data, the concentration of plastic microparticles in water and sediment varies widely, with very high values being reported near point sources such as microbead production facilities (Sweden). A conclusion that can be drawn from the data is that the high variability of the values in a geographically confined area suggests that either, nearby point sources are disproportionally important in determining the abundancy of microplastics in a location, or some external forcing is concentrating the particles in certain areas.

The interpretation of abundancy or biological effect -studies of plastic microparticles is not straightforward. For example, the variation in the size of particles used as the detection limit should be noted carefully when comparing values between separate locations. If two equal mass-concentrations of particles in the environment are considered, the one with large number of small particles would be viewed as more problematic compared to one with fewer large particles. The negative effects of microplastics can be analysed relatively independently in the laboratory, but tests based on actual environmental samples are more ambiguous to interpret. This ambiguity is a result of the uncertainty brought forth by the high number of possible harmful compounds the plastic particles could have absorbed from the environment, and the wide variety of possible plastic materials composing the microparticles. In addition, the shape of the particles could also have an effect on their biological activity, with some particles being spherical or fibrous by design, while others being more random in shape, having been derived from the breakdown of bulk plastic materials already in the environment. The partitioning of the microparticles between the water column and the sediment is also insufficiently understood, which brings further uncertainty to environmental tests.

The negative biological effects of microplastics on organisms can arise from the presence of a plastic particle in or on the organism (physical effects) or from the monomers, additives and environmentally absorbed compounds contained within the polymer matrix (toxicity). Some of the adverse physical effects observed on aquatic invertebrates included weight loss, decreased fertility and food ingestion rates as well as overall drop in reproductive output, while vertebrates experienced increased mortality rates, damage to the intestines and signs of liver stress.[95] Additionally, translocation of small sized microbeads (<10 μm) between intestinal cells and subsequent inflammation was observed in mussels. However, not all studies found adverse physical effects from exposure to microplastics, and it is uncertain what type and scale of an ecological

impact the possible adverse effects might have on the aquatic ecosystem in general. The toxic effects of a plethora of possible additives and absorbed compounds are even harder to elucidate, but some studies have found that the inclusion of microplastic particles (400-1300 μm, 0,074 wt-% in dry marine sediment) pre-absorbed with polychlorinated biphenyls increased the accumulation of these compounds in burrowing lugworms by a factor of 1,1-3,6 compared to contaminated sediment without microbeads.[100]

Overall, the ecological properties of non-biodegradable microparticles are very poorly understood. Hence, it must be stressed that more studies on the environmental abundancy and extent of microplastics, their environmental transport mechanisms and the range, magnitude and type of biological effects they might have on living organisms are needed to illuminate the scale and nature of the impact man-made particulate plastic pollution has on the natural environment.

3.1.3. Environmentally friendly replacements for microplastics

The primary negative attributes of synthetic microplastics are their non-biodegradability, accumulation in the environment and their possibly toxic nature. These qualities have caused widespread concern on their use in commercial and industrial products, which has precipitated growing interest in the industrial sector for finding more environmentally acceptable, preferably biodegradable alternatives. IUPAC[96] defines biodegradable polymer as "qualifier for macromolecules or polymeric substances susceptible to degradation by biological activity by lowering of the molar masses of macromolecules that form the substances." and polymer degradation as "Degradation that results in undesired changes in the values of in-use properties of the material because of macromolecule cleavage and molar mass decrease." It should be noted in the context of plastics, that the term bioplastics and bio-based polymer are almost wilfully misleading; the material produced (plastic) does not differ in any way or form from a similar material made out of fossil fuels. The only difference is the source of the raw material (biomass vs. oil/gas). While the use of biomass as a raw material can beneficial in itself, the behaviour of the particles produced and their impact on the natural environment is identical and equally problematic to ones produced from fossil fuels. Hence, bio-based polymers should not be separated from their petroleum-based counterparts when the environmental impact of a class of microparticles as plastic pollution is considered.

Especially the cosmetics industry has been active in finding environmentally sound alternative materials for synthetic polymers in scrubbing agents, with future or already implemented ones including ground apricot kernels, walnut shells and poppy seeds, cornmeal, seaweed, clay, pumice, silica, various waxes and bio-based polymers such as PLA.[95] The various ground shells, pits, seeds and kernels are already well established in the industry, having been in use for decades. Particularly walnut shells, which are biodegradable, readily available in sufficient quantities and induce no known adverse effects beside nut-allergies, have been proposed as a viable replacement. However, even while faced with the seemingly apparent notion that walnut shells would not interact adversely with the environment or humans, the fact that no experimental studies exist on the environmental impact of widespread use of walnut, should not be dismissed out of hand. The dark colour of walnut also poses problems in fair-coloured creams and, as a directly biomass-derived material, walnut can lower the shelf-life of a product, possibly even needing a separate sterilisation process. Glass is another potential candidate for replacing plastic microparticles in various applications. Glass beads have seen widespread use in the reflective paints in road markings, with the top three European companies totalling 200 000 tons of yearly production capacity.[95] Compared to plastic microbeads, glass beads are proposed to be environmentally friendly, but their almost total lack of elasticity limits their applicability to many of the functions plastic microbeads are utilized in. Similar limitations apply to other silica-based particles. Overall, none of the alternatives proposed offer the same kind of visual attractiveness or customizability as spherical plastic beads. Some of the alternatives are also decisively non-spherical or even ragged with sharp edges, making them non-applicable to certain products such as hand creams, where the smooth ball-bearing effect of spherical particles is the fundamental aspect of their functionality and appeal.

Some of the largest cosmetic manufacturers (such as Beiersdorf, Clarins and Shiseido) have expressed interest in replacing the plastic microbeads in their products with cellulose-based alternatives.[95] Greenpeace Asia surveyed the top 30 personal care companies based on revenue (2015) and found that six of those companies already implemented particles of cellulose or its derivates in their products.[101] In their responses however, none of the companies demonstrated genuine determination in phasing out all types of microplastics used in their product line or they were otherwise vague in their goals and the definitions of microplastic particles to be replaced. Furthermore, the origin, molecular weight or possible chemical modifications of cellulose were rarely mentioned, with most companies merely referring to the alternative materials as cellulose.

The only specific type of cellulose material mentioned was cellulose acetate also known as cellophane (**Figure 21.**), which is well established in the industrial sector as a material with many plastic-like qualities.[102] One example of cellulose acetate used as an exfoliating microbead in personal care products is CelluloScrub by Lessonia.[103] The primary attractive features of using cellulose in microparticles is the biodegradability and apparent environmental non-toxicity of the material. Moreover, the availability and number of cellulose sources is greater, more varied and
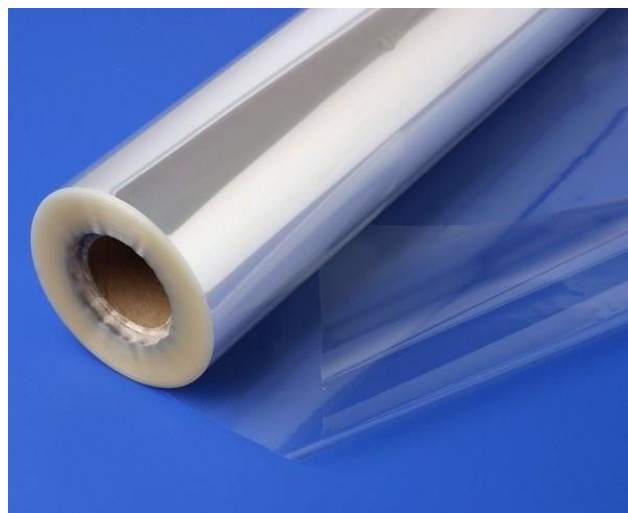
Figure 21. A roll of cellophane sheet, a plastic-like cellulose acetate used widely in the industrial sector, especially in packaging. Picture used with permission from Wikimedia Commons.[136]

the material is relatively more tuneable compared to other proposed biomass-based materials (shells, seeds, kernels). Nevertheless, in light of the practically non-existent literature on the environmental impact of widespread use of cellulosic microparticles (especially cellulose acetate), the benign nature of cellulose materials should not be presumed. Similarly to the walnut shell example mentioned in the previous paragraph, more thorough testing is needed to confirm the environmentally innocuous nature of cellulose based microparticles. Despite the lack of scientific proof, it is evident to see that cellulose-based microbeads offer a readily biodegradable alternative to synthetic plastics, with equivalent strength, abrasion and density properties, similar tunability and aquatic stability – cellulose presents a feasible way to phase out the oil-based microbeads. Various potential cellulose-based particles and their synthesis methods described in scientific literature are presented in the following sections.

3.2. Cellulose microparticles

The synthesis of cellulose-based particles of a wide range of sizes, shapes and types of chemical derivatisation have been reported in the scientific literature. These materials can essentially be divided into two, first by type of cellulose used (modified or un-modified), and second by the technique used to produce the beads (top-down or bottom-up). The wide range of possible derivatisation reactions affords a multitude of chemically modified cellulose derivates, with common ones being cellulose acetate, carboxymethylcellulose and methylcellulose. Depending on the degree of substitution, the chemical and physical properties of these derivates can differ significantly from those of unmodified cellulose. For example, chemically modified cellulose derivates are usually much more soluble in conventional organic solvents, while unmodified cellulose is largely insoluble in most available solvents (notable exceptions being NMMO·H_2O, cold aq. NaOH and numerous ionic liquids). This insolubility greatly limits the applicability of pure cellulose to many bead forming techniques. Most successful approaches rely on reducing the size of larger preformed solid particles by either mechanical grinding or enzymatic and acidic hydrolysis (top-down), or alternatively precipitating cellulose from solutions of the few viable solvents (bottom-up). Several cases of cellulose bead production are described in the following paragraphs, with special emphasis given to bottom-up methods using either modified or unmodified cellulose.

3.2.1. Chemically modified cellulose microbeads

The chemical derivatisation of cellulose usually entails various substitution reactions at the three reactive hydroxyl groups of cellulose, transforming them to esters, ethers, thiols or xanthates. The alcohol functionality at C6 can also be oxidised to a ketone, aldehyde or carboxylic acid. These cellulose derivates can then be dissolved in various solvents with relative ease and subsequently formed into beads using a range of techniques. For example, porous cellulose beads with an average diameter of 100 μm were prepared from cellulose triacetate by solvent evaporation method.[104] First cellulose triacetate was dissolved in dichloromethane along with a diluent (varying long chain alcohols), subsequently water was added to form droplets and finally dichloromethane was evaporated to leave the precipitated beads in suspension. These beads can be used in ion exchangers and gel chromatography, for example.

Cellulose acetate beads (DS = 2,5) of roughly 10 µm diameter were formed by dissolution of cellulose acetate in ethyl acetate/methanol solvent mixture, which was in turn dispersed in aqueous surfactant solution using high speed mechanical mixing (Ultra-Turrax).[105] The volatile compounds were evaporated from the mixture, and following the subsequent washing and centrifugation workup-steps, the cellulose acetate particles were isolated. Similar cellulose diacetate beads in the hundreds of µm scale were formed by first dissolving the cellulose diacetate in DMSO, then dropping the dope into an acid bath in a dropwise manner, and subsequently cross-linking the precipitated beads with epichlorohydrin.[106] Cellulose beads in the micrometre scale (10^{-6} m) have also been fabricated by the reductive amination of 2,3-dialdehyde cellulose beads with diamines.[107]

3.2.2. Cellulose composite microbeads

Cellulose beads can also be produced in conjunction with various added materials, resulting in a composite material. Some of the more simple ways to produce cellulose composites is to precipitate cellulose from a dope along with one or more dissolved polymers, or by mixing solid additives such as metallic powder into a cellulose dope. These materials have the benefit of being easily tailorable in many of their physical attributes by simply changing the ratio of the components used in their making. As an example, porous cellulose beads composed of pure cellulose or a mixture of cellulose and either of hydroxypropylmethylcellulose, a copolymer of ammonium methacrylate and other acrylates, or triethylcitrate for use in cosmetics industry have been patented.[108] In this patent, dry cellulose and other solid components are first thoroughly mixed before 50-75 wt-% water is added. The formed slurry is mixed again to form a granulate, which is then dried to produce the beads, with bead diameters being in the range of hundreds of micrometres. Despite the bead's design resembling that of various regenerated cellulose materials (such as the Freeze-dried Cellulose Beads (FDCB), described in the experimental section of this thesis), the preparation process of mixing undissolved solids with water to form the beads results in cellulose remaining in its original morphology. Hence, from the viewpoint of the cellulose raw material this method is a top-down method, as the material produced has not been regenerated or mercerized during the bead forming process.

Kobo Products, Inc. sells porous cellulose beads (Cellulobeads) with diameters between 5 and 200 μm for use in make-up and other cosmetic products.[109] These beads are prepared by mixing an aqueous solutions of sodium polyacrylate and of viscose, heating the mixture to 80° C, hydrolysing the mixture with acid and finally washing with water.[110] The beads are then modified by addition of iron, titanium or aluminium oxides for colour, by surface treatment with triethoxycaprylyl silane or isopropyl titanium triisostearate for increased hydrophobicity or by potassium succinate for moisture retention. Cellulose coated charcoal beads with immobilized heparin are used in the purification of blood coagulation factors and lipoprotein lipases.[111] These composite beads were formed by first dissolving cellulose in 1-butyl-3-methylimidazolium chloride [bmim]Cl and imidazolium heparin in 1-ethyl-3-methylimidazolium benzoate [emim][ba], and then mixing these solutions together along with charcoal beads. Ultimately, this mixture is dropped into an ethanol bath to immobilize the cellulose onto the charcoal beads.

Yu et al.[112] prepared millimetre-scale magnetic beads by adhering $CoFe_2O_4$ nanoparticles onto the surface of cellulose beads. Likewise, Luo et al.[113] produced millimetre sized magnetic cellulose beads by making a composite of cellulose with magnetite (Fe_2O_3) nanoparticles and activated carbon (**Figure 22.**). The beads were prepared by dissolving cellulose in cooled aqueous NaOH (7 wt-%)/ urea (12 wt-%), mixing in the magnetite and charcoal, and subsequently adding said mixture dropwise into an aqueous 10 wt-% NaCl bath. The authors studied the absorption of organic dyes
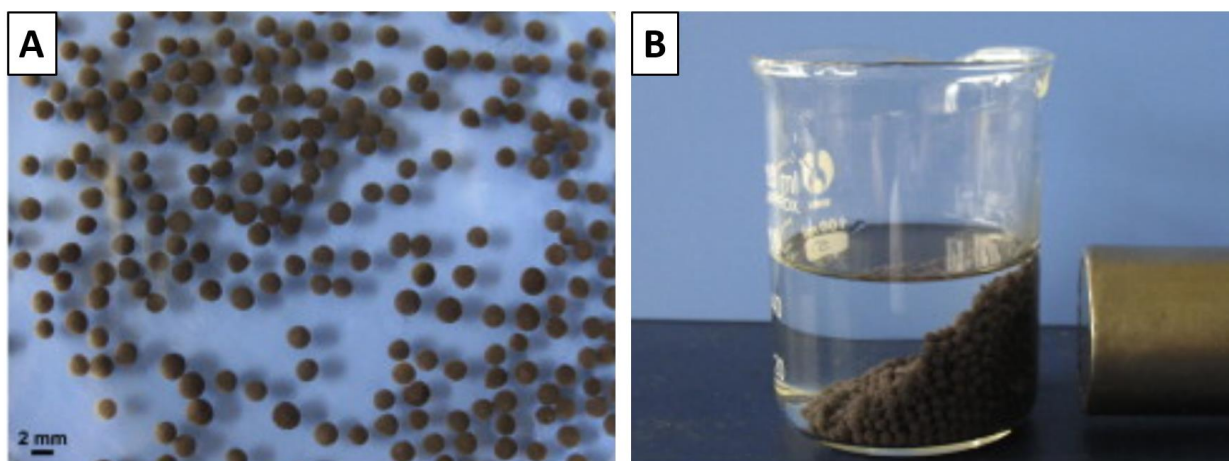
Figure 22. Magnetic cellulose beads prepared by dropwise regeneration of cellulose dissolved in aq. NaOH/urea with magnetite and charcoal additives.[149] **A:** The general appearance of the beads greatly resembles that of metal-composite beads prepared in the experimental section of this thesis. **B:** The magnetic susceptibility of the cellulose beads is evident from their attraction to the permanent magnet held to the right of the beaker. Figure modified with permission from "Luo, X. & Zhang, L. *Journal of Hazardous Materials* **171**(1) 2009 340." Copyright 2009 Elsevier.

onto the beads and found the absorption of dyes from aqueous solution into the magnetic cellulose beads highly efficient. The beads and findings were very similar to those obtained in the experimental section of this thesis. Luo *et al.*[114] were also able to produce smaller scale magnetic particles by a using a dispersion method. The method is based on the co-precipitation of aq. cellulose and magnetite nanoparticles from a dispersion in paraffin oil by the addition of 10 wt-% HCl.

The use of magnetite-cellulose composite beads for wastewater treatment would be highly advantageous. The high adsorption capacity of cellulose material towards a range of organic and inorganic compounds, such as dyes and heavy metal ions, is enhanced by the improved electrostatic interaction afforded by the embedded magnetite nanoparticles. In the case of particles produced by Luo *et al.,*[113] the addition of activated carbon nanoparticles can be used to further emphasize these adsorption capabilities. Moreover, once the beads have been saturated relative to the absorbed compounds, they can be removed from the solvent media by exploiting the high magnetic susceptibility of the magnetite nanoparticles.

3.2.3. Chemically unmodified cellulose microbeads

The chemical modification of cellulose and the production of various composite materials opens up multiple avenues of future research and a plethora of possible cellulose materials for a number of applications. Despite these obvious varietal benefits presented by the combinatorial nature of chemically modified cellulose-composite materials, the preparation of materials composed solely of unmodified cellulose gives the most information about the intrinsic properties of the biopolymer and usually the fastest process step-by-step from biomass to a usable material. The use of unmodified cellulose also retains many of the beneficial properties of the polymer, such as chemical and hydrolytic stability, biodegradability and amphiphilicity. To give an example of a production method, highly porous cellulose beads were produced from regenerated cellulose derived from paper waste.[115] Initially cellulose was mercerised in NaOH (12 wt-%), then dissolved in 1-allyl-3-methylimidozoium chloride [amim]Cl, and finally precipitated into a water bath by dropwise addition of the dope from a syringe. Sigma Aldrich has sold aqueous suspension of highly porous cellulose beads, ranging in size from 50 to 250 µm.[116, 117]

Trygg *et al.*[118] studied extensively the preparation of pure cellulose beads using an aqueous NaOH/urea solvent system. The porous cellulose beads were prepared by dissolving 4-6 wt-% cellulose in aqueous NaOH/urea and precipitating the cellulose in either a nitric acid or NaCl bath in a drop-wise fashion. The authors observed the presence of a skin-core structure in the beads when the acid concentration in the coagulation bath was above 0,5 M. The thickness of the skin did not show a notable increase between 2 and 6 M acid concentration (circa 3-6 μm), but at 10 M the skin was observed to be already 50 μm thick. Nah *et al.*[119] also observed a formation of a skin-core - structure in the synthesis of PLGA nanoparticles by way of dialysis – the skins were 40-50 nm thick, while the cores ranged from 100-300 nm (beads of varying size). Furthermore, precipitation of cellulose in the Lyocell process has been shown to form a skin-core structure radially within the fibre, which affects the resulting material qualities of the fibre.[8] In the case of the cellulose beads,[118] the coagulation process of the cellulose beads also seemed to differ somewhat at different pH: the surface of the beads at higher acid concentration appeared to show nucleation centers, whereas at lower acid concentration the coagulation seemed to happen evenly along the bead surface. The authors suggested that some competing coagulation mechanism (to diffusion) was at play in the more acidic conditions.

After the skin formation, the coagulation process inside the bead is more diffusion controlled and significantly slower than on the surface. In the case of the nitric acid bath, the diffusion of acid into the bead neutralizes the base, which causes the cellulose to precipitate. The coagulation mechanism is roughly similar when using a NaCl bath, but instead of neutralization, the cause of cellulose precipitation is the dilution of the cellulose solvent (NaOH/urea) inside the bead. Beads formed in low acid concentration (0,5-2 M) had larger fibril aggregates and rougher surfaces inside the beads compared to those formed in higher acid concentration (6-10 M). When the acid concentration is higher and the concentration and diffusion gradient is larger, the diffusion of the neutralizing and diluting species into the cellulose bead is faster. This can explain the differences in aggregate size inside the bead, as at lower acid concentration the coagulation of cellulose is slower. This way more cellulose is able to aggregate together to form larger fibrils and the specific surface area inside the bead is minimized. This aggregation is hindered by the faster diffusion at higher acid concentration. A changing cellulose concentration was also shown to have a slight effect on the inner structure of the bead. The outer parts of the core immediately under the skin were denser and the core displayed fewer and smaller pores, when the cellulose concentration in the solution was 6 wt-%

71

rather than 4 wt-%. This can be explained by the roughly equivalent bead diameter, which in the case of dropwise addition of solvent into a coagulation bath is mostly gravity and viscosity controlled. Obviously when there is a 50 % increase in cellulose content (from 4 to 6 wt-%) in the same volume, the structures formed will be denser. The method was developed further and the drug releasing properties of the cellulose beads (**Figure 23.**) were studied by Yildir *et al.*[120]
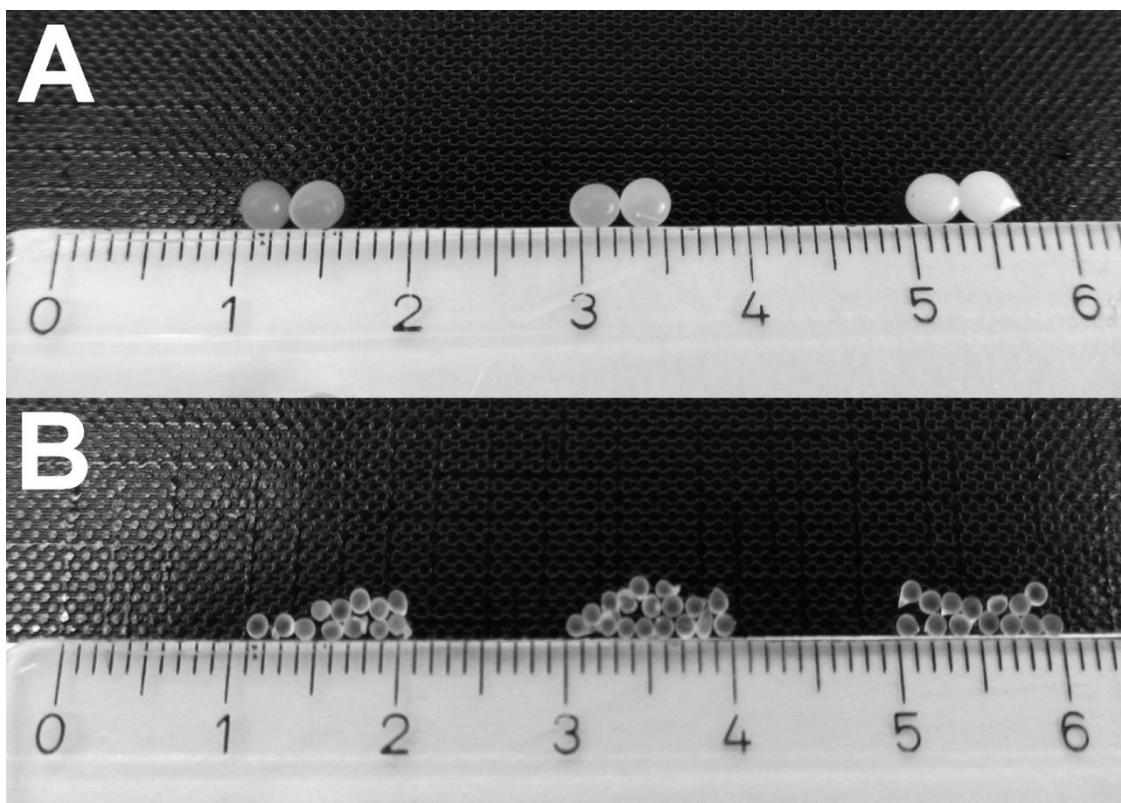
Figure 23. Cellulose beads prepared by dropwise addition of cellulose-NaOH/urea (aq.) dope into a nitric acid coagulation bath.[153] Beads pictured above (**A**) are wet and swollen, while those below (**B**) have shrunk during air-drying. Note that the dried beads are somewhat transparent, but not to the same degree as ones prepared in the experimental section of this thesis. Figure reused with permission from "Yildir, E., Kolakovic, R., Genina, N., Trygg, J., Gericke, M., Hanski, L., Ehlers, H., Rantanen, J., Tenho, M., Vuorela, P., Fardim, P. and Sandler, N. *Int. J. Pharm.* **456**(2) 2013 417" Copyright 2013 Elsevier.

In a study by Omura *et al.*[121], porous cellulose beads in the 10-100 μm range were prepared by solvent releasing method (SRM), with the aim of drug and other solute carrier in mind. Cellulose (7 wt-%) was dissolved in [bmim]Cl with DMF as co-solvent for viscosity reduction. The study was based on prior published multiple step solvent releasing method by the same authors.[122] First 0,2 g of dope is mixed with 2 g of hexane along with surfactant VPS-1001 by using a homogenizer (for the working principle of a homogenizer see section **3.3.4. Cellulose nanofibers by mechanochemical**

processing). Then the dispersion is introduced into an excess of 1-butanol to remove solvents, washed three times with 1-butanol to ensure solvent removal and finally solvent exchanged to water, toluene or acetone. The beads shrink in size and the porosity is decreased during drying, as expected. The closing of the outer pores can be beneficial, when the drug carrier aim of the study is considered. While wet, the porous particles incorporate any small solutes dissolved in the solvent medium without any noticeable discrimination. Hence, when the pores close during drying, both hydrophobic and hydrophilic compounds can be encapsulated within the material. The compounds used to study the encapsulation were non-volatile hydrophobic compounds and hydrophilic fluorescent dyes (Rhodamine B and Nile Red). The beads were dried from acetone using a supercritical CO_2 drying method. The authors did also prepare larger, 1 mm scale, cellulose beads by dropping the dope from a syringe into 1-butanol. This was followed by washing the beads with 1-butanol, solvent exchanging into water, subsequently encapsulating various compounds into the cellulose matrix and finally vacuum drying the beads. The fluorescent dye soaked beads (1 mm) were cut after drying, and the spread of the dye was shown to be uniform. The release of the dyes from inside the dried beads into water or toluene was tested by simple soaking of the beads and measuring the amount of dye released by an UV-vis spectrometer. Rhodamine B release into water plateaued at around 80 % cumulative release (from all encapsulated dye determined in a previous step) while Nile Red release into toluene reached an end point already at 10 % cumulative release. This much lower release percentage is contributed to the apparent absence of complementary interactions between toluene and cellulose, which are present between water and cellulose at least to some degree. The authors were able to limit and slow down the release of Rhodamine B by coating the beads in PMMA. The authors also managed to make disk-like cellulose beads in a further study.[123]

Druel *et al.*[124] reported in a conference abstract that they have managed to make cellulose aerogel beads from a MCC/[DBNH][CO$_2$Et] dope using a jet-cutter apparatus to cut a stream of dope before it enters a ethanol bath. The wet beads were then dried using supercritical CO_2 drying. Lin *et al.*[125] prepared cellulose beads by dropwise addition of cellulose dissolved in NaOH/urea/H_2O (4 wt-% cellulose) into an acidic coagulation bath (5 wt-% aq. HCl + 5 wt-% CaCl$_2$) and subsequent washing with excess water. Beads from both of these cases closely resemble ones obtained in the experimental section of this thesis. In the study by Lin *et al.,* the wet beads were freeze dried and some were TEMPO-oxidized prior to drying (TEMPO = 2,2,6,6-tetramethylpiperidine-1-oxyradical,

final carboxylate content 0,96-1,27 mmol/g). The crystalline morphology of the beads was studied before and after TEMPO-oxidation by WAXS and the crystallinity index of the material (cellulose II) was observed to remain unaffected. The TEMPO-oxidized beads demonstrated increased porosity on their surface, but remained otherwise intact and unaltered in appearance. Similarly to Omura *et al.*,[121] the beads were also impregnated with various cationic dyes to study their suitability in removing organic dyes from industrial wastewater (**Figure 24.**). After dyeing, the TEMPO-oxidised beads (CB-3h and CB-6h) were significantly darker in colour compared to the un-oxidized beads (CB-0h), which illustrates the increased affinity of the slightly anionic cellulose towards the cationic dyes. The authors were able to desorb the dyes out of the TEMPO-oxidized beads by exposing them to slightly acidic conditions, which allowed the beads to be recycled for use in further adsorption cycles. However, the bead's adsorption capacity diminished noticeably and consistently after each cycle.
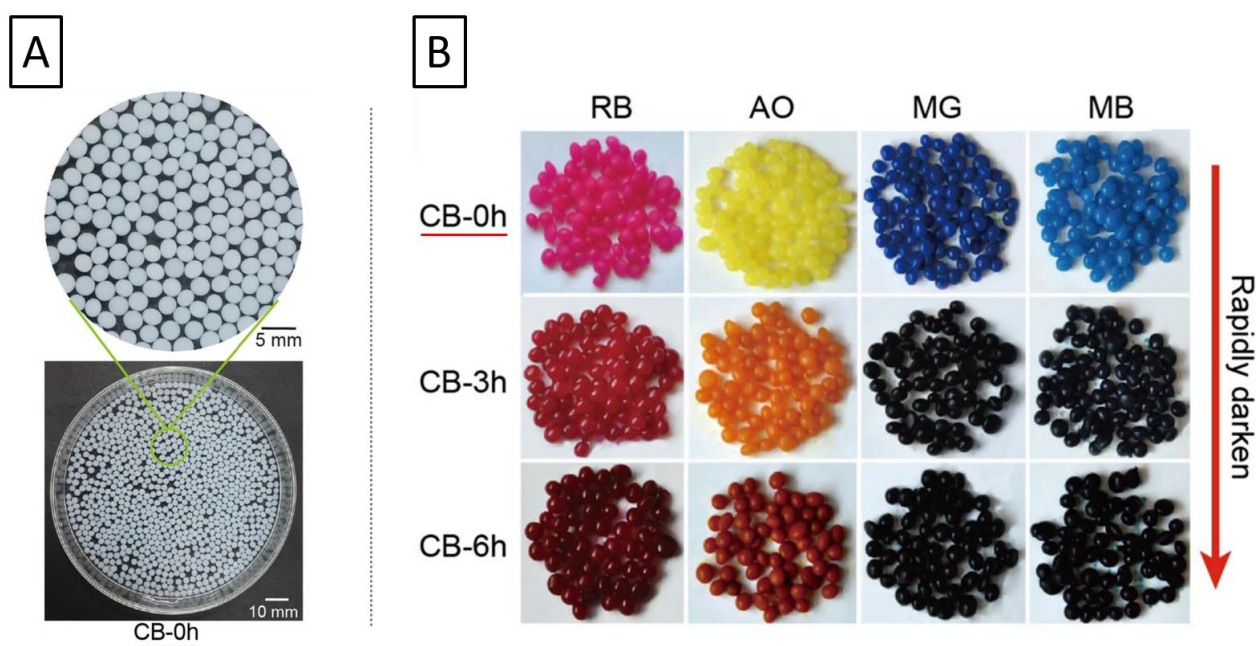
Figure 24. A: Cellulose beads prepared by dropwise addition of cellulose-NaOH/urea (aq.) dope into a nitric acid coagulation bath.[125] **B:** The same beads after adsorption of various organic dyes (**RB** = Rhodamine B, **AO** = Auramine O, **MG** = Malachite Green, **MB** = Methylene Blue). CB-0h beads (underlined in red) are pure regenerated cellulose, while CB-3h and CB-6h have been TEMPO-oxidized. Figure modified with permission from "Lin, F., You, Y., Yang, X., Jiang, X., Lu, Q., Wang, T., Huang, B. and Lu, B. *Cellulose*, **24**(11) 2017 5025." Copyright 2017 Springer Nature.

Carrick *et al.*[126] prepared smooth transparent cellulose beads in the millimetre scale, with surface roughness in the nanometre scale, by dropping a cellulose/LiCl/DMAc solution from a needle into an antisolvent bath. The procedure was based on a previous study by the same authors, in which

hollow cellulose "bubbles" were precipitated by introducing a gas-saturated drop of dope into an antisolvent.[127] Afterwards they were dried in air and acylated by reacting with undecenoyl chloride for the purpose of using them as adhesion testing material. Lower surface tension was shown to be beneficial for the droplet's ability to penetrate the antisolvent surface, and the authors singled out ethanol as their antisolvent of choice.[126] The formation of prominent "tails" on the beads was apparent already at 2 wt-% cellulose concentration in LiCl/DMAc (compared to the 7-8 wt-% observed with cellulose in [DBNH][OAc]/DMSO in the experimental part of this thesis, see section **4.3.6. Tails of beads**). Concentration of 1 wt-% and lower resulted in buckling of the particles during drying.

The authors discovered that the presence of a layer of LiCl/DMAc, which had phase-separated from the ethanol during the diffusion process, played a role in reducing the resulting roughness of the bead surface when the beads were held in the bottom layer of the bath for 24 h. The beads remained solid in this LiCl/DMAc layer, but more than likely a certain amount of restructuring of the cellulose material took place, especially on the surface. However, when the final dope concentration (LiCl/DMAc + cellulose) in the antisolvent bath was reduced from the usual 9 wt-% to 1 wt-%, there was no visible phase separation and the resulting beads had a higher surface roughness. Rewetting some of the already smooth beads with THF and subsequently evaporating the solvent decreased the surface roughness even further from 6,3 nm to 2,0 nm. The same roughness decreasing behaviour was not observed when the beads were solvent exchanged from ethanol to THF prior to drying and subsequently dried from the same THF. Neither was the roughness decreased when the beads dried from ethanol were rewetted and subsequently dried with further ethanol. THF in itself did not work as an antisolvent in this system, as the beads aggregated into non-spherical particles during diffusion. The authors did not give an explanation for the surface smoothing effect of THF. From prior trials outside the extent of this thesis, on swelling microcrystalline cellulose using cyclic ethers (such as THF), the author found that a certain amount of swelling is apparent when MCC is subjected to these solvents. This swelling-effect could be the result of the complementary intermolecular interactions these hydrogen bond-acceptor compounds have with cellulose functionalities, both the hydrophilic hydrogen bonds and the hydrophobic van der Waals and C-H···O-interactions. This would be supported by the adequate Kamlet-Taft net-basicity (β-α) of THF (0,55),[78] which lies reasonably close to values from known cellulose solvents such as [emim][OAc].[57]

3.3. Cellulose nanoparticles

The preparation of nanoscale cellulose and other polymeric particles is addressed in this chapter. First, some general aspects of the history of nanoscience, the properties of nanomaterials and definition of a nanoparticle are discussed. Next, some traditional methods of preparing cellulose nanoparticles and the two most common morphologies of cellulose nanoparticles (fibre and sphere) are covered. Finally, two alternative methods (nanoprecipitation and dialysis, both in common use with synthetic polymers) for the possible preparation of cellulose nanoparticles are described.

3.3.1. Nanomaterials

The prominence of nanomaterials and nanoscale structures in research papers from the field of chemistry, physics, materials science and medicine has grown substantially during the last two decades. This development is self-evident, when observing the use of the word "nano" in the scientific literature (**Graph 1**). The occurrence of the word "nano" in a SciFinder search is shown as a function of the year of publication between 2000 and 2017. The more than twenty-fold increase in the occurrence of the word mirrors the growing interest towards nanoscience and the establishment of new terminology in the scientific community. In essence, the concepts of nanoscience and nanotechnology refer to objects with some of their dimensions or properties
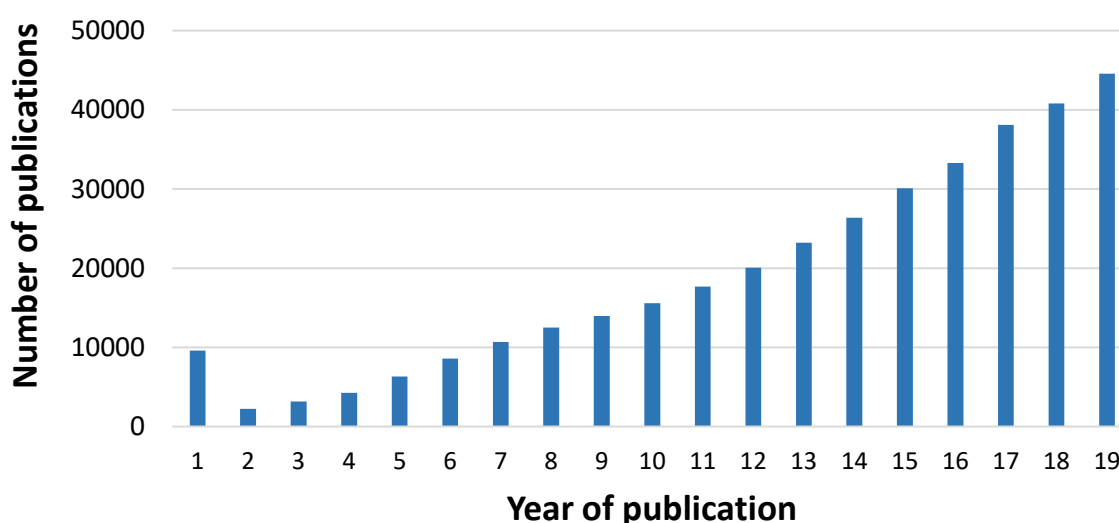
Graph 1. Number of hits occurring in the results of a SciFinder-search of publications from years 2000-2017, while using the word "nano" as the search term.

measurable in nanometres (10^{-9} m). The physicist Richard Feynman is considered to be the father of the concepts, which he portrayed in his 1959 talk "There's Plenty of Room at the Bottom", the transcript of which was later published in Caltech's Engineering and Science magazine in 1960.[128] Ultimately the ideas conveyed by Feynman led to the emergence of the fields of nanoscience and nanotechnology. However, it took a while for these ideas to take root, as what can be called modern nanoscience only took off following advances in the field of electron microscopy, which enabled scientist to glimpse at individual atoms for the first time in 1981.

The manifestation of a variety of novel attributes makes nanomaterials a highly intriguing subject for future research. Nanomaterials possess physical, chemical, and quantum mechanical properties and demonstrate phenomena unseen in macroscopic materials or in the solution state. The newly emerging physical, electrochemical, catalytic, mechanical, biological and optical behaviours, attributed to the presence of nanoscale structures, usually result from changes in phase boundary characteristics, in electrochemical environment of chemical moieties or in surface area. The nanoscale structure responsible for the changes can be the diameter of a particle or a fibre, the thickness of a coating or a film, or the porosity of a matrix. Scientists in the early parts of the 21st century were mostly approaching the subject of the preparation of nanoscaled materials from top-down, carving larger objects down to the nanoscale. However, more recently the focal point of nanomaterials research has shifted towards trying to find ways to build nanostructures from bottom-up. That way many of the characteristics of a material can be more efficiently tuned for the situation at hand. Despite these advances and the implementation of new nanomaterials in a large number of modern innovations, such as water repellent coatings and nanomedicines, scientists believe that they have only been able to discover the so called "tip of the iceberg". Many new findings have not yet been properly studied, and even more are still likely to be fully unknown to modern science.

3.3.2. Nanoparticles

A nanomaterial subtype particularly prevalent within the context of this thesis is the nanoparticles, especially those composed of cellulose. Nanoparticles are physically separate objects, which's largest dimension is measured in tens or hundreds of nanometres. Nanoparticles can be produced by breaking down larger particles or growing them from even smaller molecular or even atomic constituents. They can be spherical, elongated or flaky in shape and they can be composed of inorganic (metals, minerals, ceramics) or organic (polymers) materials. Nanoparticles derived from polymers are called Polymer NanoParticles (PNP), which are defined as solid colloidal particles, made of polymeric material, with their largest dimension in the range of 10-1000 nm.[129] These can be further divided into nanospheres and nanocapsules, both of which are roughly spherical in shape, as well as nanofibers, which are usually significantly elongate particles (**Figure 25.**). Nanospheres are solid particles composed entirely of the polymeric matrix, while nanocapsules are composed of a shell and a cavity filled with fluid (water or oil). Nanofibers are often produced from fibrous biopolymers like cellulose. These are very elongate and thin compared to the other nanoparticles, in fact the length of certain cellulose nanofibers regularly exceeds 1000 nm. Preparation pathways for polymer nanoparticles can be divided into two depending on the nature of the starting material: reworking of polymeric material or polymerization of monomers. The former pathway shows great potential in the utilisation of preformed biopolymers, whereas the latter is mostly concerned with the preparation of new materials from the viewpoint of traditional polymer chemistry.

The following sections of the thesis will focus on the use of reworking techniques in the preparation of cellulose nanoparticles. Some of the more common nanoparticle preparation methods, based on the reworking of polymeric material, include mechanochemical processing, nanoprecipitation, dialysis, salting-out, solvent evaporation and supercritical fluidics.[129] While almost all cellulose based nanoparticles are produced via mechanochemical processing methods (such as homogenization and acid hydrolysis), nanoprecipitation, dialysis and spraying methods are also discussed due to their relevance to the experimental section of the thesis and their potential in cellulose nanoparticles production.
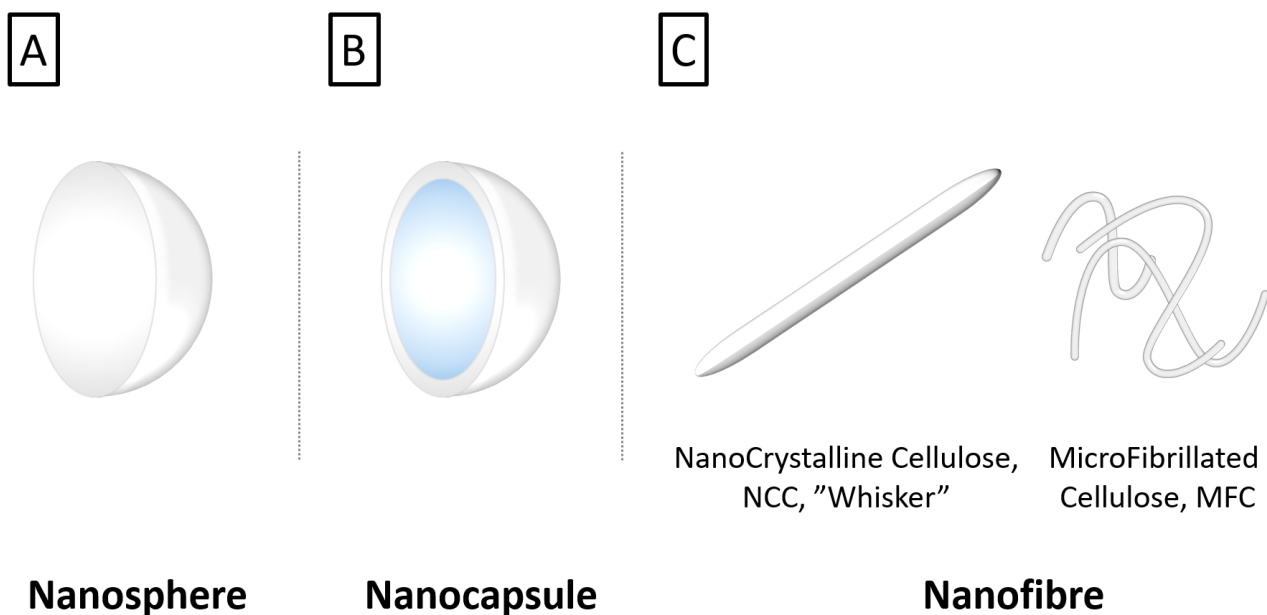
| A | B | C |

NanoCrystalline Cellulose, NCC, "Whisker"   MicroFibrillated Cellulose, MFC

Nanosphere   **Nanocapsule**   **Nanofibre**

Figure 25. Schematic presentation of the three types of PNPs: nanosphere (**A**), nanocapsule (**B**) and nanofiber (**C**). Relative particle sizes not to scale. The hollow center of a nanocapsule is often filled with water or oil. The nanofibers are set apart from the two other types by their high aspect ratio (length to width). **C**: The two subtypes of cellulose nanofibers are further set apart by their aspect ratio and rigidity – NCC is relatively stubbier and more rigid than MFC.

3.3.3. Cellulose nanoparticles

Nanoparticles composed of cellulose usually fall into one of two sub-classes depending on the aspect ratio: nanofibers and nanospheres. In this thesis, nanofibers are described as thin, elongated cellulose particles, the thickness of which are in the order of few tens of nanometres and length in the order of hundreds of nanometres to several micrometres.[1, 20, 130] Individual cellulose chains come together to form an elementary fibril, which has a roughly square cross section and a diameter of ca. 5 nm. These elementary fibrils form microfibrils with diameters of about 20 nm, albeit the diameter can vary depending on the species of plant and the life history of the individual.[19] The cellulose fibrils are much longer than they are wide, hence their aspect ratio can be as high as several hundred (length to width). Most reports of measured fibril lengths are in the range of hundreds of nanometres to several micrometres.[20] The fibres are the most crystalline, as well as the chemically and mechanically strongest parts of native cellulose. The fibrous and crystalline fractions are concentrated in the products, when native cellulose is broken down in traditional mechanical or chemical processing. This is due to the less fibrous and more amorphous parts of native cellulose

being more labile, and hence end up being the sites where the cellulose matrix is more easily broken down. Examples of cellulose nanofibers are the MicroFibrillated Cellulose (MFC)[131] and NanoCrystalline Cellulose (NCC) (**Figure 25. C**).[132] A special case of cellulose nanoparticles is Bacterial NanoCellulose (BNC), which is composed of cellulose nanofibrils polymerised from glucose monomers by bacteria.[20]

On the other hand, nanospheres are roughly spherical in shape and their average diameter is usually in the order of hundreds of nanometres, round cellulose particles being called Cellulose Nanospheres.[133] Nanospheres have a low aspect ratio, which means that the difference between the longest and shortest spatial dimension is small. The particle size of nanospheres can differ, but the common definition for polymer nanoparticles places the largest dimension between 1-1000 nm. Unlike nanofibers, which are structurally very unidimensional, the internal structure of cellulose nanospheres can be highly variable. They can be very porous and be capable of absorbing and carrying smaller compounds. They can be composed of multiple structurally differing layers or form a composite with other polymers. For example, when cellulose is in a homogeneously dissolved state, the addition of solid ingredients, such as metals or ceramics, or soluble polymers into the cellulose matrix is effortless to implement.

3.3.4. Cellulose nanofibers by mechanochemical processing

Various mechanochemical methods are very popular in the synthesis of cellulose nanofibers. Two of the most common ones are mechanical processing[131] and hydrolysis.[132] For example, cellulose can be grinded or sheared to decrease its size all the way to the nanoscale, or it can be similarly decreased in size by degrading the cellulose material by acid hydrolysis. Cellulose nanofibers formed by mechanical grinding are dubbed MicroFibrillated Cellulose (MFC) and ones produced by acid hydrolysis are called NanoCrystalline Cellulose (NCC). Synonyms for MFC include: nanofibrils, microfibrils and nanofibrillated cellulose; and synonyms for NCC include: cellulose nanocrystals, crystallites, whiskers, rod like cellulose microcrystals.

Cellulose is said to fibrillate when it is mechanically disintegrated. Fibrillated nanoscale cellulose is often counterintuitively called MicroFibrillated Cellulose (MFC),[131] when a more descriptive name for the material would be NanoFibrillated Cellulose (NFC) – a name that some in the research community are trying to popularize.[20] Some of the more common apparatuses used in cellulose fibrillation include the homogenizer,[134] the ball mill,[133] and the microfluidizer.[133] A homogenizer is a liquid fed mechanical pulveriser, in which a high starting pressure and the high frequency oscillation of the inlet valve expose particles or emulsions to high magnitude pressure changes and the resulting shear forces (**Figure 26.**). The principle of disintegration in a homogenizer is based on the collisions of particles against the piston head, the impact plates and each other. The high aspect

HOMOGENIZER APPARATUS

The media is held under high pressure

Unprocessed macroparticles

Apparatus body

Impact plate or ring

Homogenized nanoparticles

Inlet valve oscillating at high frequency
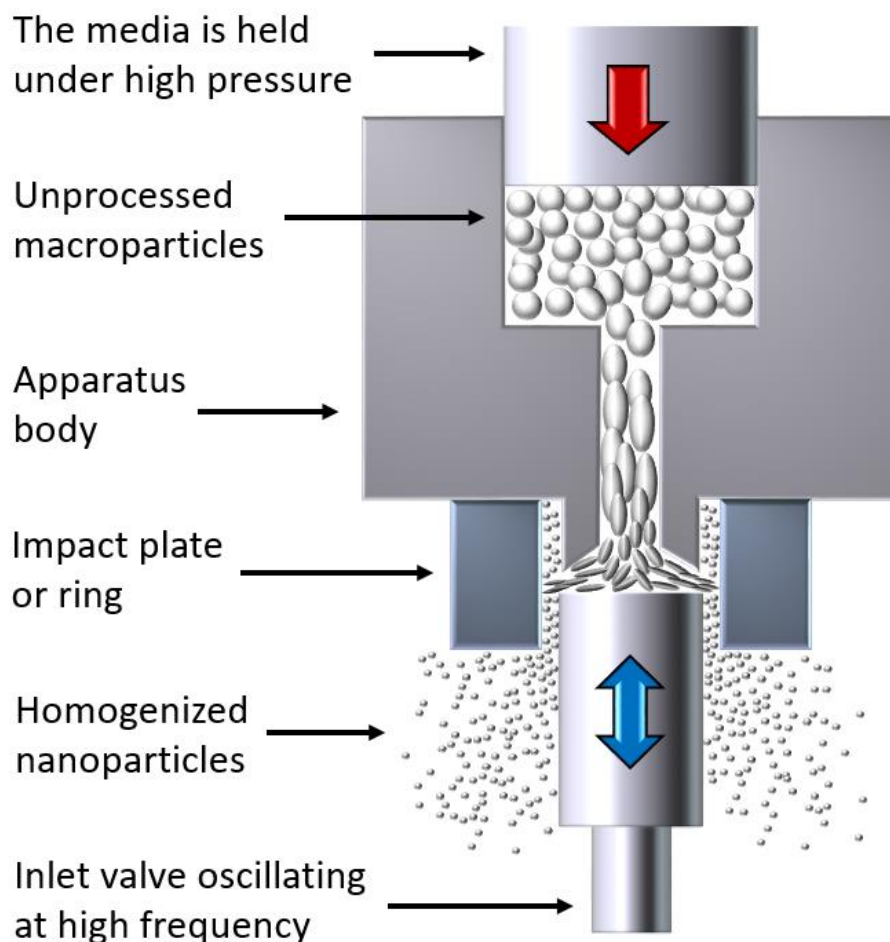
Figure 26. Schematic presentation of the working principle of a high-pressure homogenizer. The unprocessed material broken down by utilising a high starting pressure and high frequency oscillation of the inlet valve, which exposes particles to high magnitude pressure changes. The ensuing shear forces and collisions of particles with the impact plates, inlet valve, apparatus body and each other result in the disintegration of macroparticles down to nanoparticles.

ratio of native untreated cellulose is retained when it is mechanically disintegrated in a high pressure homogenizer. However, the coherent inter-fibril adhesion is greatly reduced in the process and the large-scale fibrous structure of cellulose is damaged, individual fibrils adopting a looser formation (**Figure 27.**) – the cellulose fibrils are said to delaminate.[134] The tendency of these fibrillated materials to form gels in polar solvents can be mostly attributed to the loose fibrils being prone to forming new connections with each other and form extensive networks.

Another example of mechanical nanoparticle processing is the microfluidizer apparatus.[133] In a microfluidizer, the polymeric material is subjected to high shear forces in a liquid media, which is achieved by introducing a sample stream under a high pneumatic pressure into a fixed geometry interaction chamber composed of a number of narrow channels. When entering the interaction chamber, the speed of the media and particles is accelerated up to hundreds of meters per second. Similarly to the homogenizer, the collision of the particles with each other and the chamber walls results in a drastic decrease in particle size. However, multiple runs are usually required to achieve a narrow size distribution in the sub 100 nm size range.
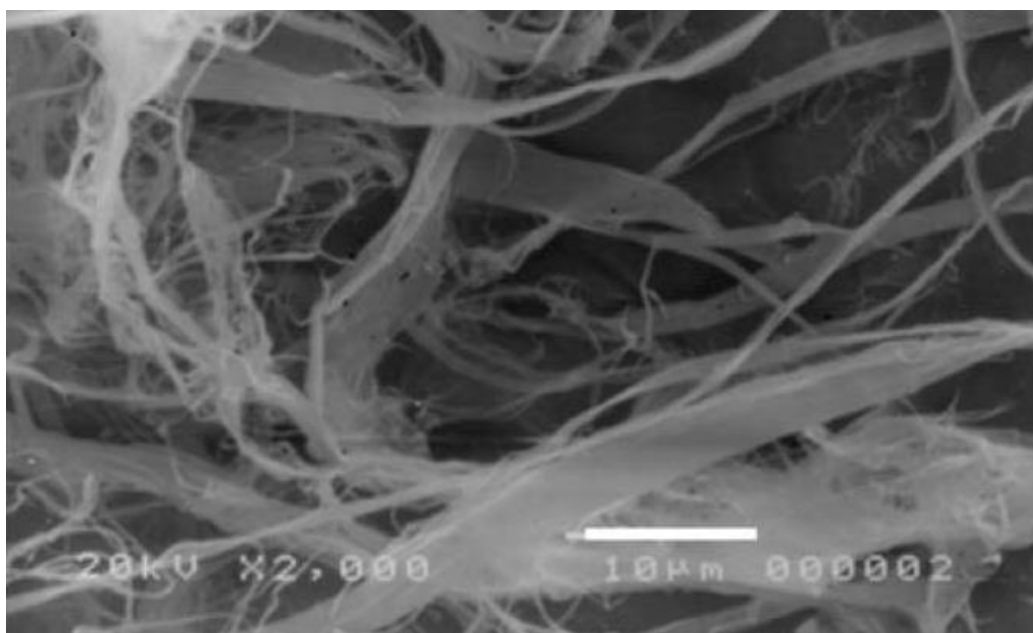
Figure 27. Microfibrillated Cellulose imaged by SEM. The starting material was processed 14 times in the homogenizer.[167] The diameter of individual fibers is 10-100 nm. Figure reused with permission from "Nakagaito, A.N. and Yano, H., *Appl. Phys. A* **80**(1) 2005 155." Copyright 2003 Springer Nature.

The preparation of MFC by mechanical processing alone has disadvantages in being highly energy consuming and being blockage-prone due to the usual small scale of the instruments. Several

different pre-treatment methods can be employed to combat these issues, with TEMPO oxidation being one of the most common ones (TEMPO oxidation is further discussed in the section **3.3.5. Cellulose nanospheres by mechanochemical processing**).[135] The primary goal of any general pre-treatment is to disrupt the strong intermolecular interactions between cellulose fibrils. This is done in order to reduce the duration and intensity of the highly energy consuming mechanical grinding, resulting in more energy efficient process. The prominence of the intermolecular interactions is usually reduced in tandem with the crystallinity of the cellulose material; a change which can be measured using various XDR-based methods (see section **1.2.6. X-Ray measurements of cellulose morphology**).

The aspect ratio of cellulose fibrils from cotton, wood or MCC is significantly lowered down to <100, when strongly acidic conditions are used to hydrolyse the material. The hydrolysis results in cellulose fibres with a rod-like appearance called "whiskers", which are still some hundreds of nanometres long and have low polydispersity (**Figure 28.**).[130, 136, 137] For example, fibrous cellulose nanoparticles can be produced by sulphuric acid hydrolysis of treated (swollen) sisal fibres.[132] The highly acidic conditions coupled with sonication lead to significant hydrolysis of the amorphous parts of the fibrils, resulting in low aspect ratio fibril aggregates and rod like fibrils.[130] The acid hydrolysed nanofibrils (NCC) are much stiffer than their fibrillated MFC-counterparts, which is due to the lack of flexible amorphous regions in the hydrolysed "whiskers".[20] However, when cellulose from other sources such as algae, bacteria or tunicates is subjected to similar acidic conditions, the resulting nanofibers have a much higher polydispersity and their length can vary between 100 nm and several μm. The nature of the acid has an effect on the characteristics of the resulting whiskers: those prepared using hydrochloric acid remain mostly uncharged and have a relatively high viscosity, while those prepared using sulphuric acid become negatively charged on the surfaces and as a result have
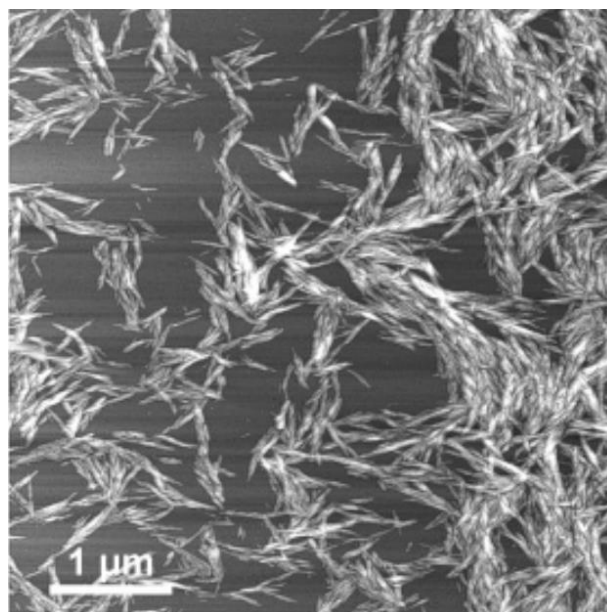

Figure 28. NanoCrystalline Cellulose, NCC imaged by AFM.[172] Figure reused with permission from "Kvien, I., Tanem B.S. and Oksman, K., *Biomacromolecules* **6**(6) 2005 3160." Copyright 2005 American Chemical Society.

much lower viscosity. This is due to the formation of sulphate esters on the nanofibril surfaces, with up to 10 % of glucose units ending up being functionalised.[138]

The coupling of a mild enzymatic hydrolysis and high pressure mechanical shearing has been shown to achieve cellulose nanofibers in a more efficient manner, than with strongly acidic hydrolysis or mechanical shearing alone.[130] The process was composed of four steps. First, a slight mechanical refining with an angle refiner to swell the fibre wall and aid in the enzymatic hydrolysis. Then an enzymatic hydrolysis using a monocomponent endoglucanase (Novozym 476), combined with mixing and subsequent denaturation of enzyme using temperature. Subsequently further washing with deionized water and mechanical refining as before. Finally, a high pressure shearing by passing the material through a high-pressure fluidizer (Microfluidizer M-110EH).

The most significant differences between the two primary cellulose nanofiber morphologies (acid hydrolysed NCC and mechanically fibrillated MFC, **Figure 29.**)[139] are the rigidity, crystallinity and aspect ratio (length to thickness) of the fibres. The acid hydrolysed cellulose whiskers (NCC) are much more rigid than their mechanically modified counterparts, their aspect ratio is lower (NCC 15-50 vs. MFC 250), they are thinner on average (NCC 2-30 nm vs. MFC 2-100 nm) and more crystalline (NCC 85 % vs. MFC 60 %).[140] However, the crystallinity of nanofibers is highly dependent on the crystallinity of the starting material and as a result, two materials with nearly identical Degrees of Crystallinity can be found in either of the two different categories. The greater rigidity of NCC is due to the apparent scarcity of flexible amorphous regions, which is due to the preferential hydrolysis
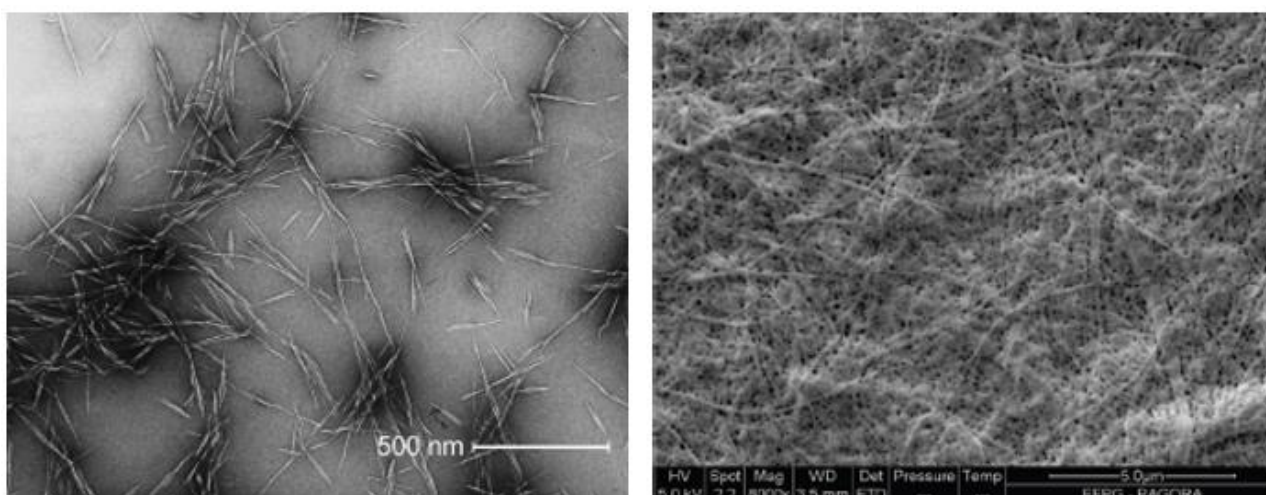

Figure 29. The different morphologies of Cellulose Nanofibers: NCC (left) and MFC (right).[174] Figure modified with permission from "Siqueira, G., Bras, J. and Dufresne, A., *Biomacromolecules* **10**(2) 2009 425." Copyright 2009 American Chemical Society.

of the more accessible amorphous regions in an acidic environment. The amorphous regions are more randomly oriented and they have a larger surface area, which allows for better access for the hydrolytic media and leads to the hydrolysis of said regions proceeding relatively faster compared to the crystalline regions. On the other hand, also crystalline cellulose is hydrolysed in the process and the degree of crystallinity of cellulose never reaches 100 %. This implies that new amorphous cellulose is constantly formed during the hydrolysis process. The aspect ratio of the fibril also has great influence on its phase behaviour in liquid medium. Low aspect ratio fibrils, such as the stubby rod-like "whiskers", are capable of forming liquid crystal phases in water[141], whereas high aspect ratio fibrils with lengths of several μm are more likely to form entangled networks leading to gels.[130] This gel formation is likely due to entanglement of fibrils at junction zones where partly disintegrated fibril aggregates come together.

3.3.5. Cellulose nanospheres by mechanochemical processing

Cellulose nanospheres are roughly spherical particles, which's largest dimension lies between 1 and 1000 nm. The native morphology of cellulose (cellulose I) is rather hard to break down to any other shape than fibre, as the elongate cellulose fibrils are the strongest part of the plant cell wall both mechanically and chemically. Thus, cellulose nanofibers are the prominent product when unmodified cellulose is subjected to mechanical homogenization. However, when the cohesion between the fibres is broken down via a pre-treatment such as mercerisation, derivatisation or regeneration, the formation of spherical nanoparticles using mechanical disintegration is achievable. This is made possible by the lack of large differences in mechanical resilience between the different spatial dimensions of the treated cellulose material, which leads to breakage of the material more evenly in all directions.

For example in a study by Hettrich *et al.*,[133] microcrystalline cellulose (Avicel) was used as a starting material to test the feasibility of producing spherical cellulose nanoparticles by using a microfluidizer apparatus (MF). Before cellulose was introduced to the high pressure shear forces, it was subjected to one of four different pre-treatment methods: grinding, hydrolysis, regeneration or derivatisation. The primary goal of all of these pre-treatments was to disrupt the strong cohesion between cellulose fibrils, which also inevitably leads to a decrease in the overall crystallinity of a cellulose material.

The hydrolysis pre-treatment of cellulose was achieved at 90° C using one of three hydrolysis agents: 20 % aqueous sulphuric acid, 40 % phosphoric acid or a molten salt $ZnCl_2 + 4H_2O$.[133] The acid hydrolyses resulted in an overall increased particle size of the starting material and prior to homogenization, the resulting suspension was shown to contain both roughly spherical and fibrous particles. After the MF-treatment, the sulphuric acid hydrolysed sample consisted of circa 500 nm particles of notched rod-like appearance, whereas the phosphoric acid and $ZnCl_2$ ones had sizes under 200 nm and a much more spherical shape (**Figure 30.**).

The grinding pre-treatments were performed on a planetary ball mill or a colloid mill with grinding times ranging from 0,5 h to 32 h. The smallest particle size was obtained after 6 h of milling, while the change is particle size distribution was negligible. When processed with a Microfluidizer, the cellulose formed a nanoscale dispersion. However, the dispersion showed a bimodal particle size distribution with local maxima at 470 nm and 3 µm. This was attributed to the agglomeration of cellulose particles in suspension. It has been show that excessive ball milling greatly decreases both the
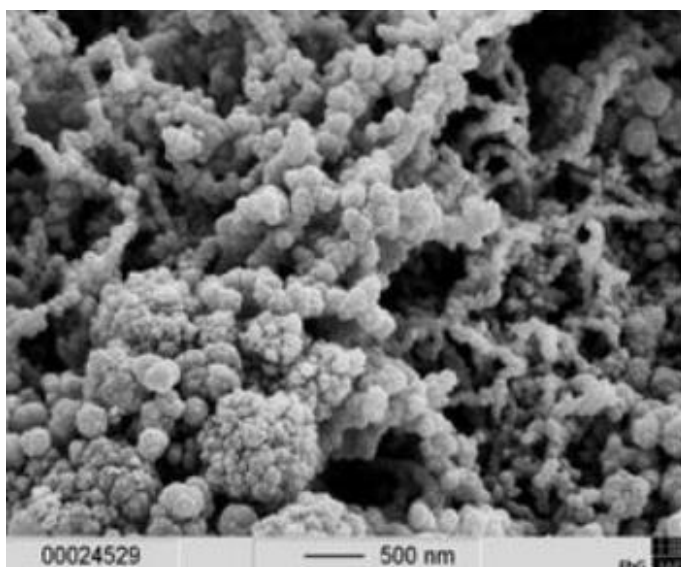
Figure 30. Cellulose Nanospheres prepared by processing $ZnCl_2$-pretreated microcrystalline cellulose in a microfluidizer apparatus.[159] Figure reused with permission from "Hettrich, K., Pinnow, M., Volkert, B., Passauer, L. and Fischer, S., *Cellulose* **21**(4) 2014 2479." Copyright 2014 Springer Nature.

particle size and crystallinity of cellulose, and in fact it is a viable way to produce amorphous cellulose.[142, 143] In the study by Yu & Wu,[143] milling time of seven hours at a milling frequency of 15 Hz already produced fully amorphous cellulose. Interestingly cryogenic ball milling, with milling times of only several minutes, leads to a major decrease in particle size but insignificant decrease in cellulose crystallinity.

The regeneration pre-treatment of cellulose was achieved by dissolving cellulose in NMMO·H_2O and subsequently precipitating it with the addition of excess isopropanol.[133] This procedure effectively removed all prior crystallinity resulting in amorphous cellulose (characterized by Raman and SAXS). As much as 23 wt-% of cellulose can be dissolved in 1:1 H_2O:NMMO.[8] The process starts by making

a homogenous slurry of cellulose in a H_2O:NMMO mixture. This mixture is called dope and the exact ratio of H_2O:NMMO can be tuned to yield the best wetting and swelling characteristics for cellulose. The best results are usually achieved with more dilute NMMO concentrations and for this reason, cellulose in these mixtures is not dissolved until the concentration of NMMO is raised. True dissolution of cellulose is achieved by removing water from the dope at increased temperatures under vacuum, with a ratio of 1:1 H_2O:NMMO holding the most dissolving power towards cellulose. The particles that resulted after the homogenization were of sizes ranging from 60 nm to 200 nm and had a general scaly appearance.[133]

Two types of chemical derivatisation pre-treatments were tested: carboxymethylation and TEMPO-oxidation (TEMPO, 2,2,6,6-tetramethylpiperidine-1-oxy-radical). Carboxymethyl cellulose (CMC) with a DS of 0,07 was produced in a heterogeneous synthesis. Dried cellulose was mixed with 11:1 volume ratio 2-propanol:methanol, while NaOH in water was added slowly to the mixture. Subsequently monochloroacetic acid was introduced to the mixture and CMC was recovered after work-up. After MF-treatment, the particles showed a tendency to form films, which became evident when a sample was prepared for SEM. An almost closed film with very small cracks was obtained, while inside the cracks the separate <300 nm particles were visible. The particles showed two types of morphology: spherical and rod-like. However, contrary to prior literature, the presence of fibrillated structures was not observed, and no hydrolysis was necessary to achieve the spherical and rod-like nanoparticles.[133] In the other pre-treatment, cellulose was TEMPO-oxidized according to a well described method from literature.[135, 144] Cellulose was suspended in an aqueous mixture of TEMPO and NaBr. Sodium hypochlorite (NaClO) was added to the mixture and the pH was kept constant at 10,5 with the addition of NaOH. The carboxyl content of the resulting cellulose was determined to be 600 mmol/kg after work-up.[145] The post-MF-treatment nanoparticles had similar morphology and film forming behaviour as CMC, and yet again no fibrils could be observed in the films. The size of the nanoparticles varied between 30-200 nm and when studied using light scattering, the presence of agglomerated particles was inferred from small peaks at 750 nm and 3,5 µm. Overall, spherical particles were obtained from all different pre-treatment pathways followed by microfluidizer-treatment, and all of the particles had more viscous suspensions compared to the starting material.

3.3.6. Polymeric nanoparticles by nanoprecipitation

Nanoprecipitation is a nanoparticle preparation method, in which a solution of polymer is introduced dropwise into an antisolvent mixed with surfactant under stirring. Due to the two solvents being miscible, a rapid diffusional mixing of the solvent and antisolvent follows when the solvent drop hits the antisolvent surface. The sudden removal of the solvent from around the polymer leads to rapid precipitation in the nanoscale.[146] The method is widely used in the preparation of Polymer NanoParticles (PNP) from a range of synthetic polymers such as poly(ε-caprolactone) (PCL),[147] polylactid acid (PLA),[148] poly(lactic-co-glycolic acid) (PLGA)[149] and polyalkylcyanoacrylates (PACA).[150] The range of choice for the polymer solvent is equally broad, with common organic solvents such as acetone[146, 151], ethanol[152], chloroform[153], THF[148] being usually favoured. In addition to being cheap, as well as extremely well studied and described in the literature, these traditional solvents have low viscosity, which is beneficial in the diffusion step of the nanoprecipitation process. Despite the widespread and common use, the application of the nanoprecipitation method to the production of unmodified cellulose nanoparticles was not encountered in the literature. This was one of the reasons the method was included in the thesis as a possible way to produce cellulose nanoparticles.

The study by Yordanov *et al.*[150] is here used as an example of an experimental nanoprecipitation process. The authors produced Dextran 40 coated PACA nanoparticles with average diameters of 238 nm (**Figure 31.**) using the nanoprecipitation method. First a stabilizing agent Dextran 40 (20 mg) was dissolved in an aqueous glucose solution (5 wt-%, 10 ml) and polybutyl cyanoacrylate (PBCA, 50-100 mg) was dissolved in 5 ml of acetone. Then the PBCA/acetone solution was added dropwise to the glucose solution while vigorously stirring with a magnetic stirrer (600 rpm). Finally acetone was evaporate in a fume hood for 5 hours, after which the rest was evaporated under vacuum. Glucose was likely added to the water phase in order to increase the surface activity of Dextran 40. High concentration of glucose in the water phase drives the solubility equilibrium of Dextran 40 away from the liquid phase towards adhering to the surface of the nanoparticles.
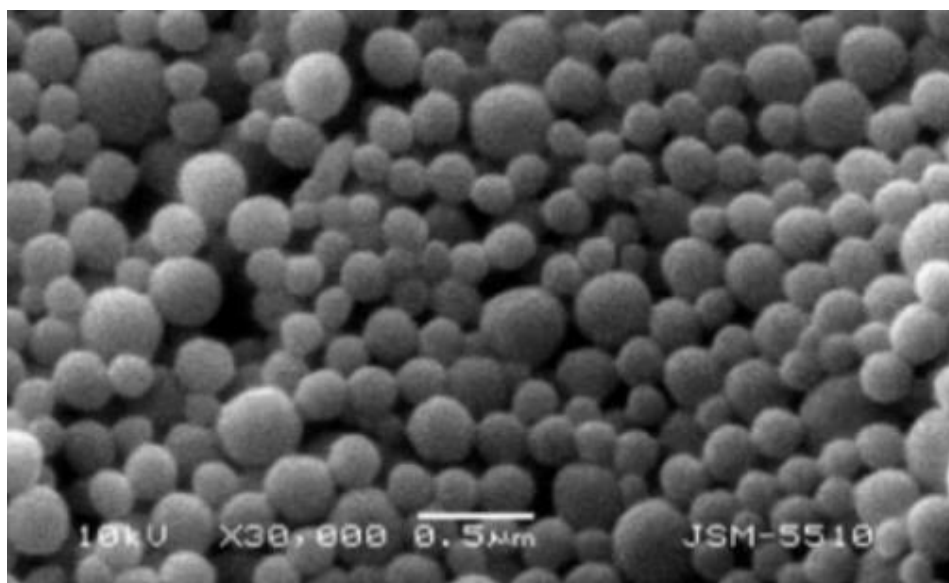
Figure 31. Dextran 40 coated PACA nanoparticles imaged by SEM.[188] Average diameter of the particles is 238 nm. Figure modified with permission from "Yordanov, G.G. and Dushkin, C.D., *Colloid Polym. Sci.* **288**(9) 2010 1019." Copyright 2014 Springer Nature.

Parameters that affect the size of the resulting particles in the nanoprecipitation method are those related to the mode of addition (unassisted dropping, jet cutting, spinning drop atomization, spinning disc atomization, dispersion),[154] rate of addition, viscosity and the final solvent-to-antisolvent ratio. Even though the surfactant is not necessary to achieve precipitation of nanoparticles, if left in solution with the nanoparticles, it helps in reducing aggregation of nanoparticles during long term storage. In addition, the effect of increasing size of the resulting particles with higher surfactant concentration suggests that the viscosity of the antisolvent plays an important role in determining the particle size.[155]

The nanoprecipitation process can be divided into three steps: nucleation, growth and aggregation.[156] All of these steps affect the size distribution of the nanoparticles and the driving force behind each of the steps is super-saturation, which is defined as the ratio of the actual polymer concentration and the solubility of the polymer in the solvent mixture. To achieve a narrow particle size distribution and a small overall particle size, the nucleation step should be optimised. The most efficient way to increase the nucleation rate of nanoprecipitation is with rapid and continuous mixing, which can be achieved with mixing reactors such as confined impinging jets reactors (CIJR). In a CIJR, turbulent forces are rapidly generated and dissipated leading to very fast and efficient mixing. This is the result of the collision of the two streams of solvent and antisolvent in very small volumes in the centre of a large interaction chamber, with mixing times in the order of milliseconds.

When the growth step of the process is emphasised, a smaller number of larger particles are formed. A dominating growth step can be achieved by poor and slow mixing. The final aggregation step is largely independent of the two prior steps, and is mostly related to the number concentration of the polymer particles in the final solvent mixture. Aggregation of particles can be diminished by decreasing polymer and subsequent particle concentration.

Nanoprecipitation is a fast and simple nanoparticle synthesis method that does not require expensive or complex machinery to work, unless the very smallest of nanoparticles are desired. One of the weaknesses of the method is that the solvents used need to be of very low viscosity, which can problematic with certain polymer materials. For instance, solvents and solvent systems capable of dissolving cellulose, and hence being candidates for use in cellulose nanoparticle preparation by nanoprecipitation, are across-the-board much more viscous than traditional polymer solvents. Fortunately, the viscosity of these cellulose solvents can be modified with the addition of an appropriate low viscosity co-solvent such as DMSO or GVL.

3.3.7. Polymeric nanoparticles by dialysis

Dialysis is a solvent exchange method based on the diffusive mixing of two miscible liquids, in which a dialysis membrane is employed to keep large molecular weight compounds and particles from exiting the dialysis bag. The method utilises the concentration gradient of the two solvents either side of the dialysis membrane in a way that allows the replacement of the solvent initially inside the dialysis bag with the one outside of the bag. The diffusive mixing of solvents A and B can be clearly seen in **Figure 32.,** where the initial concentration of solvent A inside the dialysis bag is 100 %. However, after having completely mixed with solvent B, the concentration of solvent A inside the bag is only 1 %. When the diffusion of the two solvents has finished and the two are completely mixed, the formed solvent mixture outside the dialysis bag is exchanged for a new batch of solvent B and the diffusion process begins anew. After this process has been repeated many times, the final concentration of solvent A inside the dialysis bag is practically zero.

DIALYSIS PROCESS

During the dialysis process the two solvents are dispersed inside the container via diffusive mixing. The polymer solvent A diffuses outwards through the dialysis membrane, which detains the high molecular weight polymer inside the dialysis bag. Solvent B diffuses into the dialysis bag to fill the volume vacated by solvent A.

← Diffusion

Polymer
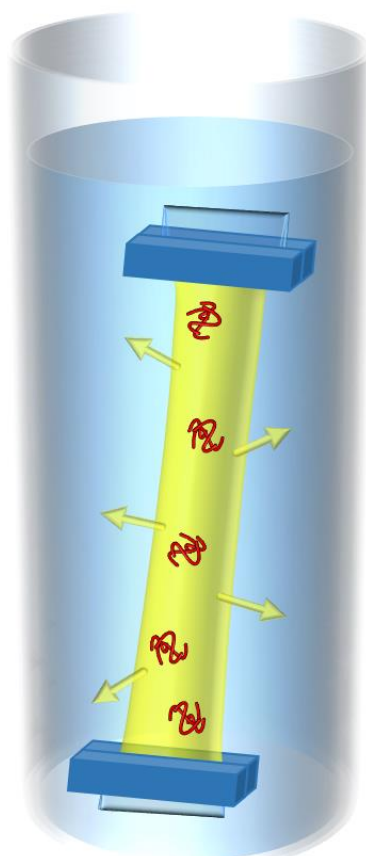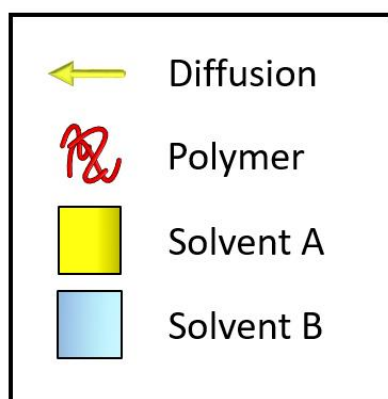
Solvent A

Solvent B

At the start of the dialysis, the concentration of solvent A inside the dialysis bag is 100 %.
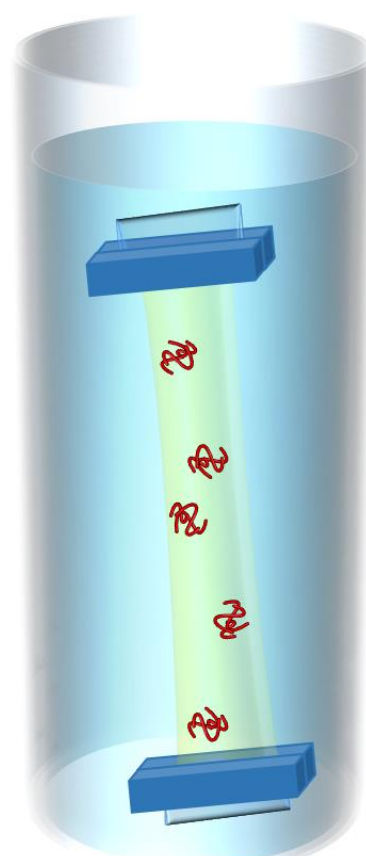
At first equilibrium, the concentration of solvent A inside the dialysis bag is 1 %, for example.

Figure 32. A schematic presentation of the principle diffusion-based mechanism of the dialysis nanoparticles preparation method. Once dialysis has commenced, the polymer solvent (solvent A) will start to diffuse outwards into the antisolvent bath, while simultaneously the antisolvent (solvent B) starts to diffuse inwards into the dialysis bag. The loss of dissolution capacity inside the dialysis bag causes the polymer to precipitate, but due to its high molecular weight, it is incapable of penetrating the dialysis membrane and exiting the dialysis bag. The yellow arrows designate diffusion direction of solvent A.

The dialysis nanoparticle preparation method is based on the precipitation of polymer inside a dialysis membrane, when a solvent for the polymer is slowly replaced by antisolvent.[129, 157] The polymer is first dissolved in a solvent miscible with the antisolvent and placed inside a dialysis bag. The ends of the bag are sealed and it is placed in a large container of the antisolvent. Gentle stirring is usually applied to enhance the mixing of the two solvents, and once the concentration gradient has levelled out, the antisolvent bath is changed in order to continue the solvent exchange process. Precipitation of the polymer occurs usually quite quickly during the dialysis process, resulting from

the loss of polymer solvent concentration inside the dialysis bag. This naturally leads to the loss of dissolving power of the solvent mixture towards the polymer. However, the continuation of the dialysis well after the precipitation is beneficial in removing the remaining solvent and other soluble impurities from the polymer particles.

The preparation of nanoparticles using the dialysis method is feasible with most polymers and a vast number of solvent/antisolvent combinations – the only general limitations being that the polymer needs to be soluble in only one of the solvents and that the two solvents need to be miscible. An additional limitation is presented by the chemical resilience of the dialysis bag, although this rarely becomes a problem, as one of the most common film materials is the remarkably stable cellulose. However, sometimes even the cellulose dialysis bag cannot withstand the solvents used. This was observed first-hand while trying to prepare cellulose nanoparticles from ionic liquids using the dialysis method within the extent of this thesis. No suitable dialysis bag material was found that could withstand the studied ILs in the traditional dialysis nanoparticle preparation setup, but dialysis was observed to be a good method for purifying particles of residual IL, once the IL was first poisoned with water or other cellulose antisolvent.

A study by Nah *et al.*[119] is used as an example of the dialysis nanoparticle preparation method. PLGA nanoparticles with an average diameter of 270 nm (**Figure 33.**) were prepared in a dialysis process. First PLGA (20 mg) was dissolved in dimethylformamide (DMF, 10 ml). Then the PLGA-solution was moved to the dialysis bag (MWCO 12,000 g/mol), which was placed inside a container filled with 1 l of water. DMF and water were left to mix for 1 hour, after which the water was replaced. This process was repeated two more times, after which the water was replaced every 3-4 hours for the next 24 hours. Finally, the dialysis bag was removed from the container and the nanoparticles contained within were extracted by freeze-drying.

The formed nanoparticles are not able to diffuse out of the dialysis bag because of a low molecular weight cut-off (MWCO) of the membrane. MWCO is expressed as the molecular weight of a compound of which 90 % is retained within the dialysis membrane during the dialysis process. However, solvent molecules are usually significantly smaller than the MWCO of the membrane, which enables their efficient diffusion across the dialysis membrane. Dialysis is a relatively slow nanoparticles preparation method and a full dialysis can take anywhere from several hours up to several days, depending on the solvents used and on the completeness of solvent exchange required. Every time the antisolvent bath is changed, full mixing of the two solvents is usually achieved within 30 min with high concentration gradients, and within several hours with low gradients.
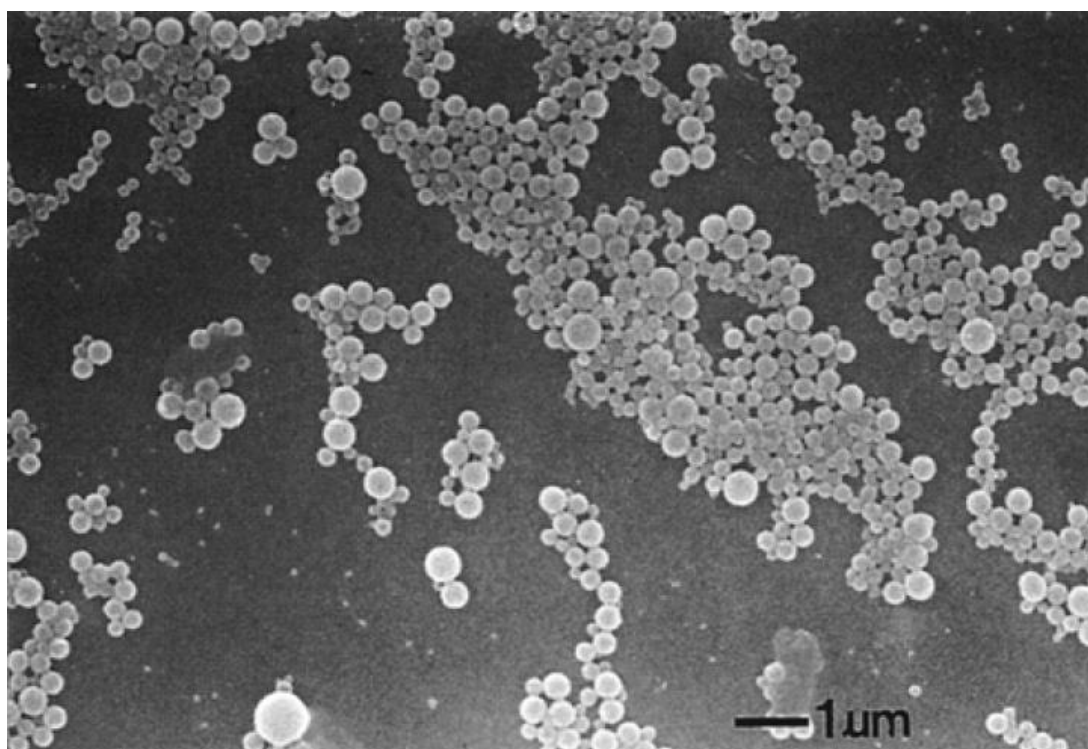
Figure 33. PLGA nanoparticles with average diameter of 270 ± 119 nm imaged using SEM.[151] Figure modified with permission from "Nah, J.W., Paek, Y.W., Jeong, Y.I., Kim, D.W., Cho, C.S., Kim, S.H. and Kim, M.Y., *Arch Pharm Res.* **21**(4) 1998 418." Copyright 1998 Springer Nature.

The dialysis nanoparticles preparation method is simple and effortless. It is very effective in removing the original polymer solvent and it does not require complex or expensive machinery. Unfortunately, the dialysis method is very slow and it is hard to scale up to larger than laboratory scale volumes. The method also produces large quantities of solvent waste, which can be very problematic recycling wise depending on the choice of solvents. For example, recycling of an ionic

liquid from a very dilute aqueous solution is both time consuming and costly, both of which hinder the applicability of the dialysis method to the preparation of cellulose nanoparticles. In addition, the chemical resilience of the dialysis film can become an issue with certain solvents, such as was observed when trying to prepare cellulose nanoparticles using ionic liquids in this thesis.

3.3.8. Polymer microspheres by spray-regeneration of dope

Spraying of a liquid media is an efficient way to coat solid surfaces or greatly increase the surface area of a solvent for effective spray drying of dissolved compounds, which is widely applied in the making of powdered milk.[158] In these instances, high fluid pressure, external gas stream, ultrasonic vibration or electrostatic interactions are used to disperse the liquid feed into a fine airborne mist. The principle forming the basis of all these techniques is collectively known as atomization, which can be further divided into primary and secondary type. Primary atomization occurs in or very near to the atomizing nozzle, while secondary atomization occurs further downstream from the atomizer when preformed droplets are fragmented further. The primary categories of atomizers are the single-fluid atomizers (pressure jet), two-fluid atomizers, rotary atomizers, ultrasonic atomizers and electrostatic atomizers, all of which have seen numerous nozzle designs developed for various spraying tasks.[159] Out of these categories, the single- and two-fluid atomizers are the most simple to implement and are by far the most common applied methods of spraying. Spraying methods in general are very useful in the preparation of polymeric particles, as they usually offer excellent control over the produced particles size and are also very high throughput methods, unlike many other particle preparation methods described in this thesis.

The high surface tension and viscosity of a fluid greatly restricts the mobility of the constituent molecules, leading to absence of flow in an atomizer, and poses significant limitations on the spraying of the bulk material using most traditional atomizing nozzles. The single-fluid sprayers are mostly applicable to the spraying of low viscosity fluids such as water and traditional organic solvents, while some of the two-fluid designs are capable of spraying even viscous fluids such as concentrated solutions of maltodextrin,[160] sodium alginate[161] and honey.[162] Two-fluid atomizers are divided into two types, internal- and external-mixing designs. In an internal-mixing atomizer, the fluid and gas jets collide inside the nozzle and are released together through an orifice, whereas in an external-mixing atomizer the two jets do not collide prior to exiting the nozzle head. Out of the

two, the external mixing atomizer is superior in the spraying of viscous fluids, as there are fewer chances for clogging of the nozzle orifices and the proper function of the atomizer is less sensitive to deviations from the ideal mixing ratio and flowrate of the two fluid components.

For example, a two-fluid fan jet atomizer was used to prepare polymeric microcapsules, with diameters as small as 30 µm, by spraying a viscous sodium alginate solution (0,5-2,5 wt-%) into a $BaCl_2$ coagulation bath placed downstream (**Figure 34.**).[161] The viscosity (90 – 4000 mPa·s) of the solution was observed to be related to the produced particle size, with more viscous solution resulting in larger particles (as high as 400 µm). Intuitively, an increase in the atomizing gas flow intensity resulted in a decrease in the particle of the particles. Despite the dynamic range of the particle size with changing viscosity or airflow, the formed particles were observed to be highly monodisperse within a single setup. Although the lowest size of the particles prepared in this study was 30 µm, the production of even smaller particles conceptualized. The particle size should continue reducing along with an increasing atomizing airflow intensity, albeit some physical limitation must exist for the size of a particle produced via an air-powered atomizing setup.
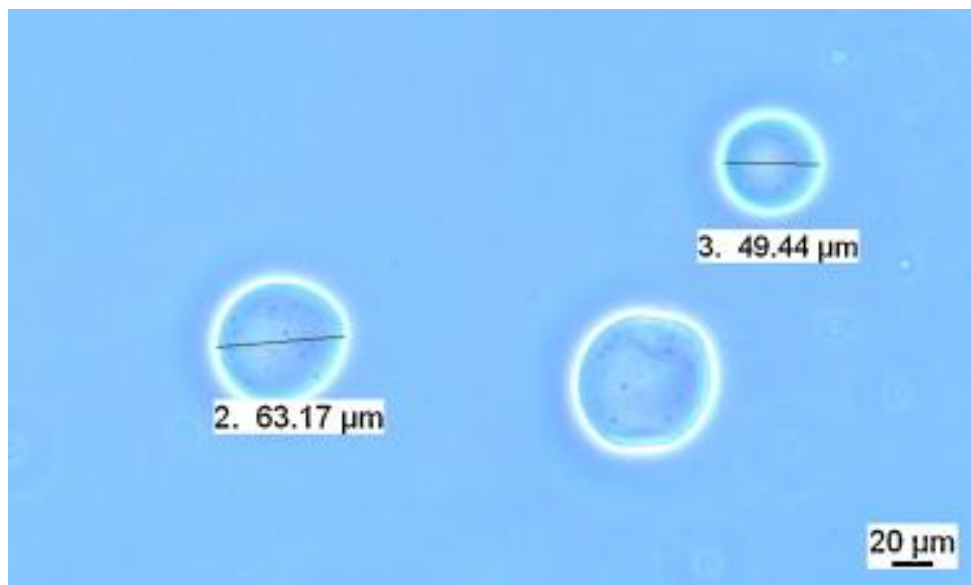

Figure 34. Picture of the alginate microcapsules produced by spraying a sodium alginate solution into a $BaCl_2$ coagulation bath.[199] The spraying was achieved by a two-fluid fan jet atomizer. Figure modified with permission from "Cerveró, J.M., Nogareda, J., Valle, Eva M Martín del & Galán, M.A. *Chem. Eng. J.* **174**(2) 2011 699." Copyright 2011 Elsevier.

4. Results and experimentals

The laboratory work conducted within the extent of this thesis is outlined in the following section. First, some experimental information about the synthesis of chemicals, the preparation of surfactant solutions and organic electrolytes, the dissolution of cellulose in the electrolytes and the analytical methods used to study the resulting cellulosic materials are presented. Following that, the main body of experimental work is divided into two parts. The first part deals with superbase IL-based organic electrolyte [DBNH][OAc]/DMSO and the preparation of micro- and millimetre scale cellulose particles via precipitation, while the second part deals with phosphonium IL-based organic electrolyte [P$_{4441}$][OAc]/GVL and the preparation of low micrometre scale cellulose particles via an UCST-like thermoresponsive phase change mechanism. The results are examined in a semi-chronological fashion, the main work being divided into sections titled according to the scientific question the experiment aims to answer, yet adjacent sections are still closely associated with each other – later experiments exploring the findings of previous experiments in greater detail.

4.1. General experimental procedures

4.1.1. Preparation of [DBNH][OAc]/DMSO (40 wt-% DMSO)

To prepare 10 g of [DBNH][OAc]/DMSO (40 wt-% DMSO), equimolar amounts of 1,5-diazabicyclo[4.3.0]non-5-ene (DBN) and glacial acetic acid were mixed in a glass vial or larger glass bottle, with a pre-determined wt-% of DMSO added afterwards. For example, 4,04 g of DBN was first placed in a container and 1,96 g of acetic acid was added via a syringe while keeping the point of the needle below the liquid surface. This was done to avoid fuming, which occurs when acetic acid is injected above the surface. Subsequently 4 g of DMSO was added to form the final electrolyte solution. The mixture was then first mixed by manual shaking and then vortexed for a short time. Afterwards the container was protected from moisture by replacing the atmosphere inside of the container with argon, sealing it with parafilm and storing it in a desiccator.

The neutralization reaction between DBN and acetic acid is exothermic and hence active cooling is needed to keep the flask temperature under control when using large reactant quantities. However,

when the reaction is done is small scale no active cooling is needed. The heat released during the neutralization also helps to keep the otherwise room-temperature-solid [DBNH][OAc] molten, until DMSO can be added to the mixture. This way the mixing of the two solvents is much faster than it would be when the IL had already solidified. Additionally, the resulting electrolyte solution is much easier to administer than the solid IL. The reactants DBN and acetic acid can be distilled before the reaction, if there is concern of purity. However, in applications not needing high purity of solvent such as the IONCELL-F, they can be usually used as purchased.[24]

4.1.2. Preparation of [P$_{4441}$][OAc]

The phosphonium IL [P$_{4441}$][OAc] used in this thesis were synthesized by Dr. Holding for his studies on the same solvent systems. While it was not part of this current thesis, the synthesis of the ILs was conducted according to a synthesis method by Holding.[10] In the case of [P$_{4441}$][OAc], tributylphosphine was placed in a 2 litre Parr reactor under inert atmosphere. A large excess of dimethyl carbonate (DMC) and methanol (two times the volume) was added and the mixture was stirred at 140° C for 24 h. When cooled, the mixture is placed in a flask and reduced to about quarter of its crude volume by rotary evaporator, whilst keeping the temperature under 40° C to avoid decomposition. This compound ([P$_{4441}$][MeCO$_3$]) is also available commercially from Iolitec GmbH.[70] Subsequently, an equimolar amount of acetic acid was added dropwise to the mixture under stirring. When the reaction was deemed to have reached completion, excess solvent was removed first under reduced pressure and later in a rotary evaporator under high vacuum at 70° C for 24 h. The resulting compound was a dark-orange viscous liquid. In this synthesis route, the tributylphosphine (or trioctylphosphine) is reacted with DMC to form tetra-alkylphosphonium methyl carbonate salt. When acetic acid is added, the methyl carbonate further neutralizes to form methanol and CO_2, leaving acetate as the counter anion for the tetra-alkylphosphonium cation.

4.1.3. Preparation of [P$_{4441}$][OAc]/GVL (30 wt-% GVL)

A predetermined amount of IL (for example 0,6 g) was weighed into a 20 ml glass vial. The easiest method of addition is via syringe when the IL was molten (i.e. it was heated), but addition of solid IL by spatula is also possible. Then an appropriate amount of co-solvent DMSO or GVL was added to the IL via a syringe. For example, to produce an electrolyte with a co-solvent concentration of 30

wt-%, 0,4 g of co-solvent would need to be added. The mixture was then first mixed by manual shaking and then vortexed for a short time. Subsequently the container was protected from moisture by replacing the atmosphere inside of the container with argon, sealing with parafilm and storing it in a desiccator.

4.1.4. Dissolution of cellulose (MCC) in [DBNH][OAc]/DMSO (40 wt-% DMSO)

To prepare a 5 wt-% solution of cellulose (MCC) in [DBNH][OAc]/DMSO, an appropriate amount of cellulose (for example 0,1 g) was weighed and added slowly to the IL/co-solvent (1,9 g) in a 20 ml glass vial. Mixing was applied with a magnetic stirrer bar (as large as could fit inside the vial) during the addition to produce an evenly dispersed suspension of MCC. This mixture was then heated to 60° C in an oil bath and mixed until the liquid appeared optically clear. After all cellulose had dissolved, the vial was left to cool at RT. The IL/cellulose mixture was stirred continuously until the cooling step when the mixing was stopped.

4.1.5. Dissolution of cellulose (MCC) in [P$_{4441}$][OAc]/GVL (30 wt-% GVL)

To prepare a 5 wt-% solution of cellulose (MCC) in [P$_{4441}$][OAc]/GVL, an appropriate amount of cellulose (for example 0,1 g) was weighed and added slowly to the IL/co-solvent (1,9 g) in a 20 ml glass vial. Mixing was applied with a magnetic stirrer bar (as large as could fit inside the vial) during the addition to produce an evenly dispersed suspension of MCC. This mixture was then heated to 70° C in an oil bath for 45 min and then placed in another oil bath heated to 120° C for 5 min. After this the liquid appeared optically clear and it was left to cool at different ambient temperatures (RT, refrigerator at 4° C, ice bath at 0° C, freezer at -16° C). The IL/cellulose mixture was stirred continuously until the cooling step when the mixing was stopped.

4.1.6. Preparation of surfactant solutions

The mixing of the original surfactant stock solutions was done by vigorous stirring using a magnetic stirrer bar, while the more dilute solutions were prepared by diluting a portion of the stock solution with further water. The Critical Micelle Concentration (CMC) of all of the studied surfactants was

retrieved from literature (Brij-52, Brij-72, Brij-76,[163] Aerosol-OT 100[164] and SDS[165]). For SDS, which has a high CMC concentration, the minimum concentration used was at least twice that of CMC. For those surfactants with lower CMC concentrations (Brij-52 and Brij-72), the minimum surfactant concentration used in the experiments was ten times higher than CMC. This minimum concentration was chosen so that the surfactant solution would be saturated and would guarantee that the formation of nanoparticles in the nanoprecipitation experiments would not be hindered by the lack of surfactant. This decision was also based on practical limitations, as the preparation of very low concentration solutions directly is inaccurate and the need to do multiple dilution steps limits the accurate determination of the surfactant concentration. This is due to the surfactant not being evenly distributed in the aqueous solution, being in the form of micelles, which showed visible concentration gradients within the 500 ml stock solution bottle. For the low CMC concentration surfactants, stock solutions of up to 5000xCMC were initially prepared, to be diluted later. The minimum used concentrations are listed in **Table 1**.

Table 1. Surfactants used in the nanoprecipitation experiments. CMC values were retrieved from literature.

Surfactant	Average Mn	CMC in water	Minimum concentration used		
Brij-52	330	0.000067 mM	10xCMC	0,00067 mM	$2,211 \cdot 10^{-4}$ g/l
Brij-72	357	0.00025 mM	10xCMC	0,0025 mM	$8,965 \cdot 10^{-4}$ g/l
Brij-76	711	0.003 mM	10xCMC	0,03 mM	0,02133 g/l
Aerosol-OT 100	444,56	0,12 w/v-% (2,7 mM)	10xCMC	27 mM	12 g/l
SDS	288,372	7 mM	2xCMC	14 mM	4,037 g/l

4.1.7. X-Ray Diffraction (XRD) measurements for determining Crystallinity Index (CI)

The Crystallinity Index of the ADCB, FDCB and UCST samples was determined using a PANalytical X'Pert Pro MPD system. The diffracted intensity of Cu Kα radiation (λ = 1.54Å, under a condition of 45 kV and 40 mA) was measured in a 2θ range between 5° and 50°. The degree of crystallinity (Crystallinity Index, CI) of the freeze-dried cellulose beads (FDCB) was evaluated by using the amorphous subtraction method on an X-Ray diffractogram.[166] This method consists of the deconvolution of the crystalline signals obtained from the X-ray diffraction pattern, while separating

and subtracting the amorphous baseline. A curve-fitting software Fityk[167] was used to calculate the CI and it accepted Gaussian,[168] Lorentzian,[169] and Voigt[170] signals. The degree of crystallinity (CI) was determined by comparing the area of the crystalline signals to total area (including amorphous background).

A fully amorphous standard with close enough resemblance to the amorphous component in the sample is needed, in order to acquire a feasible estimate of the amorphous background of the freeze-dried beads. To prepare the amorphous standard, Enocell pulp was dissolved in trifluoroacetic acid (TFA). Enocell pulp (0.100 g) was placed in a 20 ml container and TFA 99% (2ml) was added. The mixture was stirred at room temperature overnight, after which it was poured onto a petri dish and left to dry at ambient conditions for 10 h. The resulting transparent film was further dried under vacuum. All work relating to preparing the amorphous samples, measuring XRD and deconvolution of the diffractogram was done by MSc Daniel Rico del Cerro.

A WAXS sample of purified UCST microparticles can be prepared by mixing a 200 mg portion of vacuum treated dope (see section **4.4.5. Removal of GVL under vacuum**) with 40 ml acetone in a 50 ml centrifuge tube and sonicated with a probe sonicator Hielscher UP100H Ultrasonic Processor for 30 min at max amplitude and no cycling. The sample was centrifuged at 4000 rpm for 10 min, the supernatant was decanted off and replaced with a fresh batch of acetone. The resulting dispersion was sonicated for further 30 min and centrifuged again. The supernatant was again decanted of the sample, which was left to dry in the air. The resulting mass was formed into a disc and subsequently analysed using WAXS.

4.1.8. SEM-analysis of ADCB and FDCB beads and UCST microparticles

All the SEM images of the various cellulose materials were taken on a Hitachi S-4800 Field Emission Scanning Electron Microscope and sputter coated with Au-Pd alloy. The samples were all placed either on carbon tape or on the surface of a silicon wafer, which were in turn placed on the aluminium SEM stubs.

While the ADCB and FDCB beads are easily large enough to be analysed visually by eye, using a good quality camera or an optical microscope, some additional information was able to be gleaned from them by using Scanning Electron Microscopy (SEM). Silver paint was applied around one of the samples to increase the electron conductivity of the material, which allowed imaging at larger

magnifications and with higher energies. Otherwise the beads were analysed unaltered apart from the sputtered coating of AU-Pd.

Studying the shape and appearance of the UCST microparticles necessitated the use of SEM. A SEM sample of purified UCST microparticles can be prepared by mixing a 10 mg portion of vacuum treated dope (see section **4.4.5. Removal of GVL under vacuum**) with 40 ml acetone in a 50 ml centrifuge tube and sonicating it with a Hielscher UP100H Ultrasonic Processor probe sonicator for 30 min. Afterwards the sample is centrifuged at 4000 rpm for 10 min, the supernatant is decanted off and replaced with a fresh batch of acetone. The resulting dispersion is then sonicated for further 30 min, after which a small drop is placed on a silicon wafer. The material is left to dry in air for 30 min and finally placed in a vacuum oven at RT for 10 min. The particles on the wafer surface can be sputtered with Au-Pd and studied using a SEM.

4.1.9. Cellulose nanoparticles by dialysis of MCC/IL dopes

Experiment was fashioned to study the possibility of using dialysis as a way to produce cellulose nanoparticles. The nature of the dialysis bag, regenerated cellulose, raises concerns for the feasibility of using it with direct cellulose solvents such as [DBNH][OAc]/DMSO, [P$_{4441}$][OAc]/DMSO and [P$_{8888}$][OAc]/DMSO (all 30 wt-% DMSO). Hence the dialysis was first initiated with using a portion of the cellulose solvent [P$_{4441}$][OAc]/DMSO, with no dissolved cellulose content prior to dialysis, to see if the dialysis bag could hold up to the aggressive solvent. Out of the three, this particular solvent was chosen due to prior knowledge of the IL's lesser cellulose dissolving capabilities at RT compared to the other two. A 25 cm piece of 6000-8000 MWCO (molecular weight cut-off) regenerated cellulose dialysis bag was placed in 1 l of water to soak overnight. Two 5 l beakers with ion exchanged water were set up next to each other, with magnetic stirrers mixing the water in both. A dialysis clip was fastened to a stand between the beakers so that it just reached beneath the liquid surface in both beakers, when they were filled with water. In the same fashion, the length of the dialysis bag was measured beforehand so that it would not hit the stirrer bar on the bottom of the beaker when in operation. After sufficient soaking of the dialysis bag was achieved, the bag was opened gently and one end was folded and closed with a clip.

Wetting the dialysis bag once more, a 2 g sample of the IL [P$_{4441}$][OAc]/DMSO (30 wt-% DMSO) was added to the bag quickly, but carefully. Immediately after the addition of the IL, air was squeezed

out of the bag and the open end was closed the same way as the other one. The filled dialysis bag was submerged in the 5 l beaker, while the water was gently mixed. The dialysis bag was changed from the first beaker to the next after first 30 min. Afterwards it was alternated between the beakers every hour, until it was left to soak overnight after 8 hours. The water from the vacated beaker was changed after each cycle. Finally, the water was changed once more the following day after 22 h from the start of the experiment. After 24 h the dialysis bag was removed from the water, the outside surface dried gently with a non-abrasive paper, the upper clip opened and the contents poured into a 20 ml beaker, which was then covered with parafilm and placed in a refrigerator. It was found that after only 10 minutes, the sample in the bottom part of the dialysis bag started to turn cloudy and damage to the dialysis bag walls was evidenced by the appearance of visible patches of slightly opaque material. After 45-60 minutes, visible particles started appearing and after 150 min, all of the cloudiness had disappeared with only large visible brown coloured particles were observable.

The effects of the experiment on the dialysis bag were studied by optical microscopy. Control pictures of a dry and wet dialysis bags were taken from small pieces of bag (**Figure 35, A&B**). Then two parts of the dialysis bag used in the experiment were imaged: one from low down on the dialysis bag (C), showing visible surface damage from the solvent and one from higher up (D) that seemed visually unaltered from higher up on the bag. Even though the dialysis bag on inset C was not dissolved all the way through, under the microscope the scarring caused by the procedure in evident, i.e. it has a relief pattern of hills and valleys. Also the seemingly undamaged section showed some "waviness" visible in the diagonal direction, which might indicate that it did suffer some small scale deformation as well. The formed particles were also imaged under a microscope (E&F), they were large and of irregular shapes indicating an uncontrolled agglomeration of cellulose.
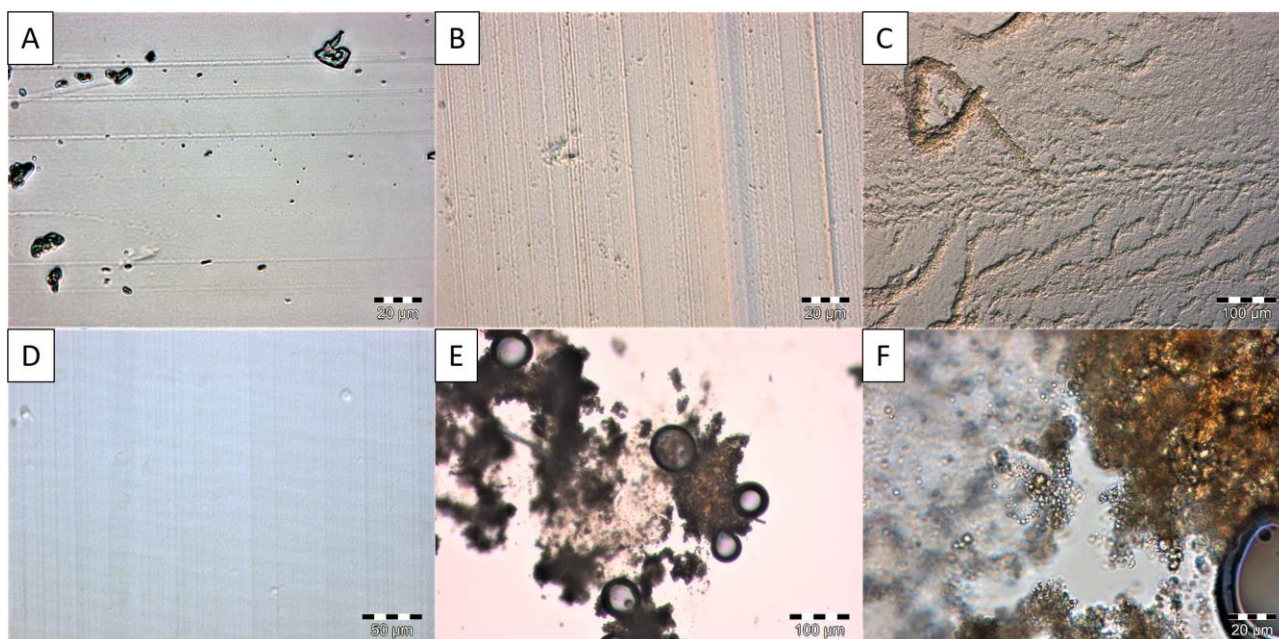
Figure 35. Optical microscope images of the cellulosic dialysis bag used in the dialysis trials and some of the formed particle aggregates. A: dry dialysis bag, B: soaked dialysis bag. C: damaged section of dialysis bag, D: mostly undamaged section of the dialysis bag, E&F: large particle aggregates formed from the dissolved dialysis bag walls.

The observations can be explained by the dissolution of the dialysis bag by the IL. When the IL is inserted into the bag, it starts to instantly dissolve the inner surface of the bag, even though the bag is wet and is immediately placed underwater. The dissolved cellulose starts to precipitate when enough water has diffused into the bag to lower the dissolving capacity of the IL. First it is seen as cloudiness, particles that are too small to see with the naked eye, but with enough time they agglomerate together to form larger visible particles.

To prove the prior assumption of lesser dissolving power of [P$_{4441}$][OAc]/DMSO, and to test whether further dialysis trials using the other solvents were necessary, the dissolving capabilities of the three ILs were tested using a piece of dry dialysis bag and no water. Into a 1 g sample of IL, a ca. 10 mg piece of dialysis bag was placed under gentle stirring of the mixture. The prior assumption concerning the dissolving power of [P$_{4441}$][OAc]/DMSO was proven, as complete dissolution of the piece of bag was observed in [DBNH][OAc]/DMSO and [P$_{8881}$][OAc]/DMSO, but [P$_{4441}$][OAc]/DMSO did not seem have had nearly as much of an impact on the material. The piece of dialysis bag was removed from the IL after 24 h and mixed with 2 ml of distilled water, while stirred vigorously for 30 min. The bag was removed and soaked overnight in 10 ml of water. Afterwards the piece of bag

was studied under the microscope and it showed similar relief pattern as did the bag used in the actual dialysis, albeit the relief was of much higher degree (**Figure 36. A**).

Figure 36. Optical microscope images of the cellulosic dialysis bag used in the dissolution and dialysis tests. A: 10 mg piece of dialysis bag immersed in [P$_{4441}$][OAc]/DMSO for 24 h, B: 10 mg piece of dialysis bag immersed in [P$_{4441}$][OAc]/GVL for 24 h, C: piece of the dialysis bag used in a dialysis test using [P$_{4441}$][OAc]/GVL as the sample to be dialysed.

A further test using [P$_{4441}$][OAc]/GVL as the solvent seemed to result in even lesser scarring of the dialysis bag (**Figure 36. B**). This result can be rationalised by thermodynamical measurements and observations described in sections **2.2.5. The role of co-solvents in the solvation of cellulose, 2.2.2. Thermodynamics of cellulose dissolution, 2.2.4. Kamlet-Taft Parameters of a cellulose solvent** and **2.4.1. UCST in [P$_{4441}$][OAc]/GVL.** Based on the findings presented in those chapters, it can be said that while GVL is a cellulose-compatible co-solvent in multiple solvent organic electrolytes, it is all around a worse solvent for cellulose than DMSO. In addition, a dialysis was run using [P$_{4441}$][OAc]/GVL (30 wt-% GVL) as the sample to be dialysed, with the setup being identical to those described earlier. Unlike with DMSO as a co-solvent, no deterioration of the dialysis bag was observed during the dialysis process. When studied under the microscope, a similar lack of deterioration was observed (**Figure 36. C**). This would imply that cellulose nanoparticles could in theory be prepared using this solvent system.

4.2. Cellulose particles from [DBNH][OAc]/DMSO solution

The following section of the experimental work describes the tests conducted with the aim of preparing cellulose micro- and nanoparticles using the [DBNH][OAc]/DMSO solvent system. The outset for the experimental work was a homogeneous dissolution of MCC in the [DBNH][OAc]/DMSO (40 wt-% DMSO) solvent system and the initial goal was to prepare cellulose nanoparticles based on the nanoprecipitation nanoparticle preparation method (see section **3.3.6. Polymeric nanoparticles by nanoprecipitation**). However, this method turned out not to be feasible for cellulose nanoparticles synthesis, being much more suited for the preparation of cellulose micro- and macroparticles. Hence, the focal point of the work shifted more towards the preparation of larger cellulose beads. This shift is also reflected in the fact that the initial tests, consisting of experiments from **4.2.2. Nanoprecipitation of cellulose from [DBNH][OAc]/DMSO dope** to **4.2.5. Effect of mixing on cellulose nanoprecipitation from [DBNH][OAc]/DMSO**, were performed with relatively large range of variation to the synthesis techniques, while the subsequent intermediate experiments were much more uniform in design. The Cellulose Bead (CB) preparation procedure also took its shape during these intermediate experiments, which were the foundation upon which the final refined method used to prepare the majority of all cellulose beads in the ADCB (Air Dried Cellulose Beads) and FDCB (Freeze Dried Cellulose Beads) experiments and their derivates was built on. The final refined procedure obtained as a result of all the tests conducted is described below. The capitalised moniker "Cellulose Bead" (or just CB) is used to refer to any of the large millimetre-scale cellulose particles produced with the [DBNH][OAc]/DMSO solvent system.

4.2.1. Basic Cellulose Bead (CB) experimental setup

A cellulose solution of various wt-% is first prepared by dissolving MCC (MicroCrystalline Cellulose) in [DBNH][OAc]/DMSO (40 wt-% DMSO). The synthesis of [DBNH][OAc], the preparation of the electrolyte and the dissolution of cellulose is described in sections **4.1.1. Preparation of [DBNH][OAc]/DMSO (40 wt-% DMSO)** and **4.1.4. Dissolution of cellulose (MCC) in [DBNH][OAc]/DMSO (40 wt-% DMSO).** Throughout the laboratory tests, the wt-% of MCC in the IL solution varied from 0,1 wt-% to 10 wt-%. Usually the concentration was between 3-5 wt-%, with 5 wt-% being by far the most common concentration.

After a homogenous MCC/[DBNH][OAc]/DMSO dope is achieved, the solution is left to cool at RT. Subsequently the dope is loaded onto a syringe of a proper size for the amount of dope, with sizes used varying from 1 ml to 200 ml. The dope is extruded at a constant rate from the syringe to a needle using a syringe pump. A connecting tube can be used to connect the syringe to a needle positioned further away from the pump. The extruding dope forms a drop on the needle tip, and once enough dope has gathered, the drop falls down into an antisolvent bath (usually pure distilled water). The drop-shape formation is driven by gravity and the property of the dope that mostly affects the process is viscosity. The antisolvent is pure distilled water, while several aqueous surfactant solutions and several non-aqueous solvents were tested during the initial studies. If a connecting tube is used, then a straight needle can be placed perpendicularly above the water surface. However, when no tube is used, the needle is gently bent 90° so that the needle tip is facing the water surface perpendicularly. The drop formation is the most consistent when the needle tip is pointing straight down.

Once the drop of dope has left the needle tip, it will fall towards the liquid surface. In most cases, the drop of dope will penetrate the surface and sink to the bottom. The instance the drop submerges, its outer surface will harden due to desolvation of cellulose. This is a result of the fast diffusion of water into the drop of dope, and partly due to the slower diffusion of [DBNH][OAc] and DMSO out of the drop. This leads to the formation of a dense precipitated cellulose network on the outer surface of the drop, which keeps the drops from merging and slows down the diffusion of the solvents from and into the interior of the bead. When all of the dope has been extruded as droplets, the beads are left to precipitate fully in the water bath. After approximately 15 min, even the last-extruded beads have turned from transparent to fully opaque greyish white. Subsequently the beads are washed multiple times (usually five times) with distilled water by replacing the water in the bath with a fresh batch. The beads are then left to soak in water for 24 h, after which they are washed once more with a fresh batch of water.

At this point the beads are either air-dried, freeze-dried or left for storage in water. The air-drying process is very simple, consisting of placing the wet beads on a petri-dish or other flat container, draining out excess water from around the beads and protecting the container from airborne dust. This last step is usually done by placing the lid on the container, but leaving it slightly ajar to let the water vapour escape. The beads are usually dry after 24 h, but if they are not, the process is continued until they are. During air-drying, the beads will change appearance from whitish opaque

to transparent, and shrink to roughly half of their original diameter. After this, the beads are ready for storage or additional treatments.

The freeze-drying process is equally simple, consisting of placing the wet beads inside containers able to stand freezing temperature, freezing with liquid nitrogen and finally placing the container in the freeze-dryer. In the vacuum of the freeze-dryer, the water in the beads sublimates, leading to dry particles usually after 24 h. In contrast to air-drying, the beads retain their pre-drying dimensions and their white colour. After this, the beads are ready for storage or additional treatments.

4.2.2. Nanoprecipitation of cellulose from [DBNH][OAc]/DMSO dope

The aim of this experiment was to prepare cellulose nanoparticles using the nanoprecipitation method (see section **3.3.6. Polymeric nanoparticles by nanoprecipitation**). Cellulose was to be dissolved in [DBNH][OAc]/DMSO (40 wt-% DMSO) and the resulting solution was to be dispersed into an aqueous surfactant solution. The hypothesis was that this would result in the precipitation of cellulose into nanoparticles as the solvent around the cellulose polymer was replaced with antisolvent (H_2O). The surfactant was presumed to help in the formation of nanoparticles by preventing excessive aggregation of particles post-precipitation. Finally dialysis was used as a clean-up method, getting rid of the [DBNH][OAc]/DMSO and excess surfactant.

A cellulose dope (1 wt-%) was prepared by dissolving 0,010 g of MCC in 1 g of [DBNH][OAc]/DMSO (40 wt-% DMSO). Separately an aqueous Brij-S10 solution (2 ml, 0,03 mM) was prepared, with the resulting solution being ten times the critical micelle concentration (CMC) of Brij-S10.[163] The cellulose dope was transferred to a syringe and added slowly (0,6 ml/3 min) to the surfactant solution under moderate stirring using a magnetic stirrer bar.

The resulting solution was let to mix for 30 min, after which a dialysis was run with a 6-8000 MWCO dialysis bag for 24 h. Before dialysis started, the mixture in the bag was coloured slightly beige and showed some turbidity. After only a minute in the dialysis bag, a grainy, particulate jelly texture was observed, with individual particles visible by eye. The dialysis was run in a similar fashion as in the dialysis trials (see section **4.1.9. Cellulose nanoparticles by dialysis of MCC/IL dopes**) and the ion exchanged water was changed after 30 min, every hour after that for the next six hours, and finally left overnight. The next morning, after 23 h, the water was changed once more and after further 1 h, the dialysis was ended.

Due to the individual particles being visible by eye, it was evident that either the formed particles were much larger than the intended nanoscale particles or they had secondarily agglomerated together. Microscopic images were taken of the particles and they were shown to be composed of large, hundreds of μm scale irregularly shaped shreds (**Figure 37.**). Based on observations made in later experiments, the particles observed were most likely the remnants of the formed Cellulose Beads (CB), which had been torn apart by the stirrer bar. The low cellulose concentration in the dope (1 wt-%) also forms mechanically weaker spheres than higher concentration ones (e.g. 5 wt-%, which was used in the formation of most of the later CBs), which aided in the breakup of the beads.
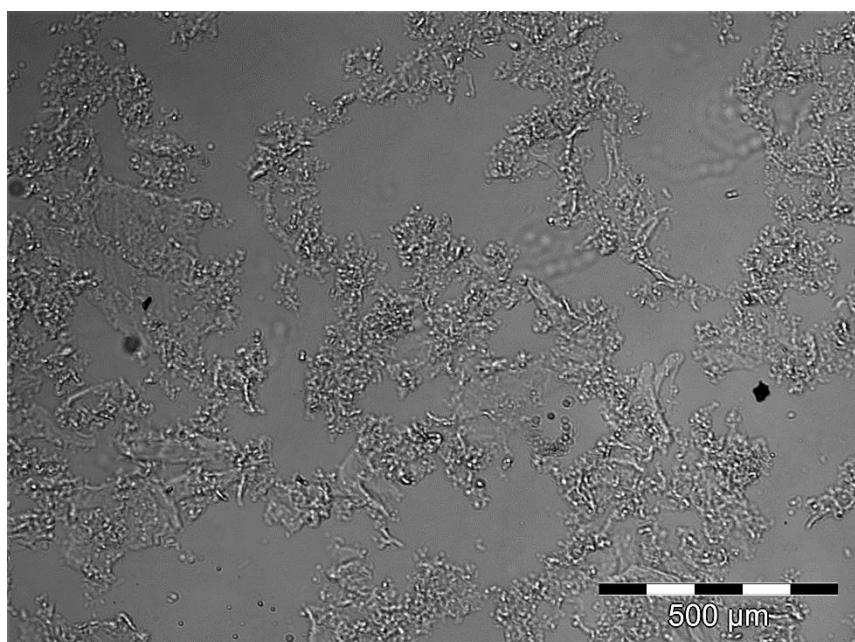
Figure 37. Optical microscope image of the precipitated cellulose material acquired in the first nanoprecipitation experiment. The large scale of the particles (hundreds of μm) points out the failure of the method for its intended purpose – nanoprecipitation.

4.2.3. Effect of surfactant on cellulose nanoprecipitation from [DBNH][OAc]/DMSO

The previous test was replicated using a number of surfactants at varying concentrations, which are listed in **Table 2**. There was a change in surfactant total volume from 2 ml to 3 ml and the concentrations varied from 2xCMC to 1000xCMC. The MCC (1 wt-%)/IL/DMSO (overall 0,5 ml) and surfactant solutions (3 ml) were also mixed together, not by hand, but by extruding the cellulose dope from a 1 ml syringe above the surfactant solution using a syringe pump (running time 2 min).

Table 2. Surfactants and their aqueous concentrations used in the nanoprecipitation tests. Actual surfactant concentrations can be calculated from values listed in section **4.1.6. Preparation of Surfactant Solution**. The test run using 100xCMC Brij-76 (red **X**) was the one were the mixing failed and the first Cellulose Beads were observed.

Surfactant	2xCMC	5xCMC	10xCMC	25xCMC	50xCMC	100xCMC	1000xCMC
Brij-72			X			X	X
Brij-76			X			**X**	X
Aerosol-OT			X	X	X		
SDS	X	X	X				

The tests were carried out in a similar manner to the previous experiment, employing a reasonably vigorous magnetic stirring to enhance the mixing of the cellulose and surfactant solutions. However, when the test using Bri-76 as surfactant at concentration of 100xCMC was carried out, the magnetic stirrer bar got stuck and hence, the efficiency of the stirring was significantly reduced compared to the other tests. As the mixing was very limited, the drops of dope falling from the end of the needle were left mostly undisturbed in the surfactant solution. Much to the surprise of the author, the drops did not disperse in the surfactant solution but were left on the bottom of the beaker as large transparent beads. The roughly 2 mm diameter particles retained the shape of the drops at the time of their impact with the liquid surface and were the first Cellulose Beads (CB) observed during this thesis. The beads that were formed are presented in **Figure 38**.

After a short while, the initially transparent beads started to turn white and were found out to be rather fragile overall, easily breaking up in response to the pressure produced when a syringe needle was tested for the purpose of solvent exchange around the particles. After several solvent exchange cycles were executed in a more careful manner, the cellulose beads were placed in pure distilled water. The products of the other tests, during which the stirring had worked as intended, were imaged using optical microscope and the formed cellulose material was very similar to those observed in the earlier test, with ragged shreds of 10^{-5} m scale cellulose particles remaining suspended in the surfactant rich solutions.
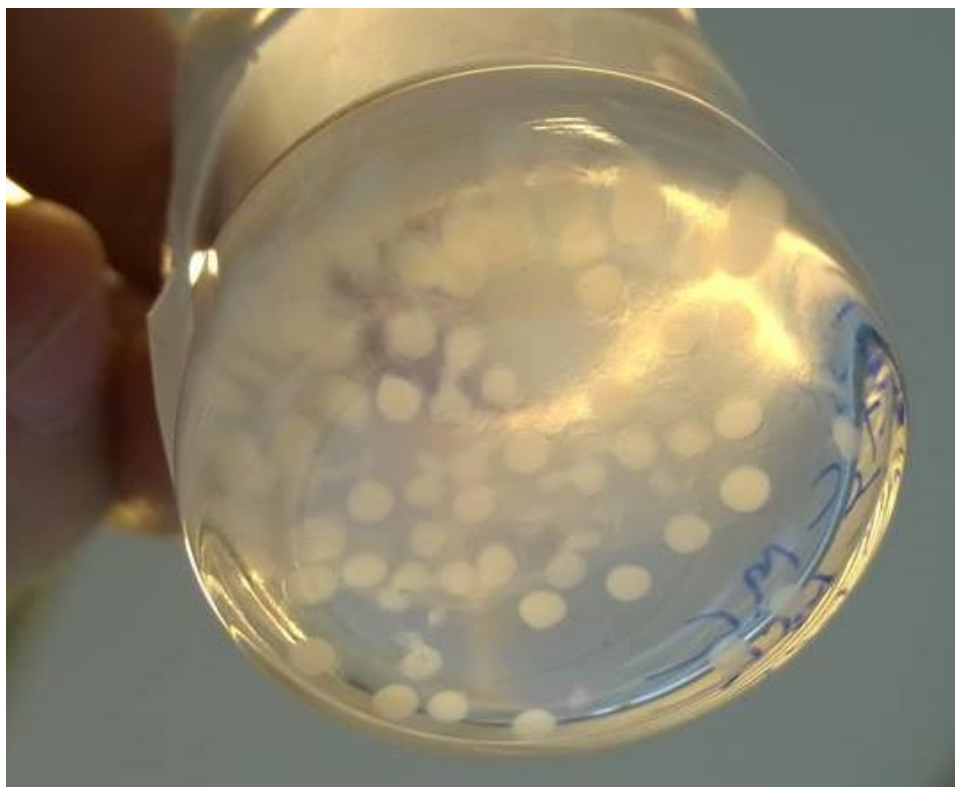
Figure 38. The first Cellulose Beads (CB) observed in making of this thesis were produced during the Nanoprecipitation 2 tests. The magnetic stirrer bar has been removed from the beaker before capture of this image.

Here the author would like to point out that the apparent failure of this one experiment truly had an unseen benefit, as the surprising findings of this failed test ultimately gave rise to more than half of the experimental content and intellectual concepts composing the finished thesis.

The results were replicated using 50xCMC Aerosol-OT 100 as the surfactant on a separate experiment, where the mixing of the surfactant solution was forgone intentionally. The beads produced were found to be identical to those prepared with Brij-76 and hence the nature of the surfactant (neutral Brij-76 or anionic Aerosol-OT 100) inconsequential to the formation of the beads.

4.2.4. Effect of temperature on cellulose nanoprecipitation from [DBNH][OAc]/DMSO

This experiment was performed at an elevated temperature of 60° C and using a 10xCMC solution of SDS as the antisolvent, but otherwise following the basic setup of the previous experiment with mixing still enabled. The rationale was that at higher temperature, the mixing at the solvent interface would be enhanced due to lowered viscosity of the surfactant solution, which in turn would be the result of increased molecular energy. This test was still performed with the aim of

producing cellulose nanoparticles and not the large scale beads discovered in the earlier test. The antisolvent was placed in a 20 ml vial, which was held in an oil bath. The vial was kept closed at all times, apart for the 2 min period when the dope was administered to the vial. The vial was kept in the oil bath for further 30 minutes after the pumping had ceased. Subsequently the vial was removed from heat and sonicated for 15 min in a water bath sonicator. Microscope images of the resulting mixture were taken on an optical microscope (**Figure 39.**).
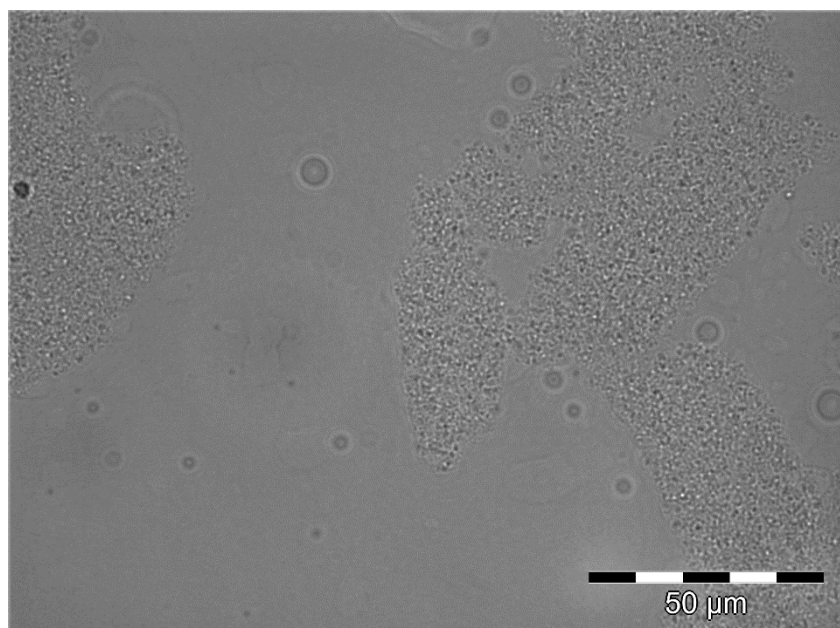
Figure 39. Optical microscope image of the mass agglomeration of particles produced in the Nanoprecipitation 3 experiment. The big "rafts" are likely the remainders of the shape of the initial drop of dope, which was shredded apart by the magnetic mixing bar.

The large "rafts" of precipitated material, with dimensions in the order tens to hundreds of μm, are easily visible from the image. These rafts are likely the result of the magnetic stirrer bar breaking apart the initial drop of dope, which's surface had precipitated upon contact with the water. The rafts seem to be composed of smaller individual particles in the size range of few μm, but those particles were not discernible using the optical microscope and did not separate upon sonication. Overall, this test was unsuccessful in procuring cellulose nanoparticles.

4.2.5. Effect of mixing on cellulose nanoprecipitation from [DBNH][OAc]/DMSO

This test was still run with the aim of producing cellulose nanoparticles via the nanoprecipitation method. In light of earlier observations, where the inserted dope either formed large sized Cellulose Beads or was broken into 10 – 100 μm scale irregular shreds by the magnetic stirrer bar, this experiment was run using a much higher intensity mixing Ultra-Turrax apparatus. The motivation behind the experiment was to expose the interface between the extruding dope and the antisolvent to as powerful a mixing as possible. This should facilitate the efficient mixing of the solvents and provide the best circumstances for the formation of nanoparticles.

Ultra-Turrax is a high power mechanical mixer working on an electric motor. The motor spins a special mixing head at rates of thousands of revolutions per minute, which induces high shear forces onto a solvent media. In this experiment setup, the dope was loaded onto a 1 ml syringe in the syringe pump and the syringe was connected to the needle via a long flexible tube (**Figure 40. A**). The needle was taped to the shaft of the Ultra-Turrax so that the tip of the needle was as close to the mixing head as possible, but was not in the way during mixing. The mixing vessel was chosen to minimize the amount of solvent needed to keep the shaft of the mixer underwater, which is necessary to guarantee adequate cooling of the mixing head and shaft. The 1 wt-% MCC dope (0,5 ml) was injected into the water bath at a rate of 0,25 ml/min. The Ultra-Turrax was set at

Figure 40. A: The setup used to test nanoprecipitation while mixing with Ultra-Turrax mechanical mixer. The syringe is connected by a flexible tube to a needle taped to the shaft of the Ultra-Turrax mix head. B: Excessive foaming resulting from the presence of 1 wt-% of Aerosol OT surfactant along with cellulose in the [DBNH][OAc]/DMSO-dope. The intensity of mixing had to be reduced to avoid further foaming.

approximately 70 % maximum intensity, which equals to roughly 16,000 rpm. Microscope images were taken of the material produced, which showed the presence of shredded cellulose particles similar in appearance, albeit significantly reduced in size (<10 μm), compared to earlier results.

In additional testing, the Ultra-Turrax experiment was altered in two ways in order to maximise the possibility of attaining nanoparticles. First in one experiment, a surfactant (1 wt-% Aerosol OT 100) was added to the dope to facilitate the mixing of the two solvents at the solvent interface. This unfortunately resulted in excessive foaming and hence the intensity setting of Ultra-Turrax had to be lowered to 60 % (**Figure 40. B**). The particles obtained were imaged on a microscope (**Figure 41. A**).

Then on a second experiment, the composition of the dope was altered from 40 wt-% DMSO to 80 wt-% DMSO, as well as substituting the antisolvent (distilled H_2O) for 100xCMC aqueous solution of Brij-52. The DMSO concentration was increased in order to lower the viscosity of the dope, which should have beneficial effects on the formation of nanoparticles by facilitating more efficient mixing at the solvent interface. The increased surfactant concentration was also hypothesized to augment the efficiency of mixing and stabilisation of nanoemulsions at the solvent interface, despite the ensuing increase in viscosity in the antisolvent bath. The material produced was imaged on an optical microscope (**Figure 41. B**).
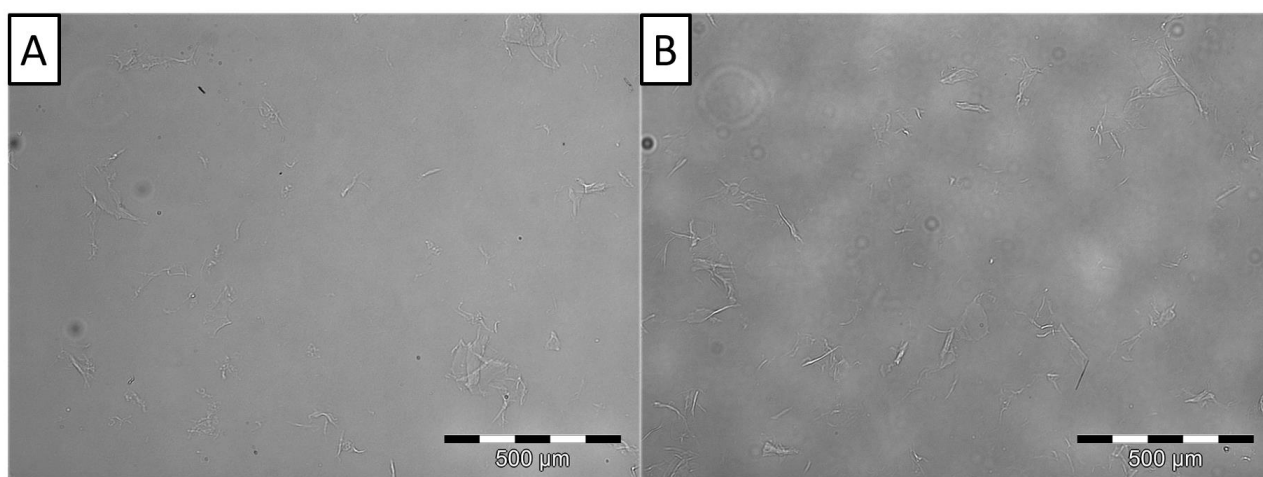
Figure 41. Optical microscope images of the cellulosic material recovered from the further two Ultra-Turrax experiments. **A:** Shreds of cellulose resulting from dope containing 1 wt-% Aerosol-OT 100 surfactant. **B:** Shreds of cellulose resulting from [DBNH][OAc]/DMSO (80 wt-% DMSO, instead of 40 wt-%) and antisolvent containing 100xCMC Brij-52. The shape of the material is a result of the extruded string of dope being shredded by the Ultra-Turrax mixer.

As can be seen from **Figure 41. A&B**, the resulting materials did not differ much from each other. Both types of particles were of an irregular shredded appearance and ranged from tens to hundreds of μm in size. The string of dope extruded from the needle tip likely precipitated instantly upon contact with the antisolvent, but was then very swiftly shredded to tiny cellulose "rafts" by the Ultra-Turrax mixer head. In the end, the nanoprecipitation method was deemed unsuitable for the [DBNH][OAc]/DMSO solvent system and this was the final test where nanoprecipitation was conducted in the orthodox manner – dope being extruded into a stirred surfactant solution with the aim of preparing nanoparticles.

4.2.6. Formation of large sized Cellulose Beads

The following intermediate experiments were aimed at elucidating the cause, properties and potential of the formation of large scale Cellulose Beads (CB) first observed during the initial tests. During these small scale experiments, most of the capabilities and limitations of the phenomenon were screened and the foundations of the cellulose bead forming process (see section **4.2.1. Basic Cellulose Bead (CB) experimental setup**) were laid for the upscaled ADCB and FDCB experiments that followed.

The first Cellulose Bead experiment was based on the findings of the second nanoprecipitation experiment. A 1 wt-% MCC in [DBNH][OAc]/DMSO (40 wt-% DMSO) was prepared and 0,5 ml of this dope was extruded into 3 ml of 50xCMC of Aerosol-OT 100 (aq.) in the same way as in **4.2.3. Effect of surfactant on cellulose nanoprecipitation from [DBNH][OAc]/DMSO**. The solidified beads were left in the solution for 30 min, after which they were washed 5 times with 20 ml of distilled water. The beads were left for several hours in the last batch of water. Before freeze-drying, all the water that readily poured out of the vial was removed and the whole container was frozen in liquid nitrogen, after which it was placed in the Labconco FreeZone 2.5 Plus freeze-dryer for 24 h. The resulting particles were completely white and opaque, but their shape had deformed considerably from their pre-dried spherical state. A single bead had an average weight of 0,15 mg and was considerably wrinkly, resembling a crushed soda cans in appearance.

4.2.7. The effect of drying method on Cellulose Bead appearance

The experiment was run in a similar fashion to the previous experiment, while varying the concentration of MCC in the dope to test what type of effect this would have on the bead forming phenomenon and the properties of the resulting beads. The setup consisted of a syringe pump, which extruded the dope (0,5 ml) through a needle placed over a beaker containing an aqueous solution of Aerosol-OT 100 (50xCMC). The MCC concentrations used and the treatments carried out on them are listed in **Table 3**. Beads containing low amounts of MCC (0,1-0,75 wt-%) broke during the initial addition step into the antisolvent and hence were not studied further. On the other hand, the high MCC composition dope (10 wt-%) was very viscous and when extruded out of the needle tip, a long tail formed on the beads. This resulted from the material stretching considerably before the connection between the needle and the drop was severed. In this case, the surface tension of the dope is not sufficiently high to contract the shape of the drop to its most stable roundish shape before impact with the antisolvent surface, leaving a tail trailing behind the drop. As the tail failed to withdraw into the head of the drop in time, it remained on the final beads when the surface of the dope hardened and the shape of the object was sealed.

Table 3. The wt-% of MCC in the [DBNH][OAc]/DMSO (40 wt-% DMSO) tested for the formation of Cellulose beads and the drying methods employed for each bead composition. (* = The beads broke during preparation. † = The beads retained very prominent tails.)

MCC wt-% →	0,1	0,25	0,5	0,75	2	3	4	5	6	7	10
Beads formed	X*	X*	X*	X*	X	X	X	X	X	X	X†
Freeze-dried					X	X	X	X	X	X	
Air-dried							X	X			

All of the beads that did not either break or retain excessive tails, were freeze-dried the same way as in **4.2.6. Formation of large sized Cellulose Beads**. A portion of the 4 and 5 wt-% beads were also air-dried out of interest. The air-drying was carried out in a very simple manner: the wet beads were placed on a petri dish in a fume hood and the water that remained was let to evaporate at RT. The process usually took from one to two days, depending on the amount of water present on the petri dish. The petri dish lid was slightly offset relative to the bottom part in order to encourage evaporation but still prevent airborne dust from settling onto the petri dish. During the drying process, the beads gradually shrunk from white opaque, roughly 2 mm sized soft spheres to transparent, hard sub-1-mm-sized beads (**Figure 42.**). The difference to freeze-dried beads was drastic and the process was observed to be irreversible. The intermediate stages of shrinkage are
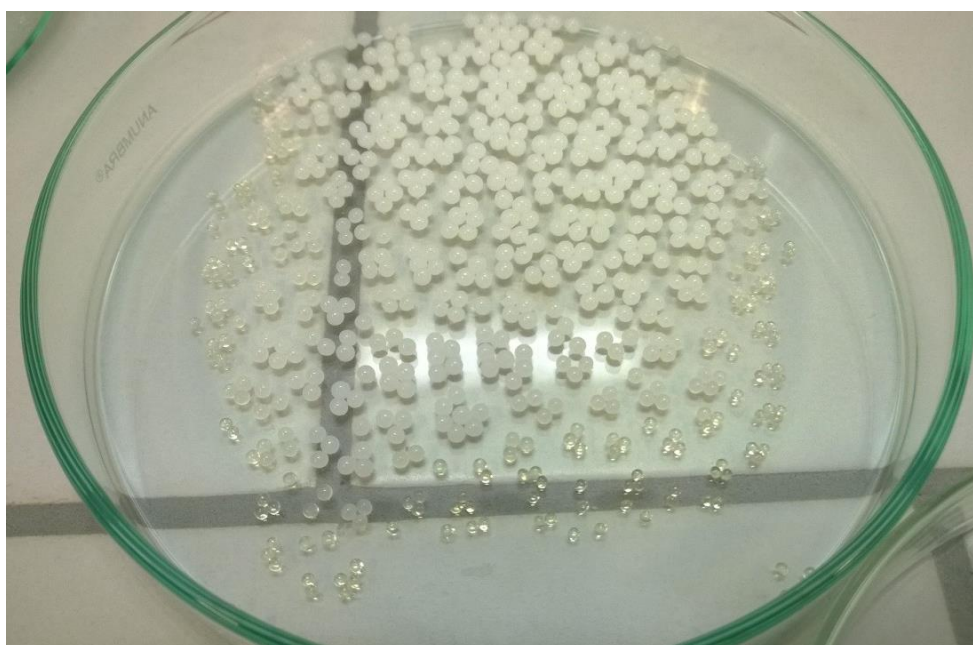

Figure 42. The shrinkage and the appearance of transparency of Cellulose Beads is evident during air-drying.

also intermediate in their colour change, turning more and more towards transparent the smaller the bead gets.The freeze-dried beads were white, opaque and identical in shape and size (1,5-2 mm) to the initially formed wet beads (**Figure 43.**). Unlike the 1 wt-% beads produced in the earlier experiment, these beads were not wrinkly or crushed but had a smooth and round surface. However, some of them did retain a small tail. The particles were weighed, the average weight calculated and based on a simple formula of the volume of a sphere, their density was estimated. As the size of the beads varied, the two extremes in diameter observed (1,5 and 2 mm) were used as the end points in the average density calculation. The density of the 1 wt-% beads from earlier is

not estimated as the particles differed greatly from the general round shape of the other beads. The results are listed in **Table 4**.

Figure 43. The freeze-dried Cellulose Beads are large (diameter ca. 2 mm), porous and opaque, while the air-dried Cellulose Beads are small (diameter <1 mm), dense and transparent.

It must be noted that the densities calculated are approximate and are presented only to give a general impression of the material density in question. Despite the inconsistencies with the 2 wt-% and 7 wt-% samples, which are composed of a very small number of beads, an expected trend of increasing density is observed side by side with the increase of MCC concentration in the dope. The estimated average densities vary from the highest 0,31 g/cm³ to lowest 0,0475 g/cm³, making the higher density beads similar to cork and the lower density similar to Styrofoam.

Table 4. The number, mass and density of freeze-dried beads derived from dope of varying MCC concentration.

MCC wt-%	Number of beads	mass of al beads (g)	mass of one bead (mg)	Density g/cm³ (1,5 mm)	Density g/cm³ (2,0 mm)	Density average
1 %	40	0,00604	0,15	-	-	-
2 %	7	0,00085	0,12	0,067	0,028	0,0475
3 %	33	0,00981	0,30	0,17	0,071	0,1205
4 %	62	0,02672	0,43	0,24	0,10	0,17
5 %	37	0,01946	0,53	0,30	0,12	0,21
6 %	19	0,01474	0,78	0,44	0,18	0,31
7 %	8	0,00586	0,73	0,41	0,17	0,29

One of the freeze-dried 1 wt-% beads and an air-dried 4 wt-% bead were submerged and soaked in water for 72 h. Both of the beads quickly sank to the bottom but did not swell or change shape during the 72 h period of submersion. The beads were subsequently removed from water and left to dry in air, resembling their appropriate non-soaked equivalents to the nicety once dry.

Five air-dried 4 wt-% beads were weighed (total mass 2,82 mg) and placed in the freeze dryer for 24 h. The beads were weighed afterwards (1,84 mg) and the result indicated a 35 wt-% loss during the freeze drying process. However, this experiment was repeated using a much larger mass of particles (ca. 1300 mg) and a significantly lower value of 3 wt-% loss was observed. These results and more are discussed in section **4.3.3. Water content of ADCB**.

4.2.8. Mass and density of Air- and Freeze-dried Cellulose Beads

Series of Cellulose Beads using dopes of varying cellulose concentrations were prepared in the same fashion as in previous experiments. The MCC concentrations used were 1, 2, 3, 4 and 5 wt-%. Each group of different MCC composition was split into two groups, one of which was freeze-dried and another which was air-dried. The two types of dried particles were identical in appearance to their prior-obtained equivalents. The number and mass of beads was determined and are listed in **Table 5**.

Table 5. The number, mass and density of beads derived from dope of varying MCC composition.

MCC wt- %	Method of drying	Number of beads	Mass (g)	Mass (mg) per bead	Density (g/cm^3) estimated using 1,8 and 0,9 mm diam.
1	Air-drying	23	0,00208	0,090	0,24
1	Freeze-drying	14	0,00136	0,097	0,031
2	Air-drying	18	0,00328	0,18	0,48
2	Freeze-drying	15	0,00279	0,19	0,061
3	Air-drying	31	0,00930	0,30	0,79
3	Freeze-drying	18	0,00461	0,26	0,084
4	Air-drying	14	0,00448	0,32	0,84
4	Freeze-drying	18	0,00554	0,31	0,10
5	Air-drying	8	0,00358	0,45	1,2
5	Freeze-drying	14	0,00613	0,44	0,14

The same expected trend of increasing density with cellulose wt-% seen in **4.2.7.** is also observed here. The 1 wt-% air-dried beads were quite flat and were stuck to the bottom of the petri dish, while the freeze-dried beads resembled crushed soda cans rather than spheres in shape. The 2 wt-% beads exhibited similar deviations from the shape of higher density beads, but to a lower degree than the 1 wt-% ones. The 3-5 wt-% air-dried beads were very close to spherical to the naked eye, while the freeze-dried beads were slightly more imperfect in their sphericity.

4.2.9. Choice of antisolvent in the production of Cellulose Beads

The basic experiment using 1 wt-% MCC dope was repeated with water (no surfactant) and varying organic solvents. The first aim of this experiment was to illuminating the role of the surfactant, or in fact the lack of one, in the Cellulose Bead formation. The second aim was to study the magnitude and type of effect the nature of the antisolvent has on the bead formation as well as to gauge the applicability for the production of Cellulose Beads. The solvents tested for bead formation were H_2O, EtOH, MeOH, isopropanol, acetone, ethyl acetate, THF, 1,4-dioxane, DMC, chloroform, acetonitrile, *n*-hexane, toluene, DMSO and GVL. At this point in the study, it was already evident that water is a very efficient antisolvent for the purpose of coagulating cellulose, as it was known that even 1 wt-% MCC drop of dope was capable of maintaining its spherical shape in the previously used aqueous surfactant solutions. Hence, in this experiment the cellulose concentration in the dope was set at 1 wt-% in order to see if any of the other solvents could outperform water.

Somewhat unsurprisingly, pure water expressed identical behaviour to the aqueous surfactant solutions described in previous experiments. The drops of dope falling from the end of the needle retained their shape to a very high degree during impact with the water surface. Initially after submersion, the beads were entirely transparent. This change was not previously as visible as it was in pure water, as the milky high concentration surfactant solutions in earlier experiments effectively concealed the initial entirely transparent appearance of the beads. However, similarly to the surfactant solutions, a change to fully opaque was observed in roughly 15 minutes. Some of the beads also had tails, which were an artefact of the dropwise method of addition and the fact that the dope is rather viscous. The surface of a drop is rather hard immediately after submersion, as the drops were observed to collide elastically with each other on numerous occasions but were never noted to coalescence to form a common phase with one another. This holds true even when a drop of dope lands on top of the previously extruded drop, which had entered the water bath only one second prior.

Ethanol, methanol and isopropanol acted in a mostly similar fashion to water. The main difference was that, while the solidification of the drop was instantaneous, the drops were rather soft and their shape slowly distorted due to flowing and flattening of the dope. The result was pancake-shaped particles, some of which had fused together into a large irregular mass. Furthermore, when air drying of the "pancakes" was tested, they stuck to the bottom of the petri dish and were

irremovable without incurring major damage to their shape. However, freeze-drying of the beads was successful and pancake shaped opaque particles were obtained.

Acetone, ethyl acetate, THF and 1,4-dioxane resulted in the almost instantaneous dispersion of the introduced drop of dope and immediate precipitation of cellulose. Unfortunately, the majority of the material agglomerated into a large mass and even the few isolated particles were highly irregular in shape and size. DCM was able to disperse the drop of dope even quicker and also less agglomeration was observed (if any). The particles were still rather large (tens to hundreds of μm) and irregular in shape. Acetonitrile resulted in strips of precipitated material, being a cross between the pancakes obtained from the alcohols and that of spaghetti strings.

Chloroform acted rather differently to the prior organic solvents in that it seemed to "dissolve" the drop of dope. No precipitation of cellulose was observed by eye or under the microscope, but a change in refractive index of the mixture was observed near the bottom. n-hexane and toluene were immiscible with [DBNH][OAc]/DMSO, which sunk to the bottom of the beaker forming a separate phase to the bulk solvents. Because of this phase separation, the already flattened dope droplets on the bottom merged together to form larger sheets and hence no particles were formed.

As a known and effective co-solvent for many cellulose dissolving systems, DMSO expectedly dispersed the drop of dope completely. GVL, also a known co-solvent, similarly dispersed the drop very effectively but left areas of slightly different refractive index. This difference is likely due to a concentration of material rich in cellulose and possibly [DBNH][OAc] present in those areas. In the end, only water performed adequately as an antisolvent for the production of Cellulose Beads (CB). The others either formed beads that were not structurally sound, did not form macroscopic particles in the first place or were not miscible with the dope.

To investigate the avenue of producing actual nanoparticles with the nanoprecipitation method, instead of the large beads, an experiment was run using 0,1 wt-% MCC dope and select few of the solvents from the previous test. The rationale of the test was that, as some of the solvents seemed to disperse the dope rather efficiently, perhaps it would be possible to emphasize on this property to disperse the dope and dissolved cellulose in the manner usual to nanoprecipitation experiments. The solvents tested were THF, acetone, toluene and DCM. THF and DCM seemed to be able to form a very good dispersion of the dope and cellulose, transforming from clear liquid into a white opaque dispersion with no particles visible to the naked eye. However, the suspension was temporary, as

the particles quickly agglomerated to form visible particles. DMSO, GVL and chloroform were not tested for this purpose as they were not suitable for the production of Cellulose Beads either due to being a partial solvent of cellulose (DMSO, GVL) or being otherwise unsuitable for wider scale use (chloroform).

4.2.10. The effect of MCC concentration on the preparation of Cellulose Beads

The motivation behind this experiment was to confirm that the cellulose bead formation works also with a higher cellulose content dope. The first test in this experiment was run using the basic setup from previous experiment with pure water as the antisolvent but a 3 wt-% MCC concentration in the dope. As expected, the bead formation proved to be just as effortless as with the 1 wt-% dope. The formed beads were washed with five batches of 40 ml water and left to soak in further 40 ml for 24 h (**Figure 44.**). Subsequently the beads were divided into two portions for air- and freeze-drying. The dried beads identical were identical to those obtained with the use of a surfactant in earlier experiments. The procured beads weighed an average of 0,289 mg.
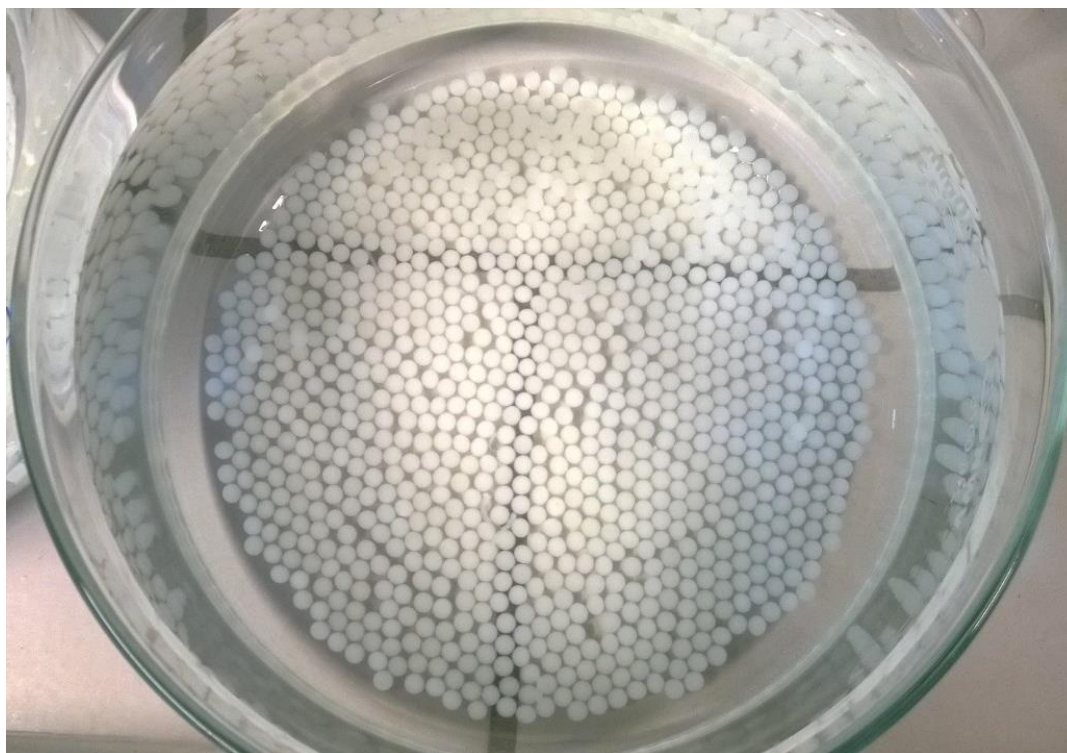

Figure 44. Wet Cellulose Beads left to soak overnight in distilled water.

Then on the second test, a large batch of Cellulose Beads (CB) was prepared using 5 wt-% MCC dope for use in determining the composition of said beads using NMR. All of the obtained beads were air-

dried (end mass 56 mg), but otherwise the experiment was identical to the previous test. Based on previous experience gained from prior experiments, the 5 wt-% cellulose concentration in the dope seemed to produce the best result both in the sense of particle properties (shape, durability, absence of a tail) as well as in ease of handling and manufactory (easy to pump, lack of "floaters", drying properties). Because of these beneficial qualities, the 5 wt-% was adopted as the general purpose MCC concentration and was widely used later on in the ADCB and FDCB experiments. In a similarly encompassing fashion, the use of a surfactant was deemed unnecessary for the formation of the Cellulose Beads and was summarily removed from the basic preparation setup.

4.2.11. Air-Dried Cellulose Beads (ADCB 1)

At this point in the study, the experimental setup for the formation of cellulose beads was well established (see section **4.2.1. Basic Cellulose Bead (CB) experimental setup**). The following experiments labelled either as ADCB (Air Dried Cellulose Beads) or FDCB (Freeze Dried Cellulose Beads) reflect this in their generally large scale or their rather derived aim.

The Basic Cellulose Bead experimental setup was used to produce beads from a 5 wt-% dope. A total of 15,8 g of dope (0,789 g of MCC) was extruded into a water filled beaker by a syringe pump at a rate of 0,22 ml/min (1 drop every 2,8 s). The needle, through which the sample was pushed, was 0,80 mm in diameter. Dropping height from needle to water surface was 6 cm and water depth was 3 cm (100 ml beaker filled with 40 ml H_2O). The drops were left in the water for 45 min, after which the water replaced twice within 5 min, with gentle stirring in between changes. Finally 80 ml of water was added to the beaker and the beads were left to soak overnight (24 h). Most of the water from each beaker was poured out and replaced with 80 ml of water. After 10 min this water was removed as well and the beads were poured onto Petri dishes. The Petri dish lid was slightly offset from the bottom to enhance water evaporation and the beads were left to dry in air for a week.

Afterwards some of the Petri dishes still had some residual "liquid" on them (probably the IL or DMSO) so all of the beads (966 beads in total, 770 mg weight in total) were placed on a Petri dish with 60 ml of water and they were left to soak overnight with the lid on. The next day the water was removed and replaced twice with 30 ml of water. Most of the water was poured off and the rest was removed using a tissue. The beads were placed in a 20 ml vial and left to dry in air for 48 h. Afterwards the weight of the 966 beads was 742 mg, which equals to 0,768 mg/bead. In this

experiment, the yield was quite excellent if one considered that 789 mg of MCC was added to the initial dope and that 742 mg of cellulose beads were procured in the end. However, taking into account the loss of dope on the vial and syringe walls, the needle and the tube, it is improbable that the total weight of the formed beads is composed of pure cellulose, but likely it incorporates some amount of water in its structure.

4.2.12. Air-Dried Cellulose Beads (ADCB 2)

This experiment was devised in order to study the viability of upscaling the Cellulose Bead forming method. The experiment was run according to the basic cellulose bead (CB) experimental setup with a 5 wt-% MCC dope. The total dope amount of 100 ml was loaded onto a 60 ml syringe at roughly 20 ml at a time to divide it into five batches (B1-B5). To prepare such a large amount of dope, the mixing of the electrolyte components and the subsequent dissolution of cellulose was undertaken in a 100 ml storage bottle. The temperature of the oil bath was also increased to 75° C to compensate for the larger mass of material, but the dissolution process still took 30 minutes to finalise. Batches B1-B4 used the 1,6 mm short-needle horizontal orientation setup, which was replaced with the more suitable vertical 0,8 mm setup in B5. The reasoning behind the needle setup is described in section **4.2.15. Needle diameter and orientation**. In this experiment the water volume was 600 ml, water depth was 11 cm, dropping height from needle tip to water surface was 10 cm for B1 and 8 cm for B2-B5. The rate of infusion was initially set at 2,5 ml/min, but due to limitations in the pumping capacity, it was later downgraded all the way to 0,67 ml/min.

The 100 ml beaker holding the newly formed beads was exchanged every 10 minutes with a new one and the beads inside were washed three times with 200 ml of water before being deposited into a separate containers for temporary storage. After the whole batch of dope was pumped through the needle and the beads had been washed, the water in the 500 ml storage container was exchanged for a fresh batch of distilled water and the beads were left to soak for 6 days. Afterwards, each batch was placed in a 100 ml beaker and washed five times with 60 ml of water and left to dry on petri dishes with their lids slightly ajar. A small portion of B3 was left in water to test their preservation in the wet state. The beads were shown to be very stable in the neutral aqueous environment, being easily dryable to both morphologies (ADCB and FDCB) even after 12 months of storage.

4.2.13. Air-Dried Cellulose Beads (ADCB 3)

This experiment was used to gauge the practical volumetric upper limits of the Cellulose Beads forming method with the laboratory equipment available. The experiment conformed to the earlier two ADCB experiments for the most part, but the simultaneous process volume was once again upscaled considerably and the practical setup of the bead forming apparatus was modified somewhat. The dropping height between the needle and the water surface was adjusted to 4 cm and the syringe pump now withheld three 60 ml syringes filled to roughly half of their maximum capacity. These syringes were connected with flexible tubes to three 0,8 mm diameter needles suspended above the water bath. The water container was a 20 l plastic box filled to approximately half of its volume. A bucket, the walls of which were perforated with 1 mm diameter holes, was suspended inside the water box so that a considerable volume of it was submerged, but so that the bottom of the bucket was still some distance above the bottom of the box. This configuration was designed so that when the drops of dope hit the water surface and are solidified, they would fall to the bottom of the bucket and remain there, while the IL/co-solvent mixture would escape through the holes and get diluted throughout the total water volume. Compared to the earlier setups, where the dope was pumped from the needle into a beaker of relatively small volume (600 ml), the new setup allowed for a more continuous running of the apparatus without the need the exchange the water (10 l) around the beads.

When the experiment was first started, the progress was monitored for several hours and it was noticed that the pump had trouble dealing with the three syringes at the rate of 0,67 ml/min/syringe. To rectify this problem the pump was set on its lowest speed of 0,33 ml/min/syringe and left to pump overnight. Unfortunately, the pump had stalled during the night and hence had stopped the production of further beads, so another syringe pump was installed into the setup and one of the syringes was transferred to that pump. This seemed to solve the performance issues, although the rate of addition was still kept at the low 0,33 ml/min level. After all of the dope had been pumped, the beads were left to sit inside the bucket for further 10 minutes, after which they were relocated into a 2,5 l volume of water and left to soak for 24 h. Afterwards the beads were transferred to a 600 ml beaker, washed four times with 500 ml of water and left to dry in a large plastic container (**Figure 45.**). After several days, all of the beads had dried and their final weight was determined to be 4,96 g. This result can be seen as acceptable considering the starting weight of 5,229 g of MCC dissolved in the electrolyte, especially when the "floaters" that

failed to penetrate the water surface and the amount of dope left in the bottle, syringes and tubes is taken into account.

Figure 45. All of the wet Cellulose Beads from the most voluminous individual experiment were left to dry in a large plastic container. The container was loosely covered to limit the accumulation of airborne dust.

4.2.14. Freeze-Dried Cellulose Beads (FDCB 1&2)

The aim of these tests was to produce larger quantities of freeze-dried particles for various analytical methods such as WAXS. The FDCB 1 experiment followed the basic Cellulose Bead (CB) experimental setup with a 5 wt-% dope. In FDCB 2, some 50 freeze-dried beads were prepared from the never-dried beads of ADCB 2 B3. After the FDCB 1 beads had soaked in water for 24 h, both batches of beads were washed with 100 ml of water and freeze-drying was performed as usual. In general, the beads are spherical in shape, but as can be seen from **Figure 46.**, a distinct oval shape is common among the beads. This shape results from flattening of the drop of dope upon impact with the water surface.

Figure 46. These Freeze-dried Cellulose Beads (FDCB) have an oval shape to them and the surface of the beads is also somewhat uneven. The diameter of the beads is ca. 2 mm.

4.2.15. Needle diameter and orientation

The various parameters relating to the needle in the basic Cellulose Bead experimental setup were studied in order to produce the best and most consistent results. These experiments followed the already established method, yet the needle diameter, orientation and shape was varied during the tests. The first parameter to be tested was the needle diameter, with the two most viable diameters being 0,8 mm and 1,6 mm due to availability at the time. After several tests and differing conditions, it was concluded that the 0,8 mm needle was the easier to handle due to its greater pliability, decreased size of beads produced and the lower tendency for the formation of tails on the beads. Hence, the 0,8 mm diameter needle was adopted for most experiments if possible.

The second parameter tested was the position of the needle on top of the water surface. First the needles were placed on the same plane as the water surface, which resulted in the drops of dope falling from the tip perpendicular to the flow direction in the needle. In this setup, the needle tip was also rotated to see whether it would have an effect on the bead morphology. When the pointed tip of the needle was placed above the axis of flow in the needle, the drop of dope gathered on the

opening of the needle head. When it was placed below the axis, the drop gathered on the pointed tip and on the outer curved surface of the needle below the tip. A flat headed "needle" was also tested for reference. Out of these three setups, the one with the pointed tip above the flow axis was deemed the most usable as the drop of dope had the shortest distance to travel and seemed to produce the reproducible results. However, it was not optimal and a separate setup where the needle was positioned perpendicularly to the water surface was devised. This setup was clearly better than the earlier one as the dope still had a short and direct path to follow on the tip, but it also could take full advantage of the sharp tip of the needle.

The perpendicular position of the needle could be achieved either by attaching a flexible tube connecting the syringe head and the needle, which allows the needle to be placed vertically while keeping the syringe pump on the counter, or by bending the needle so that it formed a gentle 90° bend along its length. The former setup has the benefit of being able to introduce the dope to a variety of positions around the syringe pump, whereas the latter necessitates that the water container is placed right next to the apparatus. On the other hand, the bended needle setup is considerably easier to setup and takes significantly less time to prepare than the tube fed needle (with the materials available to the author). Hence, the perpendicularly oriented needle with a connecting tube setup was adopted for the vast majority of Cellulose Bead tests, but some were also performed using the bended needle setup due to convenience.

4.2.16. Dropping height and floaters

The effect of the dropping height was investigated for the basic Cellulose Bead experimental setup. The experiment used 5 wt-% cellulose dope loaded onto a syringe attached to a 0,8 mm diameter needle oriented vertically above a water bath. The dropping height is determined as the distance between the needle tip and the water surface. Varying distances between 4 and >12 cm were tested in several experiments and it was found that roughly 8 – 10 cm seemed to produce the best quality beads in the most consistent manner. If the height is less than that, the drops of dope may not have enough kinetic energy to overcome the surface tension of water, and hence remain afloat on the surface. If the height is more than that, the drops might have too much kinetic energy and may equally deform so much upon impact that they are unable to penetrate the water surface.

When dope is dropped from a low height, the drops gain a flat shape as a result of the impact and/or flowing of the dope along the water surface. This is especially problematic for the lower cellulose content dopes, as their viscosity is the lowest and hence they are the most prone to shape distortion. Similarly to the low dropping height but due to different a reason, the drops of dope have a tendency of flattening on impact when the dropping height is greater than 12 cm. This flattening can be of two kinds: floating or sinking. The floating flattened beads are especially frequent with low cellulose content dope and large dropping heights, resulting from the bead having too much kinetic energy at the moment of impact. At the moment of impact, the resistance from the surface tension between water and dope causes the drop to flatten, which results in an even greater contact area between the two systems and culminates in a dope "pancake" floating on the water surface, refusing o sink. The sinking-type is more common with high cellulose content dope. The drop is deformed due to the impact, but to a lesser degree than the floating-type, and has enough kinetic energy to punch through the water surface. The beads swing from side-to-side while they sink due to their non-ideal hydrodynamic shape (slightly elliptical). The sinking beads are still usable as beads, whereas the floating material is of very irregular shape and is virtually always discarded.

A special case of floaters are beads with inclusions of air bubbles. They are a result of trapped air bubbles being extruded alongside the drops of dope, which naturally they remain afloat due to their low density. They sometimes remain quite round and could, in theory, be submerged manually to obtain beads with large holes in them. All types of floating drops are problematic due to the tendency of the floater formation to propagate. Once a floater is present on the surface, it is possible that a second drop of dope will hit it directly or partially, which will most certainly result in another floater. The more floaters present on the water surface, the more likely is the formation of even more. Due to this limitation, the initial likelihood of floater formation should be minimized and the process should not be left unattended for excessively long periods of time.

When the distance is approximately 9 cm or less, the beads do not produce audible noises when they hit the water surface. When the distance is approximately 11 cm or more, the beads make a "plopping" sound just as expected of a drop of material hitting water. However, when the distance is roughly 10 cm, the beads produce an audible high-pitched "click" sound when they hit the water surface. The sound resembles that of two hard objects colliding, such as a marble falling on a metal surface, albeit the pitch is higher. This sound seems very out of place and surprised the author when it was observed for the first time. To the best observations of the author, the sound seems originate

at the moment of impact between the drop of dope and the water surface, rather than when it hits the bottom of the container. This behaviour is yet to be explained or further examined, but might be caused by a propagation of a shock wave within the drop of dope when it meets the water surface. This shock wave could cause rippling of the dope on its upper surface and possible even the launching of a small droplet of dope free of the main drop. This could conceivably result in vibrations audible to the human ear.

4.2.17. Dyed Cellulose Beads

The aim of this test was to prepare colourful cellulose beads. The motivation to study the dyeing potential of the beads came from the possibility of applying them into consumer products, where the visual appeal of a material is disproportionally important compared to its other physical characteristics. Hence, dyed Cellulose Beads (CB) were prepared in much the same way as regular Cellulose Beads, with slight changes to the antisolvent constitution. Instead of pure distilled water, the first batch of washing antisolvent (i.e. the one after the initial water, in which the beads were formed) included a concentration of red, blue or green food colouring dye. The rationale was that, when the diffusion of solvent and antisolvent occurs between the bead and the water bath, the dye would also seep into the beads and colour them accordingly.

The blue colour in the blue food colouring is caused by Brilliant Blue (CAS: 3844-45-9), the red colour is caused by Carmine (CAS: 1390-65-4) and the green colour is caused by a combination of Brilliant Blue and Lutein (CAS: 127-40-2), which is yellow in colour (**Figure 47.**). The experiment was first run with a highly concentrated solution of food colouring, substituting the second batch of water in the washing phase with 1 ml of the food colouring solution and leaving the beads to soak for 1 h, after which the washing and drying steps were continued as normal. This procedure turned out to be good for the freeze-dried beads (FDCB), which gained a rich colouring (**Figure 48. B&E**). However, in the air-dried beads (ADCB) the colour ended up being excessively strong, the colour appearing to be almost black and the beads losing their transparency completely.
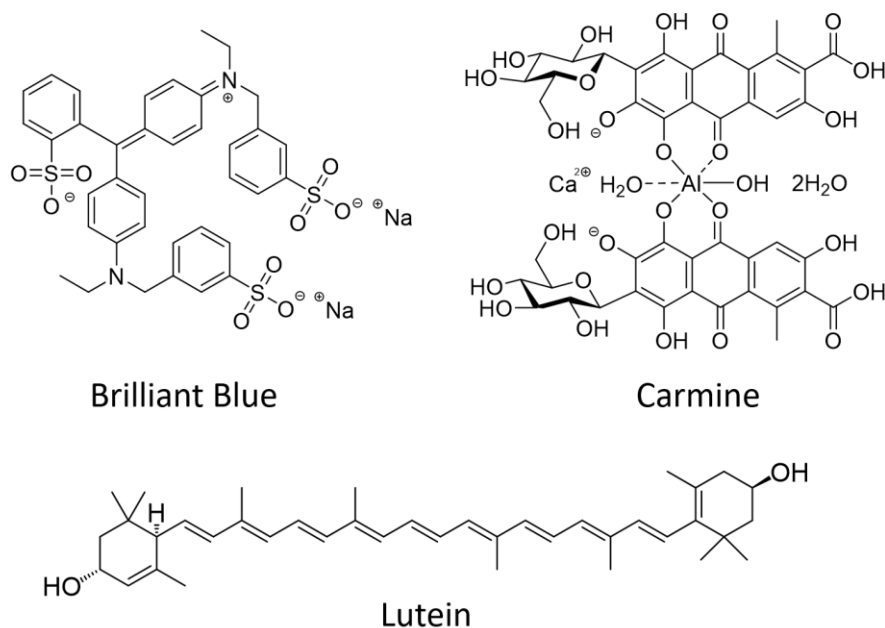
Figure 47. The three dye molecules used in the dyeing of the regenerating cellulose beads. The blue colour comes from Brilliant Blue (CAS: 3844-45-9), the red from Carmine (CAS: 1390-65-4) and the green from a mixture of Brilliant Blue and Lutein (CAS: 127-40-2).

 Hence, a second experiment was run using a significantly lower dye concentration, diluting the food colouring solution by adding 10 ml of H_2O. This procedure suited the ADCB beads much better, the beads catching an appealing tint of colour while still keeping their optical transparency to a very high degree (**Figure 48. A,D&F**). On the other hand, the FDCB beads were much more faintly dyed than in the previous experiment (not pictured). The differing colour intensity results based on the drying technique are most likely due to two factors: contraction and transparency. When the CBs are freeze-dried, they roughly keep their dimensions intact and remain opaque. This results in only the colour on the surface layer being visibly. The white colouring of cellulose additionally dilutes the colour of the freeze-dried beads. However, when the beads are left to dry in air, they contract significantly and the cellulosic material turns transparent in the process. This way the same amount of dye molecules is concentrated into a much smaller volume and, due to the transparency of the material, it is also visible within the bead to a much greater depth. This is the reason why the air-dried beads appear much more intensively coloured and at high dye concentrations lose their apparent transparency. A further close-up of beads C and E are shown in **Figure 49**.
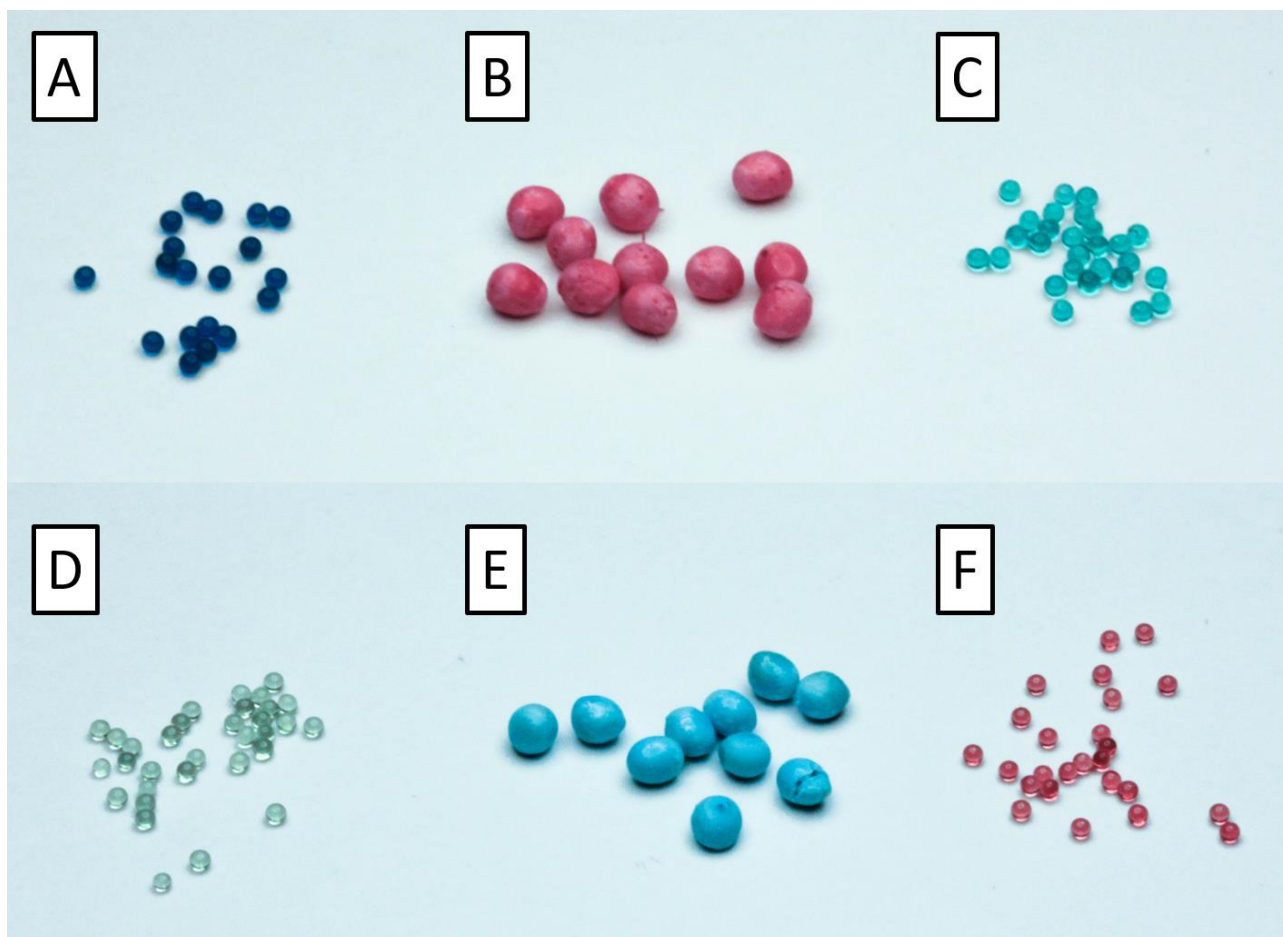
Figure 48. Some of the dyed Cellulose Beads. Beads B, C and E are dyed using the initial higher dye concentration, while beads A, D and F are dyed using the revised lower concentration.

The loss of transparency is observed in the red (Carmine) and blue (Brilliant Blue) coloured ADCB beads, but the green coloured ones are somewhat of an outlier. Unlike the blue and red ones, the ADCB beads coloured using green food colour at the higher dye concentration remained transparent after drying, but were turquoise rather than green in colour (**Figure 48. C**). This is possibly due to the green food colouring having Lutein as one of the colour constituting compounds. Lutein is a carotenoid compound that is found in many plants and is yellow in colour. If not the most hydrophobic compound possible, Lutein is definitely not hydrophilic or amphiphilic even (**Figure 47.**). In the green food colouring, it is mixed with Brilliant Blue to make a green average colour. However, the yellow Lutein does not seem to stick to the cellulose beads to the same degree as Brilliant Blue. This might be due to Lutein's lack of compatible strong intermolecular interactions with cellulose, while at the same time the sulphate groups in Brilliant Blue readily interact with cellulose hydroxyl groups. Hence, Brilliant Blue is much more likely to remain in close association with the cellulose matrix at the same time as Lutein preferably associates with the solvent.

132

Naturally, when the dye solution is washed away, the majority of dye molecules remaining in the cellulose matrix are blue rather than yellow. Why the beads do not appear as blue as with the blue food colour, is likely due to the much lower concentration of Brilliant Blue in the green food colouring relative to the blue one. At low dye concentration, the disparity between the dye components is less announced and the beads appear light green in colour (**Figure 48. D**). In this case, Lutein is probably integrated into the bead material along with the inwards diffusing water without interacting substantially with the cellulose matrix. Once the beads starts to shrink and dry, Lutein remains trapped in pores inside the bead and the overall ratio between blue and yellow dye molecules in the beads is much closer to the original ratio present in the green food colour.
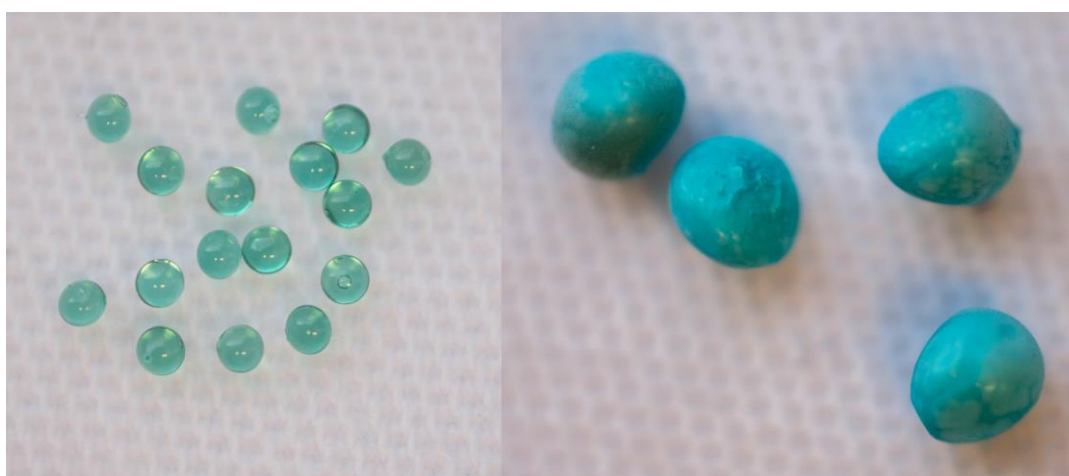

Figure 49. Close-up of Dyed Cellulose Beads C and E. The ADCB beads (left) were dyed using the green food colouring in the initial concentrated run, while the FDCB beads (right) were dyed using the blue food colouring in the later, more dilute method.

4.2.18. Magnetic Cellulose Beads

The possibility of making magnetic Cellulose Beads was investigated by loading the dope with solid magnetic materials such as metal powders. The experiment followed the basic Cellulose Bead experimental setup, but several powdery magnetic materials were mixed with the cellulose dopes before they were loaded onto syringes. In addition, some samples of dope were loaded with non-magnetic magnetic materials for reference. Once loaded onto syringes, the dopes were extruded to form the beads as usual. The magnetic materials used in the experiment were Fe-powder, Fe_3O_4-powder, Co-powder and Ni-powder. The non-magnetic reference materials used were Mn-powder, steel-powder and SiO_2-powder. The Mn- and steel-powders were coarser than the other powders and did not stay in suspension in the dope to the same degree as the other powders. Some finished magnetic beads can be seen in **Figure 50**.

Figure 50. Freeze-dried and air-dried cellulose beads containing 20 wt-% iron powder.

The amount of solid material was calculated so that it would constitute 20 wt-% of the final dry matter of the beads. However, for the Fe-beads, compositions of 50 wt-% and 10 wt-% were also prepared with aim of testing the magnetic susceptibility of the beads. Due to the presence of the metals and other solids, the colour of the dope deviated significantly from the norm. The Fe_3O_4 dope was practically black before and after being formed into beads, while the Ni & Co and to a lesser degree Fe and steel dopes were also darker in colour than the control dope (**Figure 51.**). The beads started getting slightly lighter in colour once they had soaked in the water for a while, which was almost certainly caused by the precipitation of a thin layer of opaque cellulose on the bead surface.

After freeze-drying, all of the beads turned lighter in colour, whereas the opposite happened with the air-dried beads. These changes are all in line with previous observations in section **4.2.17. Dyed Cellulose Beads**.
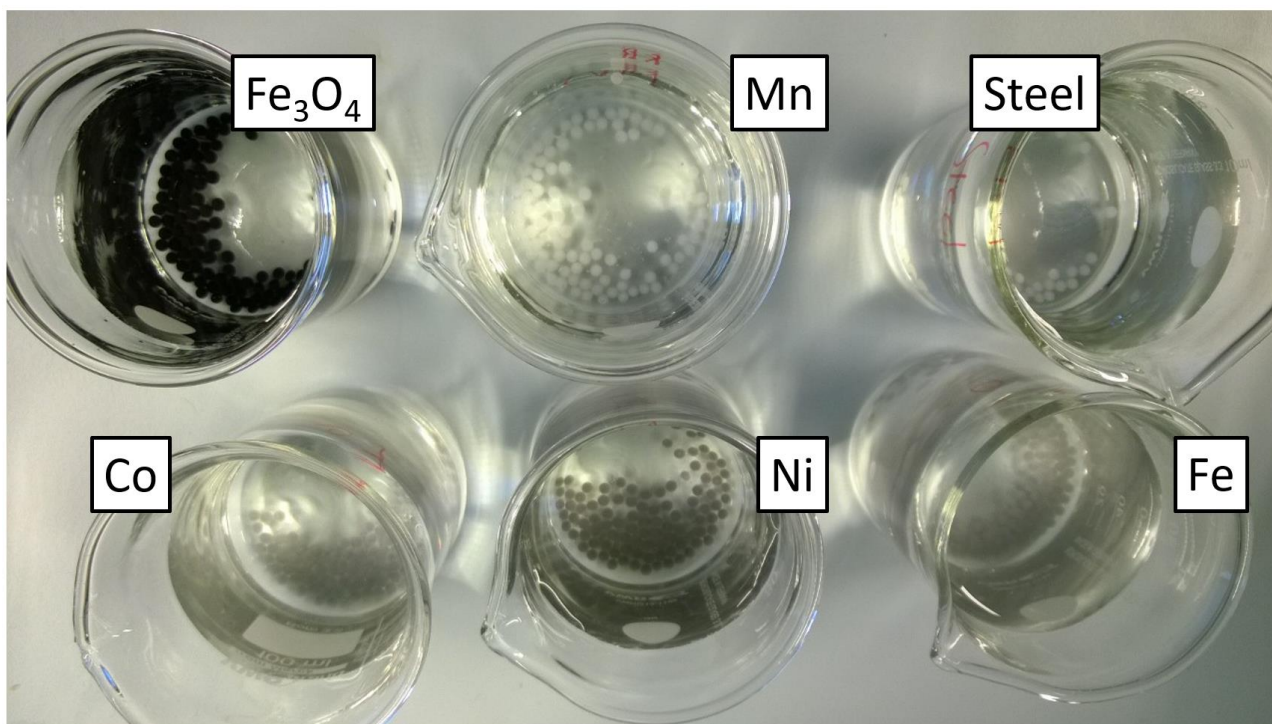

Figure 51. Freshly extruded wet cellulose beads loaded with various magnetic and non-magnetic powdery solids. The darker than normal colour of the dope, caused by the added powders, is especially evident in the case of Fe_3O_4 and Ni. The beads greatly resemble those described in section **3.2.2. Cellulose composite beads.**

Once dry, the magnetic properties of the beads were initially tested using a somewhat powerful handheld magnet. All of the beads withholding magnetic material responded to the magnet as expected, with the higher magnetic composition Fe-beads and air-dried ones seeming to interact more intensely and from further away than lower composition and freeze-dried beads. To test their magnetic properties in a quantifiable manner, the 10-50 wt-% Fe-series of beads was analysed using a Vibrating-sample Magnetometer (VSM). The relative magnetisation curves of all Fe-loaded beads fall way behind the Ni-sphere reference in magnitude, but are very consistent between the ADCB and FDCB beads of a given Fe-content (**Figure 52.**). This consistency seems rational, when considering that the Fe content of a given mass of dope (a drop) and of a single bead should be equal regardless of the drying method.
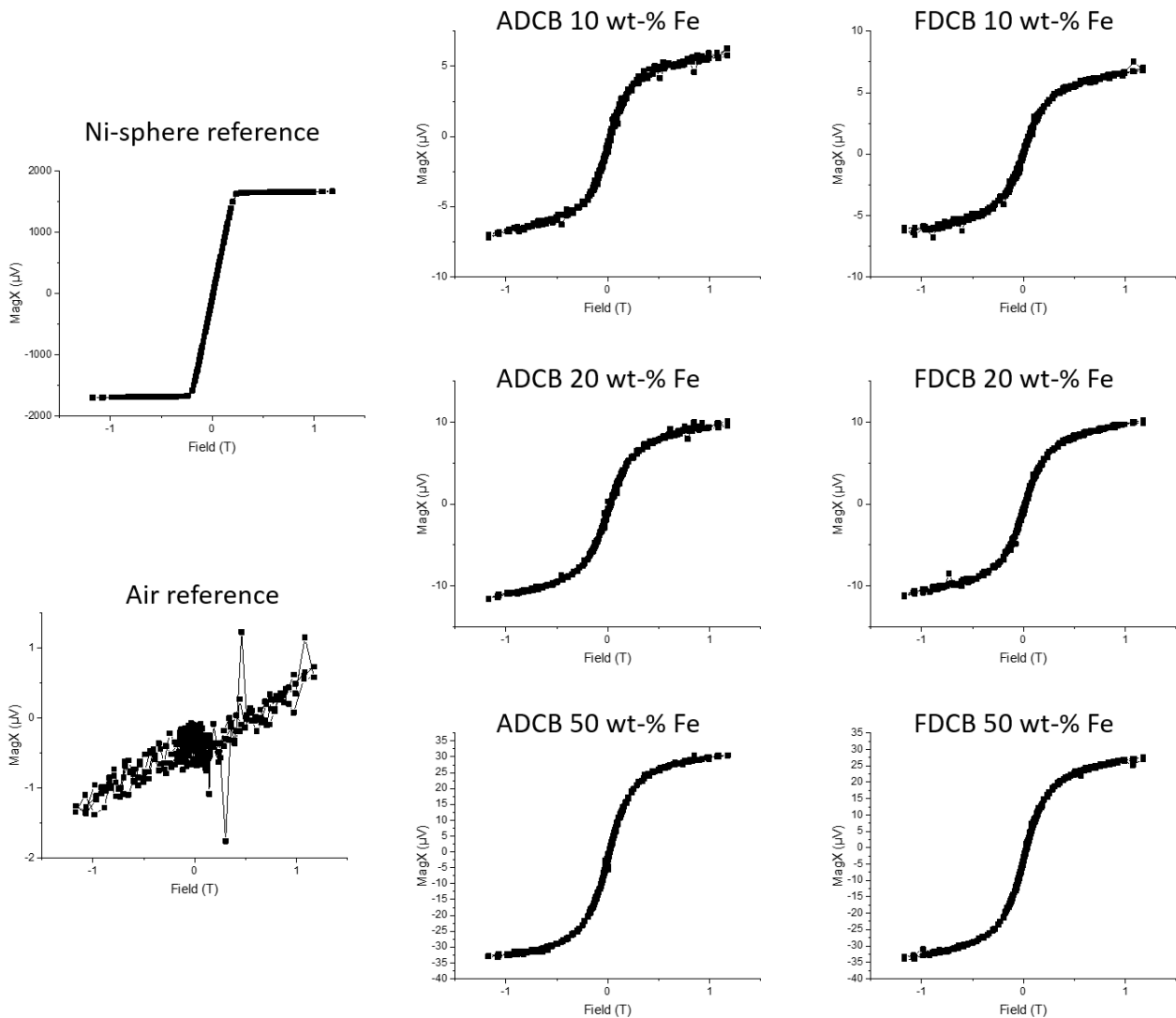
Figure 52. The magnetisation curves of the Ni-sphere/air references and the ADCB and FDCB beads with varying Fe content (10, 20 or 50 wt-%) obtained by VSM. Note the growing values in the Y-axis.

Hence, the absolute magnetisation and magnetic moment by mass values of both ADCB and FDCB beads are very closely matching in each of the three measured Fe-compositions (**Table 6.**).[171] On the other hand, the magnetisation by volume values differ significantly between the two types, which is a result of the over twelvefold difference in volume between the large FDCB and small ADCB beads. The magnetisation by volume values of even the ADCB beads fall far short of the values obtained from a solid Fe-sphere, being roughly one order of magnitude smaller at the 50 wt-% Fe-composition. These values are still easily adequate for most practical purposes where attraction to magnets would be required, the value for ADCB 50 wt-% Fe bead amounting to more than a third of the value of Ni by volume and even exceeding it by 30 % in weight.

Table 6. The magnetisation by mass and by volume of the six types of Fe-loaded Cellulose Beads. The values relative to mass are closely matching between the ADCB and FDCB beads, but naturally the values relative to volume differ significantly due to the over twelvefold difference in volume between the two types. Nonetheless, even the ADCB beads fall far short of the magnetisation values of solid Fe-metal.

Sample	σ (emu/g)	M (emu/cm^3)
ADCB 10 wt-% Fe	19,95	37,89
FDCB 10 wt-% Fe	20,46	3,07
ADCB 20 wt-% Fe	28,17	59,54
FDCB 20 wt-% Fe	31,74	4,82
ADCB 50 wt-% Fe	71,64	178,62
FDCB 50 wt-% Fe	70,97	14,46
Elemental Fe	218	1714
Elemental Ni	54	484

4.2.19. ADCB and FDCB from various Cellulose sources

The motivation behind this experiment was study whether the air- and freeze-dried beads, which were previously produced solely from MCC, could also be produced from various other cellulosic raw materials. The experiment followed the basic Cellulose Bead experimental setup and used a 5 wt-% dope of one of five different cellulose materials: Avicell, Enocell, eucalyptus pulp, birch pulp and spruce pulp (**Table 7.**). The materials were of different composition and the cellulose in them was of varying average molecular weight. Avicell is a commercial microcrystalline cellulose powder (50 μm average particles size) and is closely comparable to MCC. The Enocell, birch and eucalyptus pulps are Wiley-milled bleached, dried hardwood Kraft-pulps obtained from UPM-Kymmene Corporation.

Table 7. The different cellulose sources used to fabricate Cellulose Beads and the concentration of solid material in their respective dopes. The 5 wt-% Enocell, eucalyptus and birch pulp dopes were too viscous to load onto syringes and hence were not fabricated into beads.

Cellulose wt-%	MCC	Avicell	Enocell	eucalyptus	birch	spruce
2 %	X	X	X	X	X	X
5 %	X	X				X

The dissolution time of the materials varied from 5 minutes (Avicell), 4 h (Enocell) and 18 h (the other pulps). While the Avicell and Enocell dopes were indistinguishable from a MCC dope by eye, the viscosity of the Enocell was considerably higher (barely flowing at RT) than that of Avicell or MCC. The eucalyptus dope was similar in appearance to the prior dopes, albeit slightly more yellow. On the other hand, it did not flow at all at RT, so the viscosity was significantly higher. The birch dope was equally non-flowing, but orange in colour. The spruce dope was the clear outlier out of the five, being coloured light brown and containing small-sized undissolved particles. Additionally, it did flow comparatively well, being equivalent in viscosity to a high cellulose composition (ca. 8 wt-%) MCC dope. As the non-flowing dopes were practically impossible to load into syringe, 2 wt-% samples were prepared for all the five materials. All of the dopes flowed to some degree at this lower concentration, while the Enocell, birch and eucalyptus were still more viscous than the other three (2 wt-% and 5 wt-% MCC samples were also included as references).

The dopes able to be loaded onto a syringe (**Table 7.**) were fabricated into beads following the basic Cellulose Bead experimental setup. Enocell, eucalyptus and birch pulps demonstrated a significantly higher frequency in the formation of long tails, which is likely a result of high viscosity. Furthermore, the spruce dope was also clearly different from the others, retaining a yellow colour even in the precipitated bead form. The formed spruce beads also seemed to have some undissolved particles in them, which were suspected to be lignin. The 5 wt-% spruce dope also had issues in forming a coherent bead in the needle tip, sometimes drooping down as a larger irregular mass. The cause of this is still unknown, but is most likely related to differing viscoelastic properties between the very homogeneous MCC and heterogeneous spruce dopes. Nonetheless, all obtained beads were washed and either air- or freeze-dried. As expected, both types of MCC and Avicel beads were virtually identical in appearance. The FDCB Enocell, eucalyptus and birch beads were also practically indistinguishable from their microcrystalline equivalents, but the ADCB beads were slightly less transparent and had a more prominent yellowish hue to them. Spruce beads were clearly different from all of the other types, the FDCB beads being distinctly more elongate in their shape and truly yellow in colour, while the ADCB beads were also decidedly non-spherical and darkish brown in colour. The non-spherical shape of these beads results from their atypical drop forming behaviour and their rather low viscosity, which caused the extruded drops to launch from the needle tip in an inconsistent fashion and the shape of the drop at the moment of impact with water to be

considerably irregular. The offset colours are explained by the inclusion of the observed insoluble darkish brown particles, which are suspected to be composed mostly of lignin.

4.3. Properties of the Cellulose Beads

4.3.1. Core-Crust-ratio

The majority of the opaque and transparent beads are composed of a core and a crust that envelops it (**Figure 53.**). As can be seen in the SEM pictures, the core and crust are physically discreet (**Figure 54.** and **Figure 55.**). The thickness of the crust is not uniform, but varies quite significantly between individual beads and even within a single bead. For example, the crust in a transparent air-dried bead (diameter is 900 µm) could be ca. 50 µm thick and so the core-to-crust ratio would be roughly 17:1, while in the freeze-dried bead (diameter 1800 µm) the crust could be ca. 1600 µm thick and so the core-to-crust ratio would be as low as 1:9. In addition, the physical separation of the core and the crust is not as clear in the air-dried beads as it is in the freeze-dried beads. In the freeze dried beads there can be seen some distinction between the porosity, pore size and pore-wall thickness between the core and the crust, but similar distinction cannot be observed in the transparent air-dried beads. The origin and mechanism of formation for this Core-Crust division has remained unresolved during this thesis, but the most probable causes for such a duality are likely found in

Figure 53. Split FDCB beads displaying the variation in the core-crust ratio.

variations in the nature and speed of diffusion along the radius of the regenerating bead. In the case of the FDCB beads, this dichotomy is most likely further enforced by stresses present during freeze-drying, which causes the cellulose matrix of the bead to become physically separated into the inner and outer portions.
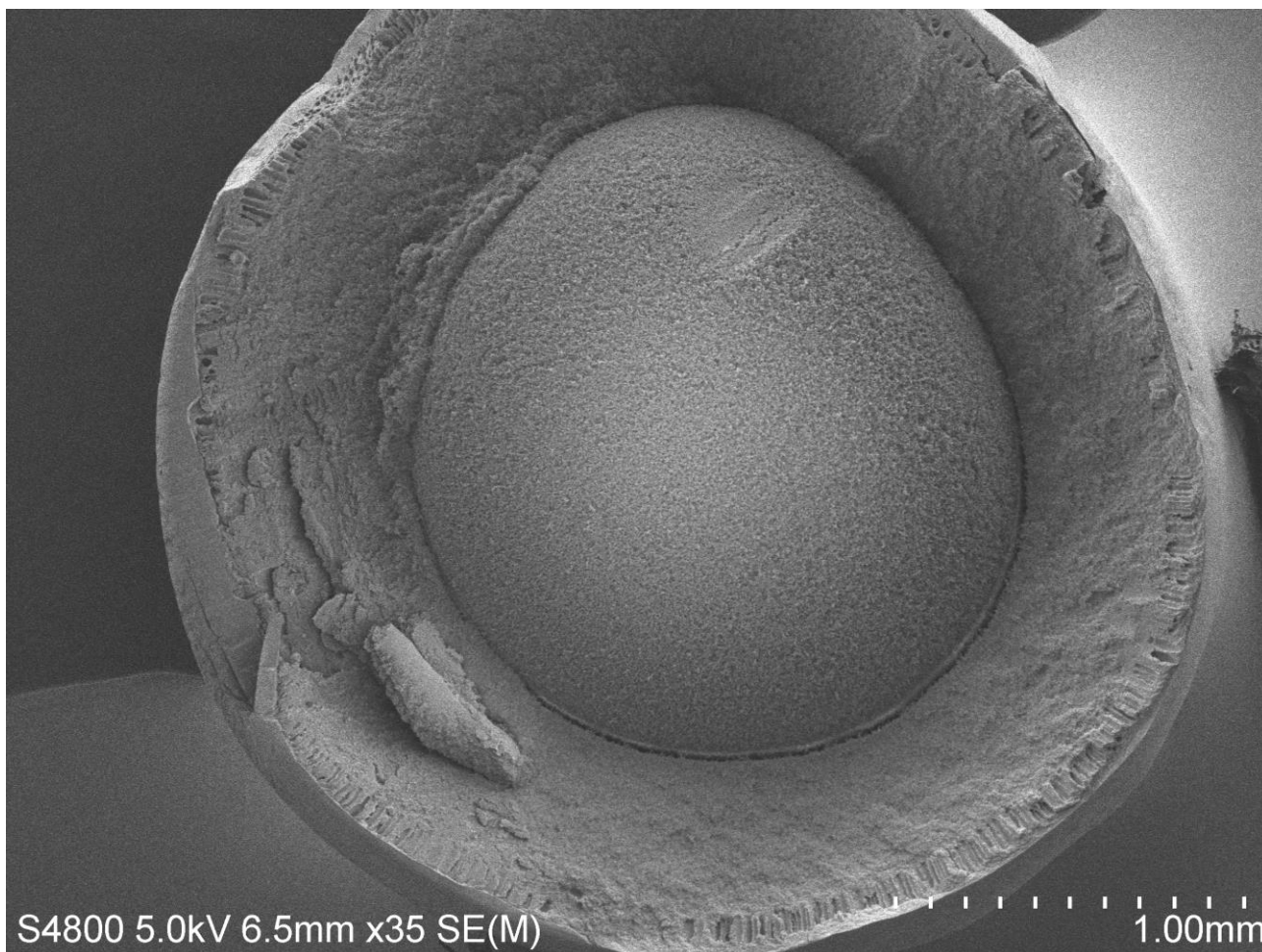

Figure 54. An SEM image of a split FDCB bead displaying the prominent core-crust duality present in the majority of cellulose beads.

The Crystallinity Index (CI) of the Cellulose Beads was studied using WAXS and values of 15 % (FDCB) and 25 % (ADCB) were obtained. In these cases the entire beads were crushed together to produce a disc of material suitable for WAXS analysis. As both of these types of beads originate from the same starting material (wet Cellulose Beads), the difference in CI between the two must rise from their different drying methods. Most likely, the CI of the wet Cellulose Beads closely matches that of the Freeze-dried beads (ca. 15 %), as the freeze-drying process allows for very limited restructuring of the cellulose network during the drying process, and hence should preserve the original CI of the treated material. This necessitates then that the CI of the ADCB beads has increased

during the drying process, which also makes sense considering how great is the restructuring of the cellulose networks from the porous starting material to the dense product. During the shrinkage, the cellulose matrix is condensed into approximately 10 % of the original volume, while still retaining the original shape of the bead. Hence, it is likely that major local restructuring of the cellulose network also leads to an increase in crystallinity of the material. Although it must be noted, that even the CI value of 25 % is modest in comparison to many cellulosic materials, making the ADCB beads still very much amorphous in comparison (see section **3.3.4. Cellulose nanofibers by mechanochemical processing)**.

In this context of crystallinity, the distribution of the crystallinity between the two structural units of the bead, core and crust, is very intriguing. Therefore, the cores and crusts of ca. 200 FDCB beads were separated manually using a scalpel to study them separately by WAXS. The analyses gave slightly different results for the two units, with the cores giving a higher value of 23 % and the shells giving a lower value of 14 %. This difference could be the result of the differing regeneration rates
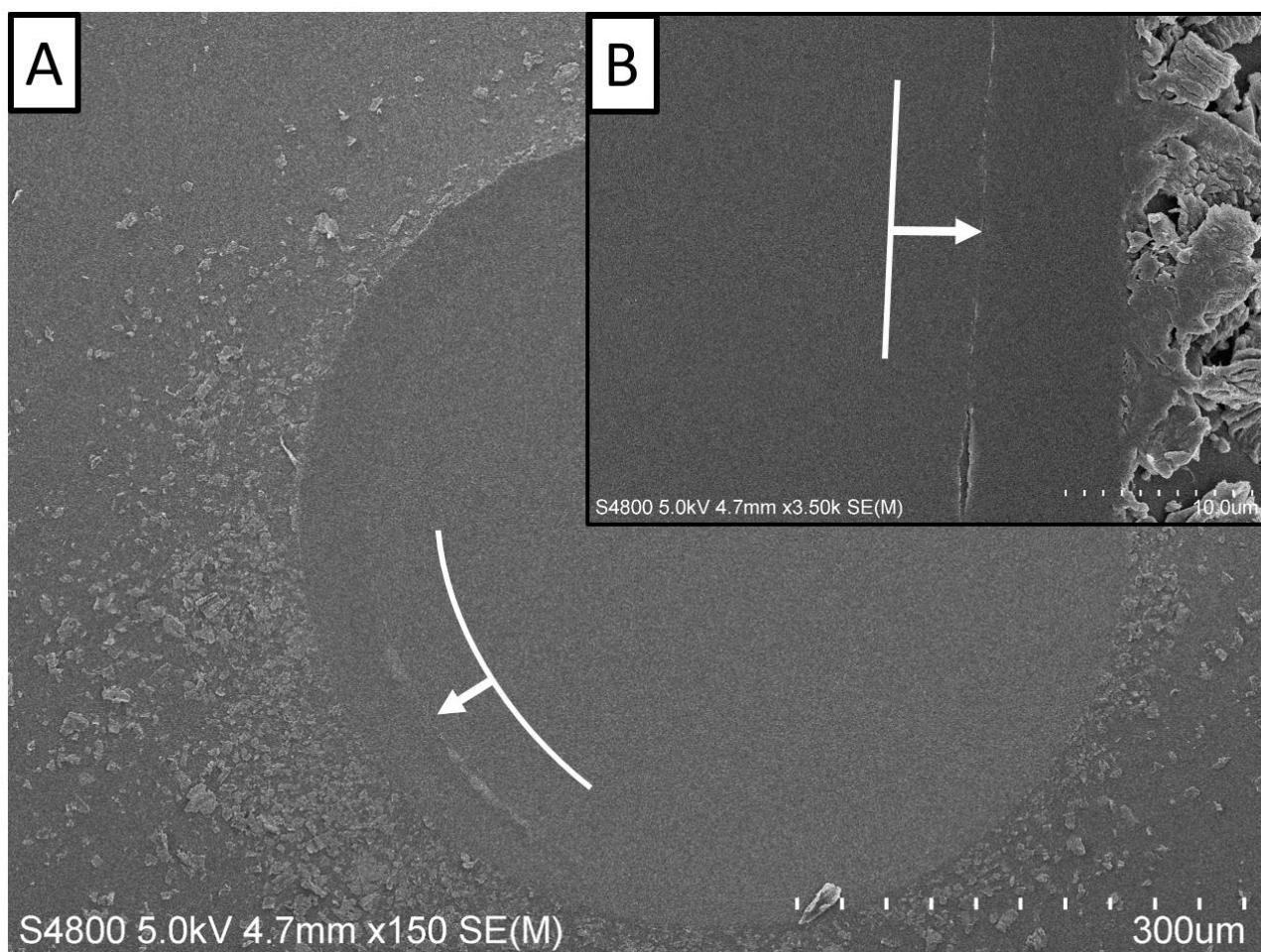

Figure 55. A: An ADCB bead cut in half using a high precision table top slicer. The core-crust division is not nearly as prominent as in the freeze-dried beads, but is still faintly visible in the larger image (white curve) and slightly more so in the larger magnification inset **B** (white line).

between the two units. The material on the outside portion of the bead is coagulated quickly during the regeneration process and hence the dissolved cellulose chains have very limited time to organise themselves into crystallites. On the other hand, the material residing in the inner portion of the bead has more time to organise itself into a relatively crystalline structure, albeit the CI would still be quite low due to the absence of directional guidance (forcing). This would lead to a positive gradient of crystallinity from the surface to the core. Unfortunately, the cores and crusts of the ADCB beads could not be separated, and hence the crystallinity gradient could not be verified with them.

4.3.2. Convection channels beneath the bead surface

Short hollow channels, positioned perpendicularly to the bead surface, are observed just beneath a freeze-dried bead's crust (**Figure 56.**). These features could be the result of a convection during the initial diffusion process. When the dope hits the antisolvent surface, the two solvents experience an extreme diffusion gradient and start travelling in opposite directions (towards or away from the core). This rush of solvents in opposite directions might be locally concentrated into areas of inwards diffusing water and outwards diffusing IL (**Figure 57.**). In such conditions, the dissolved cellulose
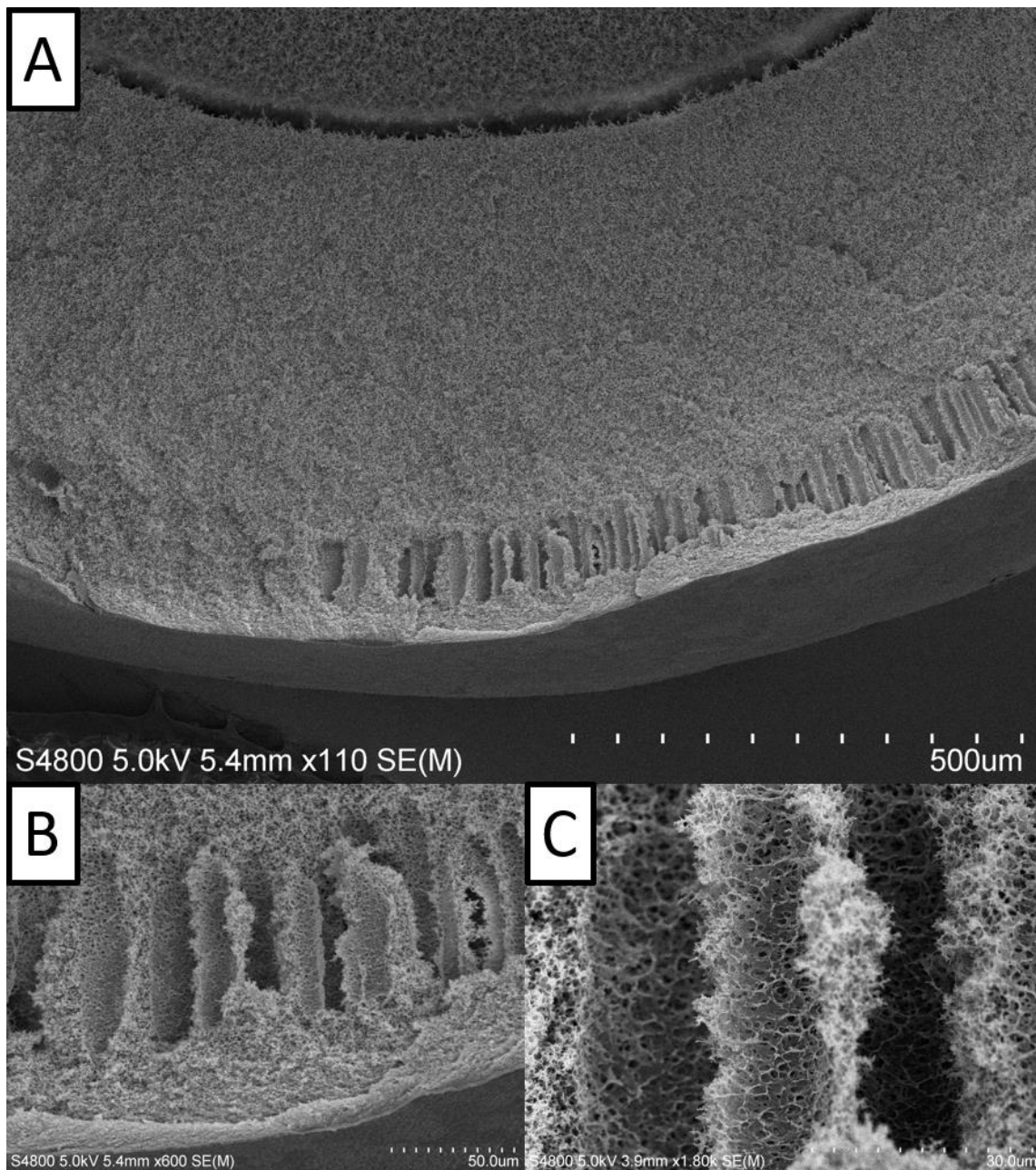

Figure 56. A: SEM image portraying the prominent convection channels present beneath the immediate surface of a FDCB-type bead. **B&C:** Larger magnification images of the convection channels, showing the high macro- and microporosity of the material.

would be transported with the IL towards the surface of the dope until it precipitates due worsening thermodynamical properties of the surrounding solvent environment. However, this initial concentrated rush of unmixed solvents would have to be very brief, as the diffusive mixing of the components would soon override any local concentrated flows.

This brief rush of IL might still allow the dissolved cellulose, which originally resided in the "voids", to be pushed towards the surface of the bead, leaving behind regions of solvent where there would be no more cellulose to precipitate. On the other hand, cellulose present in regions where water would be flowing inwards would be instantly precipitated due to desolvation of the polymer, which
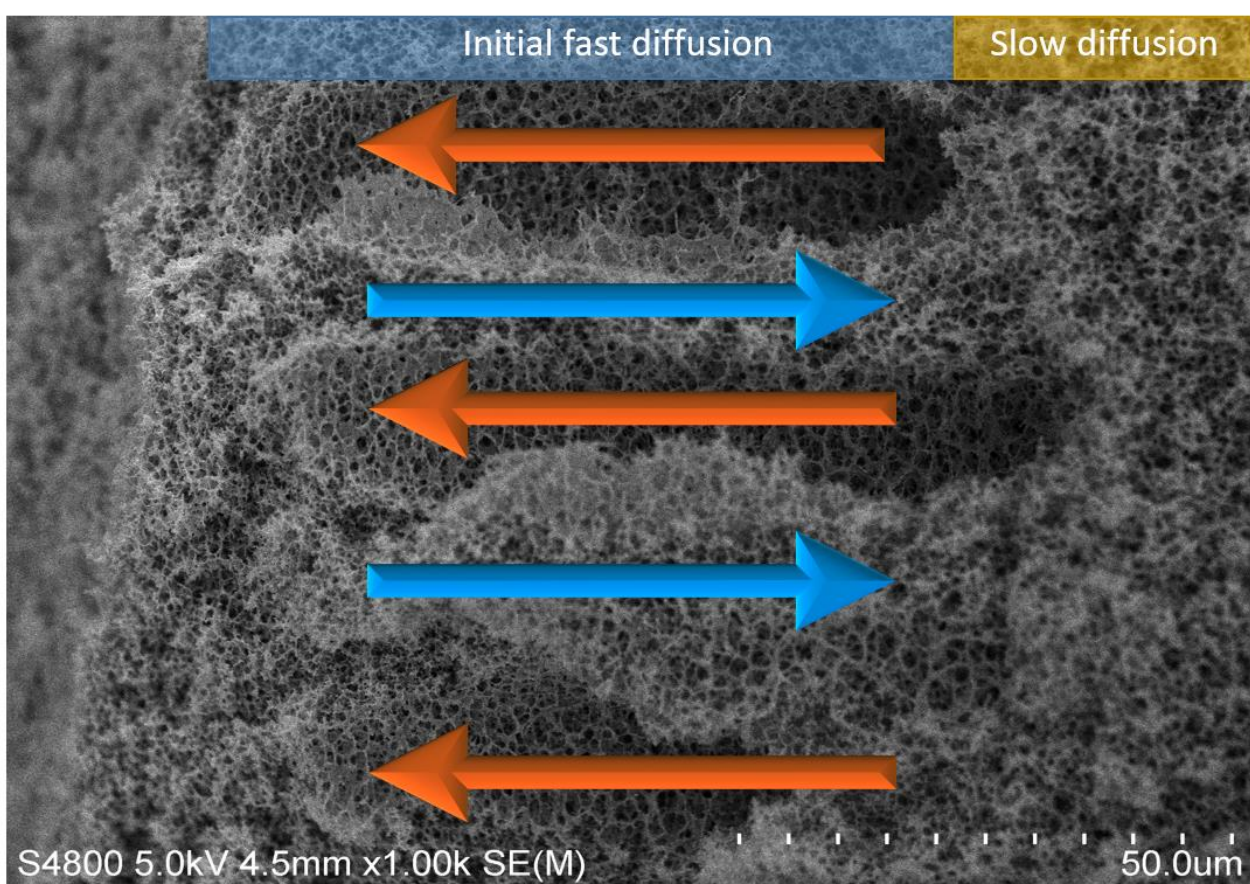
Figure 57. A possible explanation for the convection channels present beneath the surface of a FDCB bead would be the cross-directional flow of the cellulose solvent and antisolvent at the beginning of the regeneration process. The dissolved cellulose would be transported with the IL towards the surface of the dope until it would precipitate due worsening solvent conditions (wetting).

would result in the struts of material continuing all the way to the surface. Once the initial rush of solvent would be finished, the precipitated cellulose surface on the bead would slow down further diffusion of solvents. In such a case, the regeneration front would move slowly towards the center and precipitate the cellulose material evenly throughout the bead. This phase in the precipitation process would take over when the regeneration front reached the end of the convection channels. Despite the continuous outwards diffusion of further IL trough the bead surface, the solvent environment for cellulose near the surface would now on always remain thermodynamically poor, which would preserve the already formed convection channels. However, no experimental data that would prove such a mechanism for the formation of the channels has come to the attention of the author, albeit similar channels are seen with the precipitation of cellulose from N-methylmorpholine N-oxide-water solutions.[172]

4.3.3. Water content of ADCB

The water content of the air-dried beads was initially estimated by freeze-drying already air-dried beads. Mass of beads (1,289 g, approx. 2500 beads) from ADCB 2 batches B1 and B2 were transferred to a vial and frozen using liquid nitrogen. The vial was then transferred to the freeze-dryer and left to dry for 24 h, after which the vial was removed and weighed. The resulting weight loss was only 3 %. To the test whether 3 wt-% is representative of the actual water content, a separate test was implemented by heating two samples of beads (1,0 g and 0,1 g) from ADCB 4 (shaken) in an oven. The temperature was set at 105° C and the test was continued for 24 h. Cellulose does not degrade extensively at this temperature, while water evaporation is encourage by the above-boiling-point temperature. The resulting weight loss was 8,0 wt-% for a 1 g sample and 14,2 wt-% for a 0,1 g sample. Which result is closer to the truth is difficult to say. The larger sample of course has the benefit of more accurate weight determination, but at differences of this magnitude (the weight of the smaller sample would need to be almost 6 mg heavier to have the similar 8 wt-% loss) the accuracy of weighing should not be an issue.

A possible explanation for the difference could be that the test was done in a vial, which is considerably higher than it is wide. This resulted in the beads in the larger sample being stacked two or even three layers high, while the smaller sample was assembled only in one layer. The multi-layer arrangement is of course not optimal for evaporation, which might be a reason to explain the lower

weight loss in the larger sample. To further test validity of the results, some 0,4 g of the shaken ADCB beads were once again weighed into a vial and placed in the oven. This time the drying time was chosen as 72 h and the amount of beads was optimized for greatest mass, while keeping all the beads in one layer. The resulting weight-loss was 10,0 wt-%, which is between the two prior figures received from the larger and smaller samples. While this result does not give any definite answers about the actual water content inside the beads, alongside the previous results it does give a rough estimate of 3-15 wt-% for the amount of water accessible to outside atmosphere and solvent.

4.3.4. [DBNH][OAc] residue in Cellulose Beads

As is presented in section **2.3.3. Regeneration of cellulose from [DBNH][OAc] and other ILs – Case study in fibre spinning**, the IL and co-solvent diffuse out of the cellulose dope when it is submerged in an antisolvent such as water. In the case of Cellulose Bead preparation, the complete removal of the IL from the beads would be ideal for their potential future application in the cosmetic or food industries. The need to determine how thoroughly the washing and soaking steps removed [DBNH][OAc] and DMSO from the beads resulted in the utilisation of several analytical techniques. First, the elemental composition of the ADCB 1 was analysed using an elemental analyser (Elementar vario MICRO cube) for the presence of either nitrogen or sulphur, while using MCC as the reference. Neither sulphur (from DMSO) nor nitrogen (from [DBNH]) were present in the abundancy needed for detection (ca. 1 wt-%) and hence their concentration in the sample can be estimated to be relatively low. However, even if the nitrogen content of sample was 0,1 wt-%, it would still equate to relatively high concentration of [DBNH][OAc] in the beads (0,66 wt-%). Thus, additional experiments are needed to determine the amount of IL left in the samples.

To further test for the presence of [DBNH][OAc] in the beads, two NMR-experiments were employed. First, an ^{1}H-NMR experiment was run of a 1 wt-% [DBNH][OAc]/DMSO (40 wt-% DMSO) reference as well as from three 5 wt-% bead samples (ADCB 1, ADCB 4 and FDCB 3), with [P$_{4441}$][OAc]/DMSO-d$_6$ (80 wt-% DMSO-d$_6$) as the solvent. From the results, it was noted that [DBNH] was not present in any of the sampled beads in a concentration that would be observable. The spectra as well as the peaks observed are allocated in **Attachment 1.** A second diffusion-edited 1H-NMR-experiment was run of the IL reference and FDCB 3, but the result gave the same results as the earlier experiment (the spectra and peaks are allocated in **Attachment 1.**). In the end, NMR was

not sensitive enough to observe any of the possible [DBNH][OAc]-impurities left in the beads, which implies that the concentration of the IL must be in the region of 0,2 wt-% or lower.

The IL content of the beads was further investigated using the Energy-dispersive X-ray analyser (EDS) of a Scanning Electron Microscope. An ADCB bead was sliced in half with a scalpel, and examined via SEM. The EDS analyser was used to study the elemental composition of the bead material from three spots along the radius of the bead (**Figure 58.**). No indication of nitrogen ([DBNH]) or sulphur (DMSO) was observed in the spectra from any of the three points (**Attachment 3.**).

This further supports the idea that the diffusion driven washing and soaking steps used in the preparation of the Cellulose Beads are in fact very efficient in removing any traces of the original cellulose solvent [DBNH][OAc]/DMSO. Final attempt to study the concentration of electrolyte-impurities could be made by using IR to study the possible presence of a carbonyl signal originating

EDS analysis of a cut ADCB bead

⬤ = Spots on the surface of the sliced ADCB bead that were analysed using the EDS analyser.

The coarse pieces of cellulose observed on the cut surface result from the use of a scalpel as the cutting apparatus, which is not ideal for cutting this dense and resilient cellulosic material. Much smoother results are observed from the use of a high precision table top slicer.
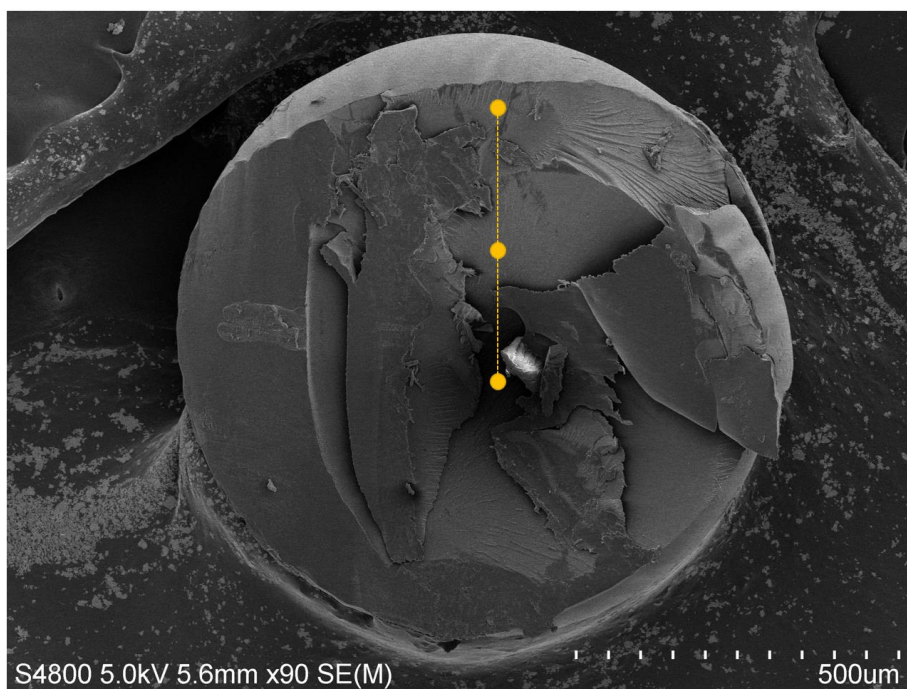
S4800 5.0kV 5.6mm x90 SE(M)　　　500um

Figure 58. The cross-section of an ADCB bead studied under SEM and analysed using EDS. The orange spots along the radius of the bead indicate the places where the elemental composition of the material was studied. No sign of nitrogen (from [DBNH]) or sulphur (from DMSO) was observed in any of the analysed points, which indicates that the residual concentration of the electrolyte solution components ([DBNH] or DMSO) is very low.

from the acetate anion or its protonated form, acetic acid. However, this method was not explored further due to time constraints.

4.3.5. Cross-linking of Cellulose Beads and their solubility in [DBNH][OAc]/DMSO

Cross-linking can be mostly simply understood as the formation of relatively short covalent connectivities between non-terminal positions of two or more polymer chains. A cross-linked polymeric material has several benefits over a non-cross-linked one. Firstly, a cross-linked polymer is usually less soluble compared to its non-cross-linked counterpart, being formed of a large network of interconnected molecules rather than individual polymer chains. Such an insoluble polymer network is more likely to form stable gels as a result of polymer swelling. In this case, the polymer can absorb impressive amounts of solvent, while the covalent bonds prevent the polymer chains from drifting too far from each other. Secondly, cross-linking of cellulose with another polymer would allow for the preparation of a wide array of polymer composites.

The cross-linking of Cellulose Beads was tested in a multitude of different experiments, with two compounds, epichlorohydrin and Poly(ethylene glycol) diglycidyl ether (PEGDE), being used as the primary cross-linking agents. The experimental details of these tests are left outside the extent of this thesis. Afterwards, a test was carried out to determine if the various types of Cellulose Beads regenerated from the [DBNH][OAc]/DMSO were insoluble in the original solvent used to form them, which if it were so would imply that the cross-linking was successful. All in all, 40 different cross-linked or un-cross-linked ADCB and FDCB beads were tested for their resilience towards dissolution in [DBNH][OAc]/DMSO (40 wt-% DMSO), the solvent they were initially crafted from. The experiment setup consisted of placing a single bead of each type in a 4 ml vial containing an excess of [DBNH][OAc]/DMSO – the cellulose concentration in these mixtures was between 0,1 – 0,2 wt-% depending on the bead.

After the porous FDCB beads had resided only 10-15 min in the solvent, they had turned considerably transparent, probably due to infiltration of the solvent into the pores of the bead and slight swelling of the cellulose matrix. After 2 hours, the unmodified control bead had clearly dissolved, while the cross-linked beads did not show much progress beyond the swelling stage. However after several more hours, even the cross-linked beads had fully dissolved. The stirring bar was suspected of breaking the FDCB beads during the process, so separate tests were run with no stirring applied. This ended up prolonging the dissolution process, but did not alter the ultimate results of the stirred experiments. Tests were also made where the vials were placed in an oil bath heated to 60° C and after 15 min on heat, all of the beads had dissolved in the solvent.

All of the tested ADCB beads withstood the IL media for 5 days at RT without any sign of dissolution or swelling. The cross-linked beads were also mixed using a magnetic stirrer bar for further 2 days, but no visible deterioration was observed in this case either. Finally, the cross-linked beads were heated at 60° C for 72 h, after which full dissolution was observed. Unfortunately, the author was not there to observe at which point the particles had fully dissolved and hence, it could have happened after 10 h or 60 h. When the unheated, and hence undissolved, un-cross-linked beads were removed from the vials, washed with water and left to dry in air, they were observed to be unchanged from their original state.

The findings of this experiment is that while the FDCB beads are prone to fast and efficient re-dissolution in the original solvent, the ADCB beads are very resilient towards dissolution and swelling, but under increased temperature do eventually dissolve. This is most likely a result of the of the great density and low porosity of the beads. Hence, there is a kinetic barrier for the dissolution of the ADCB beads at RT, but at elevated temperatures this barrier is overcome by the good cellulose solvent [DBNH][OAc]/DMSO. In addition, the fact that even all of the cross-linked FDCB and ADCB beads did eventually dissolve in the original solvent, means that the cross-linking reactions tested in this thesis were unsuccessful in creating a covalent cellulose network, and hence were deemed to have failed in cross-linking the Cellulose Beads.

4.3.6. Tails of beads

A dry Cellulose Bead might exhibit a tail, a structure which's presence or absence is already determined during or immediately after the dope dropping phase of the bead preparation process. The physical appearance of the tail and if it exists at all depends mostly on the drop height used in the experiment and on the cellulose concentration in the dope. The tail is the result of either, the droplet of dope not having enough time to assume a true spherical shape during freefall due to too short of a dropping height, or too strong of an impact with the water surface that forms a ripple within the droplet.

The presence and shape of tails varies somewhat between different bead types and consistencies. When the bead formation experiment goes according to plan, the beads have very diminutive tails resembling small studs on their surfaces. When the dope is too stretchy and the dropping height is too low, the tails are more prominent and frequent. In these cases, the length of the tails varies

between 0,5 to 3 mm, but can be as long as 10 mm if the dope is very stretchy and the dropping height is low. In the worst case the dope does not separate at all from the needle tip and a continuous chain of connected blobs is formed. The cross-section of the base of a relatively short tail on a FDCB bead can be seen on **Figure 59**.

Figure 59. SEM image of a FCB bead. The base of the tail is shown in cross-section while the tail itself is left whole.

Curiously, a considerably long tail can sometimes be seen rising up from beads that are already positioned underwater at the bottom of the container (**Figure 60.**). This behaviour is yet to be described along with proof, but some hypotheses can be made about the "rising-tails" phenomenon. The tails might be the result of a small trapped gas bubble near the surface of the dope. Once the dope has settled on the bottom, the bubble starts to rise upwards due to positive buoyancy. However, the dope is quite viscous and restricts the movement of the bubble, which ends up dragging some of the dope with it for a distance as long as 1 cm. The bubble however can not be very large, since it has not been observed with the naked eye unlike larger air bubbles that have not shown similar apart from actually floating the whole drop on the surface of the water. Thence, the credibility of this hypothesis is quite limited, but could still be partly responsible for the appearance of these rising-tails.
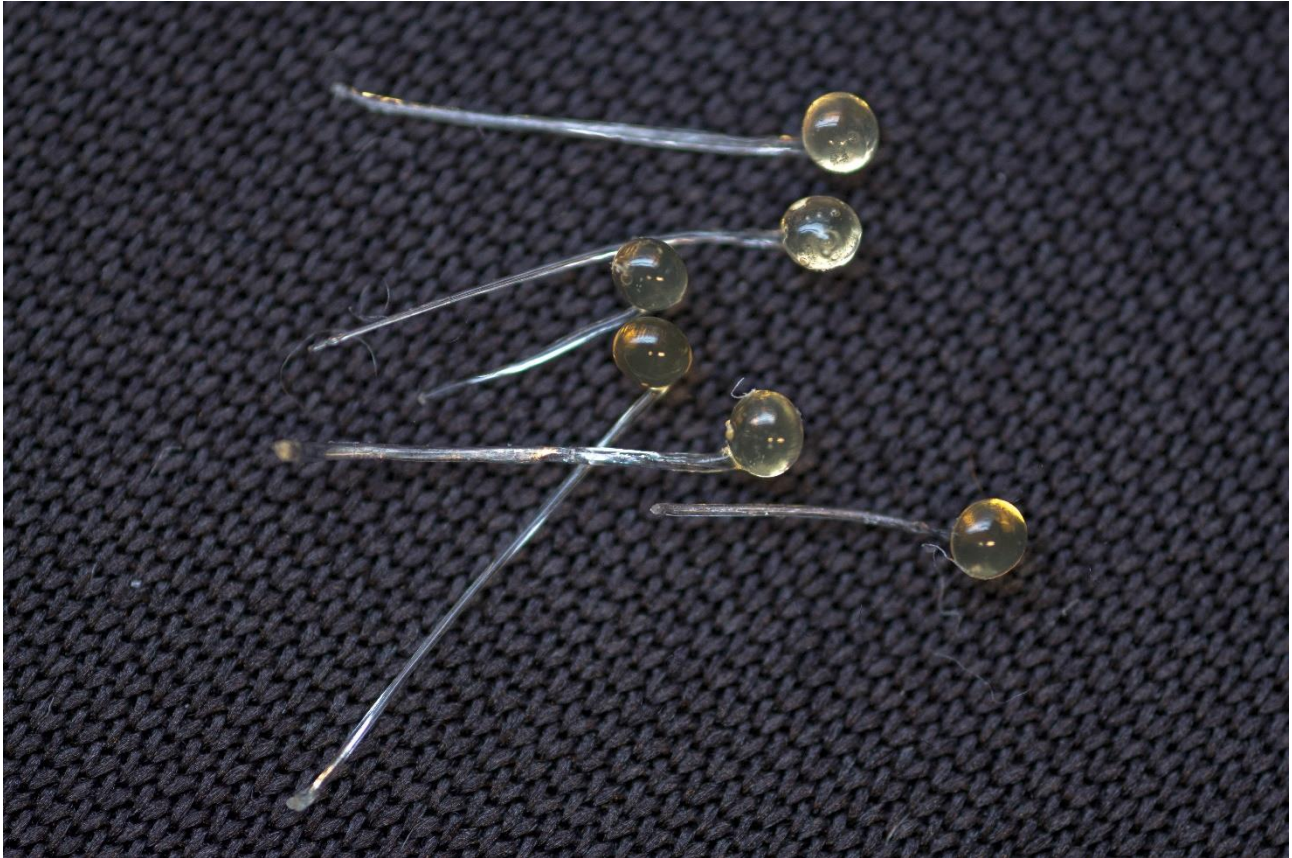
Figure 60. Sometimes the tails of the beads are observed to slowly rise upwards from the dope after the drop of dope has been submerged. The phenomenon might be caused by a trapped gas bubble or the relief of hydrostatic pressure built up as a result of the differing diffusion rates of the antisolvent water and the cellulose solvent [DBNH][OAc]/DMSO. The stronger than usual yellow tint is likely a result of somewhat inadequate washing of the beads prior to drying.

A more believable hypothesis could be made on the basis of swelling of the dope during regeneration and the subsequent release of the building pressure. When a drop of dope is submerged, water starts to diffuse towards the center of the bead while the cellulose solvent starts to diffuse outwards. However, the rate of diffusion is not the same for both solvents, with water having a faster diffusion inwards compared to the IL's outwards diffusion, as is the case with related systems such as Lyocell fibre spinning.[89] In this scenario, the cellulose on the surface of the dope has already precipitated and formed a hard layer. When the pressure inside the layer builds up due to the unequal diffusion rates, it might cause the surface to crack along a pre-existing line of weakness such as the already present small tail of the bead. Relatively water-poor dope would flow outwards through this crack to relieve the pressure build-up inside the bead, not unlike how pillow lava is formed under water. Cellulose on the surface of this newly exposed dope would very quickly

precipitate, but due to its younger age relative to the rest of the bead surface, this precipitated cellulose layer would most likely still constitute the weakest part of the bead surface. This would lead to further cracking of the surface in the rising tail, which would lead to lengthening of the tail but also to the formation of yet more weak newly precipitated cellulose surface. This positive feedback loop could then in theory lead to the formation of an impressively long tail, which's growth would be finally curtailed by a decrease in the absolute or relative diffusion rates between the two solvents.

It is easy to understand that the presence of an outwards poking appendices can be considered undesirable during the preparation of Cellulose Beads, as they deduct from the primary appealing feature of the beads – their sphericity. Although a small tail is always present in a Cellulose Bead, the formation of noticeable and obstructive tails should hence be actively avoided by changing the experimental parameters of the bead forming process. The two most important parameters that should be tuned in order two avoid or minimize the formation of tails are the dropping height and the dope viscosity. Usually the best results are obtained with a dropping height of 8-10 cm. Lower than that and the drop might not have time to acquire a spherical shape in time. Higher than that and the impact with the water surface most likely otherwise deforms the shape of the bead. The actual ideal value depends on the viscosity of the dope, which is the other important determining component. At a low viscosity, the dope material does not stretch substantially when the dope is dropping from the needle, which aids in tail reduction. Unfortunately, the low viscosity does make the material less resilient towards other deformations during the dropping or drying, which are equally undesirable. A high viscosity can be even more troublesome, causing the dope to stretch considerably before liquid-liquid contact is severed between the drop of dope and the material being extruded. In extreme cases this can lead to complete loss of separation between adjoining beads and hence a total failure in the bead forming process.

4.4. Cellulose microparticles from the UCST-like thermoresponsive phase behaviour in [P$_{4441}$][OAc]

The second experimental portion of this thesis focuses on the UCST-like thermoresponsive phase behaviour expressed by cellulose dissolved in [P$_{4441}$][OAc]/GVL and the preparation of cellulose microparticles by exploiting this phenomenon. The theoretical background and case specific details are discussed in sections **2.2.3. Thermoresponsive phase behaviour in cellulose solutions** and **2.4.1. UCST in [P$_{4441}$][OAc]/GVL.**

4.4.1. The basic UCST experimental setup

The preparation of gel-like cellulose microparticles from solutions of cellulose in [P$_{4441}$][OAc]/GVL (30 w-% GVL) is founded on a basic UCST experimental setup described here, with the details of each individual experiment varying slightly. In essence, the experiment is founded on the dissolution of cellulose by heating it with [P$_{4441}$][OAc]/GVL (30 wt-% GVL) and the subsequent cooling of the mixture. Upon cooling, these cellulose solutions produce gel-like cellulose microparticles, which can then be extracted from the solvent media and finally characterized by various analytical methods. Despite the problems associated with marrying cellulose and the concept of UCST together (as is described in section **2.2.3. Thermoresponsive phase behaviour in cellulose solutions),** all particles formed from the [P$_{4441}$][OAc]/GVL solvent system and all the experiments carried out using this system are denominated by the moniker "UCST" from here on.

For example, a 5 wt-% MCC UCST-sample can be prepared in the following manner. The [P$_{4441}$][OAc]/GVL (30 w-% GVL) electrolyte is first prepared by first synthetizing the IL (described in section **4.1.2. Preparation of [P$_{4441}$][OAc]**) and mixing it with GVL in the correct proportion in a vial. When the electrolyte mixture (2,85 g) becomes homogenous, a pre-determined amount of dry MCC (0,15 g) is carefully added to the vigorously mixed electrolyte to avoid clumping. The resulting suspension is heated to 70° C using an oil-bath heater and mixed for further 30-60 min, depending on the individual run. The electrolyte does not yet dissolve nor visibly swell cellulose at this temperature. The aim of this relatively long mixing step is to let the solvent properly wet the cellulose material, soaking into all available pores present in MCC.

After this step, the vial is rapidly heated to 120° C for 5 minutes by transferring it to a separate pre-heated oil bath. When full dissolution of cellulose is observed, the vial is removed from the oil bath, the outside surface cleaned of the oil, and the vial is left to cool at varying rates by altering the cooling method. Then the vial is left to cool at either RT, a refrigerator (4 °C) or it is first place in an ice bath for 5 min and then to the refrigerator. The different cooling rates range from slow (left to cool in air at RT) to moderate (left to cool in air at a 4° C refrigerator) to fast (placed in an ice bath for 5 min and then in the refrigerator) to very fast (placed in ice bath for 30 min and then to the -16° C freezer). This cooling step is the thermal trigger responsible for the formation of gel-like microparticles, which formed the motive of the other half of this thesis. At first, the formed particles were simply studied using an optical microscope, but sample preparation methods enabling their analysis using more powerful instruments, such as SEM and WAXS, were devised later on.

4.4.2. Cellulose nanoparticles from low concentration dope

A mixture of 0,1 wt-% MCC in $[P_{4441}][OAc]$/GVL (30 w-% GVL) was stirred for 60 minutes at 70° C using a magnetic stirrer, after which it was heated to 120° for 3 minutes. Subsequently the vial was removed from heat, placed in an ice water bath for 30 min and into the 4° C refrigerator after that. After the sample had been held in the refrigerator overnight, a 0,5 ml portion of it was prepared for dialysis. The MCC/IL/GVL solution was mixed rapidly with 1,5 ml of distilled water, which result in the immediate formation of a precipitation. The formed mixture (2 ml) was placed inside a dialysis bag and the dialysis was run using the method described in section **4.1.9. Cellulose nanoparticles by dialysis of MCC/IL dopes.**

The very low cellulose load was hypothesized to produce particles of nanometre scale as they were not visible under optical microscopy. Hence, light scattering analysis was run on the mixture and rather ambiguous results were attained. The results showed possible nanoscale particles, which scattered light in very low intensity. Therefore, the presence of particles could not be outright ruled out, even though the evidence for their existence was rather unsubstantial. To remedy this uncertainty, a test was run on pure IL/GVL mixture to see whether the observed particles were originating from cellulose or from IL. The results were equally inconclusive, suggesting the presence of somewhat smaller particles.

One explanation for the presence of "ghost particles" in seemingly homogenous solvent system could be that the solvents are not fully miscible and form local homomolecular clusters, which would result in locales of differing refractive index within the solvent. An experiment was devised to study if the two components of the IL ([P$_{4441}$][OAc] and GVL) were fully miscible by studying the evolution of the refractive index of the mixture from 100 wt-% GVL moving towards 100 wt-% [P$_{4441}$][OAc] in 10 wt-% increments of [P$_{4441}$][OAc]. The resulting graph (**Figure 61.**) shows a nearly linear relationship between the [P$_{4441}$][OAc] concentration and the refractive index of the mixture. This implies that the presence of ghost particles cannot be due to immiscibility of the two electrolyte components, but has to arise from another unrelated or related issue with the system. The origin of these ghost particles was left without further inquiry in this thesis, but possibly the ionic nature of the primary component has something to do with the phenomenon.
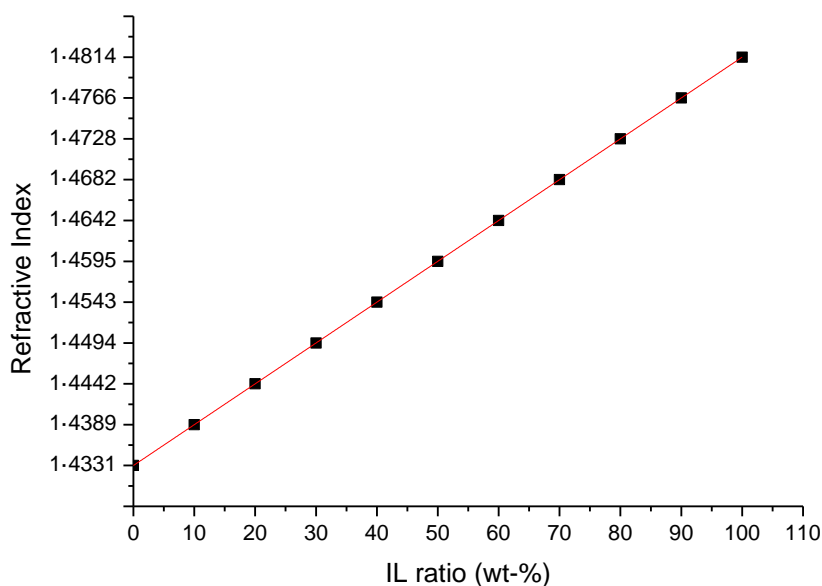

Figure 61. The refractive index of the organic electrolyte [P$_{4441}$][OAc]/GVL in relation to the proportion of [P$_{4441}$][OAc] in the mixture. The relationship is almost perfectly linear. The value for 100 wt-% [P$_{4441}$][OAc] was estimated based on the prior nine steps, as the compound is solid at RT.

4.4.3. The effect of cellulose concentration on particle formation

The next five experiments were performed in order to study possible changes in the UCST phenomenon due to changing cellulose concentration. The MCC concentration used was either 1, 2, 4, 6 or 8 wt-%. Appropriate mass of MCC was placed in a 20 ml vial and the IL was added on top of the cellulose fairly rapidly while mixing at 70° C. The vials were kept at 70° C for further 40 min, after which they were placed in an oil bath at 120° C for 5 min. Subsequently, when the solution had turned optically clear, the vial was placed in an ice water bath for 30 min and finally moved to a refrigerator for overnight. Mixing was continued until the cooling step.

After 24 h in the refrigerator, the 1 wt-% sample still remained clear and showed no visible signs of particles, while the 2 and 4 % samples were visibly opaque viscous honey-like liquids (**Figure 62.**). The 6 and 8 % samples were similarly opaque but had turned into a gel of sorts. All samples were studied under an optical microscope, where samples that had turned at least somewhat opaque (2-8 wt-%) were observed to be contain cellulosic material not in the solution phase.

Figure 62. Comparison of the 1 wt-% (left) and 4 wt-% (right) UCST dopes after 24 h storage in the refrigerator. The presence of at least partially precipitated cellulose is indicated by the opaqueness of the 4 wt-% solution.

When looking at a thicker portion of a sample, only a large opaque mass was visible, while thinner sections revealed that the material was riddled with individual microparticles with diameters of several μm (**Figure 63.**). No significant difference was observed in the size or appearance of the particles between the different MCC concentrations, but naturally the less viscous samples (2 and 4 wt-%) had a fewer number of microparticles compared to the more viscous ones. These results set

the baseline for further UCST experiments, a successful test requiring at least 2 wt-% MCC and preferably not considerably than 6 wt-%.
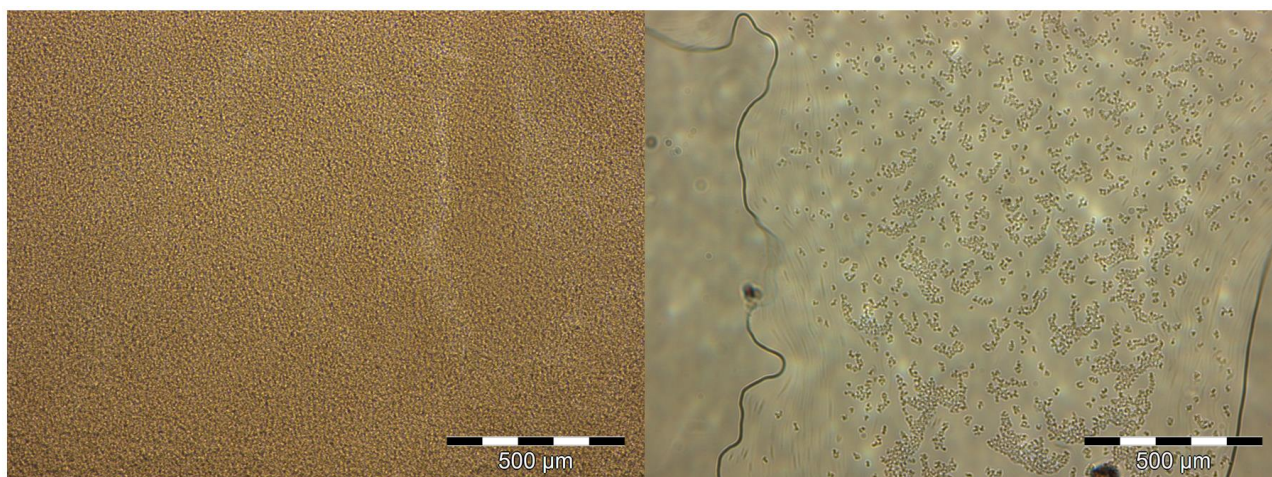

Figure 63. Optical microscope images of the UCST-dope. The image on the left is from a thick section of the sample and hence only a mass of material is observed. The image on the right is from a thin section, where the individual microparticles are clearly visible.

4.4.4. The effect of varying cooling rate on particle formation

The next three UCST experiments were run using a 5 wt-% MCC dope and varying the cooling methods (rates) to study whether the cooling rate had an effect on the particle size and morphology. The tests were run in a similar manner to prior experiments, mixing the appropriate amount of cellulose with the IL/co-solvent in a 20 ml vial while mixing and heating the dope to dissolve the cellulose. After 40 min at 70° C and 5 min at 120° C, UCST 10 was removed from heat and left to cool in the fume hood at RT, UCST 11 was transferred straight into the refrigerator and UCST 12 was placed in an ice water bath for 5 min and then placed in the refrigerator. No difference was observed in the size of the particles based on the cooling method.

Holding[10] observed a clear influence of the cooling rate on the size of the particles formed from [P$_{4441}$][OAc]/DMSO (20 wt-% DMSO), while the author did not have similarly clear findings from [P$_{4441}$][OAc]/GVL (30 wt-% GVL) in the scope of this thesis. Holding reported that when the heated mixture of cellulose in IL/co-solvent was cooled rapidly with an ice-bath/fridge combination, the particles formed were of 5,2 μm average diameter. However, when the cooling was done gently at room temperature, there was a dichotomy in the particle size: there were larger aggregates of 16 μm as well as a range of smaller particles of 1-2 μm. Some evidence suggesting that differences in

the cooling rate is the origin of the possible dichotomy of the particle size was observed in this thesis, but overall the relationship was found to be not as clear-cut as a simple slope of the temperature gradient. These disparities in the size of the particles could very well be a result of the varying degree of antisolvent (H_2O) concentration in the sample. For example, the presence of even a small amount of water in the IL could alter the thermodynamic properties of the solvent slightly, which could result in a change in the particle size that is thermodynamically or kinetically the most stable. Overall, the size-dependency is not fully understood at the moment.

4.4.5. Removal of GVL under vacuum

Even though the UCST microparticles are clearly observable using an optical microscope, the degree of magnification offered by it is inadequate to study the structure of an individual particle. Therefore, more powerful microscopes such SEM are required. However, the particles need to be extracted from volatile components for imaging in the high vacuum chamber of the SEM. To this end, an experiment was devised to find out if the co-solvent GVL was removable in vacuum. These extracted materials are suitable for additional analyses such as WAXS.

The experiment was run according to the basic setup using a 5 wt-% MCC dope, usual dissolution temperatures (70° C and 120° C) and 5 min ice-water cooling before refrigeration. No precipitation had appeared after 6 h, but a small sample was transferred to a petri dish and placed inside a vacuum oven kept at RT overnight. After 22 h the main batch of the sample in the refrigerator was still clear but the sample in the vacuum oven had turned to an opaque gel. On an optical microscope, this opaqueness was proven to be the result of the formation of particles identical to ones observed before. Compared to dope that had not been vacuum treated, the dope was much more viscous, resembling a paste rather than a viscous liquid.

To test this method further, a new subsample (0,18 g) taken out of the main batch of UCST 18, as well as subsample (0,1 g) of UCST 10 (aged at RT for four weeks), were weighed and placed inside the vacuum oven at RT. After 72 h, the UCST 18 sample had lost 28,38 wt-% of its mass and UCST 10 had lost 28,94 wt-%. The weight ratio of components in the 5 wt-% MCC dope is 5:66,5:28,5 (MCC:$[P_{4441}][OAc]$:GVL). As cellulose and $[P_{4441}][OAc]$ are practically non-volatile in comparison to GVL, all the weight loss observed must be due to the evaporation of GVL. Hence, a loss of 28,5 wt-% in a sample would indicate that all of the GVL has evaporated. The 28,38 wt-% loss of UCST 18 can

be approximated to the full removal of GVL. However, the 28,89 wt-% of loss from UCST 10 is slightly above what would be expected just from GVL. This excess mass is most likely small amounts of water that the hygroscopic material has attracted during its aging period in the lab.

In a subsequent experiment, a larger 0,6 g subsample taken from the main batch of UCST 18 was weighed at several intervals in the vacuum oven to study how long a time was needed to remove the co-solvent GVL from the sample. It was found that 2 hours was enough to remove 20,53 wt-% from the sample and 5 hours was enough to remove 23,60 wt-%. However, the loss of GVL retarded greatly after this period, as only circa 24 wt-% had been lost after 24 h and 25,29 wt-% was removed after 72 h. The value measured after 24 h is approximate (measured value 15,56 wt-%) as the vacuum oven had been opened several times before the measurement, giving opportunities for the hygroscopic material to attract water. The final loss of 25,29 wt-% is also notably less than that observed in the previous drying experiment, which is probably the result of increased bulk of the sample. The mass of cellulose "gel", within from which GVL must be removed, was noticeably thicker than that present in the earlier trial. This would work to hinder the evaporation of GVL from the centre of the mass. One could argue that the opening of the oven doors and hence the addition of water to the hygroscopic dope would also play a role in retarding the evaporation of GVL. In this scenario, the added water would make the cellulose move from a "gel-like" state to truly precipitated on the surfaces of the mass as a result of dilution of the solvent and addition of antisolvent. However, this was found out not to be the case as later trials, where the doors of the oven were not opened during the 72 h drying period, resulted in a similar circa 25,5 wt-% total loss of mass.

The effect of the timing of vacuum drying on the produced particles was studied by placing a drop of the dope on a silicon wafer before it had had time to cool as well as after 60 min in the refrigerator. A few drops of acetone was also dropped on the latter sample, which was aged with the acetone for 5 min before it was placed in the vacuum oven. Both of these tests produced particles of similar shape and size compared to those obtained from the dope aged 24 h in the refrigerator. Although these tests did not show any beneficial qualities over samples aged longer in the refrigerator, the fact that similar particles to refrigerator aged ones could be produced by placing the dope in the vacuum oven without secondary cooling makes the experiment pathway simpler.

4.4.6. Hygroscopic nature of vacuum dried MCC/[P$_{4441}$][OAc] dope

It was noticed on the previous experiment that, when the leftovers of the vacuum-dried sample were left to interact with laboratory air at RT, they attracted noticeable amounts of moisture – they were hygroscopic. The effects were observed on the paste where, in parts of the yellowish homogenous opaque material, elongate wisps of white material discernible by eye had appeared after 24 h. To study whether the microparticles had merely agglomerated together or whether proper precipitation of the material had occurred, part of the sample was sonicated in acetone at 0,1 wt-% constitution (lower concentration than in previous tests). Unlike material sonicated immediately after drying, this failed to produce a suspension. Hence, it is likely that the material had slowly precipitated as irregular large sized particles as the water concentration increased. When the dissolution capacity of the solvent fell low enough, the initially gel-state material formed masses of cellulose that did not possess the microparticle morphology anymore.

4.4.7. Shape and morphology of the cellulose microparticles

As mentioned in section **4.4.5. Removal of GVL under vacuum**, the UCST microparticles were clearly visible under an optical microscope. However, the isolation of the microparticles was not very easy as filtering of the gel did not work, and the addition of more co-solvent or antisolvent led to more extensive gelling of cellulose. In order to study the particles further, several methods of regeneration and purification of the particles from the electrolyte mixture were devised. These methods are described in the following paragraphs.

Studying the general shape and morphology of the gel-state microparticles was most easily achieved on an optical microscope, while more-thorough investigations were carried out on a SEM. For the purpose of optical microscopy, the particles were simply deposited as-is onto a sample slide. The particles for SEM (or for WAXS & CP-MAS) were further purified with methods described in earlier sections. In all cases, the co-solvent GVL was evaporated in a vacuum oven at RT, which was followed by the removal of the IL by washing and regenerating the material either slowly, by soaking in water for two weeks, or rapidly, by sonicating in acetone. The regenerated particles were then dried in a nitrogen stream (water regenerated, analysed by WAXS) or in air (acetone regenerated, analysed by WAXS, SEM and CP-MAS).

After only the evaporation of GVL, the previously slightly opaque viscous liquid turned into an opaque paste and the particles formed clusters on the SEM analysis disc (**Figure 64. A**). The clusters of particles were clearly glued together by [P$_{4441}$][OAc], as when the magnification was increased too much, the clusters started to melt (**Figure 64. B**). When pressurized nitrogen was used to blow some of the clusters away, individual particles were left stuck to the analysis disc. These particles were observed to have a general shape of a "doughnut", i.e. having a hollow centre (**Figure 64. C**). This kind of shape is usually observed when spherical particles are dried, and the solvent leaving the particles causes them to burst and turn partially inside out. This shape change is likely to have occurred in the SEM analysis chamber itself, when the particles were exposed to a vacuum higher than the GVL removing step. Albeit probably not having been formed as a result of the same conditions as the cellulose particles in this thesis, somewhat similar doughnut-shapes have been previously observed for other polymer particles.[173, 174] The IL was subsequently washed away by sonicating the material in acetone, which resulted in regeneration of the cellulose from the gel-like phase to a solid. A further SEM analysis captured a multitude of particles, which had a very high surface area and sizes ranging from several micrometres to the nanoscale. The general shrivelled appearance of the particles suggests that they have further collapsed during the regeneration process from gel to solid.
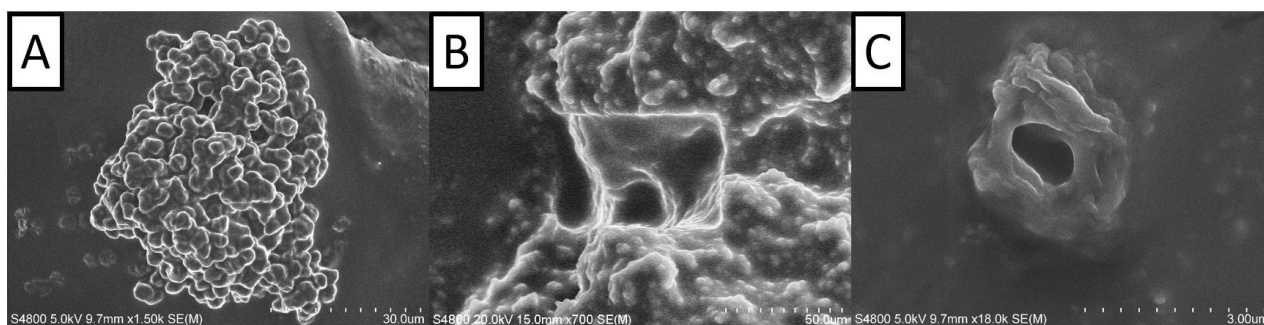

Figure 64. GVL-evaporated UCST microparticles imaged using SEM. **A:** A large cluster of microparticles. **B:** The presence of [P$_{4441}$][OAc] in and around the beads is evidenced by the temperature (energy) induced melting of the sample. **C:** Individual UCST microparticle demonstrating the peculiar "doughnut" shape.

Reference WAXS-spectra were obtained from a cooled liquid sample of [P$_{4441}$][OAc]/GVL, as well as from a single crystal of [P$_{4441}$][OAc], which had formed during a 4-month storage in a fridge.[70] Comparing to these references, several different regenerated microparticles were analysed. The WAXS-spectra of the GVL-evaporated sample shows that no evidence of characteristic cellulose I or II peaks are present (**Figure 65.**). The broad signals at 8° and 22° are from the [P$_{4441}$][OAc]/GVL

background, while the sharp peaks (35 nm dimension, larger than known cellulose dimensions) correspond roughly to those obtained from the single crystal $[P_{4441}][OAc]$. When a sample of GVL-evaporated microparticles was aged for one month, the sharp peaks were enhanced in the diffractogram, whereas the broad background was decreased. This evidence supports a model of slow co-precipitation of the IL with cellulose – IL-crystals are forming in close association with the gel-state cellulose microparticles, growing in size to up to 60 nm (FWHM=0,14). The method of regeneration by soaking in water (see earlier paragraph) was used to prepare a fully regenerated sample from the GVL-evaporated paste. When the wet material was analysed, it afforded a spectra with only two small cellulose peaks (21° and 23°, characteristic of cellulose II) standing out from the water background. Subsequently the sample was dried under a nitrogen stream for 1 min and then 5 min. After each drying step, the water background was perceived to decrease in intensity at them same time as the cellulose peaks were increasing. Of course, the increase of the cellulose signals is partly due to the increase of cellulose concentration in the sample, but it is also proof that the thermodynamically more stable cellulose II is formed, when the gel-state microparticles are regenerated in water. Naturally, only a portion of the cellulose forms crystallites, while the rest form amorphous material. When the acetone regenerated material was analysed by WAXS, a fully amorphous material was observed, with no presence of the cellulose-II-characteristic peaks at 21° and 23°. The amorphous nature of the material was also supported by a CP-MAS analysis, which showed the absence of the C4 peaks centered at 88 ppm, which are characteristic of cellulose I and II.[70]
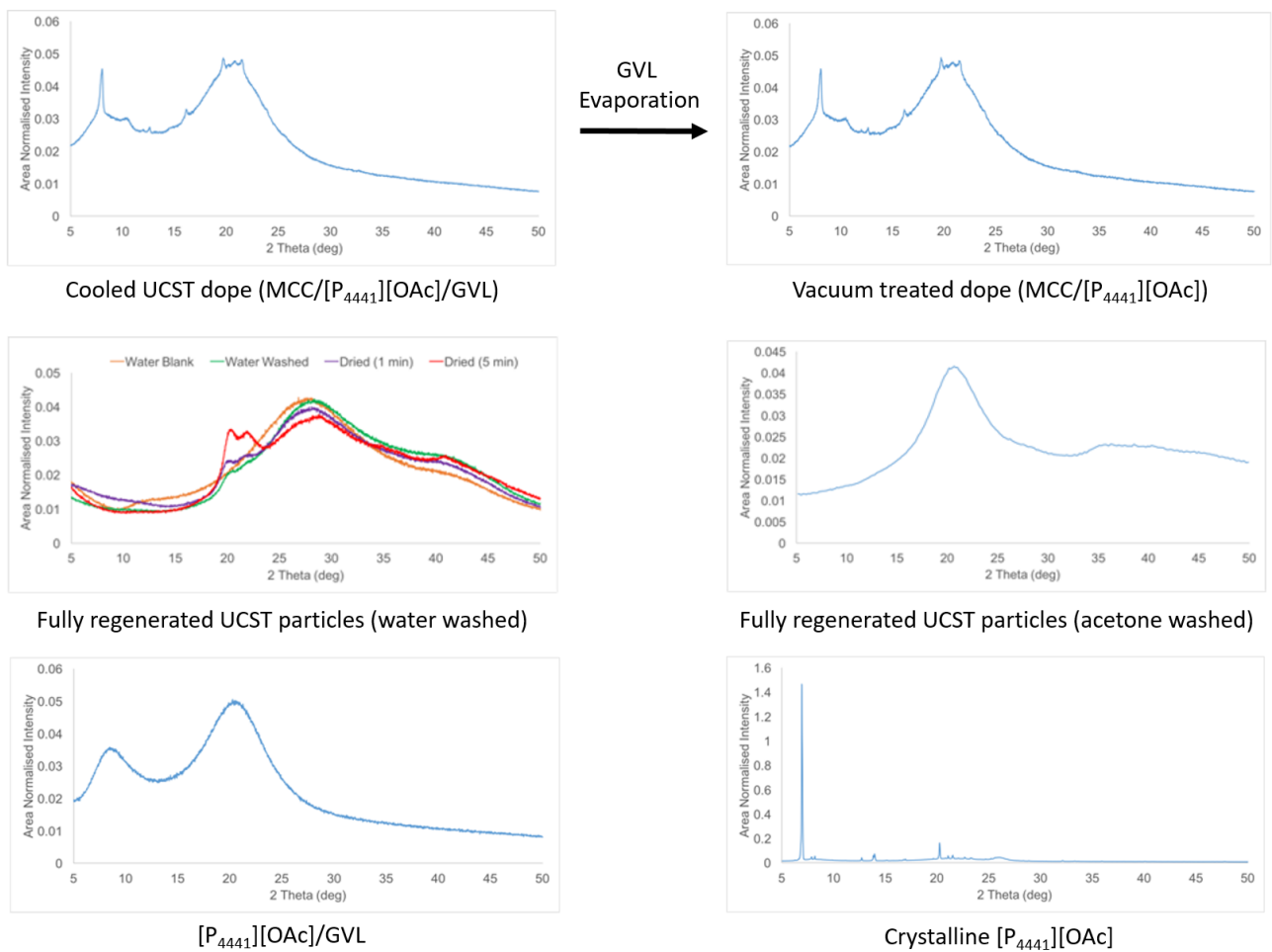
Figure 65. WAXS diffractograms of UCST particles before and after various washing and extraction methods.

While the fully regenerated cellulose material is of either amorphous or cellulose II morphology, the morphology of the "gel-state" is rather more ambiguous.[70] Despite this ambiguity, some deductions about the morphology of the formed microparticles can be made. According to the WAXS analyses, either the material is not regenerating in any crystalline morphology or the particles constitute such a small portion of the total material that they do not give discernible crystalline cellulose diffraction patterns. Moreover, as there is no outside force applied to help in macromolecular assembly, cellulose regenerates in morphologies that do not confer mechanical strength to the structure, apart from the cellulose II crystallites.

5. Conclusions

Cellulose as a material has been profoundly rooted in the development of human societies, where it has been main component in innovations such as firewood, paper or guncotton, which have heavily influenced the progress of humankind. Traditionally, cellulose has only been soluble in a few selected solvent systems and so has been problematic to chemically modify. In recent years, advances in the knowledge and understanding of ionic liquids have made the homogeneous dissolution of cellulose feasible. A homogeneous solution of cellulose is a versatile platform for further modification of the polymer and a convenient way to remodel the cellulose matric into new forms.

Cellulose as a material is extremely abundant in nature and widely used in a plethora of applications. However, these applications are comparably low-tech and hence also of low economical value. This makes the refining of low cost cellulose raw materials into high technology applications highly desirable. Especially in the face of impending ecological and climatic predicaments, the chemical resilience, biological compatibility and renewability of cellulose make it an attractive basis for innovations with sustainable growth in mind. A fitting example of such an innovation would be a cellulose-based alternative for cosmetic microbeads, which are accumulating in the aquatic environment and adversely affecting the animals living in it. Such cellulose particles have been designed during the course of this work.

Novel cellulose macro- and microparticles have been prepared from two cellulose solvents systems, [DBNH][OAc]/DMSO and [P_{4441}][OAc]/GVL. The two types of particles and their preparation methods are very different and distinct. The large beads are prepared using remarkably simple hands-on method, while the small particles are prepared by exploiting a thermally triggered gelation of cellulose. Both particles are scientifically interesting and observations made during their preparation provide new insight to the field of cellulose materials chemistry.

5.1. Acknowledgements

6. References

1. Klemm, D., Heublein, B., Fink, H.-. & Bohn, A. *Angewandte Chemie - International Edition* **44**(22) 2005 3358. DOI 10.1002/anie.200460587.

2. French, A.D. *Cellulose* **24**(11) 2017 4605. DOI 10.1007/s10570-017-1450-3.

3. Klemm, D., Philipp, B., Heinze, T., Heinze, U. & Wagenknecht, W. General Considerations on Structure and Reactivity of Cellulose: Section 2.4-2.4.3In *Comprehensive Cellulose Chemistry*, Wiley-VCH Verlag GmbH & Co. KGaA 2004, p. 130-165.

4. Swatloski, R.P., Spear, S.K., Holbrey, J.D. & Rogers, R.D. *Journal of the American Chemical Society* **124**(18) 2002 4974. DOI 10.1021/ja025790m.

5. Brydson, J.A. *Plastics Materials* , 6th. p., Butterworths, London 1995.

6. Hopkinson, B. *Trans.Roy.Soc.London (A)* **213** 1914 437.

7. Worden, E.C. *Nitrocellulose Industry*, D. Van Nostrand Company, Michigan 1911.

8. Fink, H., Weigel, P., Purz, H.J. & Ganster, J. *Progress in Polymer Science* **26**(9) 2001 1473. DOI //dx.doi.org/10.1016/S0079-6700(01)00025-9.

9. Krueger, R. *Chemiefasern/Textilindustrie* **44**(1-2) 1994 24.

10. Holding, A.J. 2016, *Ionic Liquids and Electrolytes for Cellulose Dissolution*, University of Helsinki.

11. Chakar, F.S. & Ragauskas, A.J. *Industrial Crops and Products* **20**(2) 2004 131. DOI //doi.org/10.1016/j.indcrop.2004.04.016.

12. Zeronian, S.H. & Inglesby, M.K. *Cellulose* **2**(4) 1995 265. DOI 10.1007/BF00811817.

13. Collinson, S.R. & Thielemans, W. *Coordination Chemistry Reviews* **254**(15) 2010 1854. DOI //doi.org/10.1016/j.ccr.2010.04.007.

14. Chen, H. & Qiu, W. *Biotechnology Advances* **28**(5) 2010 556. DOI //doi.org/10.1016/j.biotechadv.2010.05.005.

15. *World population trends | UNFPA - United Nations Population Fund* 2015, Available: http://www.unfpa.org/world-population-trends (Retrieved Apr 10,2017).

16. T. Clough, M. *Green Chemistry* **19**(20) 2017 4754. DOI 10.1039/C7GC01776F.

17. Mullin, L., P., Sillett, S., C., Koch, G., W., Tu, K., P. & Antoine, M., E. *Tree Physiology* **29**(8) 2009 999. DOI 10.1093/treephys/tpp037 [doi].

18. Koch, G.W., Sillett, S.C., Jennings, G.M. & Davis, S.D. *Nature* **428**(6985) 2004 851.

19. Hult, E., Larsson, P.T. & Iversen, T. *Polymer* **42**(8) 2001 3309. DOI //doi.org/10.1016/S0032-3861(00)00774-6.

20. Klemm, D., Kramer, F., Moritz, S., Lindström, T., Ankerfors, M., Gray, D. & Dorris, A. *Angewandte Chemie International Edition* **50**(24) 2011 5438. DOI 10.1002/anie.201001273.

21. Koblitz, W., Kiessig, H. & Hess, K. *Zeitschrift für Elektrochemie, Berichte der Bunsengesellschaft für physikalische Chemie* **58**(10) 1954 872. DOI 10.1002/bbpc.19540581010.

22. Hearle, J.W.S. *Journal of Polymer Science* **28**(117) 1958 432. DOI 10.1002/pol.1958.1202811722.

23. Fink, H. & Philipp, B. *Journal of Applied Polymer Science* **30**(9) 1985 3779. DOI 10.1002/app.1985.070300918.

24. Sixta, H., Michud, A., Hauru, L., Asaadi, S., Ma, Y., King, A.W.T., Kilpelainen, I. & Hummel, M. *Nordic Pulp & Paper Research Journal* **30**(1) 2015 43. DOI 10.3183/NPPRJ-2015-30-01-p043-057.

25. Wang, H., Gurau, G. & Rogers, R.D. *Chemical Society Reviews* **41**(4) 2012 1519. DOI 10.1039/C2CS15311D.

26. Ardizzone, S., Dioguardi, F.S., Mussini, T., Mussini, P.R., Rondinini, S., Vercelli, B. & Vertova, A. *Cellulose* **6**(1) 1999 57. DOI 1009204309120.

27. Atalla, R.H. & Vanderhart, D.L. *Science* **223**(4633) 1984 283.

28. Pérez, S. & Mazeau, K. Conformations, Structures, and Morphologies of CellulosesIn *Polysaccharides*, CRC Press 2004, p. 41.

29. Nishiyama, Y., Langan, P. & Chanzy, H. *Journal of the American Chemical Society* **124**(31) 2002 9074. DOI 10.1021/ja0257319.

30. Wada, M., Heux, L., Nishiyama, Y. & Langan, P. *Biomacromolecules* **10**(2) 2009 302. DOI 10.1021/bm8010227.

31. Goldberg, R.N., Schliesser, J., Mittal, A., Decker, S.R., Santos, Ana Filipa L O M, Freitas, V.L.S., Urbas, A., Lang, B.E., Heiss, C., Ribeiro da Silva, Maria D M C, Woodfield, B.F., Katahira, R., Wang, W. & Johnson, D.K. *The Journal of Chemical Thermodynamics* **81** 2015 184. DOI 10.1016/j.jct.2014.09.006.

32. Wada, M., Chanzy, H., Nishiyama, Y. & Langan, P. *Macromolecules* **37**(23) 2004 8548. DOI 10.1021/ma0485585.

33. Newman, R.H. *Cellulose* **15**(6) 2008 769. DOI 10.1007/s10570-008-9225-5.

34. Foster, C.E., Martin, T.M. & Pauly, M. *Journal of Visualized Experiments : JoVE* (37) 2010 1745. DOI 10.3791/1745.

35. Park, S., Baker, J.O., Himmel, M.E., Parilla, P.A. & Johnson, D.K. *Biotechnology for Biofuels* **3** 2010 10. DOI 10.1186/1754-6834-3-10.

36. Ruland, W. *Acta Crystallographica* **14**(11) 1961 1180. DOI 10.1107/S0365110X61003429.

37. Graenacher, C. United States US1943176 A, 1934.

38. Johnson, D.L. United States US3447956 A, 1969.

39. Ebner, G., Schiehser, S., Potthast, A. & Rosenau, T. *Tetrahedron Letters* **49**(51) 2008 7322. DOI //dx.doi.org/10.1016/j.tetlet.2008.10.052.

40. Cai, T., Zhang, H., Guo, Q., Shao, H. & Hu, X. *Journal of Applied Polymer Science* **115**(2) 2010 1047. DOI 10.1002/app.31081.

41. Vitz, J., Erdmenger, T., Haensch, C. & S. Schubert, U. *Green Chemistry* **11**(3) 2009 417. DOI 10.1039/B818061J.

42. Wilkes, J.S. & Zaworotko, M.J. *Journal of the Chemical Society, Chemical Communications* **0**(13) 1992 965. DOI 10.1039/C39920000965.

43. King, A.W.T., Parviainen, A., Karhunen, P., Matikainen, J., Hauru, L.K.J., Sixta, H. & Kilpeläinen, I. *RSC Advances* **2**(21) 2012 8020. DOI 10.1039/C2RA21287K.

44. Walden, P. *Bulletin de l'Academie Imperiale des Sciences de St.-Petersbourg* 1914 405.

45. Atefi, F., Teresa Garcia, M., D. Singer, R. & J. Scammells, P. *Green Chemistry* **11**(10) 2009 1595. DOI 10.1039/B913057H.

46. Hallett, J.P. & Welton, T. *Chemical reviews* **111**(5) 2011 3508. DOI 10.1021/cr1003248.

47. Niedermeyer, H., P. Hallett, J., J. Villar-Garcia, I., A. Hunt, P. & Welton, T. *Chemical Society Reviews* **41**(23) 2012 7780. DOI 10.1039/C2CS35177C.

48. *FluoroChem: 1,5-Diazabicyclo[4.3.0]non-5-ene* Available: http://www.fluorochem.co.uk/Products/Search?searchType=C&searchText=%203001-72-7 (Retrieved 24.10.2017).

49. *Sigma Aldrich: 1,5-Diazabicyclo[4.3.0]non-5-ene* Available: http://www.sigmaaldrich.com/catalog/product/sial/33471 (Retrieved Oct 24,2017).

50. Ranke, J., Stolte, S., Störmann, R., Arning, J. & Jastorff, B. *Chemical Reviews* **107**(6) 2007 2183. DOI 10.1021/cr050942s.

51. King, A.W.T., Asikkala, J., Mutikainen, I., Järvi, P. & Kilpeläinen, I. *Angewandte Chemie International Edition* **50**(28) 2011 6301. DOI 10.1002/anie.201100274.

52. Holding, A.J., Heikkilä, M., Kilpeläinen, I. & King, A.W.T. *ChemSusChem* **7**(5) 2014 1422. DOI 10.1002/cssc.201301261.

53. McNulty, J., Capretta, A., Cheekoori, S., Clyburne, J.A.C. & Robertson, A.J. *Chimica Oggi* **22**(11-12) 2004 13.

54. Le, K.A., Rudaz, C. & Budtova, T. *Carbohydrate Polymers* **105**(Supplement C) 2014 237. DOI 10.1016/j.carbpol.2014.01.085.

55. Kuzmina, O., Bhardwaj, J., Rizal, ., Sheril, Dasitha, ., Nandula, Mariadaria, ., Livia, Griffith, J., Potthast, A., Rahatekar, S., James, ., Stephen & Welton, T. *Green Chemistry* **19**(24) 2017 5949. DOI 10.1039/C7GC02671D.

56. Ishikawa, T. & Margetic, D. Physico-Chemical Properties of OrganosuperbasesIn *Superbases for Organic Synthesis: Guanidines, Amidines, Phosphazenes and Related Organocatalysts*, ed. by e.T. Ishikawa, John Wiley & Sons, Ltd 2009, p. 9-48.

57. Parviainen, A., King, A.W.T., Mutikainen, I., Hummel, M., Selg, C., Hauru, L.K.J., Sixta, H. & Kilpeläinen, I. *ChemSusChem* **6**(11) 2013 2161. DOI 10.1002/cssc.201300143.

58. Ishikawa, T. General Aspects of OrganosuperbasesIn *Superbases for Organic Synthesis: Guanidines, Amidines, Phosphazenes and Related Organocatalysts*, 1. publ. p., Wiley, Hoboken 2009, p. 1-8.

59. Raczynska, E.D., Maria, P.C., Gal, J.F. & Decouzon, M. *The Journal of organic chemistry* **57**(21) 1992 5730. DOI 10.1021/jo00047a029.

60. Luo, H., Baker, G.A., Lee, J.S., Pagni, R.M. & Dai, S. *The Journal of Physical Chemistry B* **113**(13) 2009 4181. DOI 10.1021/jp901312d.

61. Inoue, Y., Yoshimura, S., Kiyono, S., Nobori, T. & Yamamoto, Y. Japan JP2006036709A, 2006.

62. Omotowa, B.A., Phillips, B.S., Zabinski, J.S. & Shreeve, J.M. *Inorganic chemistry* **43**(17) 2004 5466. DOI 10.1021/ic049483o.

63. Zhang, Q., Yuan, H., Fukaya, N., Yasuda, H. & Choi, J. *Green Chemistry* **19**(23) 2017 5614. DOI 10.1039/C7GC02666H.

64. Ahmad, W., Ostonen, A., Jakobsson, K., Uusi-Kyyny, P., Alopaeus, V., Hyväkkö, U. & King, A.W.T. *Chemical Engineering Research and Design* **114** 2016 287. DOI 10.1016/j.cherd.2016.08.032.

65. D'Andola, G., Szarvas, L., Massonne, K. & Stegmann, V. US WO2008043837A1, 2008.

66. Remsing, R.C., Swatloski, R.P., Rogers, R.D. & Moyna, G. *Chemical Communications* **0**(12) 2006 1271. DOI 10.1039/B600586C.

67. Payal, R.S. & Balasubramanian, S. *Physical Chemistry Chemical Physics* **16**(33) 2014 17458. DOI 10.1039/C4CP02219J.

68. Rabideau, B.D., Agarwal, A. & Ismail, A.E. *The Journal of Physical Chemistry B* **117**(13) 2013 3469. DOI 10.1021/jp310225t.

69. Rabideau, B.D. & Ismail, A.E. *Physical Chemistry Chemical Physics* **17**(8) 2015 5767. DOI 10.1039/C4CP04060K.

70. Holding, A.J., Hummel, M., Zwiers, H., Leskinen, M.L.K., Rico del Cerro, D., Hietala, S., Sixta, H., Nieger, M., Kemell, M., Helminen, J.K.J., Aseyev, V., Tenhu, H., Kilpeläinen, I. & King, A.W.T. *In press* .

71. Hauru, L.K.J., Hummel, M., King, A.W.T., Kilpeläinen, I. & Sixta, H. *Biomacromolecules* **13**(9) 2012 2896.

72. Doherty, T.V., Mora-Pale, M., Foley, S.E., Linhardt, R.J. & Dordick, J.S. *Green Chemistry* **12**(11) 2010 1967. DOI 10.1039/C0GC00206B.

73. Hauru, L.K.J., Hummel, M., Nieminen, K., Michud, A. & Sixta, H. *Soft matter* **12**(5) 2016 1487. DOI 10.1039/C5SM02618K.

74. Medronho, B., Romano, A., Miguel, M.G., Stigsson, L. & Lindman, B. *Cellulose* **19**(3) 2012 581. DOI 10.1007/s10570-011-9644-6.

75. Medronho, B. & Lindman, B. *Advances in Colloid and Interface Science* **222**(Supplement C) 2015 502. DOI //doi.org/10.1016/j.cis.2014.05.004.

76. Work, W.J., Horie, K., Hess, M. & Stepto, R.F.T. *Pure and Applied Chemistry* **76** 2009 1985. DOI 10.1351/pac200476111985.

77. Cai, J. & Zhang, L. *Macromolecular Bioscience* **5**(6) 2005 539. DOI 10.1002/mabi.200400222.

78. Kamlet, M.J., Abboud, J.L.M., Abraham, M.H. & Taft, R.W. *The Journal of organic chemistry* **48**(17) 1983 2877. DOI 10.1021/jo00165a018.

79. Huo, F., Liu, Z. & Wang, W. *The Journal of Physical Chemistry B* **117**(39) 2013 11780. DOI 10.1021/jp407480b.

80. Rinaldi, R. *Chemical communications (Cambridge, England)* **47**(1) 2011 511. DOI 10.1039/C0CC02421J.

81. Gericke, M., Liebert, T., Seoud, O.A.E. & Heinze, T. *Macromolecular Materials and Engineering* **296**(6) 2011 483. DOI 10.1002/mame.201000330.

82. Xu, A., Zhang, Y., Zhao, Y. & Wang, J. *Carbohydrate Polymers* **92**(1) 2013 540. DOI //doi.org/10.1016/j.carbpol.2012.09.028.

83. Hauru, L.K.J., Hummel, M., Michud, A. & Sixta, H. *Cellulose* **21**(6) 2014 4471. DOI 10.1007/s10570-014-0414-0.

84. Dong, B.K., James, J.P., Seong Mu, J. & Wha, S.L. *Textile Research Journal* **75**(4) 2005 331. DOI 10.1177/0040517505054852.

85. Hummel, M., Michud, A., Tanttu, M., Asaadi, S., Ma, Y., Hauru, L.K.J., Parviainen, A., King, A.W.T., Kilpeläinen, I. & Sixta, H. Ionic Liquids for the Production of Man-Made Cellulosic Fibers: Opportunities and ChallengesIn *Cellulose Chemistry and Properties: Fibers, Nanocelluloses and Advanced Materials*, ed. by O.J. Rojas, Springer International Publishing, Cham 2016, p. 133-168.

86. Stepan, A.M., Michud, A., Hellstén, S., Hummel, M. & Sixta, H. *Industrial & Engineering Chemistry Research* **55**(29) 2016 8225. DOI 10.1021/acs.iecr.6b00071.

87. *H&M rewards Finnish cotton recycling innovation* Good News from Finland 2016, http://www.goodnewsfinland.com/h-m-rewards-the-finnish-cotton-recycling-innovation/.

88. Berggren, R., Berthold, F., Sjöholm, E. & Lindström, M. *Journal of Applied Polymer Science* **88**(5) 2003 1170. DOI 10.1002/app.11767.

89. Biganska, O. & Navard, P. *Biomacromolecules* **6**(4) 2005 1948. DOI 10.1021/bm040079q.

90. de Oliveira, Heitor Fernando Nunes & Rinaldi, R. *ChemSusChem* **8**(9) 2015 1577. DOI 10.1002/cssc.201500272.

91. Cowie, J.M.G., Maconnachie, A. & Ranson, R.J. *Macromolecules* **4** 1971 57. DOI 10.1021/ma60019a013.

92. Suzuki, H., Muraoka, Y., Saitoh, M. & Kamide, K. *British Polymer Journal* **14**(1) 1982 23. DOI 10.1002/pi.4980140105.

93. de Oliveira, H.F.N., Clough, M.T. & Rinaldi, R. *ChemSusChem* **9**(23) 2016 3324. DOI 10.1002/cssc.201601108.

94. Hirosi Sobue, Heinz Kiessig & Kurt Hess *Zeitschrift für Physikalische Chemie* **43B**(1) 1939 309. DOI 10.1515/zpch-1939-4324.

95. Scudo, A., Liebmann, B., Corden, C., Tyrer, D., Kreissig, J. & Warwick, O. 2017, *Study for the European Commission: Intentionally added microplastics in products*, The ENDS Report, https://www.endsreport.com/article/57986/study-for-the-european-commission-intentionally-added-microplastics-in-products.

96. McNaught, A.D. & Wilkinson, A. *IUPAC. Compendium of Chemical Terminology (the "Gold Book")*.
, 2nd ed. p., Blackwell Scientific Publications, Oxford 1997.

97. Lassen, C., Foss Hansen, S., Magnusson, K., Norén, F., Bloch Hartmann, N.I., Rehne Jensen, P., Gissel Nielsen, T. & Brinch, A. 2015, *Microplastics : occurrence, effects and sources of releases to the environment in Denmark - Environmental project No. 1793*, The Danish Environmental Protection Agency, Copenhagen.

98. Setälä, O., Fleming-Lehtinen, V. & Lehtiniemi, M. *Environmental Pollution* **185** 2014 77. DOI //doi.org/10.1016/j.envpol.2013.10.013.

99. Lusher, A.L., Tirelli, V., O'Connor, I. & Officer, R. *Scientific Reports* **5** 2015 14947.

100. Besseling, E., Wegner, A., Foekema, E.M., van, d.H. & Koelmans, A.A. *Environmental science & technology* **47**(1) 2013 593. DOI 10.1021/es302763x.

101. *Greenpeace Asia - Global Cosmetics and Personal Care companies' Microbead commitment ranking* 2016, Available: https://secured-static.greenpeace.org/korea/Global/korea/publications/reports/oceans/2016/EN_CorporateRankingDetails_final.pdf (Retrieved 22.2.2018).

102. Morice, C., Radigue, B. & Winckler, C. *Household and Personal Care Today* **10**(5) 2015 .

103. *CelluloScrub - Lessonia* Available: http://www.lessonia.com/index.php?rub=celluloscrub_2 (Retrieved 22.2.2018).

104. Motozato, Y. & Hirayama, C. *Journal of Chromatography A* **298** 1984 499. DOI //dx.doi.org/10.1016/S0021-9673(01)92747-5.

105. Sandig, B., Michalek, L., Vlahovic, S., Antonovici, M., Hauer, B. & Buchmeiser, M.R. *Chemistry – A European Journal* **21**(44) 2015 15835. DOI 10.1002/chem.201501618.

106. Bai, Y. & Li, Y. *Carbohydrate Polymers* **64**(3) 2006 402. DOI //doi.org/10.1016/j.carbpol.2005.12.009.

107. Lindh, J., Ruan, C., Strømme, M. & Mihranyan, A. *Langmuir* **32**(22) 2016 5600. DOI 10.1021/acs.langmuir.6b01288.

108. Schweikert, K., Egorova, M., Juch, R., Lefevre, F. & Westenfelder, H. European Union EP2907498A12015.

109. *Kobo Products Inc., Microspheres, Microsphere Complexes and Composites* Available: http://www.koboproductsinc.com/products_Categories.aspx?mPage=Microspheres (Retrieved 23.04.2017).

110. Cassin, G. US20050255135 A1.

111. Park, T., Lee, S., Simmons, T.J., Martin, J.G., Mousa, S.A., Snezhkova, E.A., Sarnatskaya, V.V., Nikolaev, V.G. & Linhardt, R.J. *Chemical Communications* (40) 2008 5022. DOI 10.1039/B809791G.

112. Yu, X., Kang, D., Hu, Y., Tong, S., Ge, M., Cao, C. & Song, W. *RSC Advances* **4**(59) 2014 31362. DOI 10.1039/C4RA05601A.

113. Luo, X. & Zhang, L. *Journal of Hazardous Materials* **171**(1) 2009 340. DOI 10.1016/j.jhazmat.2009.06.009.

114. Luo, X. & Zhang, L. *Biomacromolecules* **11**(11) 2010 2896. DOI 10.1021/bm100642y.

115. Voon, L.K., Pang, S.C. & Chin, S.F. *Materials Letters* **164** 2016 264. DOI //doi.org/10.1016/j.matlet.2015.10.161.

116. *Cellulose, beaded C7704* Available: http://www.sigmaaldrich.com/catalog/product/sigma/c7704 (Retrieved Apr 23,2017).

117. *Cellulose, beaded C8454* Available: http://www.sigmaaldrich.com/catalog/product/sigma/c8454 (Retrieved Apr 23,2017).

118. Trygg, J., Fardim, P., Gericke, M., Mäkilä, E. & Salonen, J. *Carbohydrate Polymers* **93**(1) 2013 291. DOI //doi.org/10.1016/j.carbpol.2012.03.085.

119. Nah, J.W., Paek, Y.W., Jeong, Y.I., Kim, D.W., Cho, C.S., Kim, S.H. & Kim, M.Y. *Archives of pharmacal research* **21**(4) 1998 418. DOI 10.1007/BF02974636.

120. Yildir, E., Kolakovic, R., Genina, N., Trygg, J., Gericke, M., Hanski, L., Ehlers, H., Rantanen, J., Tenho, M., Vuorela, P., Fardim, P. & Sandler, N. *International journal of pharmaceutics* **456**(2) 2013 417. DOI //doi.org/10.1016/j.ijpharm.2013.08.047.

121. Omura, T., Imagawa, K., Kono, K., Suzuki, T. & Minami, H. *ACS Applied Materials & Interfaces* **9**(1) 2017 944. DOI 10.1021/acsami.6b13261.

122. Suzuki, T., Kono, K., Shimomura, K. & Minami, H. *Journal of colloid and interface science* **418** 2014 126. DOI 10.1016/j.jcis.2013.12.014.

123. Imagawa, K., Omura, T., Ihara, Y., Kono, K., Suzuki, T. & Minami, H. *Cellulose* **24**(8) 2017 3111. DOI 10.1007/s10570-017-1342-6.

124. Druel, L., Niemeyer, P., Milow, B. & Budtova, T.Cellulose-[DBNH][CO2Et] rheological properties and aerogel beads made with JetCutting technique, 5th EPNOE International Polysaccharide Conference 2017 2017, , s. 136.

125. Lin, F., You, Y., Yang, X., Jiang, X., Lu, Q., Wang, T., Huang, B. & Lu, B. *Cellulose* **24**(11) 2017 5025. DOI 10.1007/s10570-017-1473-9.

126. Carrick, C., Pendergraph, S.A. & Wågberg, L. *ACS Applied Materials & Interfaces* **6**(23) 2014 20928. DOI 10.1021/am505673u.

127. Carrick, C., Ruda, M., Pettersson, B., Larsson, P.T. & Wagberg, L. *RSC Advances* **3**(7) 2013 2462. DOI 10.1039/C2RA22020B.

128. California Institute of Technology, Feynman, R.P., *There's Plenty of Room at the Bottom,* Pasadena, CA 1960.

129. Rao, J.P. & Geckeler, K.E. *Progress in Polymer Science* **36**(7) 2011 887. DOI //doi.org/10.1016/j.progpolymsci.2011.01.001.

130. Pääkkö, M., Ankerfors, M., Kosonen, H., Nykänen, A., Ahola, S., Osterberg, M., Ruokolainen, J., Laine, J., Larsson, P.T., Ikkala, O. & Lindström, T. *Biomacromolecules* **8**(6) 2007 1934. DOI 10.1021/bm061215p.

131. Turbak, A.F., Snyder, F.W. & Sandberg, K.R. *J. Appl. Polym. Sci.: Appl. Polym. Symp.; (United States)* **37** 1983 .

132. Morán, J.I., Alvarez, V.A., Cyras, V.P. & Vázquez, A. *Cellulose* **15**(1) 2008 149. DOI 10.1007/s10570-007-9145-9.

133. Hettrich, K., Pinnow, M., Volkert, B., Passauer, L. & Fischer, S. *Cellulose* **21**(4) 2014 2479. DOI 10.1007/s10570-014-0265-8.

134. Nakagaito, A.N. & Yano, H. *Applied Physics A* **80**(1) 2005 155. DOI 10.1007/s00339-003-2225-2.

135. Saito, T., Okita, Y., Nge, T.T., Sugiyama, J. & Isogai, A. *Carbohydrate Polymers* **65**(4) 2006 435. DOI //dx.doi.org/10.1016/j.carbpol.2006.01.034.

136. Fumagalli, M., Sanchez, F., Molina Boisseau, S. & Heux, L. *Soft Matter* **9**(47) 2013 11309. DOI 10.1039/C3SM52062E.

137. Kvien, I., Tanem, B.S. & Oksman, K. *Biomacromolecules* **6**(6) 2005 3160. DOI 10.1021/bm050479t.

138. Araki, J., Wada, M., Kuga, S. & Okano, T. *Journal of Wood Science* **45**(3) 1999 258. DOI 10.1007/BF01177736.

139. Siqueira, G., Bras, J. & Dufresne, A. *Biomacromolecules* **10**(2) 2009 425. DOI 10.1021/bm801193d.

140. Rojas, J., Bedoya, M. & Ciro, Y. Current Trends in the Production of Cellulose Nanoparticles and Nanocomposites for Biomedical ApplicationsIn *Cellulose - Fundamental Aspects and Current Trends*, ed. by M. Poletto & H.L.O. Junior, InTech, Rijeka 2015, p. Ch. 08.

141. de Souza Lima, M. Miriam & Borsali, R. *Macromolecular Rapid Communications* **25**(7) 2004 771. DOI 10.1002/marc.200300268.

142. T. Paakkari, R. Serimaa & H. Fink *Acta Polymerica* **40**(12) 1989 731. DOI 10.1002/actp.1989.010401205.

143. Yu, Y. & Wu, H. *AIChE Journal* **57**(3) 2011 793. DOI 10.1002/aic.12288.

144. da Silva Perez, D., Montanari, S. & Vignon, M.R. *Biomacromolecules* **4**(5) 2003 1417. DOI 10.1021/bm034144s.

145. Kim, U. & Kuga, S. *Journal of Chromatography A* **919**(1) 2001 29. DOI //dx.doi.org/10.1016/S0021-9673(01)00800-7.

146. Fessi, H., Puisieux, F., Devissaguet, J.P., Ammoury, N. & Benita, S. *International Journal of Pharmaceutics* **55**(1) 1989 . DOI //dx.doi.org/10.1016/0378-5173(89)90281-0.

147. Zili, Z., Sfar, S. & Fessi, H. *International journal of pharmaceutics* **294**(1–2) 2005 261. DOI //doi.org/10.1016/j.ijpharm.2005.01.020.

148. Legrand, P., Lesieur, S., Bochot, A., Gref, R., Raatjes, W., Barratt, G. & Vauthier, C. *International journal of pharmaceutics* **344**(1–2) 2007 33. DOI //doi.org/10.1016/j.ijpharm.2007.05.054.

149. Nehilla, B.J., Bergkvist, M., Popat, K.C. & Desai, T.A. *International Journal of Pharmaceutics* **348**(1) 2008 107. DOI //dx.doi.org/10.1016/j.ijpharm.2007.07.001.

150. Yordanov, G.G. & Dushkin, C.D. *Colloid and Polymer Science* **288**(9) 2010 1019. DOI 10.1007/s00396-010-2226-6.

151. Dalpiaz, A., Vighi, E., Pavan, B. & Leo, E. *Journal of Pharmaceutical Sciences* **98**(11) 2009 4272. DOI 10.1002/jps.21710.

152. Stella, B., Arpicco, S., Rocco, F., Marsaud, V., Renoir, J., Cattel, L. & Couvreur, P. *International journal of pharmaceutics* **344**(1–2) 2007 71. DOI //doi.org/10.1016/j.ijpharm.2007.06.006.

153. Kim, E., Yang, J., Choi, J., Suh, J., Huh, Y. & Haam, S. *Nanotechnology* **20**(36) 2009 365602. DOI 10.1088/0957-4484/20/36/365602.

154. Gericke, M., Trygg, J. & Fardim, P. *Chemical Reviews* **113**(7) 2013 4812. DOI 10.1021/cr300242j.

155. Moinard-Chécot, D., Chevalier, Y., Briançon, S., Beney, L. & Fessi, H. *Journal of colloid and interface science* **317**(2) 2008 458. DOI //doi.org/10.1016/j.jcis.2007.09.081.

156. Lince, F., Marchisio, D.L. & Barresi, A.A. *Journal of colloid and interface science* **322**(2) 2008 505. DOI //doi.org/10.1016/j.jcis.2008.03.033.

157. Zhang, C., Chung, J.W. & Priestley, R.D. *Macromolecular rapid communications* **33**(20) 2012 1798. DOI 10.1002/marc.201200335.
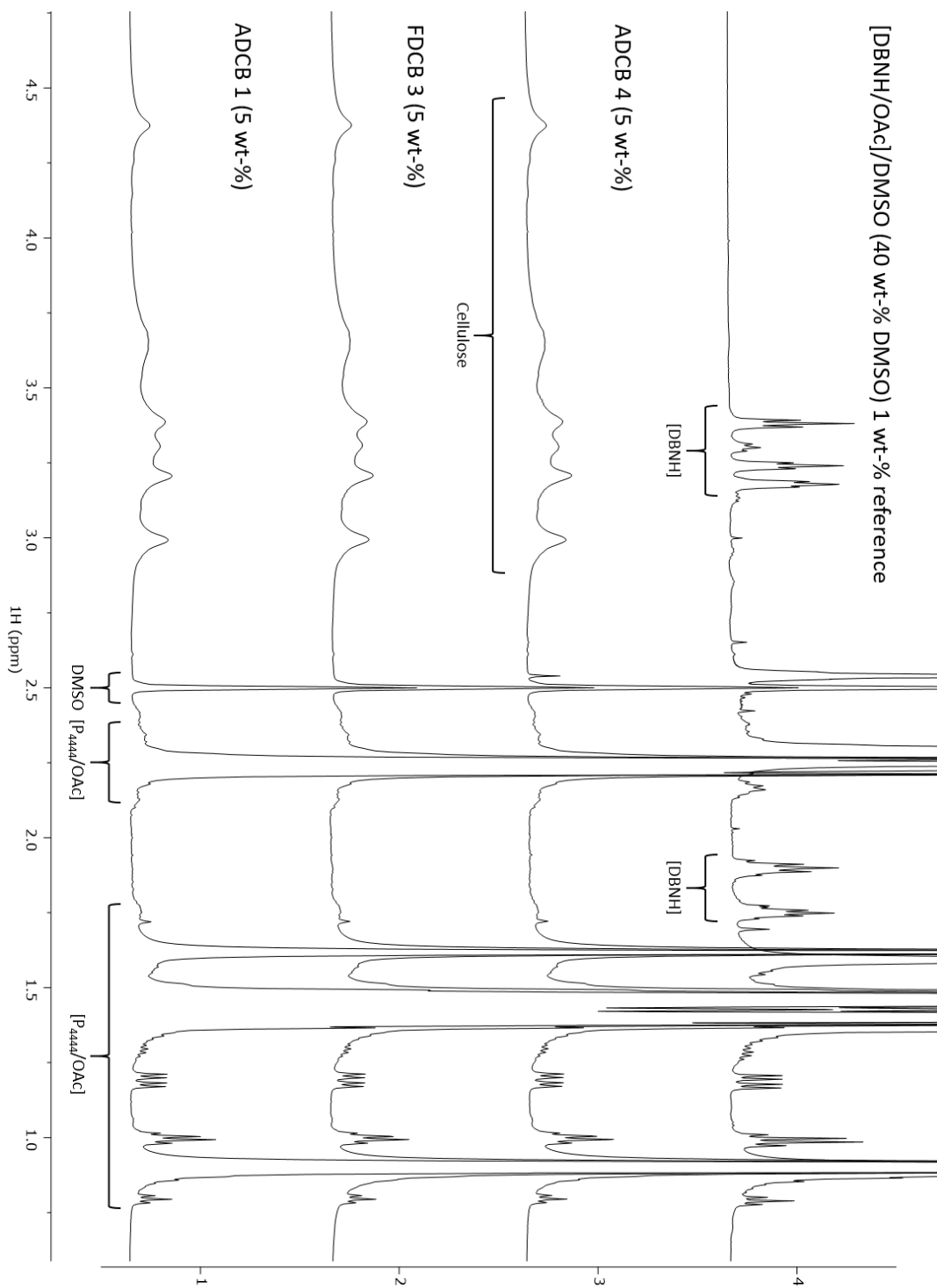
158. Foerster, M., Gengenbach, T., Woo, M.W. & Selomulya, C. *Colloids and Surfaces B: Biointerfaces* **140** 2016 460. DOI //doi.org/10.1016/j.colsurfb.2016.01.012.

159. Nasr, G.G., Bendig, L. & Yule, A.J. *Industrial sprays and atomization*, Springer, London [u.a.] 2002.

160. Mlkvik, M., Stähle, P., Schuchmann, H.P., Gaukel, V., Jedelsky, J. & Jicha, M. *International Journal of Multiphase Flow* **77** 2015 19. DOI //doi.org/10.1016/j.ijmultiphaseflow.2015.06.010.

161. Cerveró, J.M., Nogareda, J., Valle, Eva M Martín del & Galán, M.A. *Chemical Engineering Journal* **174**(2) 2011 699. DOI //doi.org/10.1016/j.cej.2011.09.063.

162. Katarzyna, S., Paulina, G. & Kamińska-Dwórznicka Anna *Polish Journal of Food and Nutrition Sciences* **65** 2015 109. DOI 10.2478/pjfns-2013-0012.

163. Hait, S. & Moulik, S. *Journal of Surfactants and Detergents* **4**(3) 2001 303. DOI 10.1007/s11743-001-0184-2.

164. *Cytec Solvay Group AEROSOL® OT-100* Available: https://www.cytec.com/products/aerosol-ot-100-2 (Retrieved 27.07.2017).

165. *Thermo Fisher Scientific Sodium Dodecyl Sulfate (SDS), Lauryl* Available: https://www.thermofisher.com/order/catalog/product/28364 (Retrieved 27.07.2017).

166. Thygesen, A., Oddershede, J., Lilholt, H., Thomsen, A.B. & Ståhl, K. *Cellulose* **12**(6) 2005 563. DOI 10.1007/s10570-005-9001-8.

167. Wojdyr, M. *Journal of Applied Crystallography* **43**(5-1) 2010 1126. DOI 10.1107/S0021889810030499.

168. Hult, E., Lena, Iversen, T. & Sugiyama, J. *Cellulose* **10**(2) 2003 103. DOI 1024080700873.

169. He, J., Cui, S. & Wang, S. *Journal of Applied Polymer Science* **107**(2) 2008 1029. DOI 10.1002/app.27061.

170. Garvey, C.J., Parker, I.H. & Simon, G.P. *Macromolecular Chemistry and Physics* **206**(15) 2005 1568. DOI 10.1002/macp.200500008.

171. Cullity, B.D. & Graham, C.D. *Introduction to magnetic materials* , 2. ed. p., IEEE Press [u.a.], Piscataway, NJ 2009.

172. Biganska, O. & Navard, P. *Cellulose* **16**(2) 2009 179. DOI 10.1007/s10570-008-9256-y.

173. Meeuwissen, S.A., Kim, K.T., Chen, Y.C., Pochan, D.J. & Hest, J C M van *Angewandte Chemie : International Edition* **50**(31) 2011 7070. DOI 10.1002/anie.201102167.

174. Kudaibergenov, S.E., Tatykhanova, G.S., Arinov, B.Z., Kozhakhmetov, S.K. & Aseyev, V.O. *Express Polymer Letters* **2**(2) 2008 101. DOI 10.3144/expresspolymlett.2008.14.
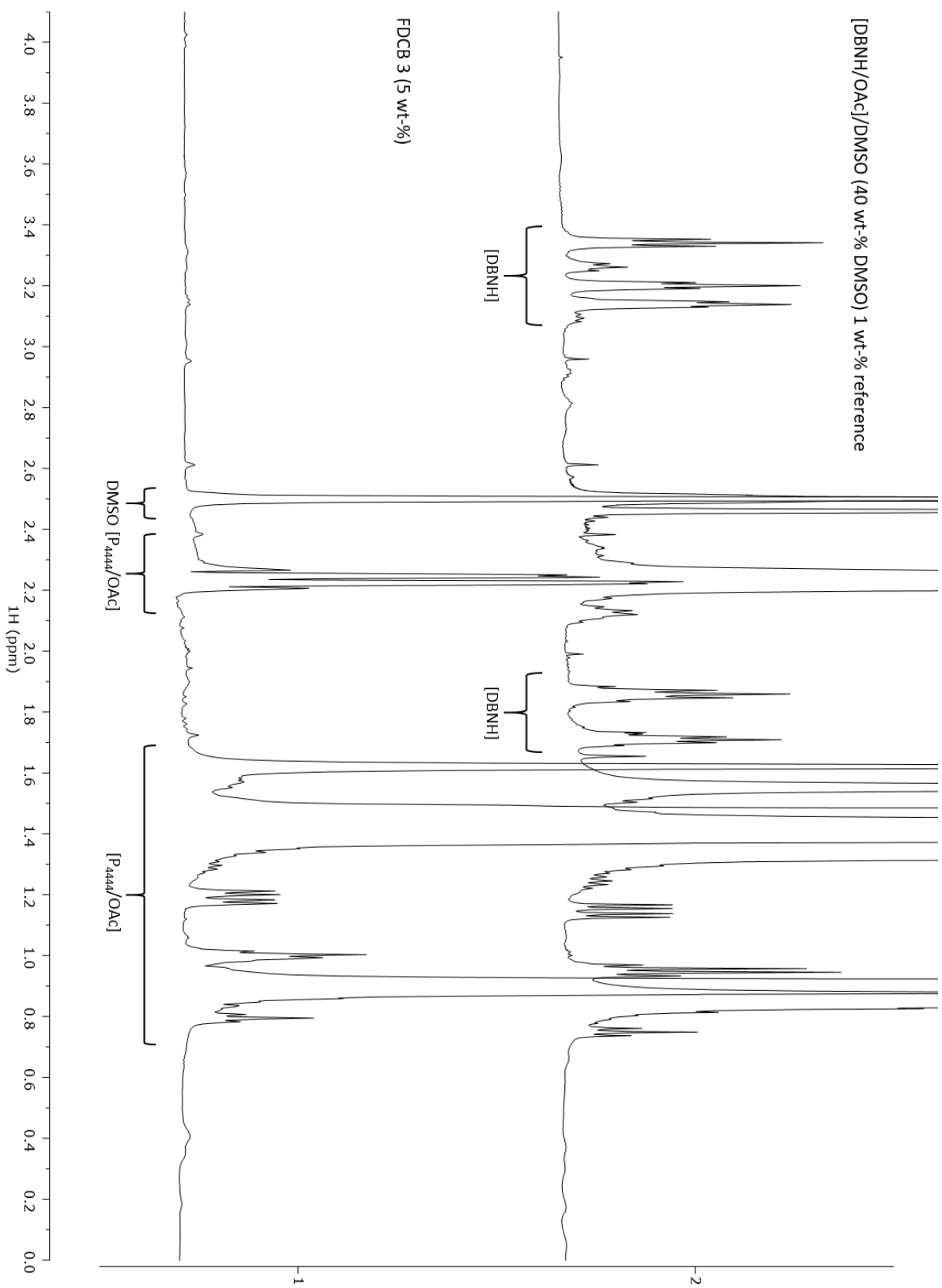
7. Appendix

7.1. Attachments:

Attachment 1.

Attachment 3.

Electron Image 1